NASA CONTRACTOR REPORT

NASA CR-2072

CORRELATION OF STRESS-WAVE-EMISSION CHARACTERISTICS WITH FRACTURE IN ALUMINUM ALLOYS

by C. E. Hartbower, W. G. Reuter,
C. F. Morais, and P. P. Crimmins

Prepared by
ADVANCED TECHNOLOGY
AEROJET SOLID PROPULSION COMPANY
Sacramento, Calif.
for

NATIONAL AERONAUTICS AND SPACE ADMINISTRATION • WASHINGTON, D. C. • JULY 1972

1. REPORT NO. NASA CR-2072	2. GOVERNMENT ACCESSION NO.	3. h.
4. TITLE AND SUBTITLE CORRELATION OF STRESS-WAVE-EMISSION CHARACTERISTICS WITH FRACTURE IN ALUMINUM ALLOYS		5. REPORT DATE July 1972
		6. PERFORMING ORGANIZATION CODE
7. AUTHOR(S) C.E. Hartbower, W. G. Reuter, C. F. Morais,& P.P. Crimmins		8. PERFORMING ORGANIZATION REPORT #
9. PERFORMING ORGANIZATION NAME AND ADDRESS Advanced Technology Aerojet Solid Propulsion Company Sacramento, California		10. WORK UNIT NO.
		11. CONTRACT OR GRANT NO. NAS 8-21405
		13. TYPE OF REPORT & PERIOD COVERED
12. SPONSORING AGENCY NAME AND ADDRESS National Aeronautics and Space Administration Washington, D. C. 20546		Contractor Report Final
		14. SPONSORING AGENCY CODE

15. SUPPLEMENTARY NOTES

16. ABSTRACT

This report presents the findings of a study to correlate stress-wave-emission characteristics with fracture in welded and unwelded aluminum alloys tested at room and cryogenic temperatures. The stress-wave-emission characteristics investigated were those which serve to presage crack instability; viz., a marked increase in (1) signal amplitude, (2) signal repetition rate and (3) the slope of cumulative count plotted versus load. The alloys were 7075-T73, 2219-T87 and 2014-T651, welded with MIG and TIG using 2319 and 4043 filler wire. The testing was done with both unnotched and part-through-crack (PTC) tension specimens and with 18-in.-dia subscale pressure vessels. In the latter testing, a real-time, acoustic-emission, triangulation system was used to locate the source of each stress-wave emission. With such a system, multiple emissions from a given location were correlated with defects found by conventional nondestructive inspection.

17. KEY WORDS Aluminum alloys Welding Stress-wave-emission characteristics	18. DISTRIBUTION STATEMENT

19. SECURITY CLASSIF. (of this report) Unclassified	20. SECURITY CLASSIF. (of this page) Unclassified	21. NO. OF PAGES 232	22. PRICE $3.00

MSFC - Form 32'

FOREWORD

This document reports on an investigation by the Aerojet Solid Propulsion Company from July 1968 to November 1971, to determine the correlation between acoustic emission and fracture in selected aluminum alloys under Contract NAS 8-21405. The work was administered under the direction of Mr. W. Clotfelter of the NASA Marshall Space Flight Center.

Aerojet personnel who participated in the investigation include C. E. Hartbower, Associate Scientist, W. G. Reuter, Senior Engineer; C. F. Morais, Test Engineer and P. P. Crimmins, Manager of the Metallurgy Section of Advanced Technology, Aerojet Solid Propulsion Company, Sacramento, California.

CORRELATION OF STRESS-WAVE EMISSION CHARACTERISTICS
WITH FRACTURE IN ALUMINUM ALLOYS

viii

ix

I.   INTRODUCTION

A.   DEVELOPMENT OF THE TECHNOLOGY

1.   Historical Background

The use of stress-wave emission as a nondestructive inspection technique has been under development for over a decade. The technique is based upon the elastic energy which is spontaneously released when a material undergoes plastic deformation and/or cracking. Thus, stress-wave emission constitutes a unique nondestructive inspection method in that the material defect when propagating, transmits its own signal, with the sensor acting as the receiver. In other words, the material undergoing crack growth both generates and transmits the signal (stress wave emission) which then can be detected by suitable instrumentation and the source located using seismic techniques.

In Germany, Kaiser[1]* reported what was apparently the first comprehensive investigation of stress-wave emission in 1950. In the U.S.A., the researches of Schofield, et al[2-4] and studies at Aerojet-General Corporation[5-28] were largely responsible for triggering the current high activity in this new field of nondestructive inspection. Dunegan[29-32] at the University of California Lawrence Radiation Laboratory also did pioneering work in this area, but most of his early research was for the U.S. Atomic Energy Commission and, therefore, was not publicized. Graduate studies at Michigan State University started working in this field around 1960 and continue to work with the stress-wave emission phenomenon[33-36]. Likewise, other colleges and universities have been encouraging work on the phenomenon in the last five years[37-45].

---

*References 1-45 are listed on pages 81 - 84.

In addition to the above references, an extensive literature survey was undertaken during this program. The articles dealing with the general area of acoustic emission technology uncovered and reviewed during this survey are shown in Appendix A. Although this background is extensive, no reported work was found which involved application of the technique to monitoring of crack initiation and growth at cryogenic temperatures. Primarily, the work has involved room temperature laboratory tests and the monitoring of structures, principally pressure vessels, also at room temperature. The results of these prior programs are incorporated in this report where applicable to the results of this study.

2. Subcritical Crack Growth

Examination of failed rocket motor cases has indicated the typical failure origin to be a small crack or crack-like flaw. The flaw is sometimes sufficiently large to cause fracture on initial loading and sometimes it is so small that the structure can withstand many load cycles or a prolonged period of sustained stress before the flaw attains critical size for failure. From service-failure analyses, it is clear that fabricated structures and even raw materials contain defects of various kinds. Service life then is controlled by (1) the initial flaw size, (2) the rate of slow crack growth in the environment of the proof test and/or service, and (3) the flaw size (critical crack size) to cause fracture at the operating stress. The latter is determined by a quantitative measure of fracture toughness. The rate of subcritical crack growth and the threshhold stress intensity below which slow crack growth will not occur is determined by laboratory evaluation and can be monitored by nondestructive inspection using the Stress-Wave Analysis Technique (SWAT). The initial flaw size is estimated by quality control and verified by proof test.

The basic philosophy of the proof test is that once a pressure vessel has withstood the proof pressure, subsequent loading to a lesser pressure will not produce failure. Obviously, this assumes that there will be no fatigue

2

cracking in service and no slow crack growth of existing subcritical defects due to time-dependent mechanisms such as hydrogen, stress corrosion and/or strain aging. Without SWAT, experience shows that failure can occur in proof testing as a result of undetected subcritical crack growth. Moreover, when a material is susceptible to slow crack growth, the concept of the proof test is invalid; i.e., after proof testing, tankage can fail at a lesser load if stress-corrosion, strain aging, hydrogen or cyclic loading are involved in service. There are numerous examples to illustrate the fact of subcritical crack growth in proof testing as well as in service.

Consider the second-stage Minuteman, a 42-in.-dia rocket motor case which was proof tested with inhibited water with three cycles of ninety seconds each to 1.1 of the mean expected operating pressure (MEOP). One chamber failed "prematurely" during the fourth cycle (a test-rig malfunction on the first cycle necessitated a fourth cycle to proof pressure). The failure occurred after 40 seconds at pressure during the last cycle of proof testing. Thus, the chamber withstood a total of 220 seconds at maximum pressure. The fabricator's failure analysis reported that failure initiated in the ID surface, in the fusion and heat-affected zone of the center girth weld. No cracks were found by nondestructive inspection prior to proof testing. The only explanation for such a failure is subcritical crack growth during proof testing.

Consider also a first-stage Polaris rocket motor case which was proof tested with inhibited water at 1150 psig and held at pressure for 180 seconds, with two or more pressure cycles. In the early development of the Polaris, there were numerous failures in proof test, and some had all the characteristics of subcritical crack growth. One chamber, for example, failed after 120 seconds at proof pressure on the second test cycle. The chamber had been inspected by magnetic-particle, dye-penetrant, radiographic and visual procedures; all failed to reveal cracking. Another Polaris

chamber failed after the second proof cycle <u>during</u> <u>the</u> <u>first</u> <u>few</u> <u>seconds</u> <u>of</u> depressurization, after withstanding a total of 360 seconds at proof pressure.

The above examples show that incipient flaws in a pressure vessel can increase in size as a result of proof testing. The concern here is not only with those pressure vessels that fail during proof test (an economic loss) but also with those that suffer subcritical crack growth without failure in the proof test. The latter then enter service with enlarged cracks which may be subject to additional slow crack growth at service loads. However, if the proof test does not fail the pressure vessel and if a system is employed to detect and locate flaw(s) undergoing subcritical crack growth, the information gained from the proof test outweighs the damage done by slow crack growth. Furthermore, with the safeguard of SWAT, proof testing significantly above the pressure anticipated in service can be advantageous. For example, if a vessel survives the first cycle to 1.5 MEOP, then the largest flaw that can be present in the successfully proof-tested tankage is smaller than that at 1.1 MEOP[*]. Thus, a vessel which survives the first cycle at a proof pressure of 1.5 MEOP is less likely to fail in service because of the significantly smaller defects demonstrated to be present by the proof test. However, if SWAT is not used to detect flaw growth and permit unloading before a crack reaches critical size, the higher proof pressure (1.5 MEOP) will increase the probability of failure in the proof test itself.

The examples of subcritical crack growth cited in earlier paragraphs involved high-strength materials. Some who are primarily concerned with lower-strength materials will take comfort in this. However, one other example should be considered. During the routine air-leak test of a large

---

[*] C. F. Tiffany, F. A. Pall, "An Approach to the Prediction of Pressure Vessel Minimum Fatigue Life Based Upon Applied Fracture Mechanics," Boeing Doc. D2-22437 (163). Unlimited Distribution. ASTM Special Committee on Fracture Testing of High Strength Sheet Materials Fifth Report, Materials Research & Standards, Vol. 4(3), March 1964.

steel pressure vessel, a catastrophic brittle failure occurred at a pressure of about 3,200 psig, even though the vessel previously had passed two hydro-static tests at 7,500 psig. The pressure vessel was in the form of a sausage-shaped flask. about 15-ft long with a 19-1/2-in. ID and a 1-1/4-in. minimum wall thickness; it was manufactured in accordance with ASTM Spec. A372 Class 4, modified to a minimum yield strength requirement of 80,000 psi. Investigation of the failure[*] revealed that, following the hydrostatic tests, prior to leak test, the pressure vessel.had been galvanized twice, including a five to eight hour warm-acid-stripping operation prior to the second galvanize. Hydrogen embrittlement arising from the acid stripping was suspected to be a factor contributing to the brittle failure. Standard Charpy V-notch impact tests revealed the 15-ft-lb transition to be 100°F and the FATT to be 125°F; the drop-weight NDT was approximately 80°F. Thus, the brittle condition of the steel was confirmed by the high transition temperatures of the pressure-vessel material (although the material met all requirements of the applicable ASTM specification). Nevertheless, the failure was considered to be unusual inasmuch as the pressure vessel had successfully passed two cycles of proof test to 7,500 psig and then failed at 3,200 psig in a routine air-leak test.

Positive assurance of the structural integrity of pressure vessels depends upon determination of (1) the initial flaw size, (2) the rate at which pre-existing flaws grow under operating conditions, and (3) the maximum flaw size the material can tolerate under operating conditions. Before proof testing (or leak testing, as in the preceding example), the only basis for estimating the initial flaw size is a knowledge of the quality-control procedures employed during fabrication. For example, if X-ray is the

* R. C. Bates and H. D. Greenberg, "A Study of the Fracture Resistance of Steel Pressure Vessels by Means of Charpy, Drop-Weight, and Full-Size Burst Tests," AIME Met. Soc. Conf., Vol. 31, APPLICATION OF FRACTURE TOUGHNESS PARAMETERS TO STRUCTURAL METALS, Edited by H. D. Greenberg, Chairman of the Symposium Committee, Gordon and Breach Sci. Pub. New York, 1964.

is the nondestructive inspection method used, then the largest crack in the pressure vessel at the time of proof testing might be estimated as being 2 percent of the thickness. If the critical crack size at the proof pressure is less than 2 percent of the wall thickness, then the pressure vessel may fail during proof test. (With acoustic emission as a nondestructive inspection method employed during proof test, one should be able to detect the growth of such a defect at loads well below the proof pressure and discontinue the test before failure occurs.) If there are no cracks in the pressure vessel of critical size at proof pressure, then one can estimate the largest flaw at the start of service to be no larger than the critical crack size at the proof pressure. This then is the estimated initial flaw size.

B.   SCOPE OF THE RESEARCH

The objective of the research reported here was to investigate the correlation of stress-wave-emission characteristics with fracture of aluminum alloys in environments of particular interest for liquid-rocket-engine tankage. Selected aluminum alloys were investigated, including 7075-T73, 2219-T87 and 2014-T6. The 2014-T6 alloy was TIG welded with 4043 and 2319 filler wire and MIG welded with 4043. The materials were tested as smooth (unflawed) tension specimens and as part-through-crack (PTC) tension specimens at room and at cryogenic temperatures. In addition, 18-in.-dia subscale pressure vessels were tested using a computerized SWAT system for detection and location of stress-wave sources.

6

II. SUMMARY

Previous programs at Aerojet have extensively utilized the stress-wave-analysis technique (SWAT) as a crack-monitoring system at room and elevated temperature. One observation common to the earlier studies, regardless of the material investigated, is that the stress-wave-emission signals have characteristics which serve to identify plane-strain instability and presage plane-stress instability. The characteristics which have been found to serve as a precursor of failure are (1) a marked increase of the amplitude of the signals as observed in real time on an oscilloscope, (2) a marked increase in the signal repetition rate (count per second) and (3) a marked increase in the slope of the cumulative count-versus-load plot.

Room-temperature data from PTC-tension tests in the study reported herein confirmed the usefulness of the above characteristics and provided a precursor of the plane-strain instability. However, the characteristic marked increase in acoustic-emission count rate observed at room temperature was not generally observed in cryogenic testing PTC-tension specimens. Nevertheless, crack growth was detected in all of the cryogenic tests and at loads sufficiently below critical stress intensity to permit unloading and confirmation by conventional non-destructive inspection. Highlights of the findings upon which these general observations were based are summarized below.

Laboratory Tension Tests. Acoustic-emission measurements in cryogenic testing were found to be complicated by the following factors:

1. bubbling (boiling) of the cryogenic medium

2. formation of ice on the tooling above and below the cryostat

3. low sensitivity of the Model 2242 accelerometer used in low-temperature testing.

Solution to these problems was obtained in the testing of tension specimens by the use of 60 KHz to 600 KHz band-pass filtering, meticulous care to avoid the formation of ice around the cryostat, and the use of a Model 2213 acclerometer mounted on a wave guide extending out of the cryogenic bath.

Larger cumulative counts were obtained from unnotched tension specimens than from part-through-crack tension specimens. The large count recorded from the unnotched specimens occurred primarily as a precursor at loads close to failure. The following tabulation summarizes the results of both the room-temperature tests and the cryogenic-temperature tests where ice was eliminated and a model 2213 accelerometer was used mounted on a wave guide.

PRECURSOR IN NOTCHED AND UNNOTCHED TENSION TESTS

Test	Material	Temp.	Condition[a]	Specimen	Thousands of Counts[b]
Unnotched Tension	2014	RT	BM	C	120
			WM	22	1,750
			WM	25	240
	2219	RT	BM	13	145
			WM	28	1,000
			WM	27	61
	2014	-320	BM	D	35
			BM	E	70
			BM	F	140
			BM	G	120
			WM	36	300
	2219	-320	BM	H	200
			BM	I	40
			BM	J	70
			BM	K	90
			WM	32	35
PTC-Tension	2014	RT	BM	2	60
			WM	3	330
			WM	21	200
	2219	RT	BM	18	Neg.[c]
			WM	29	50
			WM	30	100
	2014	-320°F	BM	8	Neg.[c]
			BM	9	Neg.[c]
			WM	26	Neg.[c]
	2219	-320°F	BM	19	Neg.[c]
			WM	31	Neg.[c]
			WM	34	Neg.[c]

- -

(a) BM, base-metal test; WM, weld-metal test.
(b) increase in count occurring in the precursor of failure.
(c) no significant increase in count just before failure.

From the above summary, it will be seen that at room temperature both the unnotched and the PTC-tension specimens gave useful precursors, but at cryogenic temperature, there was little or no warning of failure in the plane-strain (PTC) tension tests.

Two instrumentation considerations were found to affect the room-temperature precursor, viz., the trigger level used in counting, and the scale factor used in plotting cumulative count versus load. If the trigger level is set close to the background noise, this is effectively an increase in gain and the precursor gives an early warning of failure. If a higher voltage trigger setting is used (effectively less gain), the warning comes just before failure. If the X-Y plot of count is recorded at 10^6 full scale, the precursor may be somewhat indeterminant. With high sensitivity, a 10^5 full-scale count setting for the X-Y plot provided the best precursor.

The lack of precursor in the PTC-tension tests at cryogenic temperature points up (1) the advantage of proof testing tankage at room temperature where large counts generally presage failure and (2) the need for a real-time acoustic-emission triangulation system in cryogenic testing. In cryogenic testing, the computer, using the triangulation technique, determines the location of each signal source, and, thus permits judgements based on multiple emissions from a single source. In general, single events are disregarded but multiple emissions from a single location serve as the precursor of failure at cryogenic temperature.

Pressure Vessel Tests. At room temperature the pressure-vessel tests demonstrated that acoustic emission monitoring can be employed to detect and locate growing defects in the aluminum alloys tested, and provides the basis for terminating a pressure test prior to failure. A marked increase in both the count rate and stress-wave amplitude (as observed on an oscilloscope in real time) served as precursors of failure. The existence of the Kaiser effect during structural loading also was verified in the room temperature tests; i.e., significant SWE activity was not observed in successive cycles until prior pressure levels were exceeded. However, when defects (or deliberate flaws) were at the onset of instability, the Kaiser effect no longer was operative. Practical application of the Kaiser effect lies in its use to determine prior maximum pressure (stress) levels.

At cryogenic temperature the pressure-vessel tests again demonstrated the capability to detect and locate stress-wave-emission sources in real time. Moreover, in spite of the low sensitivity of the transducer used in cryogenic testing, it was still possible to detect and approximately locate the failure origin in each vessel. Multiple emissions from weld defects and/or deliberate flaws served to indicate incipient failure.

In the 2219-T87 cryogenic test, the error in defect source location based on signal triangulation was approximately 4 inches; a similar error (1 to 3-in.) in source location was observed in the room-temperature test of the same material. During each pressure-vessel test, multiple emissions were observed from the defect area which indicated potential failure. Inspite of the error, the indicated source was within the zone which would have to be ultimately inspected using conventional NDT methods to establish the size, orientation and location of the source defect.

A comparison of the performance of the 2219 and the 2014 pressure vessels indicated that the 2219 alloy was much superior to the 2014 alloy both at room temperature and −320°F. At both temperatures, the 2219 chambers burst at hoop stresses approximating the uniaxial ultimate strength level; whereas, at cryogenic temperature the 2014 alloy burst at a hoop stress significantly below the ultimate strength. The poor performance of the 2014 alloy may have been at least in part the result of 2014 welding problems which required extensive weld repair to remove weld porosity and cracking in the 2014 material. However, from an acoustic-emission-monitoring standpoint, i.e., the ability to detect and locate flaw propagation, there appeared to be no difference between the two alloys.

III. TEST PROCEDURE

A. MATERIALS

The aluminum alloys evaluated during this program included 2014-T651, 2219-T87 and 7075-T73. The nominal chemical compositions of these materials are shown in Table I. The 7075-T73 alloy was procurred from a commercial source (Reynolds Metals Co.) while the 2014 and 2219 alloys were supplied by NASA-MSFC.

The parent metal ' sile and metallurgical properties are shown in Table II and Figures 1 through 3, respectively. Both the tensile and metallurgical properties are considered typical of the materials tested. The microstructures indicate varying degrees of residual cold working and also contain relatively large amounts of non-metallic inclusions. The microstructures shown in Figures 1 through 3 are representative of the materials employed to fabricate both the tensile specimens and the subscale pressure vessels.

Welding was performed using both 2319 and 4043 filler wires. The nominal compositions of these materials are shown in Table III. Both alloys were used in fabricating tensile specimens while the subscale pressure vessels were welded only with the 2319 alloy.

B. FABRICATION OF TEST SPECIMENS

1. Uniaxial Tensile Specimens

Table IV shows the test plan for the uniaxial tensile program. Various specimen configurations were employed as discussed in subsequent sections of this report.

TABLE I

NOMINAL CHEMICAL COMPOSITION OF ALUMINUM PLATE MATERIALS EVALUATED

Element	Alloy Type		
	2014	2219	7075
Silicon	0.50 – 1.2	0.20	0.50
Iron	1.0	0.30	0.7
Copper	3.9 – 5.0	5.8 – 6.8	1.2 – 2.0
Manganese	0.40 – 1.2	0.20 – 0.40	0.30
Magnesium	0.20 – 0.80	0.20	2.1 – 2.9
Chromium	0.10	–	0.18 – 0.40
Zinc	0.25	–	5.1 – 6.1
Titanium	0.15	0.02 – 0.10	0.20
Zirconium	–	0.10 – 0.25	–
Aluminum	Bal.	Bal.	Bal.

TABLE II

PARENT METAL TENSILE PROPERTIES[1] OF ALUMINUM ALLOYS

Alloy	Specimen No.		Ultimate Strength (ksi)	0.2% Offset Yield Strength (ksi)
2014-T6	4-12		70.5	62.6
	4-11		70.1	62.8
		Avg	70.3	62.7
2219-T87	19-2		68.3	56.4
	19-1		67.8	56.1
		Avg	68.1	56.3
7075-T73	73-1		73.8	67.0
	73-2		65.5	60.0
		Avg	69.7	63.5

(1) All specimens oriented parallel to the direction of plate rolling.

TABLE III

NOMINAL COMPOSITION OF ALUMINUM FILLER MATERIALS

Element	Alloy Type	
	2319	4043
Silicon	0.20	4.5 – 6.0
Iron	0.30	0.8
Copper	5.8 – 6.8	0.03
Manganese	0.20 – 0.40	0.05
Magnesium	0.20	0.05
Zinc	0.10	0.10
Titanium	0.10 – 0.20	0.20
Zirconium	0.10 – 0.25	–
Vanadium	0.05 – 0.15	–
Aluminum	Bal.	Bal.

TABLE IV

SUMMARY OF TEST SPECIMENS

Flaw	Specimen Thickness (in.)	Test Temp.	2014-T6 Parent	DC TIG Weld 4043 Filler	DC TIG Weld 2319 Filler	MIG Weld 4043 Filler	2219-T87 Parent	7075-T73 Parent
PTC*	0.180	75°F	X	X				
PTC	0.300	75°F	X	X	X	X	X	X
None	0.300	75°F	X	X	X	X	X	X
PTC	0.500	75°F	X	X				
PTC	0.180	-320°F	X	X				
PTC	0.300	-320°F	X	X	X	X	X	X
None	0.300	-320°F	X	X	X	X	X	X
PTC	0.500	-320°F	X	X				
PTC	0.300	-423°F	X	X				
None	0.300	-423°F	X	X				
SEN	0.300	75°F	X				X	X

- - -- - - - - - - - - - - - - - -

*Fatigue precracked part-through-crack tensile specimen.
**Fatigue precracked single-edge-notch-tensile specimen.

The parent metal specimens were obtained with the longitudinal axis oriented parallel to the plate rolling direction and tested in the as-received (-T73, -T87, or -T651) condition. Both 0.3 and 0.5-in. thick materials were supplied; 0.18-in. thick specimens were machined from the 0.3-in. thick material by removing stock equally from both sides of the plate. No surface preparation was required for the 0.3 and 0.5-in. thick specimens.

Table V shows the welding parameters used in fabricating the weld tensile specimens. Both tungsten-inert-gas (TIG) and metallic-inert-gas (MIG) welding processes were employed. Welding head oscillation (TIG welding process) was employed to make the second (filler) weld pass; all weldments were tested in the as-welded condition with the reinforcement removed prior to testing.

Figures 4 through 6 show typical weldment macrosections. The characteristics of these macrosections vary, depending on the number of welding passes, filler metal and weld process employed. All weldments were dye penetrant and X-ray inspected. No cracks were detected; however, scattered fine porosity was observed in most of the weldments produced. Some scattered large porosity was also observed in the TIG weldments in the 0.18-in. thick plate, although the larger porosity was not generally observed in the weldment areas from which the test specimens were obtained. The porosity detected through nondestructive inspection is evident in the macro-sections shown in Figures 4 through 6; in other respects, the macrostructure is considered typical for these materials and weld processes.

2. <u>Subscale Pressure Vessels</u>

Subscale pressure vessels were fabricated using both the 2014 and 2219 aluminum alloys. The vessel configuration is shown in Figure 7 while Table VI schematically shows the fabrication sequence employed for

TABLE V

TYPICAL WELDING PARAMETERS USED IN PREPARING
TENSILE SPECIMEN WELDMENTS

Weld Process	DC-TIG				MIG
Nominal Thickness, (in.)	0.18	0.312*	0.312*	0.5*	0.312
Filler Metal	4043	4043	2319	4043	4043
Joint Design	Butt	Single "V"	Single "V"	Double "V"	Single "V"
Included Angle	–	60°	60°	60°	60°
Root Land, (in.)	–	0.050/0.060	0.050/0.060	0.050/0.060	0.050/0.060
Amps	165	170	170	240	120
Volts	9.5	9.5/9.7	9.5/9.7	9.5	32
Head Travel Speed (in./min)	8	8	8	5	10
Wire Feed (in./min)	12.5	40/60	40/60	70	215
Wire dia, (in.)	1/16	1/16	1/16	1/16	1/16
Gas (cfm)	50	50	50	50	50
Helium	95%	95%	95%	95%	95%
Argon	5%	5%	5%	5%	5%

*Weld Head Oscillator used on 2nd weld pass of 0.3-in. thick and both passes on 0.5-in. thick material.

	HEADS		CYLINDER	
	2014 A1	2219 A1	2014 A1	2219 A1
	T451 CONDITION	T-37 CONDITION	T-651 CONDITION	T-37 CONDITION

HEADS

2014 A1 — T451 CONDITION
- Shear Spin
- Age to T651 Condition (10 hrs at 340°F)
- Machine Outer Diameter
- Prepare Girth Weld (Single "V", 30° v bevel – 0.06 in. land)
- Drill and Tap ANPT Fitting (3/4 in. – 14)

2219 A1 — T-37 CONDITION
- Shear Spin
- Age to T87 Condition (24 hrs at 325°F)
- Machine Outer Diameter
- Prepare Girth Weld (Single "V", 30° beve – 0.06 in. land)
- Drill and Tap ANPT Fitting (3/4 in. – 14)

CYLINDER

2014 A1 — T-651 CONDITION
- Roll Form
- Prepare Long. Weld (Single "V", 30° bevel – 0.06 in. land)
- Prepare Girth Weld (Single "V", 30° bevel – 0.06 in. land)
- Weld Longitudinal Joint (TIG–2319 Filler Wire)
- Inspect (X-Ray Dye Penetrant)
- Trim Length
- Prepare Girth Weld (Single "V", 30° bevel – 0.06 in. land)

2219 A1 — T-37 CONDITION
- Roll Form
- Prepare Long. Weld (Single "V", 30° bevel – 0.06 in. land)
- Prepare Girth Weld (Single "V", 30° bevel – 0.06 in. land)
- Age to T87 Condition (24 hrs at 325 °F)
- Weld Longitudinal Joint (TIG – 2319 Wire)
- Inspect (Dye Penetrant, X-Ray)
- Trim Length
- Prepare Girth Weld (Single "V", 30° bevel – 0.06 in. land)

- Weld Girth Joints TIG – 2319 Wire)
- Inspect Girth Welds (X Ray, Dye Penetrant)

Table VI. Fabrication Sequence Used in Processing the Subscale Pressure Vessels

18

each material. Both aluminum alloys were TIG welded using 2319 filler wire. The cylinder-section longitudinal weld was produced using head oscillation (2nd filler pass) while the girth welds were not. The welding parameters are shown in Table VII (0.3 in. thick plate and 2319 filler wire). All chambers were tested in the as-welded condition; the weld reinforcement was not removed.

As indicated in Table VI, all vessel welds (both girth and longitudinal) were dye penetrant and X-ray inspected. In general, the 2219 vessels required minimal repair and usually only for removal of scattered porosity. Conversely, the 2014 alloy vessels required extensive weld repair for removal of excessive porosity, non-metallic or tungsten inclusions and cracks. Most of the defects, including all of the cracks, were removed during repair of the 2014 vessels. However, as indicated in subsequent sections of this report, some porosity and tungsten inclusions were not removed and were found to be sources of SWE; tungsten inclusions remaining in the longitudinal weld of the 2014 vessel tested at room temperature were found to be the origin of failure.

C. TEST SPECIMENS AND FRACTURE TESTING

1. Specimen Configuration and Test Procedure

Smooth (unflawed) and part-through-crack tension specimens were tested of each alloy. The part-through-crack (PTC) tension specimen was originally developed for the purpose of simulating flaws of the type frequently encountered in service. PTC-tension specimens are sometimes used to obtain information on the effects of realistic flaws in terms of fracture strength versus crack depth or area; the test also is used to obtain plane-strain fracture-toughness data (K_{Ic}). Figures 8 and 9 show the specimen designs used. The PTC tests were performed in two major series. Initially, transverse weld tensile specimens (Figure 8) were tested followed by a second series of specimens incorporating a longitudinal weld (Figure 9).

19

TABLE VII

TYPICAL WELDING PARAMETERS
USED IN WELDING SUBSCALE PRESSURE VESSELS

Weld Process	TIG[*]
Nominal Thickness	0.312 in.
Filler Metal	2319
Joint Design	Single "V"
Included Angle	60°
Root Land	0.060 in.
Amps	175
Volts	9.5
Head Travel Speed	8 in./min.
Wire Feed	50-65 in./min.
Wire Dia.	1/16 in.
Gas	50 cfm
Helium	75
Argon	25

---

*Weld Head Oscillator used on 2nd weld pass of vessel longitudinal weld.

This procedure was employed to evaluate effects of high localized strain (transverse weld) vs lower fracture strain (longitudinally welded) on the stress-wave-emission weld-fracture characteristics. Note that two specimen sizes were used in cryogenic testing; at −423°F, because of cryostat space limitations, a smaller specimen was tested (1.5-in. gage width by 11-in. long).

Two loading systems were used in the program: (1) a Baldwin-Tate-Emery 60,000-lb hydraulic testing machine and (2) a 50,000-lb Research Incorporated Material Test System. Initially, the specimens were instrumented with two post-yield strain gages. If there had been specimen misalignment in the tensile machine, the output of the two gages on an X-Y recorder would have shown bending. When it was confirmed that there was no significant bending, a single axial strain gage was used in the remainder of the program.

The initial tests of unflawed specimens produced a high rate of stress-wave emission at very low load. Figure 10 is a plot of both stress versus strain as measured by an axial electric-resistance strain gage, and acoustic-emission count rate versus strain. Note the high initial stress-wave count rate followed by a short period of relative inactivity and then a rising count rate just before failure. Experimentation showed that the high initial SWE counts were due to deformation at the specimen pin holes and if the pin holes were preloaded in compression in the manner shown in Figure 11, the initially high count rate was substantially reduced or eliminated. All of the subsequent tension specimens were preloaded in this manner. Note that with this type of preloading, the precracked section was unstrained in the preloading operation.

2. Fracture Mechanics Considerations

Fracture testing was done with a PTC-tension specimen. The PTC surface flaws were started from an electric-discharge-machined slot in one surface of the test specimen. The slots were then extended by tension-tension bending fatigue in a Burke milling machine converted for this use.

The specimen was loaded as a cantilever beam. By use of different initial slot configurations and sizes, different flaw shapes (a/2c) and sizes were produced for testing. Although the PTC-tension specimen is not recommended by ASTM Committee E-24, it is used by many investigators for determining K_{Ic}.

The plane-strain value of fracture toughness is generally considered a more fundamental unit of fracture toughness than the plane-stress value because, within certain limits of crack and specimen size, it is independent of specimen dimensions. Furthermore, plane-strain fracture toughness is concerned with the most dangerous type of flaw; viz, a flaw which initiates catastrophic fracture before growing through the thickness. With such a flaw, both initial growth and instability are controlled by the plane-strain fracture toughness, K_{Ic}.

The expression used for calculating the plane-strain fracture toughness value was:

$$K_{Ic} = FG(1.21\pi A0)^{1/2}/\phi$$

where FG = gross stress and ϕ is the commonly tabulated elliptic integral

$$\int_{o}^{\pi/2} (1 - k^2 \sin^2\theta)^{1/2} \, d\theta$$

where $k = 1-(A0/C)^2$, and C and A0 are one half the major and minor axes, respectively, of an ellipse. With a plastic-zone correction, the equation becomes

$$K_{Ic} = FG(1.21\pi A0)^{1/2}/[\phi^2 - 0.212 \, (FG/FTY)^2]^{1/2}$$

where FTY is the 0.2 percent offset yield strength.

If the elliptic-integral function and plastic-zone correction are represented by Q, the equation becomes

$$K_{Ic}^2 = 1.21\pi A0 \cdot FG^2/Q \qquad \text{(Eq 1)}$$

Figure 12 is a plot of the flaw shape parameter Q as a function of flaw depth-to-length ratios (A0/2C) for various fracture stress levels.

The criteria used for assessing the validity of the K_{Ic} measurements were as follows: (a) gross failure stress should not exceed the yield strength (FG/FTY < 1) and (b) the crack depth should not exceed 50% of the specimen thickness (A0/B $\leq$ 0.5).

Paris and Sih* have an approximate solution for a semi-elliptical surface crack. This approximation gives the stress intensity

$$K_{Ic}^2 = \left[1 + 0.12(1-A0/C)\right] \frac{FG(\pi A0)^{1/2}}{\phi} \left[\frac{2B}{\pi A0} \; \text{TAN} \; \frac{\pi A0}{2B}\right]^{1/2} \qquad \text{(Eq 2)}$$

at the end of the semi-minor axis (A0). Paris and Sih estimate the accuracy of the above equation to be within about $\pm 5\%$ for A0/2C from 0.5 to 0.05 and for A0/B from zero to 0.5. For A0/B up to about 0.75, the accuracy is still probably better than $\pm 10\%$.

In using the solution of Paris and Sih, if the crack-tip plastic-zone subtends a major portion (say half) of the distance between the crack front and the back of the test specimen, the use of the equation is doubtful. In this connection, it should be noted that the crack-tip plastic-zone extends much further ahead of the crack as it approaches the back surface than it does near midthickness; the free-surface effect extends into the thickness of the specimen for a distance which is proportional to $(K_{Ic}/FTY)^2$.

---

*Paris, P. C. and Sih, G. C., "Stress Analysis of Cracks" ASTM Special Technical Publication (STP) 381, pp.30-33, April 1965.

Thus, when the thickness and/or the crack depth is less than some critical value that is proportional to $(K_{Ic}/FTY)^2$, the constraint-relieving influence of the free surfaces will result in fictitious K_{Ic} measurements. On the basis of these observations, Brown and Srawley have suggested another criterion for valid K_{Ic} measurements, viz, that the crack depth should exceed $2.5\ (K_{Ic}/FTY)^2$ in., where FTY is the 0.2% offset yield strength.

Figure 13 compares the Irwin and Paris approximations; for all practical purposes the two gave the same value of K_{Ic}. In this study, the thickness of the material under test was sometimes less than 1.0 $(K_{Ic}/FTY)^2$ and almost always less than $2.5\ (K_{Ic}/FTY)^2$. For example, with a fracture toughness of the order of 30 ksi-in.$^{1/2}$ and a yield strength of 60 ksi at room temperature.

$$(K_{Ic}/FTY)^2 = 0.250\ \text{in.}$$
$$2.5\ (K_{Ic}/FTY)^2 = 0.625\ \text{in.}$$

and for a yield strength of 70 ksi at $-320°F$

$$(K_{Ic}/FTY)^2 = 0.184\ \text{in.}$$
$$2.5\ (K_{Ic}/FTY)^2 = 0.459\ \text{in.}$$

and for a yield strength of 80 ksi at $-423°F$

$$(K_{Ic}/FTY)^2 = 0.141\ \text{in.}$$
$$2.5\ (K_{Ic}/FTY)^2 = 0.352\ \text{in.}$$

Thus, according to the $2.5\ (K_{Ic}/FTY)^2$ criterion, few of the data are valid, and yet from Figure 14, it will be seen that the calculated values of K_{Ic} were remarkably constant when plotted as a function of (1) normalized crack depth, a/Q, (2) crack-depth-to-thickness, A0/B, ratio and (3) crack-depth-to length, A0/2C, ratio. Moreover, when the tests were invalidated by too deep a crack (A/B > 0.5) and/or when the gross stress exceeded the yield

strength (FG/FTY > 1.0), as shown in Figure 14, there was little or no difference between the valid and "invalid" test results.

3. Acoustic-Emission Instrumentation for Tension Testing

The basic instrumentation system used in Phase 1 of the investigation (transversely welded specimens) is shown schematically in Figure 15. The system consisted of (1) an Endevco piezoelectric accelerometer, (2) voltage amplification, (3) filtering, (4) an oscilloscope, (5) tape recorder, (6) electronic counter-printer, and (7) X-Y plotter. With this system, a real-time data display was obtained on both X-Y plotters and an oscilloscope, while all data were taped for record purposes. To compensate for the change in transducer sensitivity at the respective testing temperatures, the tape-recorded data were played back at a constant SWAT-system sensitivity (triggering level) for a given temperature of test, and for different temperatures of test, an adjustment was made in the playback triggering level.

In Phase 1 of the investigation (transversely welded test specimens), a Hewlett-Packard electronic-counter and strip-chart-printout system was used; whereas, in Phase 2 (longitudinally welded specimens) a Dunegan totalizer was used. In Phase 1, the gain was constant, and the trigger level was adjusted to the background noise. The gain for the system shown in Figure 15, then, was fixed at 100 db. In the Dunegan system, on the other hand, the trigger level was constant at 0.707 volt RMS (1 volt pk-to-pk) and the gain was adjusted so that the background noise was increased to the trigger level. In both phases, the basic-system gain was 100 db; with the Dunegan system, the set-point adjustment resulted in a gain variation of 100 db plus or minus 10 db. The Dunegan system was selected for the phase-2 investigation because of the convenience and efficiency of real-time recording on an X-Y plotter.

The method used during this program for developing the total number of stress-wave emissions (cumulative count) in reality produces a value weighted by SWE amplitude, specimen and sensor geometries. This method was used because of the complexity of a data-reduction system which produces one and only one count for each burst-type stress wave, as compared to the simplicity of counting each signal excursion above the noise level as an individual stress wave. Large-amplitude burst-type stress waves with typical sensor (and/or specimen) resonant decay provide many counts rather than just a single count. In other words, in general, the larger-amplitude burst-type stress wave with its longer ring-down time provides a larger number of SWE counts than does a smaller-amplitude burst-type stress wave. Primarily because of this fact, the cumulative-total count obtained in this program is weighted by the relative amplitude of the stress waves and is possibly more nearly a measure of the released energy than a measure of the number of burst-type stress-wave emissions.

Figures 16 and 17 and the following tabulation illustrate the effect of SWAT-system trigger-level setting on the plot of cumulative count versus load. Note that in the case of 7075-T73 parent metal tested at -320°F, the cumulative count increased markedly as the triggering level was set increasingly close to the background-noise level.

Specimen No.	Test Temperature, °F	Trigger Level, volts	Cumulative Count
73-3	-320	0.35	25,000
		0.26	52,500
		0.18	145,000

Likewise, in the case of 2014-T6 TIG welded with 4043 filler wire,

Specimen No.	Test Temperature, °F	Trigger Level, volts	Cumulative Count
PT43-10	-423	0.26	550,000
		0.07	1,115,000
-20	-423	0.26	420,000
		0.07	710,000
-30	-423	0.26	435,000
		0.07	820,000

the cumulative count increased markedly with decreasing triggering voltage. This is the result of the increased SWAT-system sensitivity provided by the lower triggering level and the progressively smaller amplitude of stress-wave emissions that are detected as the system sensitivity is increased.

D. HYDROTEST PROCEDURE AND INSTRUMENTATION FOR SUBSCALE PRESSURE VESSELS

1. Details of Hydrotest Procedure

The nominal hydrotest procedure which was employed in testing both at room temperature and cryogenic temperature is shown below; variations in this procedure, if employed, are indicated in discussions of the results obtained with each vessel.

1st Cycle – pressurized to 50% of FTY without a part-through-crack (PTC), held at maximum pressure for 30 seconds and then depressurized.

2nd Cycle – pressurized to 75% of FTY without a PTC, held at maximum pressure for 30 seconds and then depressurized.

3rd Cycle – pressurized to 90% of FTY without a PTC, held at maximum pressure for 30 seconds and then depressurized.

If the chamber did not fail during the above pressurizations, a PTC flaw was introduced and the three steps were repeated in the indicated order. If failure did not occur during the sixth pressurization, the chamber pressure was increased until failure occurred. The PTC type semi-elliptical defect was introduced in the center of the longitudinal weld using a 1-1/2-in. diameter x 0.020 in. thick grinding wheel. The longitudinal axis of the flaw was oriented parallel to the vessel longitudinal axis. Varying PTC lengths and depths were employed depending on the vessel being tested; the actual depth and length is indicated in discussion of each vessel tested.

The room-temperature tests were conducted using uninhibited water as the filler and gaseous nitrogen as the pressurizing media. The pressurized gas was obtained through a cumulator from several banks of gaseous nitrogen. Figure 18 shows the 2014-T6 aluminum pressure vessel prior to testing and is typical of the test set-up employed for both room and -320°F testing. A nominal pressurization rate of 100 psi/min was employed for the room temperature tests although this was also varied as indicated in subsequent discussions. A single strain gage (Type SR-4) was mounted in the parent metal area adjacent to the longitudinal weld at the center of each vessel tested at room temperature and was employed in conjunction with pressure gages to monitor and control both the pressure level and pressurization rate.

The cryogenic tests at -320°F were conducted using liquid nitrogen as the test media. The chambers were initially filled with fine sawdust in order to reduce the volume of liquid nitrogen required for chamber fill and thus reduce the energy release occurring upon chamber failure. Pressurization was accomplished using a cumulator of several banks of gaseous nitrogen. The vessels were mounted in the vertical position; rubber pads coated with silicone were used to prevent direct contact with the metal support structure and thereby eliminate possible sources of extraneous emissions due to relative motion between the vessel and retaining fixture.

28

A nominal pressurization rate of 50 psig/min was employed for the tests at -320°F. Strain gages were not mounted on the chambers for the cryogenic tests; the pressure level and pressurization rate was controlled by monitoring gages at the pressurization system cumulator. The overall test procedure for the -320°F tests was to fill the chamber with dry powder, then with the liquid nitrogen, and pressurize immediately (within five minutes) after the vessel was filled with liquid nitrogen. Successive refills with liquid nitrogen were required after each pressurization cycle. With this procedure, a vessel temperature of -320°F and minimum "boil off" was attained.

2. Acoustic Emission Instrumentation System for Pressure Vessel Testing

The ASPC-SWAT Mobile Laboratory shown in Figure 19 was used to monitor the pressure vessel hydrotest. Figure 20 shows a schematic diagram of the sixteen (16) channel Acoustic-Emission-monitoring system contained within the van. When a defect propagates in the monitored structure, the associated energy release is detected by the transducer mounted on the vessel. The detected energy pulse is converted to an electrical signal which is preamplified, amplified, filtered to remove extraneous background noise and then transmitted to the SWAT system for triangulation and display of the detected impulse. Figure 21 shows typical burst type stress wave data at two different sweep rates and indicates the type of data to which the SWAT system is tuned.

For the tests reported herein, the trigger level of the SWAT system was set to varying sensitivity levels depending on the background noise encountered. These signals were band-pass filtered (30 KHz - 60 KHz) with a gain of 60 dB.

The SWAT system computer is programmed to operate on the detected acoustic emission data. A main and a test subroutine triangulation program is employed.

The triangulation program (main program) for a test vehicle is written so that location of the acoustic-emission sources can be automatically furnished as data output. Through this system, various data handling techniques can be automatically accomplished and displayed in real-time so that decisions or actions may be taken. The computer, functioning as process control, also can be programmed to make decisions and react to any pre-established situation such as applications involving continuous surveillance of critical components.

The main program provides real-time triangulation to the acoustic-emission source. This program locates the individual sources on a video display as an X-Y coordinate on a background representing the test article in flat pattern. The main program also services the time clock and counters which show total counts for each sensor when it is the first sensor activated. These counts are transmitted to and tabulated by a teletype at programmable clock intervals determined by the operator.

The subroutine test program provides the necessary instructions to post the first four sensor numbers that are activated, the corresponding three delta-time differences in microseconds and the test time in hundredths of hours. This information is posted by the teletype in tenths of microseconds and is used during the test calibration and post-test set up procedure in conjunction with the acoustic-emission simulator. This program also can be used for monitoring small, simple test articles where only a tabular format is desired. A typical teletype record for the subroutine program is shown below:

1st Channel	2nd Channel	T_1	3rd Channel	T_2	T_3	4th Channel	Test Time
5	3	23	6	38	41	4	0.03

The numbers listed under the channel headings are the channel numbers identified in the order of acoustic-emission arrival. The numbers presented under T_1, T_2 and T_3 headings represent arrival time in microseconds between the 1st and 2nd channels, 1st and 3rd channels and 1st and 4th channels, respectively. Readout time per pulse is 7-1/2 sec.

Data display is accomplished by visual and graphical means in real time during the test; display time per pulse is in microseconds. The video display is on a television monitor which also shows the sensor locations on an overlay plan view of the test article. The sources of detected stress waves are posted on the screen of the monitor so that their location can be determined in relation to critical structure areas such as welds. Particular attention is paid to areas indicating multiple emissions from a single source since this can be indicative of subcritical flaw growth. Video tape records of the monitor display also are made for subsequent data analysis if required.

Analog records were made of the detected stress wave emissions for each of six channels used to monitor the pressure vessels during hydrotest. These records were made using a fourteen channel Sangamo 3500 tape recorder operating in a direct record mode. A seventh channel was used for tape synchronous control.

In addition, a Dunegan Research Corporation Totalizer system was used to plot the cumulative stress wave emission count vs pressure for each hydrotest cycle. The output from one channel, corresponding to one of the sensors mounted at the center of the cylindrical section, was monitored using the totalizer system.

3. SWAT Sensor Location and Attachment

The room temperature tests were monitored using Endevco Model 2213 accelerometers, while Endevco Model 2242 accelerometers were used for the tests at -320°F. The location of each of the sensors on

31

the pressure vessels are shown schematically in Figure 22. Figure 18 shows a vessel prior to hydrotest, while Figure 23 shows a sensor attached to the vessel; the strain gage attached to the vessels for room temperature testing is also shown. Figure 22 also represents the video display for the SWAT system since the computer was given coordinates which would place the sensors as shown on the display.

For the tests performed during this program, the sensor pattern was arranged around the cylindrical section longitudinal weld. Since the pressure vessels were tested in the as-welded condition, the weld area was significantly lower in strength than the base metal; a PTC type notch was also inserted in the longitudinal weld in the event failure did not occur during the initial pressurizing cycles.

In addition to the sensors, one pulser (test transducer) was located on the vessel. This unit provided a means of introducing an artificial stress wave into the test article to check the SWAT system operation both during set-up and while the vessel was under load. The location of the pulser is shown in Figure 22, while Figure 24 shows a closeup of the pulser attached to the vessel. The pulser location was varied during the test program.

The sensor and pulse attachment method is shown schematically in Figure 25. The pulser was attached through an isolation stud which was attached to the vessel using adhesive (dental cement). For the room temperature tests, the sensors were mechanically attached to individual mounting blocks which were held in place by wrap-around, expandable shock cords as shown in Figure 23. A light film of Dow Corning Silicone was applied between the chamber and aluminum block, and between the aluminum block and sensor to provide a continuous film contact. For tests at -320°F, the sensors were attached to the vessel using anodized aluminum studs (flange dimensions of 1/2" hex, dia, thickness 0.125", an overall length of 0.245"). The studs were individually bonded to the pressure vessel using a 7343 basin resin and the sensors mechanically attached to the mounting stud.

IV. TEST RESULTS

A. FRACTURE TOUGHNESS

1. Parent Metal

The fracture toughness values as obtained from the part-through-crack (PTC) tension tests are summarized in Table VIII. Note that a slight increase in toughness was indicated at cryogenic temperature. Note also that the second batch of 2014-T6 was somewhat tougher than the first batch supplied by NASA-MSFC for the contract.

It was noted that the fatigue precrack was interrupted by delimination-type cracking in some of the 7075-T6 and 2219-T87 specimens. The following data from specimens with and without delimination-type cracking show that the delamination-type flaws resulted in a higher apparent plane-strain fracture toughness than the flaw-free material.

Material	Test Temp.	Internal Flaws	K_{Ic} Toughness	
			Irwin	Paris
7075-T6	75	Delam.	33.9-39.5 Av(3) 37.5	30.0-38.8 Av(3) 34.8
	75	Clear	31.6	29.9
2219-T87	75	Delam.	33.7-33.8 Av(2) 33.8	32.2-34.7 Av(2) 33.4
	75	Clear	19.4	19.0
	-320	Delam.	42.3	43.1
	-320	Clear	32.6-36.0 Av(2) 34.3	30.4-34.7 Av(2) 32.6

2. Welded Plate

The fracture toughness values as obtained from the PTC-tension tests of welded plate are summarized in Table IX. Note that in the transversely welded specimens where the notch was wholly contained in the

TABLE VIII

SUMMARY OF PARENT-METAL APPARENT FRACTURE TOUGHNESS
PART-THROUGH-CRACK (PTC) TENSION TESTS

Alloy	Temp. (°F)	Thick. (in.)	Plane-Strain Toughness[a] (ksi-in.$^{1/2}$)	
			First Batch	Second Batch
2014-T6	75	0.17	26.5-28.2 Av(2)27.3	
		0.31	28.9-30.0 Av(3)29.6	34.4-34.5 Av(2)34.4
		0.47	26.9-35.1 Av(3)31.9	
	-320	0.17	28.1-30.8 Av(3)29.3	
		0.31	28.5-33.9 Av(3)31.2	38.2-38.3 Av(2)38.2
		0.47	29.8	
	-423	0.31	34.0-36.0 Av(2)35.0	
2219-T87	75	0.30	33.7-33.9 Av(2)33.8	33.0
	-320	0.30	32.6-42.3 Av(3)37.0	37.3-38.4 Av(2)37.8
7075-T73	75	0.30	31.6-39.5 Av(4)36.0	
	-320	0.30	39.1	

- - - - - - - - - - - - - - - - -

(a) First and Second Batch refer to different test series.

TABLE IX

SUMMARY OF WELD APPARENT FRACTURE TOUGHNESS
PART-THROUGH-CRACK (PTC) TENSION TESTS

Alloy	Temp. (°F)	Thick. (in.)	Plane-Strain Toughness (ksi-in.$^{1/2}$)	
			Transverse Weld	Longitudinal Weld
2014-T6 4043 wire TIG Welded	75	0.18	12.0-18.2 Av(3)14.2	
		0.30	16.1-18.0 Av(3)17.1	
		0.49	15.7-20.0 Av(2)17.8	
	-320	0.20	13.5-19.6 Av(2)16.5	
		0.31	12.5-20.6 Av(3)17.3	
		0.50	13.2-23.8 Av(3)20.0	
	-423	0.31	16.6-20.0 Av(3)18.5	
2014-T6 4043 Wire MIG Welded	75	0.31	12.1-17.0 Av(3)15.2	
	-320	0.31	15.7-20.8 Av(3)17.7	
2014-T6 2319 Wire TIG Welded	75	0.31	17.7-21.1 Av(3)19.9	30.3
	-320	0.31	18.8-23.1 Av(3)18.5	37.8
2319-T87 2319 Wire TIG Welded	75	0.34	-	32.4-32.7 Av(2)32.5
	-320	0.34	-	38.3-39.4 Av(2)38.8

deposited weld metal, the fracture toughness values were low and not signifi-
cantly different irrespective of parent metal, filler wire or welding process.
In the longitudinally welded PTC tension tests, the part-through-crack was
centered on the weld joint and extended into the heat-affected base metal on
either side of the joint. Note that the apparent fracture toughness as
determined in the longitudinally welded plate was approximately the same as
that of the parent metal.

B.   ACOUSTIC EMISSION

1.   Stress-Wave Emission as a Precursor of Failure

        Most of the materials testing done previously at Aerojet
using SWAT as a crack monitoring system has been at room or elevated tempera-
ture. One observation common to all the earlier studies, regardless of the
material investigated, is that the stress-wave-emission signals have char-
acteristics which serve to identify plane-strain instability and presage
plane-stress instability. The characteristics which have been found to
serve as a precursor of failure are (1) a marked increase of the amplitude of
the signals as observed in real time on an oscilloscope, (2) a marked increase
in the signal repetition rate (count per second) and (3) a marked increase in
the slope of the cumulative count-versus-load plot. These characteristics
were first identified at Aerojet in a study for the Office of Naval
Research[19] However, the characteristics were observed to be dependent
upon material toughness.

        In highly tough HY-80, HY-150, D6aC (austenitized at 1750°F
and tempered at 1100°F), and 6A1-4V (aged at 1250°F) where there was no
detectable pop-in by either crack-opening-displacement gage or stress-wave
emission, the failure process was identified by an increasing stress-wave
count, starting at approximately the load corresponding to deviation from
linearity in the crack-opening-displacement chart. In the more brittle D6aC

steel (austenitized at 1750°F and tempered at 600°F) and 7075-T6 aluminum, plane-strain instability was identified by an order-of-magnitude increase in stress-wave amplitude and the final failure process was identified by an increasing stress-wave count, generally starting at approximately the plane-strain pop-in. In the extreme embrittlement of D6aC austenitized at 1550°F, fracture occurred directly from the plane-strain pop-in with only two or three stress waves before the final unstable burst of crack growth.

In the ONR study, the plane-strain (K_{Ic}) instability was identified by acoustic emission but the acoustic emission monitoring system used did not have sufficient amplification and/or sensitivity to detect a precursor for the K_{Ic} instability. However, in a recent study for the Advanced Research Projects Agency[28], an improved acoustic-emission detection system demonstrated that acoustic emission can also provide warning of the plane-strain (K_{Ic}) instability. This study and the Navy study were based on room-temperature testing.

Figure 26 illustrates the precursor in a part-through-crack (PTC) tension test of 2014-T6 at room temperature. The results at cryogenic temperature and other factors affecting the precursor are discussed in subsequent sections of this report.

a. Precursor in Room Temperature Testing

In this investigation, the effect of trigger level on the precursor was investigated. It was found that the trigger level used in counting the stress-wave emissions had a marked effect on the precursor. For example, in Figure 27 the data from 2014-T6 specimen 8-8, tested at 73°F, were played back at trigger levels of 0.059, 0.070, 0.090 and 0.12 volt. Note that at the highest trigger level, the precursor occurred just before fracture; whereas, at the lowest trigger level, the precursor appeared to occur at about 25% of the failure load. In Figure 28, it will be seen that at an 0.15-volt trigger level 2219-T87 specimen 19-7 showed no precursor

whatsoever; whereas, at an 0.07-volt trigger level there was an unmistakable precursor. Because the choice of trigger level is arbitrary, selection of a quantitative value of load corresponding to the onset of crack instability does not appear to be meaningful.

The effect of trigger level on the precursor is best understood by a consideration of the background "noise" level. If the background noise increases (band widens) as the load is increased, the stress-wave count could be affected if, at the start of the test, the triggering voltage is set just above the background "noise" level. Comparisons between the background "noise" band widths at the start of loading and near fracture are presented in Figures 29, 30, and 31. At room temperature, the background "noise" band at the start of loading was relatively narrow; while near fracture, the band was relatively wide. At cryogenic temperatures, where plastic deformation would be minimized, the width of the band was essentially the same near fracture as at the start of loading. This suggests that the broadened band near fracture in the 75°F tests was the result of plastic-zone formation. In Figures 29 through 31, no attempt was made to photograph burst-type stress waves; when they appeared in the photographs, it was by chance. Figure 32 schematically shows the effect of background "noise" at three triggering levels for room-temperature tests. To simplify the illustration, no burst-type stress waves are shown until failure. As the load is increased, the net section yielding and the plastic zone at the crack tip increases and, consequently, the continuous emission increases (see Figures 29 and 30, 75°F PTC tests). At a low-voltage trigger level, the background "noise" increases to trigger-level one at a relatively low load, producing an anomalously low precursor. At trigger-level three, the specimen is practically at the failure load before the background "noise" has increased to the trigger voltage, giving little or no precursor (see Figure 27 for actual test data).

b. Precursor at Cryogenic Temperatures

Examination of the cumulative count versus load curves for cryogenic-temperature tests indicated that the precursor of failure is likely to be very short at cryogenic temperatures, often less than 1 sec. In Figure 17, for example, there was a sharp upward turn in the curves just before failure, but the warning time was very short.

Figure 33 schematically shows the effect of trigger level at cryogenic temperature (-320°F). At cryogenic temperature there was little or no increase in the background-noise band (see Figures 29 through 31). However, at cryogenic temperature there were many stress waves starting almost immediately on applying load, including a large number of small stress waves interspersed with much larger amplitude stress waves. The latter, because of the ring-down characteristic of the signal, were counted as several stress waves rather than one. Effectively, then, the electronic counter produced an integration of the size and number of stress waves. At a low-voltage trigger setting (level 1), the small stress waves, as well as the large, were counted, producing a rapid increase in cumulative count at a low load. At trigger-level three, on the other hand, the small stress waves were not counted and the count-versus-load plot tended to look more like the room-temperature precursor curves (see Figure 34 for actual test data).

Figure 35 was obtained from a -320°F cryogenic test of 7039-T61 aluminum using a WOL configuration (B = 1.00 in. and W = 2.00 in.). The instrumentation used in this test for NERVA was comparable to that used in the NASA-Huntsville study. The specimen gave over 220,000 counts before it failed, and the plot provided a more or less typical precursor to failure. However, it is apparent that the counter triggering level affected the nature of and the ability to detect the precursor. Figure 36 is a comparison between the curves presented in Figures 16 and 35 (comparable SWAT systems) indicating a difference in the results obtained from the PTC tests of 7075-T6 and the

WOL tests of 7039-T61. Whether this difference at essentially constant trigger level is attributable to differences in the alloys or in the specimen configurations is not known.

Several factors are believed to affect the precursor in cryogenic testing including, in addition to trigger level, the noise produced by ice cracking and the low sensitivity of the transducer used in cryogenic testing. These factors are evaluated in subsequent sections of this report.

2. Effect of Delamination

The following data were obtained from 7075-T73 parent metal PTC-tension specimens tested at room temperature with and without delamination flaws in the fracture surfaces.

Material	Specimen	Delam.	Crack (in.) AO	Crack (in.) 2C	Trigger Level (volts)	Cumulative Count x 10^3
7075-T73	73-6	Yes	0.084	0.382	0.32	3,310
	73-7	Yes	0.105	0.382	0.32	3,330
	73-10	No	0.110	0.380	0.07	212
2219-T87	19-7	Yes	0.126	0.398	0.07	55

Figure 37 shows the 7075-T73 fracture surfaces with the delamination-type cracking. Note that the delamination caused an order-of-magnitude higher acoustic emission count. Delamination observed in the 2219-T87 specimens, on the other hand, did not generate a high count.

3. Procedural Variables

a. Effect of Tape Playback

In the course of the investigation, there were a number of occasions when tape-recorded data were played back for purposes of evaluating the effect of trigger level or adjusting the trigger level to compensate for loss of transducer sensitivity at cryogenic temperature.

In tape playback, even using an instrumentation-type tape recorder with high frequency response, there is a considerable loss of data, as will be seen from Figure 38. Figure 38a is an X-Y plot of cumulative stress-wave count versus load for 2219-T87 Specimen No. 32 as recorded in real time during the cryogenic test at 10^6 full scale. Figure 38b for the same test was obtained by tape playback at 10^5 full scale. From a comparison of the two jumps, one at 47.5 kips and another at 50.7 kips (failure load), and the indicated cumulative total count in the two plots, it will be seen that the loss of stress wave data can be very significant.

	Stress Wave Emission			
	Event Count		Cumulative Total	
Load (kips)	Real Time	Play Back	Real Time	Play Back
47.5	10,000	1,300	42,000	6,600
50.7	45,000	9,000	110,000	23,700

Likewise, the real-time plot of RMS voltage versus load when compared with the playback plot shows the same loss of precursor data (Figures 39a and 39b). The reason for the discrepancy is that the minimum signal the tape recorder will record and play back is 150 mv whereas the noise level for these tests was on the order of 30 mv meaning that tape playback does not include data between 30 and 150 mv. The limited frequency response of the tape recorder (300 KHz) may also be a factor.

41

b. Effect of Filter Level

Band-pass filtering has long been recognized as an essential part of any acoustical-emission detection system. Variations in machine or environmental noise from day to day sometimes necessitates changes in the filtering level; however, an attempt is made to minimize such changes because of the effect of filter level on the cumulative count. Consider, for example, the following data for unnotched, 2219-T87 longitudinally welded, tension specimens No. 27 and 28, and also 2219-T87, longitudinally welded, PTC-tension specimens No. 29 and 30.

Specimen No.	Test Temperature (°F)	High-Pass Filter KHz	Trigger Level (set Point)	Cumulative SWE Count
27	75	90 + 90	8.5	0.13×10^6
28	75	40 + 40	5.0	2.02×10^6
29	75	90 + 90	8.0	0.08×10^6
30	75	40 + 40	5.0	1.18×10^6

As seen from these data, reducing the filter level from 90 KHz to 40 KHz increased the cumulative count by an order of magnitude. The difference in set point was an adjustment in signal gain in the Dunegan system, and not a change in trigger level. In the Dunegan system, the trigger level is fixed at 0.707 volt. When filtering at 40 KHz, more background noise was detected and therefore less gain was required to bring the signal up to a level just under the 0.707-volt trigger level. Figure 40 schematically illustrates this condition. With the quieter system provided by 90 KHz filtering, a higher set point (gain) was required to bring the signal up to a level just under the 0.707-volt trigger level.

4. Kaiser Effect in Welded Aluminum

    Figure 41 is a comparison of data from longitudinally welded, unnotched, tension specimens 22, 27 and 28 which indicates an increase in stress-wave activity in the range of 5 to 10 kips load. When the specimens were loaded for a second time, the activity in this range completely disappeared. This behavior is consistent with the Kaiser effect.

    Joseph Kaiser in Germany in 1950 was the first not only to use electronic instrumentation to listen to the subaudible sounds produced by the deformation of metals but also to observe that acoustic emission activity is irreversible. In other words, acoustic emission is not generated during the reloading of a material until the stress level exceeds its previous high. This irreversible phenomenon is now known as the "Kaiser effect".

    One of the specimens (No. 27) shown in Figure 41 was subjected to a third load cycle. For the third cycle, a Model 2213 accelerometer was spring mounted on the specimen. The data were filtered at a band width of 60 KHz to 600 KHz with approximately the same gain as in the previous cycles, viz., 100 db. The following tabulation of stress-wave-count data illustrates the marked drop in count in each successive cycle at a given load and the marked increase in count just before failure in the 3rd cycle (the precursor of fracture).

Specimen	Cycle	Date	Load	Count	Max. Load	Total Count
27	1	11-3-70	36.85	134,000[a]	36.85	134,000[a]
	2	11-3-70	36.85	3,200[b]	38.30	3,500[b]
	3	9-29-71	36.85	730	40.65	610,000[c]

(a) High count resulting from the peak in stress-wave activity at 10 kips
(b) Kaiser effect
(c) Precursor

43

Figure 42 shows the precursor as seen in the 3rd cycle; the specimen fractured at 40.65 kips. Note the Kaiser effect in that the stress-wave activity began at about 38 kips, the maximum load of the 2nd cycle.

The fact that welded specimens showed increased stress-wave activity at about 10 kips whereas unwelded (parent-metal) specimens did not, suggests that the activity at low load could be the relieving of residual welding stresses. Figure 43 is a comparison of welded and unwelded, unnotched, room-temperature tests. Note that the parent-metal specimen showed virtually no stress-wave activity until there was a tooling problem, at which time the specimen was unloaded, the situation corrected and then reloaded.

A comparison of data from PTC specimens 21, 29 and 30 also indicated an increase in stress-wave activity in the range of 5 to 10 kips load. These are part-through-crack (PTC), longitudinally welded, tension specimens of 2014 and 2219 aluminum. From Figure 44 note that when the filter level was reduced from 90 KHz to 40 KHz, the evidence of activity at 10 kips was markedly increased, and when the specimen was loaded a second time, the activity completely disappeared. This behavior is consistent both with the Kaiser effect and with what would be expected if the first load cycle had produced a stress relief.

5.   Effect of Flaw Size

In general, flaw size appeared to have little or no effect on the SWE cumulative count.

Material Wire	Specimen No.	Test Temperature, °F	Crack, in.		Trigger Level, volts	Cumulative Count
			AO	2C		
2014-T6	PT43-13	75	0.118	0.730	0.35	86,500
4043 Wire	-23	75	0.138	0.560	0.35	50,500
TIG	-33	75	0.165	1.090	0.35	68,500
2014-T6	PT43-11	75	0.091	0.290	0.14	22,500
4043 Wire	-21	75	0.091	0.477	0.14	23,500
TIG	-31	75	0.064	1.500	0.14	30,500

The plots of cumulative count versus load corresponding to the tests in the above tabulation are presented in Figures 45 through 48.

Figures 49 and 50 and the following data illustrate a case where increasing crack size appeared to be attended by an increase in cumulative SWE count.

Material Wire	Specimen No.	Test Temperature, °F	Crack, in.		Trigger Level, volts	Cumulative Count
			AO	2C		
2014-T6	PT19-1	75	0.098	0.300	0.32	13,500
2319 Wire	-2	75	0.126	0.520	0.32	28,500
TIG Welded	-3	75	0.114	1.090	0.32	32,500

However, the difference in count was not great and may not be significant.

Comparisons of notched (PTC) and unnotched tension tests revealed a result that at first appeared to be anomalous. As indicated below some of the transversely welded specimens gave higher counts in the unnotched tests than in the PTC-tension tests. In subsequent tests of the longitudinally welded specimens, both parent metal and welded 2014-T6 specimens confirmed that the smooth, unflawed specimens generated larger counts than PTC-tension tests at both 75°F and -320°F.

Material	Specimen No.	Test Temperature (°F)	High Pass Filter (KHz)	(set point) Trigger Level	Cumulative SWE Count x 10^3
2014-T6 Parent Metal					
Unnotched	4	75	90 + 90	8.0	4000
	5	75	90 + 90	8.0	4600
	6	75	90 + 90	8.0	3000
PTC	1	75	180 + 180	3.0	22
	2	75	90 + 90	8.0	53

45

Material	Specimen No.	Test Temperature (°F)	High Pass Filter (KHz)	(set point) Trigger Level	Cumulative SWE Count x 10^3
2014-T6 Parent Metal (cont.)					
Unnotched	E	-320	60 + 60	7.5	120
	G	-320	60 + 60	7.0	180
	F	-320	60 + 60	6.0	360
PTC	8	-320	54 + 54	7.0	103
	9	-320	50 + 50	6.0	90
2014-T6 Welded with 2319 Wire					
Unnotched	22	75	90 + 90	8.0	1800
PTC	21	75	90 + 90	8.0	250
Unnotched	25	-320	60 + 60	3.8	720
	36	-320	54 + 54	8.0	350
PTC	26	-320	60 + 60	5.0	150

Likewise, both parent-metal and longitudinally welded 2219-T87 tests showed that the smooth, unflawed specimens generated either larger counts or about the same count as PTC-tension tests at both 75 and -320°F.

Material	Specimen No.	Test Temperature (°F)	High Pass Filter KHz	Level Trigger (set point)	Cumulative SWE Count x 10^3
2219-T87 Parent Metal					
Unnotched	12	75	90 + 90	8.0	1000
	13	75	90 + 90	8.0	1500
PTC	18	75	90 + 90	8.0	1
Unnotched	J	-320	60 + 60	4.0	70
	K	-320	60 + 60	1.1 + 20db	150
PTC	19	-320	60 + 60	9.2	100
	20	-320	60 + 60	3.5	170

Material	Specimen No.	Test Temperature (°F)	High Pass Filter KHz	Trigger Level (set point)	Cumulative SWE Count x 10³
2219-T87 Welded with 2319 Wire					
Unnotched	27	75	90 + 90	8.0	2200
	28	75	40 + 40	5.0	1200
PTC	29	75	90 + 90	8.0	800
	30	75	40 + 40	5.0	1200
Unnotched	32	-320	54 + 54	–	310
	33	-320	60 + 60	6.7	550
PTC	31	-320	54 + 54	7.0	200
	34	-320	54 + 54	7.0	150

The explanation for the high counts obtained with smooth (unnotched) tension specimens as compared with PTC-tension tests is the result of continuous emission occurring in the smooth specimens during the final stage of the failure process. Figure 51 illustrates this in unwelded 2014-T6 material. Note that at 37 kips, the smooth specimen had generated a count of only 3×10^3; the PTC failed at 36.9 kips with a count of 53×10^3. At 44 kips, the smooth-specimen count had increased to 130×10^3 with an unmistakable precursor of failure. Likewise, consider the case of welded specimens No. 21 and 22. At 33 kips, the smooth specimen No. 22 had generated a count of only 40×10^3; PTC specimen No. 21 failed at 32.8 kips with a count of 250×10^3. At failure (36.9 kips) the smooth-specimen count had increased to 1800×10^3.

A comparison of longitudinally welded PTC test No. 26 and smooth specimen No. 36 at -320°F showed the same trend as the room temperature tests. At 38 kips, the smooth specimen had generated a count of 33×10^3; the PTC specimen failed at 37.9 kips with a count of 150×10^3. At failure (42.3 kips) the smooth specimen count increased to 350×10^3.

6. Relationship Between Acoustic-Emission Count and Stress-Intensity Factor

Dunegan and Harris [31] previously showed a relationship between stress-intensity factor and acoustic-emission cumulative count in rising-load-to-failure tests of 7075-T6 aluminum. In Figure 52, note that data obtained from four initial crack lengths grouped into a single curve fitting the theoretical fourth-power curve. Unfortunately the plots of such data did not always conform to a fourth power curve; in another study, Dunegan and Harris reported the exponent to vary between the 6th and 8th power. Later, constant-load, stress-corrosion studies at Aerojet [14] indicated a direct proportionality between stress-intensity factor and cumulative stress-wave count in single-edge-notch tension specimens (Figure 53). It was hypothesized that the difference between the LRL and Aerojet test results could be the result of a difference in the monitoring system trigger level. At LRL the counter trigger level was set to include the continuous emission produced by plastic deformation; whereas, in most Aerojet studies, the trigger level was set above the continuous emission, focusing on the burst-type stress-wave emission associated with incremental crack growth. However, differences from test to test, even with a supposedly constant data-acquisition system, have been encountered and as yet not explained.

The importance of the relationship between stress intensity factor and acoustic emission lies in the possibility of estimating flaw sizes and failure load based on in-service, real-time, nondestructive inspection of a flawed structure utilizing acoustic emission. However, before this can be realized, much has to be learned about the variables affecting the count-versus-K relationship.

A limited number of tests was made during this program using a single-edge-notch (SEN) tension specimen to facilitate the calculation of stress-intensity factor as a function of increasing crack length as measured by crack-opening displacement.

With the SEN-tension specimen configuration, the 7075-T73 alloy generated a much higher stress-wave count than either of the other two alloys tested. Figure 54 is a plot of cumulative stress-wave count versus applied stress intensity as calculated from the measured load and crack-opening displacement for duplicate specimens. No explanation was found for the discrepancy between the curves. Table X presents the data from the duplicate 7075-T73 tests.

The data from the SEN-tension tests of the 2014-T651 and 2219-T87 alloys are shown in Tables XI and XII. Figure 55 is a plot of cumulative stress-wave count versus applied stress intensity for the same materials. The data from duplicate specimens of 2014-T651 alloy did not fall on a common curve at low load, but as the load and crack length (COD) approached the critical stress-intensity factor, tne data appeared to fall on a common curve. From Figure 55, note that the 2219-T87 alloy as compared with the 2014-T651 alloy generated a higher stress-wave count initially and at fracture. The critical stress intensity was approximately 48 ksi-in.$^{1/2}$ in the 2014-T651 alloy with a total stress-wave count to failure of 22,000, and 68 ksi-in.$^{1/2}$ in the 7075-T73 alloy with a total count to failure of 110,000 and 79 ksi-in.$^{1/2}$ in the 2219-T87 alloy with a total count to failure of 45,000. Thus, based on these data there did not appear to be correlation between toughness and cumulative count indicating other variables such as material type and condition are important factors in this relationship.

Figure 56 illustrates the excellent correlation that can be found between crack-opening-displacement (COD) measurements and acoustic-emission count rate. Note that at approximately the load at which there was both pop-in and deviation from linearity in the COD-load X-Y plot, there was a marked increase in the rate of stress-wave emission. The stress-intensity corresponding to the load at this point of instability was 25.7 ksi-in.$^{1/2}$.

TABLE X

SUMMARY OF STRESS-WAVE-EMISSION STRAIN-GAGE FRACTURE DATA
7075-T73 ALUMINUM ALLOY - 0.30-IN. THICK
Single-Edge-Notch Tensile

Specimen No.	Crack Length (in.)	Applied Load (lbs)	Applied Stress Intensity (ksi-in.$^{1/2}$)	Axial Strain (μ-in.)	Cumulative Stress Wave Emission Count
73-14	1.14	2,000	8.4	280	5,170
	1.12	3,000	12.3	425	7,975
	1.12	4,000	16.3	560	11,009
	1.11	5,000	20.2	695	13,078
	1.10	6,000	24.2	840	14,094
	1.11	7,000	28.3	990	14,958
	1.12	8,000 [a]	32.8	1145	18,985
	1.15	9,000	38.5	1310	27,087
	1.18	10,000	44.2	1470	38,430
	1.21	11,000	50.3	1650	51,725
	1.27	12,000	59.9	1850	79,501
	1.30	12,460 (Fail)	64.9	1960	112,750
73-15	1.04	2,000	7.6	230	6,353
	1.05	3,000	11.5	370	11,258
	1.06	4,000	15.4	505	18,510
	1.06	5,000	19.4	635	29,793
	1.06	6,000	23.1	775	37,838
	1.06	7,000	26.9	915	44,666
	1.06	8,000	30.9	1050	49,672
	1.07	9,000 [b]	35.1	1190	55,932
	1.12	10,000	42.0	1360	69,384
	1.15	11,000	47.5	1510	81,000
	1.18	12,000	54.4	1675	93,000
	1.23	13,000	62.5	1845	114,000
	1.30	13,680 (Fail)	72.1	2000	134,000

[a] COD pop-in occurred at 8 kips or 32.8 ksi-in.$^{1/2}$
[b] COD pop-in occurred at 9.3 kips or 37 ksi-in.$^{1/2}$

50

TABLE XI

SUMMARY OF STRESS WAVE EMISSION-STRAIN GAGE-FRACTURE DATA
2014-T651 ALUMINUM ALLOY – 0.30-in. THICK
Single-Edge- Notch Tensile

Specimen No.	Crack Length (in.)	Applied Load (lbs)	Applied Stress Intensity (ksi-in.$^{1/2}$)	Axial Strain (μ-in.)	Cumulative Stress Wave Emission Count
4-18	1.01	2,500	8.5	400	2,800
	1.01	5,000	16.9	840	2,561
	1.02	7,500	25.7	1320	7,570
	1.14	10,000	40.3	1920	17,055
	1.21	10,600 (Fail)	46.4	2120	22,500
4-19	1.08	1,000	3.7	15	1,071
	1.07	2,000	7.4	140	1,150
	1.07	3,000	11.0	275	1,361
	1.07	4,000	14.6	410	1,436
	1.07	5,000	18.4	540	1,546
	1.07	6,000[a]	22.2	670	1,702
	1.08	7,000	26.1	805	3,039
	1.13	8,000	31.7	965	7,398
	1.19	9,000	38.6	1130	12,787
	1.32	9,870 (Fail)	50.2	1360	28,762

- - - - - - - - - - - - - - - - - -

(a) COD pop-in occurred at 6.9 kips or 25.7 ksi-in.$^{1/2}$ (see Figure 56).

51

TABLE XII

SUMMARY OF STRESS WAVE EMISSION-STRAIN GAGE-FRACTURE DATA
2219-T87 ALUMINUM ALLOY – 0.30-IN. THICK
Single-Edge-Notch Tensile

Specimen No.	Crack Length (in.)	Applied Load (lbs)	Applied Stress Intensity (ksi-in.$^{1/2}$)	Axial Strain (μ-in.)	Cumulative Stress Wave Emission Count
19-15	1.11	2,000	3.2	235	8,429
	1.10	3,000	12.2	375	10,300
	1.09	4,000	16.0	515	13,145
	1.10	5,000	20.3	665	14,166
	1.10	6,000	24.4	815	14,600
	1.10	7,000	28.6	960	15,047
	1.12	8,000	33.4	1105	15,720
	1.15	9,000[a]	38.9	1260	16,759
	1.19	10,000	45.6	1420	17,245
	1.24	11,000	53.5	1605	17,822
	1.48	11,900 (Fail)	79.1	1880	45,000

- - - - - - - - - - - -

(a) COD deviation from linearity occurred at 9.5 kips or 41.5 ksi-in.$^{1/2}$

The value of K_{Ic} for 2014-T6 as determined by PTC-tension tests was

$$28.9 - 30.0$$

$$\text{Av(3)} \quad 29.6 \text{ ksi-in.}^{1/2}$$

A comparison between the apparent K_{Ic} value as determined from COD pop-in or deviation from linearity in the SEN-tension tests and the K_{Ic} values determined from PTC-tension tests is presented in the following room-temperature data summary:

Alloy	Plane-Strain Fracture Toughness	
	SEN-Tension	PTC-Tension
2014-T6	25.7	28.9 - 30.0
		Av(3) 29.6
2219-T87	31.0 - 33.9	33.7 - 33.9
	Av(2) 32.5	Av(2) 33.8
7075-T6	32.8 - 37.0	31.6 - 39.5
	Av(2) 34.9	Av(4) 36.0

Thus, the two tests provided essentially the same K_{Ic} values.

7. Effect of Test Temperature

The following data indicated a marked effect of test temperature on cumulative count in the 2014-T6 alloy.

Material Wire	Specimen No.	Test Temperature, °F	Crack, in. AO	2C	Trigger Level, volts	Cumulative Count
2014-T6	4-4	-320	0.125	0.290	0.25	200,000
Unwelded	4-8	-423	0.110	0.255	0.25	750,000

When an approximate correction was made for the loss of accelerometer sensitivity at -423°F, an even greater difference in cumulative count between -320 and -423°F was indicated.

Material Wire	Specimen No.	Test Temperature, °F	Crack, in. AO	2C	Trigger Level, volts	Cumulative Count
2014-T6	PT19-1	75	0.098	0.300	0.32	13,500
2319 Wire	-4	-320	0.095	0.300	0.32	85,000
	-4	-320	0.095	0.300	0.18 (a)	358,000
2014-T6	PT43-15	75	0.193	0.430	0.79	325
4043 Wire	-45	-320	0.185	0.450	0.18 (a)	77,500

(a) trigger level corrected to compensate for the loss of sensitivity at -320°F.

The curves and crack photographs for the above data are presented in Figures 57 through 60.

The high count recorded in the cryogenic tests was suspected to be the result of ice formation in the cryostat and on the tooling. To verify this observation, specimen I was subjected to a succession of loadings. Figure 61 is the plot of cumulative count (TSWE) versus load as produced on an X-Y recorder during loading; on this first cycle of loading at -320°F the load was dumped at 32.5 kips after recording 500,000 counts. After the 1st cycle, the LN_2 was removed from the cryostat. When the tooling had warmed to above 32°F, the specimen was replaced and LN_2 added preparatory to the

2nd cycle. Figure 62 is the plot of TSWE versus load for the 2nd cycle; the load was dumped at 51.0 kips. At 32.5 kips (the maximum load applied in the 1st cycle) the TSWE count was 850,000 as compared to 500,000 in the 1st cycle. The cryostat was then redesigned, removing all insulation from the inner diameter surface. After redesign and starting with a dry cryostat and dry tooling, the specimen was subjected to a 3rd cycle at -320°F (Figure 63a). At 32.5 kips, the count was only 55,000. At 56.3 kips the load was dumped, and immediately the specimen was reloaded to failure at 57.7 kips (Figure 63b). In the 4th cycle (to failure) the count at 32.5 kips was an order of magnitude lower than in the 3rd cycle. Thus, in the 1st and 2nd cycles, the Kaiser effect was not observed because of ice on the cryostat and associated tooling; whereas, in the 3rd and 4th cycles, after taking precautions to eliminate ice formation, the Kaiser effect was observed.

The precursor of failure was not evident because of the scale factor (10^6) used in the X-Y recording. However when Figure 63b was replotted to 10^5 counts full scale, the precursor was evident (Figure 64).

In the cryogenic tests of transversely welded specimens, a Model 2242 accelerometer was mounted on the specimen, immersed in the cryogenic bath. During subsequent tests of longitudinally welded specimens, a Model 2213 accelerometer was mounted on a rod attached to the specimen and extending out of the cryostat. Using the latter procedure, the sensor temperature remained above -100°F which is the lowest temperature that can be employed without a significant loss in sensor sensitivity. Also with this procedure, the sensor was isolated from the cryogenic bubbling which had been a source of extraneous background noise.

In the following tabulations, from a comparison of data obtained at 75°F and at -320°F, it will be seen that there was little difference in the cumulative acoustic-emission count for either the notched or unnotched tests. In other words, the count for both notched and unnotched specimens was essentially the same at -320°F as it was at room temperature. Thus, with an improved cryostat design and care to avoid ice formation on the tooling, the large counts previously obtained in cryogenic testing were eliminated.

Material	Specimen No.	Test Temperature (°F)	High Pass Filter KHz	(Set Point) Trigger Level	Cumulative SWE Count
Unnotched 2014-T6	C	75	60 + 100	2.1*	0.15×10^6
	E	-320	60 + 60	7.5	0.19×10^6
	G	-320	60 + 60	7.0	0.18×10^6
	F	-320	60 + 60	6.0	0.36×10^6
PTC-Tension 2014-T6	2	75	90 + 90	8.0	0.065×10^6
	8	-320	54 + 54	7.0	0.085×10^6
	9	-320	50 + 50	6.0	0.090×10^6
Unnotched 2014-T6 (2319 Wire)	22	75	90 + 90	8.0	1.8×10^6
	25	-320	60 + 60	3.8	0.72×10^6
	36	-320	54 + 54	8.0	0.35×10^6
PTC-Tension 2014-T6 Welded (2319 Wire)	21	75	90 + 90	8.0	0.28×10^6
	26	-320	60 + 60	5.0	0.15×10^6
Unnotched 2219-T87	13	75	90 + 90	8.0	0.14×10^6
	H**	-320	60 + 60	6.0	0.29×10^6
	J	-320	60 + 60	4.0	0.07×10^6
	K	-320	60 + 60	1.1	0.15×10^6
	L**	-320	60 + 60	6.0	0.80×10^6
Unnotched 2219-T87 Welded (2319 Wire)	27	75	90 + 90	8.0	0.13×10^6
	32	-320	54 + 54	–	0.11×10^6
PTC-Tension 2219-T87 Welded (2319 Wire)	29	75	90 + 90	8.0	0.08×10^6
	31	-320	54 + 54	6.0	0.20×10^6
	34	-320	54 + 54	7.0	0.15×10^6

*Specimen C, like the other specimens in this tabulation, was tested with 100 db of gain. However, the data for specimen C were filtered at a band width of 60 KHz to 600 KHz and the totalizer was triggered at a set point of 2.1 (20 to 40 db range).

**Specimens F, H and L were tested before redesign of the cryostat; these specimens had the highest count of the cryogenically tested, parent-metal, unnotched specimens.

8. Effect of Transducer Sensitivity in Cryogenic Testing

In addition to the problem of icing in the tooling and cryo-
stat, there was also a problem with low sensitivity in the transducer used
for cryogenic testing. Both of these problems were suspected to have contri-
buted to the lack of precursor in a number of the cryogenic tests.

Consider the data in the following tabulation where the earlier
testing was done using a Model 2242 accelerometer spring mounted on the test
specimen, immersed in the cryogenic bath; and the later testing was done with
a Model 2213 accelerometer mounted on a rod, outside the cryogenic bath.

Material Wire	Specimen No.	Specimen Thickness, in.	Test Temperature, °F	Crack, in. AO	2C	Trigger Level, volts	Cumulative Count x 10^3
2014-T6	PT43-41	0.210	-320	0.055	0.244	0.3[a]	47
2043 Wire	-43	0.314	-320	0.122	0.406	0.3[a]	43
	45	0.496	-320	0.185	0.450	0.3[a]	23
2014-T6 Unwelded	8	0.319	-320	0.127	0.479	7[b]	100
2014-T6 2319 Wire	26	0.319	-320	0.151	0.514	5[b][c]	155

(a) transversely welded specimens tested in 1969.
(b) set point for Dunegan totalizer, tested in 1971.
(c) longitudinally welded specimen

The amplification (gain) used both in 1969 and in 1971 was approximately 100 db.
The sensitivity of the transducers, however, was appreciably different; viz.,
10 pk mV/pk g voltage sensitivity for the 2242 and 44 pk mV/pk g for the 2213
accelerometer. The sensitivity of the 2242 accelerometer is only slightly
affected by temperature down to and including -320°F. The 2213 mounted on
the end of a rod was operating at about +40°F and, therefore, also was unaffected
by the temperature of the bath.

The plots of acoustic-emission count versus load for the 1969 tests using the 2242 accelerometer are shown in Figure 65; the flaws are shown in Figure 66. Note that there was little or no precursor of failure. The acoustic-emission produced by crack growth in these tests was probably obscured by ice as well as the low sensitivity of the 2242 accelerometer.

The plots of acoustic-emission count versus load for the tests using the 2213 accelerometer mounted on a rod, outside the cryogenic bath are shown in Figure 67. Note that there was no longer a high count at low load, but a typical, gradual, stepped increase in count with increasing load. However, there was still no definite precursor of failure. The unwelded specimen showed a marked increase in count at failure but it occurred in only two bursts right at failure.

a.   Response of 2242 and 2213 Accelerometers

Specimen No. 27 was 2219-T87, longitudinally welded with 2319 wire, without a deliberate flaw. The specimen had two prior load cycles at room temperature, one to 36.85 kips and another to 38.30 kips. In the third loading at room temperature, a 2213 accelerometer was spring mounted on the test specimen. The data were filtered at a band width of 60 KHz to 600 KHz with 100 db of gain. The Dunegan totalizer was triggered at a set point of 2.0 (20 to 40 db range). Because of the prior loading to 38.3 kips, one would not expect a significant count before 38 kips (Kaiser Effect). There was in fact a count of about 700 up to 38 kips. Failure occurred at 40.65 kips. Between 38 and 40 kips, there was an unmistakable precursor, with an increase in count of 61,000 in this interval of load (see Figure 41).

Specimen C was 2014-T6 parent metal without a deliberate flaw, tested at 70°F. Two transducers were mounted on the test specimen; one was a Model 2242 accelerometer and the other was a Model 2213 accelerometer. The data were filtered at a band width of 60 KHz to 600 KHz with 100 db of gain.

58

The Dunegan totalizer was triggered at a set point of 2.1 (20-40 db range) for the 2213 accelerometer and 6.5 (0-20 db range) for the 2242 accelerometer. With these settings, the background noise associated with the 2242 accelerometer was just above the trigger level and the background noise associated with the 2213 was just below the trigger level.

The acoustic-emission data for Specimen C at intermediate load (25 to 35 kips) are shown in Figure 68a. At 10^5 full scale range, the 2242 showed a gradual increase in count as a result of its set point; whereas, the 2213 showed no count at all. When the range was changed to 10^4, the 2242 showed even more clearly the steady increase in count as the result of background noise, but no incremental increases until about 30 kips when there was a jump of 2600 counts recorded by the 2242 accelerometer and 3200 counts by the 2213 accelerometer. This was followed by several bursts of emission at about 32 kips; in these bursts the Model 2242 count increased by 8700 and the Model 2213 count increased by about 26,000. Thus, in the intermediate load range, the 2242 accelerometer failed to record some of the small bursts of activity, and when it did record, the count was smaller than that recorded by the 2213 accelerometer.

Figure 68b for Specimen C shows that the Model 2213 accelerometer started to detect continuous emission from plastic deformation in the test specimen at about 42 kips. From this load until the specimen was unloaded at 44 kips, the Model 2213 recorded an increase in count of 123,000; whereas, the Model 2242 recorded an increase of only 6,500. These data show that at loads near fracture where the precursor would be expected, the 2213 accelerometer gave larger counts for individual bursts and larger cumulative count than the 2242 accelerometer. Thus, it appears that in cryogenic testing with Model 2242 accelerometers, as conducted in the first phase of this study, the low sensitivity of the Model 2242 accelerometer could explain the lack of precursor in many of the tests. However, the lack of precursor in the second-phase testing remains to be explained.

59

In the next section where the effects of a wave guide will be discussed, it will be shown in PTC-tension specimen No. 3 that even with signal attenuation in the wave guide, the 2213 accelerometer recorded larger jumps than the spring-mounted 2242 accelerometer.

b.   Attenuation of Signal in the Wave Guide

Specimen No. 28 was 2219-T87, longitudinally welded with 2319 wire, without a deliberate flaw. The specimen had two prior loadings at room temperature, one to 32.5 kips and the second to 40.0 kips. In the third loading, two Model 2213 accelerometers were used, one mounted on the end of a wave guide and the other spring mounted on the test specimen. The wave guide consisted of a 1/2-in.-dia round of aluminum, stud mounted on the shank of the test specimen, with a bend to bring the end of the rod up out of the cryogenic bath. With this set-up the end of the rod where the sensor was mounted was about +40°F. The length of the wave guide was 20 inches.

The third loading of specimen No. 28 was done at room temperature. The data were filtered at a band width of 60 KHz to 600 KHz with 100 db of gain. The Dunegan totalizer was triggered at a set point of 1.0 (20 to 40 db range) for the 2213 accelerometer spring mounted on the test specimen and at a set point of 2.0 (20 to 40 db range) for the 2213 accelerometer mounted on the wave guide

Acoustic-emission data at approximately 10 kips are shown in Figure 69a. At 10^3 full-scale range, the spring-mounted 2213 accelerometer gave an average count in 19 bursts of 10 counts per burst as tabulated in Table XIII, whereas, the wave-guide mounted 2213 accelerometer gave an average count in 19 bursts of 4.5 counts per burst.

60

TABLE XIII

INCREASE IN COUNT

2213 ACCELEROMETER

BURST	SPRING MOUNTED	WAVE GUIDE
a (1)	9.5	7.0
b	–	1.0
c	7.0	9.2
d	9.5	8.6
e	.3	1.3
f	–	.5
g	2.0	–
h	.9	–
i	1.2	–
j	2.2	.7
k	6.5	2.2
l	12.2	7.0
m	15.3	8.8
n	11.5	7.5
o	39.5	18.0
p	–	.6
q	2.8	–
r	17.5	1.5
s	49.5	12.0

---

(1)See Figure 69a.

At 15 kips, the range was changed to 10^4 full scale. At this range, the wave-guide mounted accelerometer did not show any activity until somewhat over 40 kips, and the spring-mount accelerometer showed only one significant burst (200 counts) prior to 40 kips (Kaiser Effect).

At slightly over 40 kips, the spring-mounted accelerometer recorded several small bursts and the start of continuous emission (Figure 69b). The wave-guide mounted accelerometer did not record continuous emission and did not show the onset of fracture until just before failure (41.25 kips). Thus, there appears to have been signal attenuation in the wave guide.

Specimen 3 was 2014-T6, longitudinally welded with 2319 wire; the specimen contained a part-through-crack. Two transducers were used in the test, one a Model 2242 accelerometer spring mounted on the test specimen and the other a Model 2213 accelerometer mounted on the wave guide. The data were filtered at a band width of 60 KHz to 600 KHz with 100 db of gain. The Dunegan totalizer was triggered at a set point of 2.6 (20 to 40 db range) for the Model 2213 accelerometer on the wave guide and at a set point of 6.5 (0 to 20 db range) for the Model 2242 accelerometer spring mounted on the test specimen. With these settings both transducers were just inside the noise (continuous emission) band. Figure 70 shows the strip-chart recording of load versus cumulative count for the first cycle of loading. Note that even with the attenuation in the wave guide, the 2213 accelerometer recorded larger jumps than the 2242 accelerometer.

On the second load cycle to failure (at 33.45 kips) the low sensitivity of the spring-mounted 2242 accelerometer was apparent; in Figure 71, note the marked precursor from the 2213 accelerometer with a count of 330,000 as compared with only 42,000 from the 2242 accelerometer.

Note that 2219-T87 specimen No. 28 with the 2213 accelerometer mounted on a wave guide (Figure 69) gave little precursor, whereas, 2014-T6 specimen No. 3 also with the 2213 accelerometer mounted on a wave guide (Figure 71) gave an unmistakable precursor. No explanation was found for this difference; however, the comparison does involve two different alloys.

C. SUBSCALE PRESSURE VESSEL RESULTS

1. Room Temperature Test of 2014-T6 Aluminum Pressure Vessel

The following tabulation indicates the hydrotesting sequence used for the 2014 vessel tested at room temperature.

Cycle	Pressure (psi)	Pressure Rate (psi/min.)	Hold at Max. Load (sec)	Pre-Flaw
1	0-460	150	30	No
2	0-690	150	30	No
3	0-880	150	Failed on rising load at 886 psig	No

The failed chamber is shown in Figure 72, while Figure 73 shows close up views of the chamber fracture.

As indicated by the above data, the vessel burst at 880 psig during rising load after previous pressurizations to 460 and 690 psig. The fracture path was entirely within the cylinder longitudinal weld. Based on the nominal chamber wall thickness of 0.312-in., the stress level (Pr/t where P is the pressure, r is the chamber radius and t is the wall thickness) at failure approximated 24 ksi which is slightly below the 0.2% offset yield strength of 29 ksi previously determined for this base-metal filler-wire (2014-T6 - 2319) combination.

Figure 74 shows the pressure vs strain data obtained using a strain gage attached to the parent metal in the center section of the vessel; no plastic deformation was produced in this area during any of the pressure cycles.

Figure 75 is a plot of the cumulative stress wave emission vs pressure for the three hydrotest cycles. The data were obtained by monitoring the SWE detected by Sensor No. 3 located at the center of the cylindrical section. Note in Figure 75 that the Kaiser Effect was observed as indicated by the fact that significant SWE were not detected during the second or third pressurization cycle until the maximum prior pressure (460 psi and 690 psi, respectively) was exceeded. Although no SWE were detected at hold during the first pressure cycle (460 psi), SWE were observed during the first few seconds of hold (690 psi) in the second cycle. During the third cycle, significant bursts of SWE were detected above 690 psi and continued until vessel failure occurred at 880 psi. From the data in Figure 75, it is obvious that sufficient warning was obtained from these SWE data to permit depressurization and prevent failure of the vessel.

Figures 76 through 78 are plots showing the locations of the SWE detected during each pressurizing cycle; each plot is a reproduction of the SWE data as displayed on the SWAT system monitor in real-time during the test. In general, more randomly located SWE are observed during the first cycle and from different areas than the SWE observed during the second and third cycles. However, each of the plots show multiple emissions from two general areas of the vessel longitudinal weld toward the center of the cylindrical section. This is reflected by the increased size and darkening of the emission sources as shown on the monitor screen and in these plots. As indicated in Figure 78, the origin of failure corresponded to one of these multiple emission sources on the longitudinal weld.

Figure 79 schematically shows the location of defects observed on X-rays of the longitudinal weld prior to testing. Two areas of tungsten and/or non-metallic inclusions were observed in the X-rays and are located in the same areas from which the multiple emissions were detected by the SWAT system.

Figures 80 and 81 show the fracture face and defects observed on the fracture surface, respectively; both porosity and nonmetallic inclusions or lack of fusion are shown. The weld locations of the defects are schematically shown in Figure 78 and generally correspond to the weld locations of SWE detected during vessel pressurization.

In addition to fractographic examination of the fracture surfaces, ultrasonic and dye penetrant inspection techniques were used in an attempt to identify possible defects associated with the random emission sources shown in Figures 76 through 78; no defects were observed at any of these locations.

From the above discussion, it is apparent that the cumulative plot of the SWE provided a clear precursor of impending failure and through real time triangulation of the detected emissions, it was possible to locate the source of the emissions and subsequent failure origin. Such data could have been employed to terminate loading, locate the potential failure origin and repair the vessel.

2. Room Temperature Test of 2219-T87 Aluminum Pressure Vessel

The following tabulation indicates the significant test data for the 2219 pressure vessel tested at room temperature.

Cycle	Pressure Level (psi)	Pressure Rate (psi/min)	Hold (sec)	Pre-Flaw
1	0 – 300	75	30	No
2	0 – 400	75	30	No
3	0 – 400	200	30	No
4	0 – 400	75	30	Yes
5	0 – 500	75	30	Yes
6	0 – 680	100	–	Yes
7	0 – 860	100	–	Yes
8	0 – 600 600 – 1250	200 50	–	Yes
9	0 – 1400	100	–	Yes (Double)*
10	0 – 1500	100	–	Yes (Double)*
11	0 – 1530·(Failure)	100	–	Yes (Double)*

* A second PTC flaw (0.30-in. deep x 0.60-in. long) was added in the longitudinal weld between the eighth and ninth pressurizing cycles.

Figure 82 shows the failed chamber while Figure 83 shows a close-up view of the chamber fracture.

As indicated by the above tabulation, the vessel burst during the eleventh pressurizing cycle at 1530 psig after prior pressurizations to various levels as high as 1500 psig. Based on a nominal wall thickness of 0.35-in. (includes weld reinforcement), the stress level (Pr/t) at failure was approximated 37 ksi. Failure originated at a part-through-crack type flaw which was ground approximately 0.60-in. long and 0.10-in. deep in the longitudinal weld of the chamber after the third pressurizing cycle. Based on these results, the apparent K_{Ic} is 23 ksi-in.$^{1/2}$ (calculated using equation (1)).

Figure 84 shows the fracture face which was contained entirely within the longitudinal weld. No weld defects such as porosity or

lack of fusion or secondary failure origins were observed on the fracture surface. The PTC defect from which failure originated is shown in Figure 84 as is a second PTC defect introduced following the eighth pressurizing cycle.

Figure 85 shows the pressure vs strain plot for the final two pressurizing cycles and indicates elastic behavior in the parent metal cylindrical section where the strain gage was located (refer Figure 22).

Figure 86 shows plots of cumulative SWE vs pressure for the hydrotesting of the 2219-T87 vessel. The data were obtained by monitoring channel No. 4 in the center of the chamber (refer Figure 22). In addition to counts due to SWE, most of the plots show the count increases from the pulser signals generated throughout the test to check the SWAT system operation.

Figure 86a is a plot of cumulative SWE versus pressure for the first three cycles (unflawed condition). The Kaiser effect is apparent from the data for the second load cycle; the data for the third cycle (loaded to the same maximum pressure as obtained during the second cycle) shows that the Kaiser Effect is not dependent on loading rate within the ranges studied in that no significant SWE were detected when loading to the same pressure level at 200 psi/min vs prior loadings at a pressurization rate of 75 psi/min.

Figures 86b and 86c are plots of the cumulative SWE count vs pressure for cycles four through nine. Prior to the fourth loading cycle, one PTC (length 2c of 0.6-in. and depth of 0.10-in.) was introduced in the longitudinal weld (shown in Figure 84). Again, the Kaiser effect was evident in that a pressure greater than 400 psi was required before SWE were detected and each succeeding loading required a higher pressure before increased SWE activity was observed. No SWE were observed during any of the hold periods except for the fifth cycle when limited SWE activity was observed during the first five seconds of hold.

68

Figure 86d is a plot of the cumulative SWE count versus pressure for cycles 10 and 11. Prior to the ninth loading cycle, a second PTC (length, 2c, of 0.6-in. and depth, a, of 0.13-in.) was introduced in the longitudinal weld, as shown in Figure 84. Again the Kaiser Effect was observed.

From Figure 86, it is apparent that there were multiple precursors of failure providing sufficient time to terminate loading prior to failure. Note the relatively large SWE bursts detected during the sixth, seventh, tenth and eleventh cycles. The burst-type SWE detected at the end of the tenth cycle is of particular interest. These SWE must have been associated with extension and reorientation of the preflaw introduced in the longitudinal weld since, during the eleventh cycle, flaw extensions were detected from the PTC area of the chamber at lower pressures than 1500 psig. Apparently when fracture instability is approached, the Kaiser effect is no longer observed. Failure occurred during the eleventh cycle at 1530 psig which is only slightly higher than the maximum pressure reached during the prior cycle. In all these instances, sufficient warning of defect propagation was obtained to permit depressurization prior to failure.

Figures 87 through 94 show the location of the SWE detected during the indicated pressurization cycles. These schematics also show the locations of the cylinder section longitudinal weld and the two PTC flaws introduced into the weld after the third and eighth cycles. As indicated in Figures 87 and 88, only randomly located SWE were detected during the first pressurizations without a preflaw; no SWE activity was detected from the weld area. Following introduction of the first preflaw (Figure 89), only a few random SWE were detected when the vessel was pressurized to the prior maximum pressure (400 psig); during this cycle two SWE were detected from the preflaw region near maximum pressure. On subsequent loading to 500 psig (Figure 90) and 680 psig (Figure 91) multiple emissions were detected near maximum pressure from the region of the preflaw; random SWE were also detected although essentially no SWE activity was detected from the weld area except in the region of the preflaw. From Figures 90 and 91, it is apparent that a variation of approximately

69

2-in. exists in the SWE source triangulation since the SWE grouping for the preflaw in both instances is approximately 2- to 3-in. from the actual preflaw location.

Figure 92 shows that a large number of randomly located SWE were detected during the seventh pressurizing cycle (to 850 psig). The data in Figure 92 also shows a grouping of SWE from the region of the preflaw. Comparison with the cumulative SWE count in Figure 86b shows that these SWE were detected almost exclusively above the maximum pressure (680 psig) of the sixth cycle. Further, from Figure 92, it is apparent that a large number of random SWE sources were obtained during the seventh cycle which were primarily small amplitude emissions since no large jumps were observed in the corresponding cumulative SWE plot.

Figures 93 and 94 show that in comparison to previous cycles, relatively few and only randomly located SWE were detected during the last pressure cycles. Data are not shown for the ninth cycle to 1400 psig since no SWE sources were displayed on the SWAT system monitor during this cycle. No SWE were detected from the weld or PTC preflaw regions during pressurization to 1250 psi (eighth cycle). Figure 94 shows the SWE locations for both the tenth (1500 psi) and eleventh (failure at 1530 psi) pressurizations; while only a few SWE sources are shown, these represent large SWE as indicated by the SWE cumulative count plots in Figure 86d. The last SWE detected near failure originated from the region of the PTC preflaw although offset approximately 4-in. from the true location of the flaw.

Figure 95 schematically shows the longitudinal weld defects indicated by X-ray examination of the cylinder longitudinal weld prior to testing. Except for seven locations of single porosity, the weld was clear. This would verify the lack of SWE activity from the weld area during testing. Ultrasonic and dye penetrant inspection was performed of non-weld areas of the vessel cylinder section after hydroburst from which random SWE were detected during testing. No defects were indicated by these examinations.

3. Cryogenic Temperature (-320°F) Test of 2014-T6 Aluminum Pressure Vessel

The significant data for each pressurization of the 2014-T6 vessel tested at -320°F is shown below.

Cycle	Pressure Level	Pressure Rate (psig/min.)	Hold (sec)	Pre-Flaw
1	0 - 550	100	30	No
2	0 - 975	100	Failed on Rising Load @ 975 psig	Yes

Figure 96 shows the chamber pieces within the test cell immediately following failure while Figure 97 shows the chamber pieces reassembled. As indicated in Figures 96 and 97, the chamber fragmented into approximately 20 pieces on failure. Figure 98 schematically shows the fracture surfaces in the longitudinal weld region with failure originating (Point A) from the cylinder longitudinal weld near the PTC defect introduced into the cylinder longitudinal weld following the first pressurization. It is also possible that a secondary failure origin is located at Point B on the longitudinal weld although the SWE data indicates failure originated in the region of Point A.

Based on a failure pressure of 975 psig, the gross stress (Pr/t) at fracture approximated 29 ksi. With a PTC length of 0.5-in. and depth of 0.1-in., the apparent K_{Ic} associated with this defect was 16 ksi-in.$^{1/2}$ calculated using equation (1). The measured value of K_{Ic} based on transversely welded PTC tension tests was 18.5 ksi-in.$^{1/2}$.

Figure 99 is a plot of cumulative SWE (detected by sensor No. 3 located in the center of the cylinder section) vs pressure for both load cycles. The unusually high SWE count during the initial portion of the first pressure cycle is due to the bubbling action produced when the relatively warm

gaseous nitrogen used for pressurization made contact with the liquid nitrogen in the vessel. The initial SWAT system trigger level was set on the basis of static conditions prior to pressurization. When the GN_2 was introduced into the vessel, the bubbling action caused the background noise level to greatly exceed the SWAT system trigger level. The system was immediately readjusted to a higher trigger level; however, when the bubbling action stopped, the trigger level was too high to detect the continuous emission which probably occurred on further pressurization during the first cycle.

In order to circumvent this noise problem, the SWAT system trigger level was set at 150 psig during the second loading cycle. As shown in Figure 99, discrete incremental increases in the SWE cumulative count subsequently were observed throughout the loading cycle. There was also a slight increase in the slope of the cumulative SWE vs pressure plot which has been associated with defect formation and growth, and the onset of failure. Both observations (discrete jumps and slope increase) could have been employed to terminate pressurization prior to fracture.

Figures 100 and 101 show the locations of SWE detected during each cycle. These plots represent the plan view of the test article and the SWAT video display observed on the system monitor in real time during the test. The plots also show the location of the preflaw introduced after the first cycle and the fracture branching (Points A and B, refer also to Figure 98) which occurred from the main fracture path along the cylinder longitudinal weld. The SWE are generally randomly located within the cylinder zone, except for the region around Point A on the longitudinal weld from which multiple emissions were detected. SWE were also detected from this area immediately before failure indicating the primary failure origin was at Point A. No SWE were detected from the remaining area of the longitudinal weld including the region at Point B which possibly corresponded to a secondary failure origin.

72

Figure 79 schematically shows the location of weld defects observed in the X-rays of the longitudinal weld. Only scattered porosity was observed except for two areas of multiple, alligned porosity. Areas requiring repair after the initial longitudinal weld was made also are shown and indicate the extensive repair welding required to produce relatively acceptable welds in this material. The locations of the fracture branching from the main fracture path and the possible primary (A) and secondary (B) fracture origins are also shown in Figure 79. Figures 102 through 104 show magnified views of the fracture surface at A and B. The region of multiple porosity near Point A is readily apparent in Figure 103 and is thought to be a source of multiple SWE detected from this area during both pressurization cycles.

Ultrasonic and dye penetrant examination of the chamber did not identify any defects at the locations of the random emissions shown in Figures 100 and 101.

4. Cryogenic Temperature (-320°F) Test of the 2219-T87 Pressure Vessel

The following tabulation shows the significant data for each cycle for the 2219-T87 test @ -320°F.

Cycle	Pressure Level (psig)	Pressure Rate (psig/min.)	Hold (sec)	Pre-Flaw
1	0 - 550	100	30	No
2	0 - 1000	100	30	Yes
3	0 - 1000	100	180	Yes
4	0 - 1000	100	120	Yes
5	0 - 945	100	Failed on Rising Load @ 945 psig	Yes

Because of potential damage to the test cell, the maximum pressure without failure was limited to 1000 psig; if failure did not occur when the chamber was pressurized to this level, the PTC defect was successively enlarged before subsequent pressurizations.

73

Figure 105 shows the failed chamber in the test cell and shows that there was significantly less fragmentation in comparison to the 2014-T6 chamber tested at -320°F. Figure 106 shows the cylinder section and a close up view of the PTC defect inserted in the longitudinal weld while Figure 107 shows the longitudinal weld fracture surfaces.

As indicated by the above tabulation, chamber failure occurred during the fifth pressurization at 945 psig after prior excursions to pressures up to 1000 psig. The gross stress (based on Pr/t) at failure was 28.5 ksi while the net section stress based on the section (0.08 in.) remaining under the PTC defect approximated 80 ksi. The initial defect dimensions were 1.5 in. long and 0.15 in. deep and were successively increased to 2.0 in. long x 0.19 in. deep for the 3rd cycle, 2.45 in. long x 0.25 in. deep for the 4th cycle and 3.0 in. long x 0.3 in. deep prior to the final cycle. The apparent K_{Ic} at failure (945 psi) calculated using Equation (1), the Kobayashi correction for deep crack, and the final defect size was 48 ksi-in.$^{1/2}$.

Figures 108 through 110 are plots of the cumulative SWE vs pressure for the last three loading cycles. These plots were obtained by monitoring channel 3. Since excessive background noise was encountered during the 1st and 2nd cycles, data are not shown for these pressurizations. To eliminate the background noise problems (due to bubbling action of the pressurizing GN_2), the SWAT system trigger level was determined at 350-400 psig during each cycle. Although this generally significantly improved the SWE data obtained, background noise still was detected primarily because the system trigger level was set as close as possible to the background noise level. This is particularly true in the plot for the 3rd cycle where the SWAT system was saturated by the background noise above a pressure level of approximately 425 psi. The background noise also was a problem during the fourth cycle near maximum pressure. Consequently, the SWAT system sensitivity was further reduced for the 5th cycle. As indicated in Figure 110, this adjustment eliminated the background noise problem while still enabling the detection of SWE.

From Figure 110, it is apparent that there was no well defined precursor of failure during the fifth cycle although there were discreet steps in the SWE cumulative count indicating the occurrence of defect formation or propagation which would permit depressurization prior to failure.

Figures 111 through 113 are plots showing the locations of SWE displayed on the SWAT system monitor during the 3rd, 4th and 5th cycles. The locations of the longitudinal weld and PTC flaw introduced into the weld following the second cycle are also shown. Plots for the 1st and 2nd cycles are not shown because of the excessive background noise due to the nitrogen bubbling. As indicated in these figures, larger or multiple emissions (heavy black dots) were detected in the location of the longitudinal weld and the preflaw during the 3rd, 4th and 5th cycles. During the 5th cycle, emission sources were detected from along the longitudinal weld, and multiple emissions were detected from the region of the PTC flaw including three emissions immediately prior to failure. From these plots, it is apparent that an error of approximately 3-in. existed between the actual preflaw location and the location indicated by the SWAT system. However, these data, in combination with the corresponding cumulative SWE plots (Figure 109), would have permitted depressurization prior to failure and location of the defect for repair.

Figure 95 schematically shows the results of X-ray examination of the longitudinal weld prior to testing of the vessel. From this figure, it is apparent that the weld was essentially free of detectable defects; only two single pores (both less than 0.030-in. dia.) were located by this examination. Following testing, ultrasonic and dye penetrant examination was also performed of the cylinder area adjacent to the longitudinal weld included in the area monitored by the SWAT system. No defects were detected by these post-testing examinations.

5. Discussion of Pressure Vessel Test Results

The tests performed at room temperature demonstrated that acoustic emission monitoring can be employed to detect and locate defects on the aluminum alloys tested and provides the means of terminating loading of a pressure vessel prior to failure. Both increasing cumulative SWE count and increasing SWE amplitude (as observed on the oscilloscope in real time) were verified to be precursors of failure. The existence of the Kaiser effect during structural loading was also verified through the room temperature tests in that significant SWE activity was not observed until prior pressure levels were exceeded. Within the test conditions evaluated, the Kaiser effect was independent of pressurization rate and was not affected by the introduction of a semi-elliptical preflaw (not precracked) in the vessel longitudinal weld. Practical application of the Kaiser effect lies in its use to determine prior maximum pressure (stress) levels and to determine whether or not over pressurization occurred during prior service cycles.

Based on the SWE data, failure of the 2014 vessel originated from a group of tungsten inclusions which were shown in the X-rays of the cylinder longitudinal weld and which were visible in the fracture face. The presence of these defects was detected through multiple SWE from the same area during each pressurizing cycle. SWE detected immediately before failure identified this location as the failure origin. Failure of the 2219 vessel tested at room temperature originated from a part-through-crack (PTC) defect introduced in the longitudinal weld. This failure origin was also identified by SWE during the final cycles; however, in comparison to the room temperature 2014 test, the number of emissions detected near failure was small.

The lack of large numbers of SWE immediately before failure of the 2219 vessel probably was the result of a large number of prior cycles to pressures near the failure pressure; such a procedure would tend to blunt the preflaw and thus minimize subcritical extension of the defect before failure. This hypotheses is further supported by the fact that the notch

was inherently blunt (0.01 in. min radius) in comparison to the natural defects in the 2014 aluminum vessel and that the failure stress based on the net section beneath the PTC defect was significantly higher than the uniaxial transverse weld ultimate strength of this filler wire-base metal composition. However, the presence of the preflaw (and the second preflaw introduced after the 8th cycle) was identified and located by multiple emissions detected during the lower pressure cycles and probably resulted from plastic zone formation at the notch. Thus, these data, in conjunction with the cumulative SWE counts could have been used to terminate loading and locate and subsequently repair the defects. This capability was actually demonstrated during the 6th, 7th and 10th cycles when large jumps in the cumulative SWE count were used as a basis to depressurize the vessel without failure; pressurization during the 10th cycle was successfully accomplished without failure from a pressure only 30 psi lower than the failure pressure.

The tests performed at -320°F also demonstrated the capability to detect and locate SWE sources in real time. However, problems were encountered due to:

1. excessive background noise from the "bubbling action" of the gaseous/liquid nitrogen and

2. low sensitivity of the transducer at cryogenic temperatures

By adjusting the system sensitivity after the pressurizing media-temperature of the test-vehicle had stabilized, it was possible to minimize the effects of nitrogen bubbling.

Although the system sensitivity of the transducer used in the cryogenic testing was low in comparison to that used in the room temperature tests, the SWE data were still useful to detect and locate the failure origin in each vessel. The cumulative SWE count for both vessels indicated slight

increases in slope and discrete steps in the curve, both of which are indicative of defect formation or propagation and provide a basis for depressurization prior to failure. The real-time location of the SWE sources indicated that failure of the 2219 vessel occurred at the preflaw in the longitudinal weld. The failure origin of the 2014 vessel was correlated with the origin shown by analysis of the fracture surfaces and the presence of corresponding defects (aligned porosity) shown by examination of prefailure X-rays of the longitudinal weld. However, in view of the relatively low cryogenic temperature sensitivity of the sensors commonly used with acoustic monitoring systems, it is considered desirable, when monitoring structures at cryogenic temperatures, to provide for insulation or heating of the sensor thereby insuring that the sensor temperature does not drop below approximately -110°F. Alternatively, studies should be undertaken to develop a sensor with high sensitivity at cryogenic (down to -425°F) temperatures.

In the 2219-T87 cryogenic test the error in defect-SWE source location was approximately 1 to 4 inches; a similar error (1 to 3-in.) in source location was observed in the 2219 room temperature test. This error can be improved by detailed analysis and determination of SWE propagation rates in these materials. However, during each vessel test multiple emissions were observed from the defect area, which indicated potential failure, and the indicated source was within the zone which would have to be ultimately inspected using other NDT methods to establish the true nature and location of the defect.

A comparison of the performance of the 2219 and the 2014 pressure vessels indicates that the 2219 alloy was much superior to the 2014 alloy both at room temperature and -320°F. At both temperatures, the 2219 chambers burst at hoop stresses approximating the uniaxial ultimate strength level whereas the 2014 alloy at cryogenic temperatures burst at a stress level significantly lower than the ultimate strength. This same relative advantage in 2219 vs 2014 was encountered during chamber fabrication where extensive weld repair was required to remove weld porosity and cracking in the 2014 material. From an acoustic emission monitoring standpoint and the ability to detect and locate flaw propagation, there appeared to be no difference between the two alloys.

78

V.   CONCLUSIONS

1.   Stress Wave Emission monitoring can be used to detect and locate sub-critical crack growth in 2219, 2014 and 7075 aluminum alloy structures both at room and cryogenic (-320 and -423°F) temperatures.

2.   **At room temperature,** the stress wave emission precursor of failure is a marked increase in (1) signal amplitude, (2) signal repetition rate and (3) the slope of the cumulative count plotted vs load. These precursors are observed during uniaxial tensile testing and during the hydroburst of sub-scale pressure vessels; multiple emissions from a single location also serve as a precursor of failure during the vessel hydrotests.

3.   **At cryogenic temperatures (-320°F and -423°F),** a pronounced increase in signal amplitude and repetition rate immediately before failure is not observed. However, multiple emissions from a single location serve to locate defects and indicate incipient failure.

4.   The problems encountered during cryogenic testing resulted from low sensitivity of the transducer when immersed in the cryogenic bath at -320°F or -423°F, and noise resulting from ice formation. Band pass filtering and the use of wave guides to mount the transducer out of the cryogenic bath (sensor temperature approximately -110°F) provide solutions to these problems.

5.   When monitoring structures at cryogenic temperatures, insulation or heating of the sensor should be provided to insure the sensor temperature does not drop below -110°F. Alternatively, a sensor with high sensitivity at cryogenic temperatures (down to -423°F) should be developed.

6.   The error in locating the source of multiple emissions is well within the zone which would be inspected using conventional NDI methods in order to establish the size and orientation of the flaw generating the acoustic emission.

7. The fabrication characteristics and hydroburst performance of the 2219 alloy is much superior to the 2014 aluminum alloy. However, from an acoustic-emission-monitoring standpoint, i.e., the ability to detect and locate flaw propagation, there appears to be no difference between the two alloys, filler metals (2319 and 4043) or weld processes (TIG and MIG) investigated.

REFERENCES

1. J. Kaiser, "Untersuchungen uber das Auftreten Gerauschen Beim Sugversuch," Ph.D. Thesis, Techn. Hochsch., Munchen, (1950), and Arkiv Fur das Eisen-huttenwesen, 24, 43-45, (1953).

LESSELS & ASSOCIATES

2. B. H. Schofield, R. A. Bareis, and A. A. Kyrala, "Acoustic Emission Under Applied Stress", WADC Technical Report 58-194, (April 1958).

3. B. H. Schofield, "Acoustic Emission from Metals, Its Detection, Character-istics, and Source," Proceedings of the Symposium on Physics and Non-destructive Testing, Southwest Research Institute, San Antonio, Texas, (October 1963).

4. B. H. Schofield, "Acoustic Emission Under Applied Stress", ASD-TR-53-509, Part I, (April 1963), Part II, (May 1964).

AEROJET PUBLICATIONS

5. A. T. Green, C. S. Lockman, and R. K. Steele, "Acoustic Verification of Structural Integrity of Polaris Chambers," Modern Plastics, 41, 137-139, (July 1964).

6. A. T. Green, C. E. Hartbower, and C. S. Lockman, "Feasibility Study of Acoustic Depressurization System," Report NAS 7-310, Aerojet-General Corporation, (February 1965).

7. C. E. Hartbower, W. W. Gerberich, and P. P. Crimmins, "Monitoring Sub-Critical Crack Growth by an Acoustic Technique," Weld Imperfections Symposium, Lockheed Research, Palo Alto, California, (September 1966). Published in WELD IMPERFECTIONS, Addison-Wesley, Menlo Park, Calif.

8. C. S. Lockman, A. T. Green, and R. K. Steele, "Acoustic Monitoring During Proof Testing," Weld Imperfections Symposium, Lockheed Research, Palo Alto, California, (September 1966). Loc cit.

9. C. E. Hartbower, W. W. Gerberich and P. P. Crimmins, "Characterization of Fatigue-Crack Growth by Stress-Wave Emission", NAS 1-4902, (June 1966). Available from NASA, P.O. Box 5700, Bethesda, Md. 20014.

10. A. T. Green, C. S. Lockman, S. J. Brown, and R. K. Steele, "Feasibility Study of Acoustic Depressurization System," NASA CR-55472, (March 1966).

11. A. T. Green, Stress-Wave Detection, Saturn S-II, NASA CR-61161, (December 1966).

12. W. W. Gerberich and C. E. Hartbower, "Some Observations on Stress-Wave Emission as a Measure of Crack Growth," International Journal of Fracture Mechanics, 3, 3, (September 1967).

13. W. W. Gerberich and C. E. Hartbower, "Monitoring Crack Growth of Hydrogen Embrittlement and Stress Corrosion Cracking by Acoustic Emission, "Conference on Fundamental Aspects of Stress Corrosion Cracking, Ohio State University, (September 1967).

14. C. E. Hartbower, W. W. Gerberich, and P. P. Crimmins, "Mechanisms of Slow Crack Growth in High-Strength Steels," AFML-TR-67-26, Vol. 1, Aerojet-General Corp., (February 1967). Also "Monitoring Subcritical Crack Growth by Detection of Elastic Stress-Waves," American Welding Society Meeting, Houston, Texas, (October 1967). THE WELDING JOURNAL, Vol. 47(1), p. 1-s, Jan 1968. Received the Spraragen Award as best research paper published in the WELDING JOURNAL in the year 1968.

15. A. T. Green, "Testing of 10-inch Glass Hemispheres Using Stress-Wave Analysis Technique," N00014-67-C-0333, Naval Ship Research and Development Center, (September 1967).

16. A. T. Green and C. E. Hartbower, "Stress-Wave Analysis Technique for Detection of Incipient Failure," Aerojet-General Corp., Presented at ORNL Conference on Incipient Failure Diagnosis for Assuring Safety and Availability of Nuclear Power Plants, Gatlinburg, Tennessee, (October 1967). Published in the PROCEEDINGS of the AEC Conference.

17. W. G. Reuter, A. T. Green, C. E. Hartbower and P. P. Crimmins, "Monitoring of Crack Growth in Ti-6Al-4V Alloy by the Stress Wave Analysis Technique", Report on NASA Houston Contract NAS 9-7759, Dec. 1968.

18. C. E. Hartbower, W. W. Gerberich, and P. P. Crimmins, "Spontaneous Strain Aging as a Mechanism of Slow Crack Growth," Presented at the American Welding Society Annual Conference, Chicago, Illinois, (April 1968). The WELDING JOURNAL, Vol. 47(10), Oct. 1968.

19. C. E. Hartbower, W. W. Gerberich, and H. Liebowitz, "Investigation of Crack-Growth Stress-Wave Relationships," Engineering Fracture Mechanics, Vol. I(2), p. 291, August 1968. Also C. E. Hartbower, W. W. Gerberich, W. G. Reuter, and P. P. Crimmins, "Stress-Wave Characteristics of Fracture Instability in Constructional Alloys," AD-674-881, Aerojet-General Corp., (July 1968). Copy of ONR Final in NCEL Library.

20. G. S. Baker, "Acoustic Emission and Prefracture Processes in High-Strength Steels," AFML-TR-67-266, Aerojet-General Corporation, Wright-Patterson AFB, (March 1968).

21. C. E. Hartbower and P. P. Crimmins "Fracture of Structural Metals as Related to Pressure-Vessel Integrity and In-Service Monitoring", presented at the ICRPG/AIAA 3rd Solid Propulsion Conference (AIAA Paper 68-501), Atlantic City, June 1968.

22. W. W. Gerberich and W. G. Reuter, "Theoretical Model of Ductile Fracture Instability Based on Stress-Wave Emission," ONR Contract Report N00014-66-C0340, Aerojet-General Corp., Sacramento, California (February 1969).

REFERENCES (Cont'd)

23. C. E. Hartbower, W. G. Reuter and P. P. Crimmins, "Mechanisms of Slow Crack Growth in High-Strength Steels and Titanium", Final Technical Report AFML-TR-67-26, Vol. II, June 1969 on Contract AF 33(615)-2788 for the period April 1967 - April 1969, 199 pages.

24. A. T. Green, Development of a Nondestructive Testing Technique to Determine Flaw Criticality, ARPA Contract F33615-68-C-1705, Aerojet-General Corp., Sacramento, California, (August 1969).

25. C. E. Hartbower, Application of SWAT to the Nondestructive Inspection of Welds, Technical Note, Aerojet-General Corp., Sacramento, California, (September 1969). The WELDING JOURNAL, Vol. 35(2), Feb. 1970.

26. C. E. Hartbower, F. J. Climent, C. Morais, and P. P. Crimmins, Stress-Wave-Analysis Technique Study of Thick-Walled Type A302-B Steel Pressure Vessels, NASA NAS9-7759, Aerojet-General Corp., (July 1969).

27. A. T. Green, "Detection of Incipient Failures in Pressure Vessels by Stress-Wave Emission," Nuclear Safety, 10, 4-18, (January-February 1969).

28. A. T. Green and C. E. Hartbower, "Development of a Nondestructive Testing Technique to Determine Flaw Criticality", Interim Technical Report on ARPA Contract F33615-68-C-1705 (ARPA Order No. 1244, Code 8D10), May 1970.

UNIVERSITY OF CALIFORNIA

29. H. L. Dunegan, D. O. Harris, and C. A. Tatro, "Acoustic Emission Research Status Report, December 1963-August 1964", UCID-4868 Rev. 1, Lawrence Radiation Laboratory, (November 1964).

30. H. L. Dunegan and C. A. Tatro, "Passive Pressure Transducer Utilizing Acoustic Emission," Review of Scientific Instruments, 38, 8, (August 1967).

31. H. L. Dunegan, D. O. Harris, and C. A. Tatro, "Fracture Analysis by Use of Acoustic Emission," Engineering Fracture Mechanics, 1, 105-122, (June 1968).

32. H. Dunegan and D. Harris, "Acoustic Emission-A New Nondestructive Testing Tool," Ultrasonics, 7, 160-166, (July 1969).

MICHIGAN STATE UNIVERSITY

33. C. A. Tatro, "Sonic Techniques in the Detection of Crystal in Metals", Progress Report, Division of Engineering Research, Michigan State University, East Lansing, Michigan, (January 1959).

34. C. A. Tatro and R. G. Liptai, "Acoustic Emission from Crystalline Substances", Proceedings of the Symposium on Physics and Nondestructive Testing, Southwest Research Institute, San Antonio, Texas, 145-174, (October 1962).

35. R. G. Liptai, "An Investigation of the Acoustic Emission Phenomenon," Ph.D. Thesis, Michigan State University, East Lansing, Michigan, (1963).

36. R. B. Engle, "Acoustic Emission and Related Displacements in Lithium
     Fluoride Single Crystals," Ph.D. Thesis, Michigan State University,
     East Lansing, Michigan (1966).

UNIVERSITY OF MICHIGAN

37. L. D. Mitchell, "An Investigation of the Correlation of the Acoustic
     Emission Phenomenon with the Scatter in Fatigue Data," Ph.D. Thesis,
     University of Michigan, Ann Arbor, Michigan (1965).

38. J. N. Kerawalla, "An Investigation of the Acoustic Emission from
     Commercial Ferrous Materials Subjected to Cyclic Tensile Loading",
     Ph.D. Thesis, University of Michigan, Ann Arbor, Michigan (1965).

39. A. B. L. Argarwall, "An Investigation of the Behavior of the Acoustic
     Emission from Metals and a Proposed Mechanism for its Generation,"
     Ph.D. Thesis, The University of Michigan, Ann Arbor, Michigan (1968).

40. J. R. Frederick, "Use of Acoustic in Nondestructive Testing," Semi-
     Annual Report 01971-2-T, March-August 1969, University of Michigan,
     Ann Arbor, Michigan (November 1969).

41. N. G. Sankar, "Unload Emission Behavior of Material and Its Relation
     to the Bauschinger Effect," Ph.D. Thesis, University of Michigan,
     Ann Arbor, Michigan (1969).

OTHER COLLEGES

42. D. M. Egle, "A Comprehensive Analysis of an Acoustic Emission Detection
     System", Ph.D. Thesis, Tulane University, New Orleans, Louisiana (1965).

43. R. H. Chambers, "New Techniques in Nondestructive Testing by Acoustical
     and Exo-electron Emission," AD-691-230, Arizona University, Tuscon,
     Arizona (July 1969).

44. C. K. Day, "An Investigation of the Plastic Bursts of Microstrain in
     Zinc As Sources for Acoustic Emission," M.S. Thesis, Washington State
     University, Pullman, Washington (1969).

45. J. C. Spanner, "A Selective Review on the Utilization of Acoustic
     Emission Techniques for Materials Research and Structural Integrity
     Analysis", M.S. Thesis, Washington State University, Pullman,
     Washington (1970).
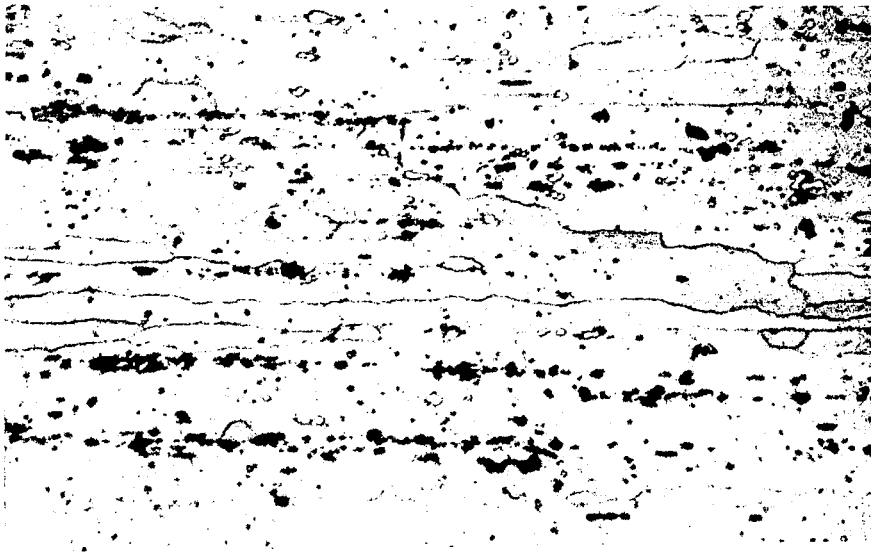
Longitudinal
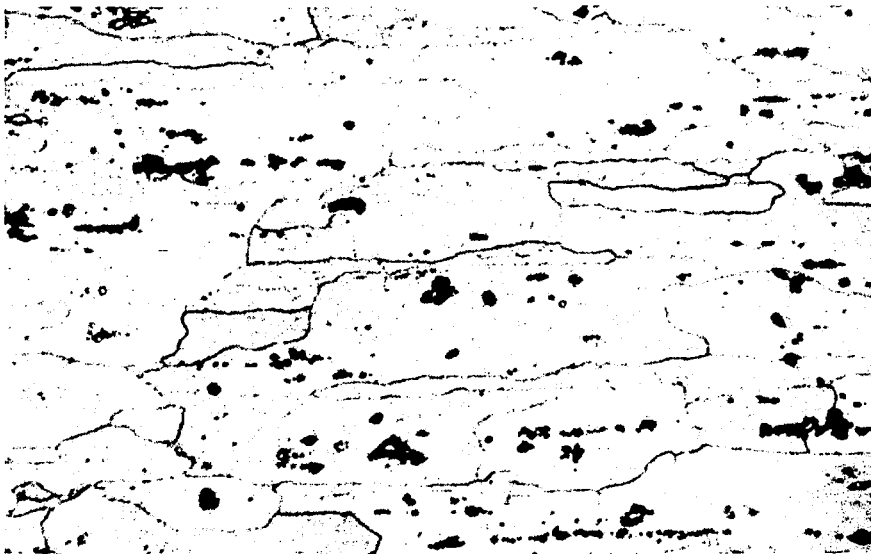
Transverse

Etch: Kellers   Mag: 150X

Figure 1.   Typical Microstructure of 2014-T651 Aluminum
            Alloy 0.3-in. Thick Plate Material
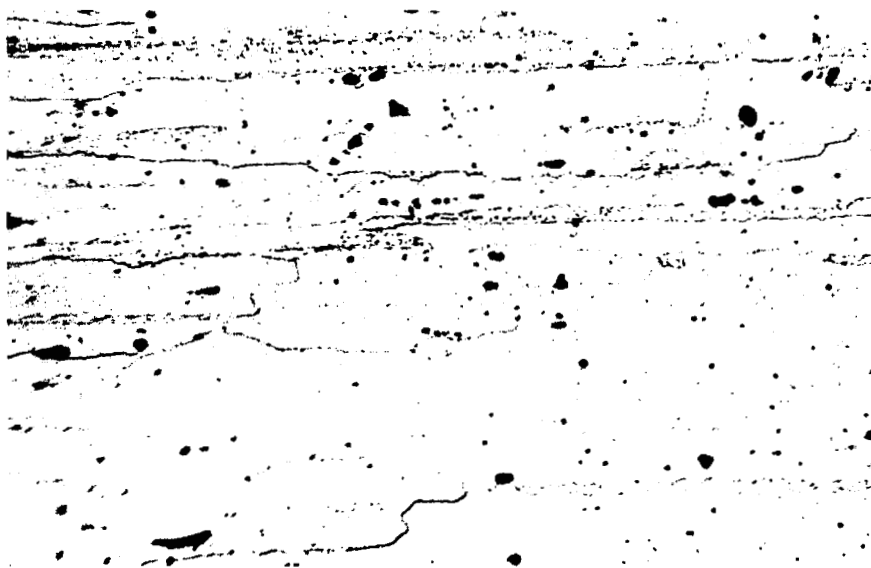
Longitudinal
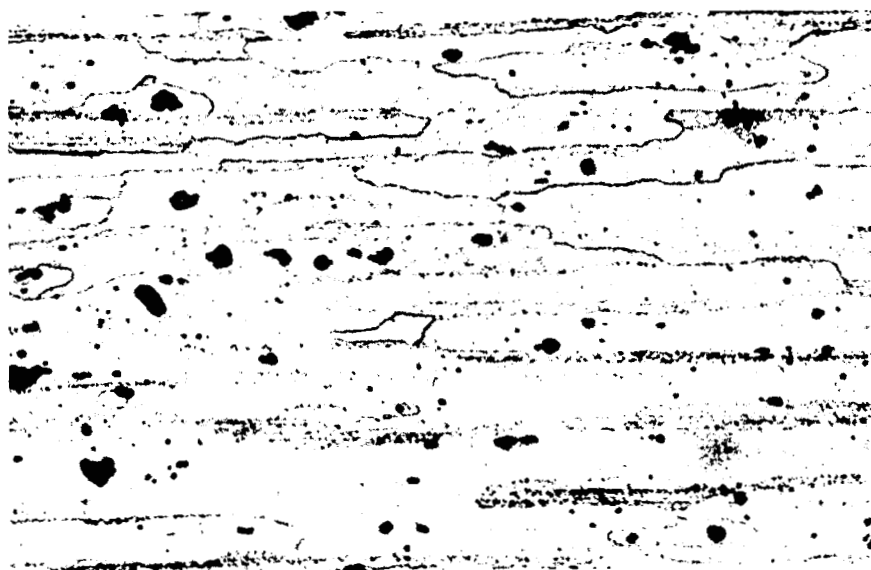
Transverse

Etch: Kellers   Mag: 150X

Figure 2. Typical Microstructure of 7075-T73 Aluminum
Alloy 0.3-in. Thick Plate

Longitudinal
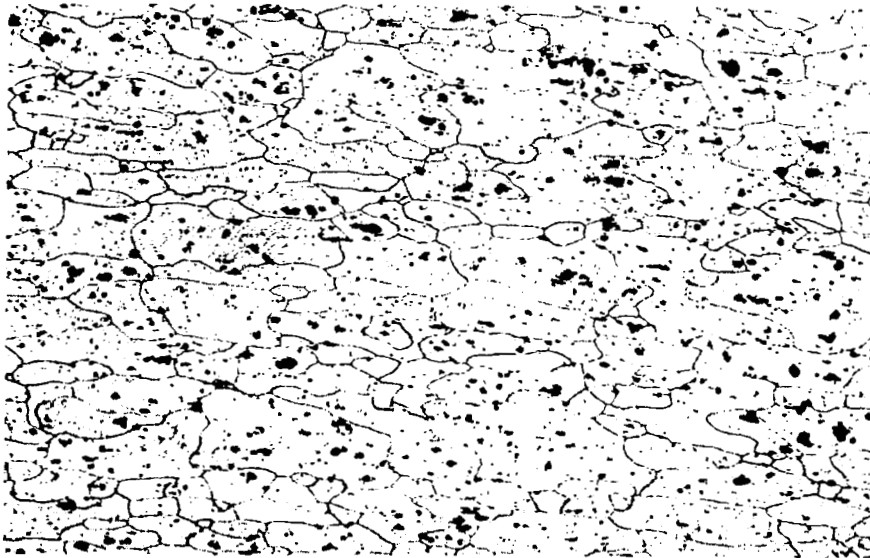
Transverse

Etch: Kellers   Mag: 150X

Figure 3.   Typical Microstructure of 2219-T87 Aluminum
            Alloy 0.3-in.-Thick Plate Material.
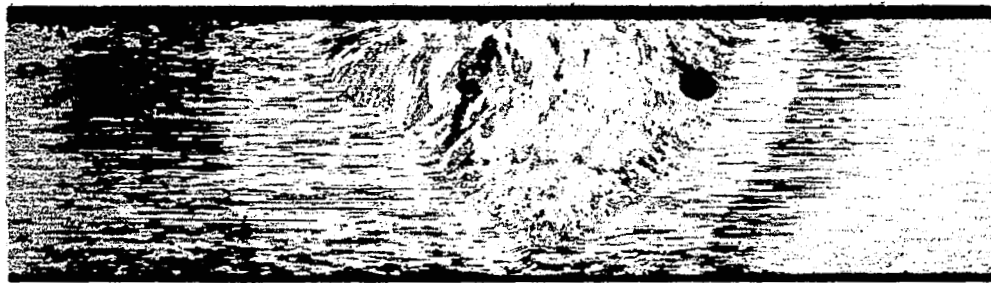
0.18-in.
Thick
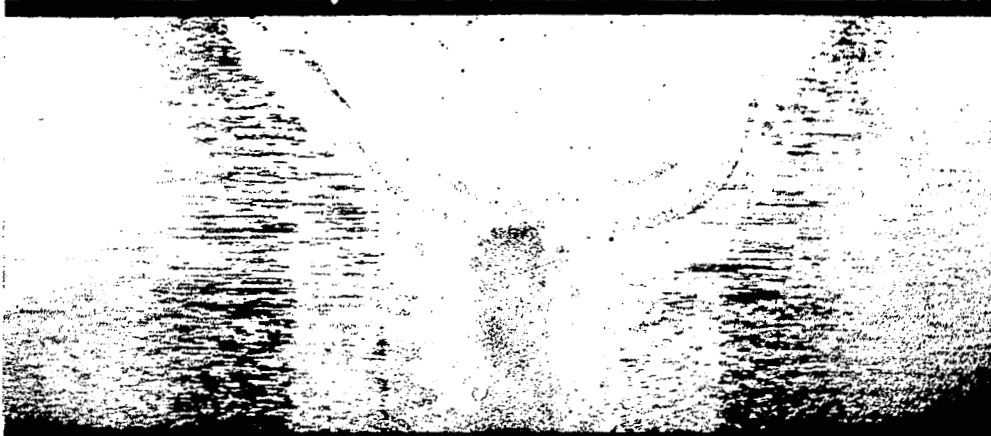
0.30-in.
Thick
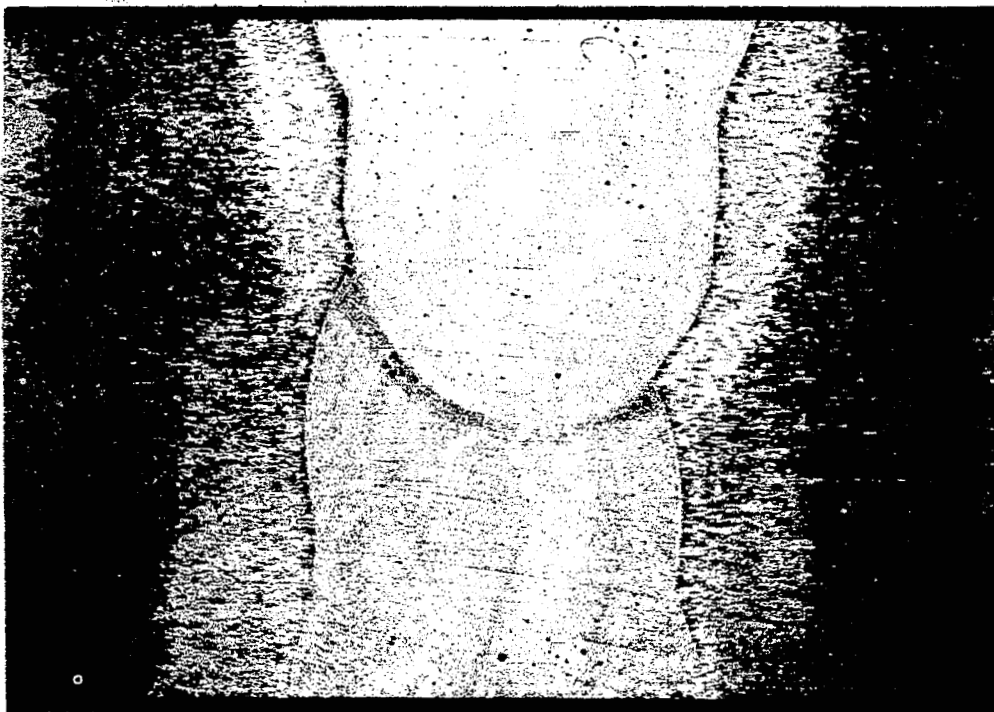
0.50-in.
Thick

Etch: Kellers   Mag: 8X

Figure 4.   Typical Macrostructure of TIG Welds (4043 Filler Wire)
            in 2014-T651 Aluminum Alloy Plate

Figure 5. Typical Macrostructure of MIG Weld (4043 Filler Wire) in 0.3-in. Thick 2014-T651 Aluminum Alloy Plate

Etch: Kellers   Mag: 8X

Figure 6. Typical Macrostructure of TIG Weld (2319 Filler Wire) in 0.3-in. Thick, 2014-T651 Aluminum Alloy Plate

HEMISPHERICAL HEADS
(MADE FROM 0.70 IN.
THICK PLATE)

48 IN.

0.32 IN. NOMINAL THICKNESS
(AS RECEIVED)

3/4 IN. ANPT FITTING
(BOTH ENDS)

B

B

17.5 IN. DIA (NOMINAL)

A

WELD JOINT (DETAIL B)

SURFACE FLAW
(IF REQUIRED - SEE TEST PLAN)

DETAIL A

30°

30°

30°

DETAIL B-B

0.32 IN. (NOMINAL)

LOCALLY REDUCE THICKNESS OF HEAD
TO MATCH CYLINDER SECTION
THICKNESS AT WELD JOINT.

0.050
0.060

LAND
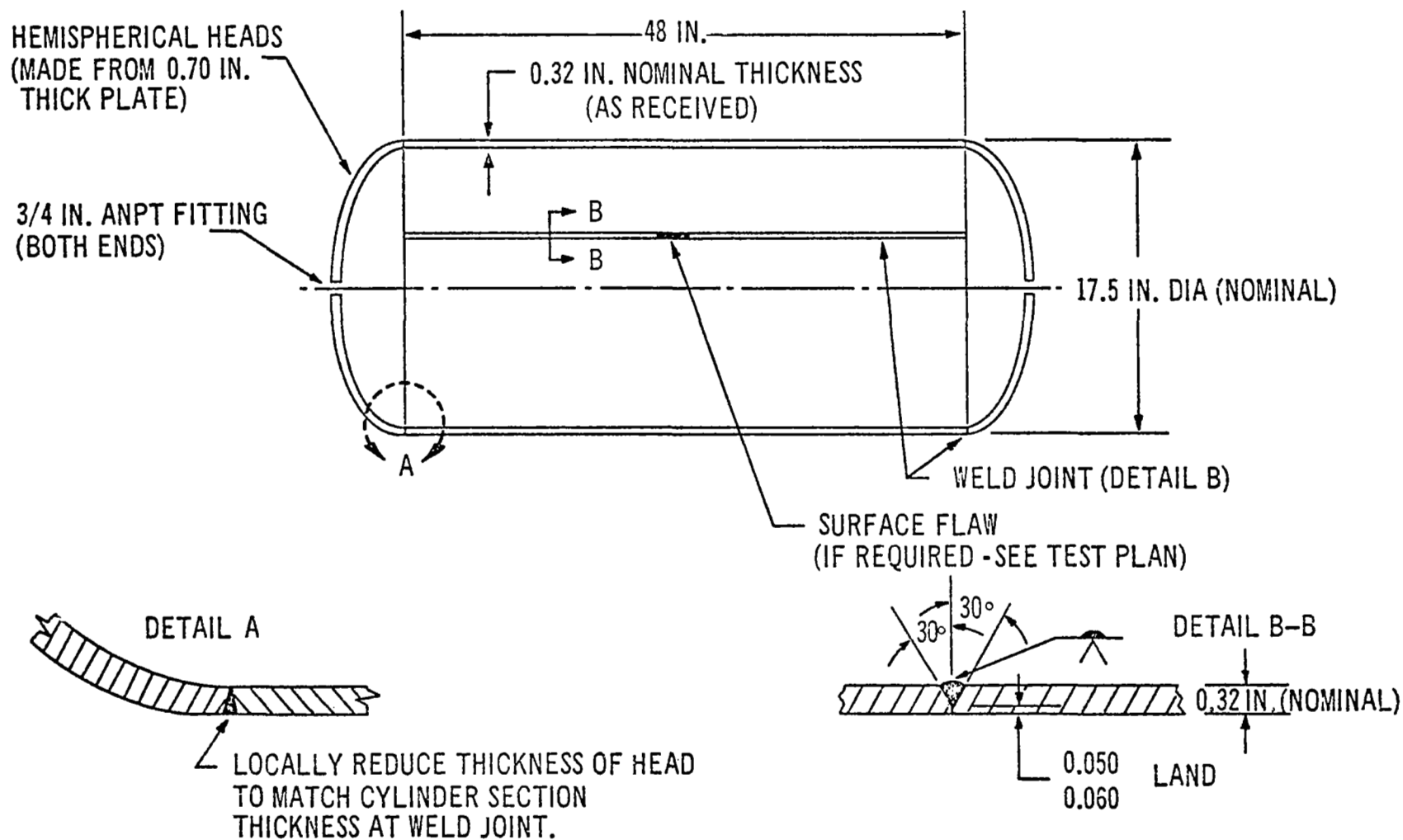
Figure 7.   Subscale Pressure Vessel Design
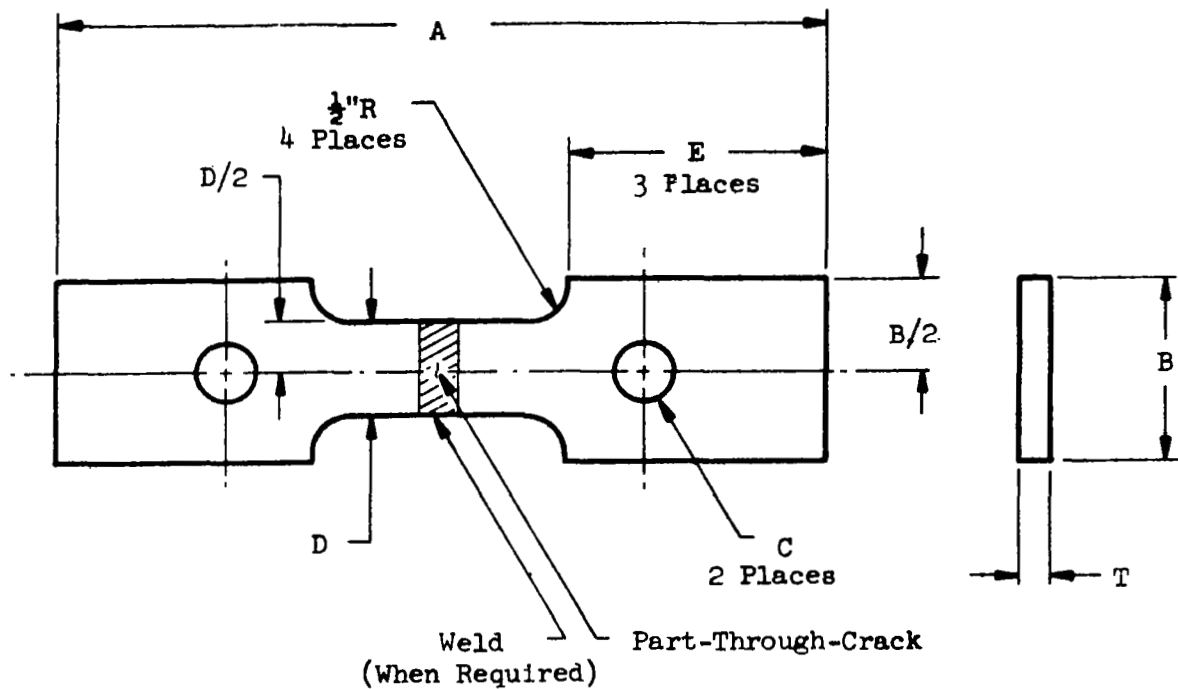
Test Temperature	A	B	C	D	E
Room and -320°F	16.00	4.00	1.25	3.00	5.00
-423°F	11.00	2.50	1.00	1.50	3.50

Figure 8. Part-Through-Crack Tension Specimen and Knife-Edge
Attachments to Accommodate the Crack-Opening-
Displacement Gage
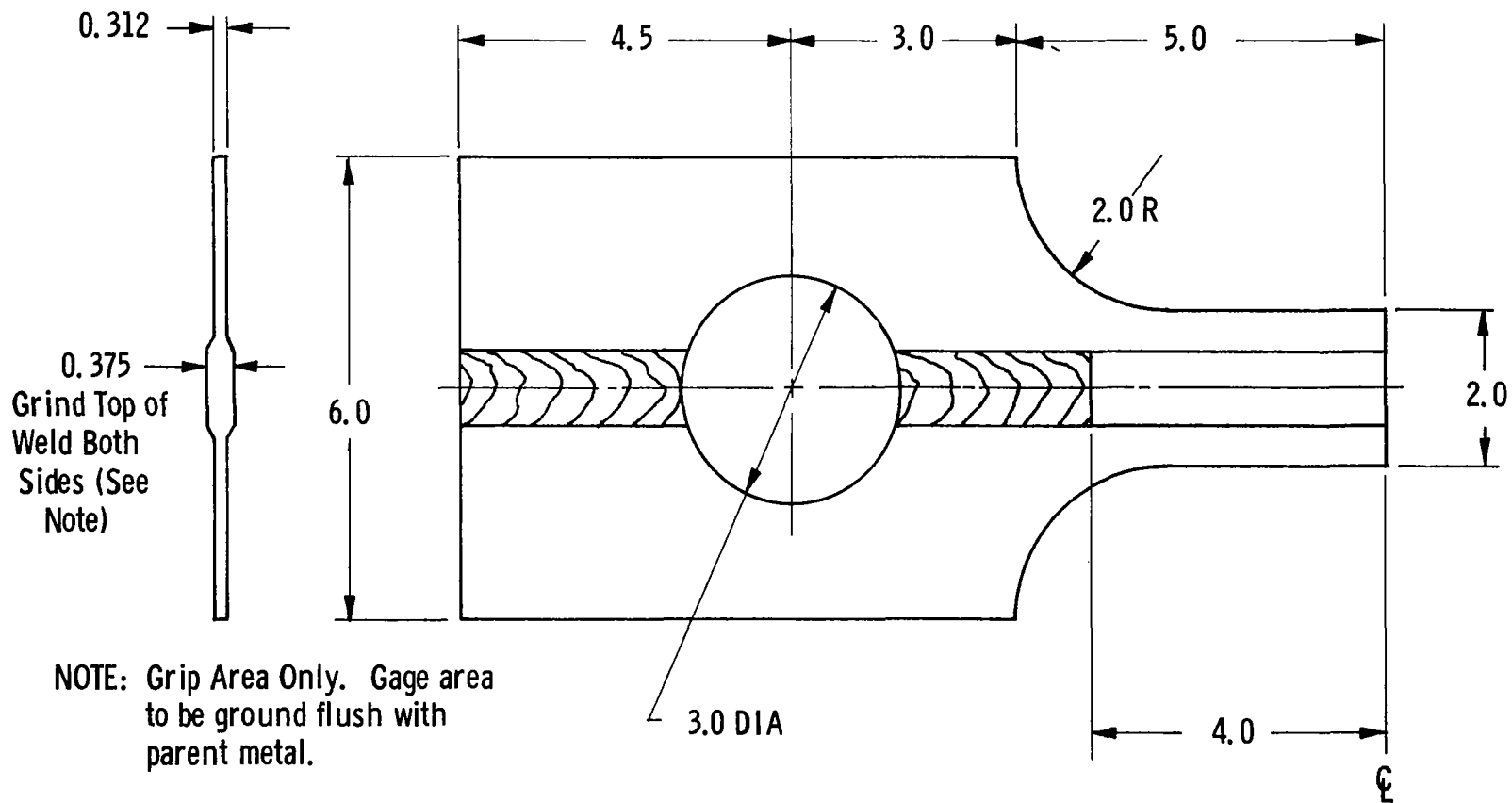
Figure 9. Longitudinally Welded Unflawed and Part-Through-Crack Tension Specimen. (Room and -320°F Tests)

TENSILE SPECIMEN 4-12   2014-T6
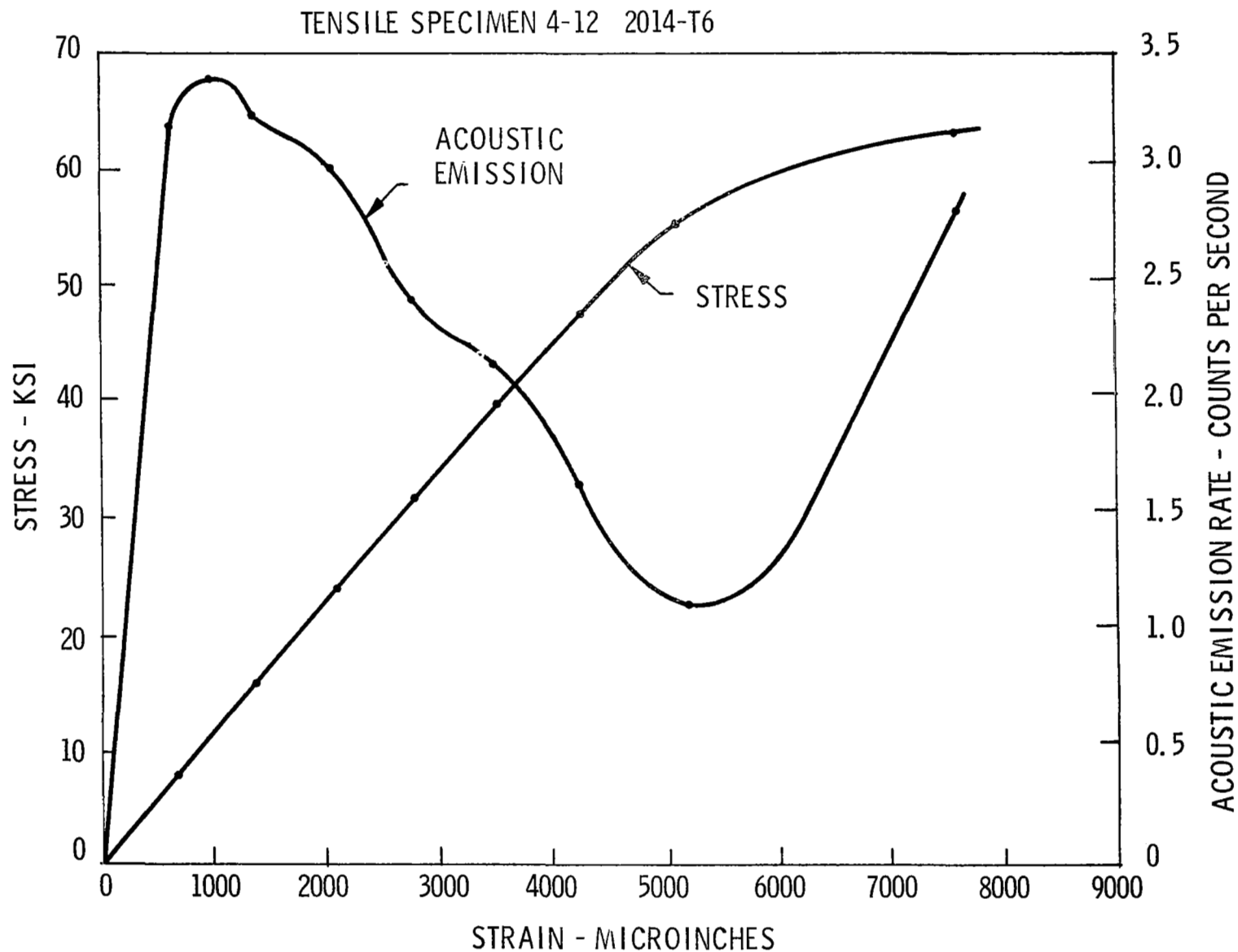
Figure 10.   Effect of Pin-Hole Irregularities on Acoustic-Emission Count Rate on Initial Loading.
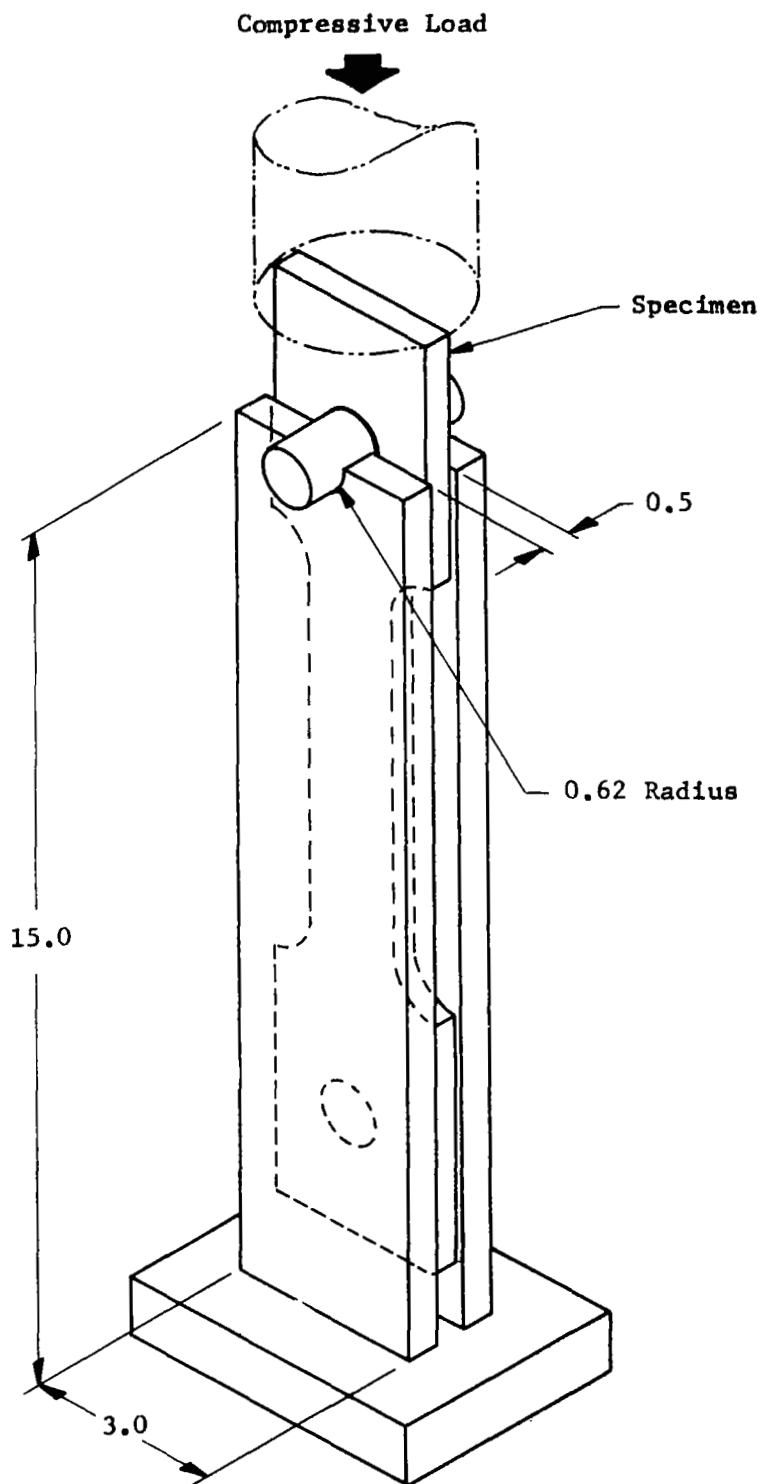
Figure 11. Fixture for Compressive Loading Specimen Loading Holes

95
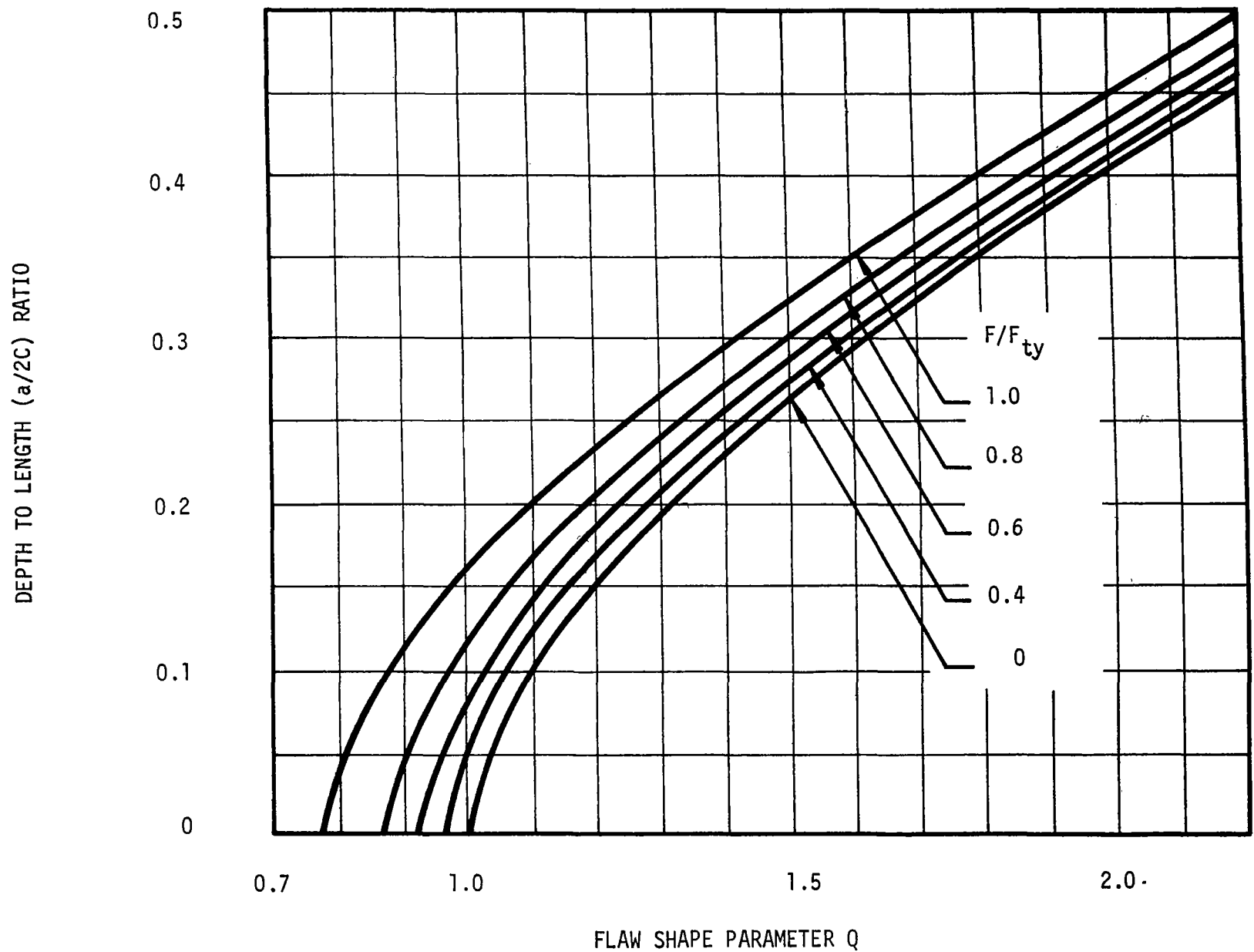
Figure 12. Flaw Shape Parameter, Q, for Surface and Embedded Flaws
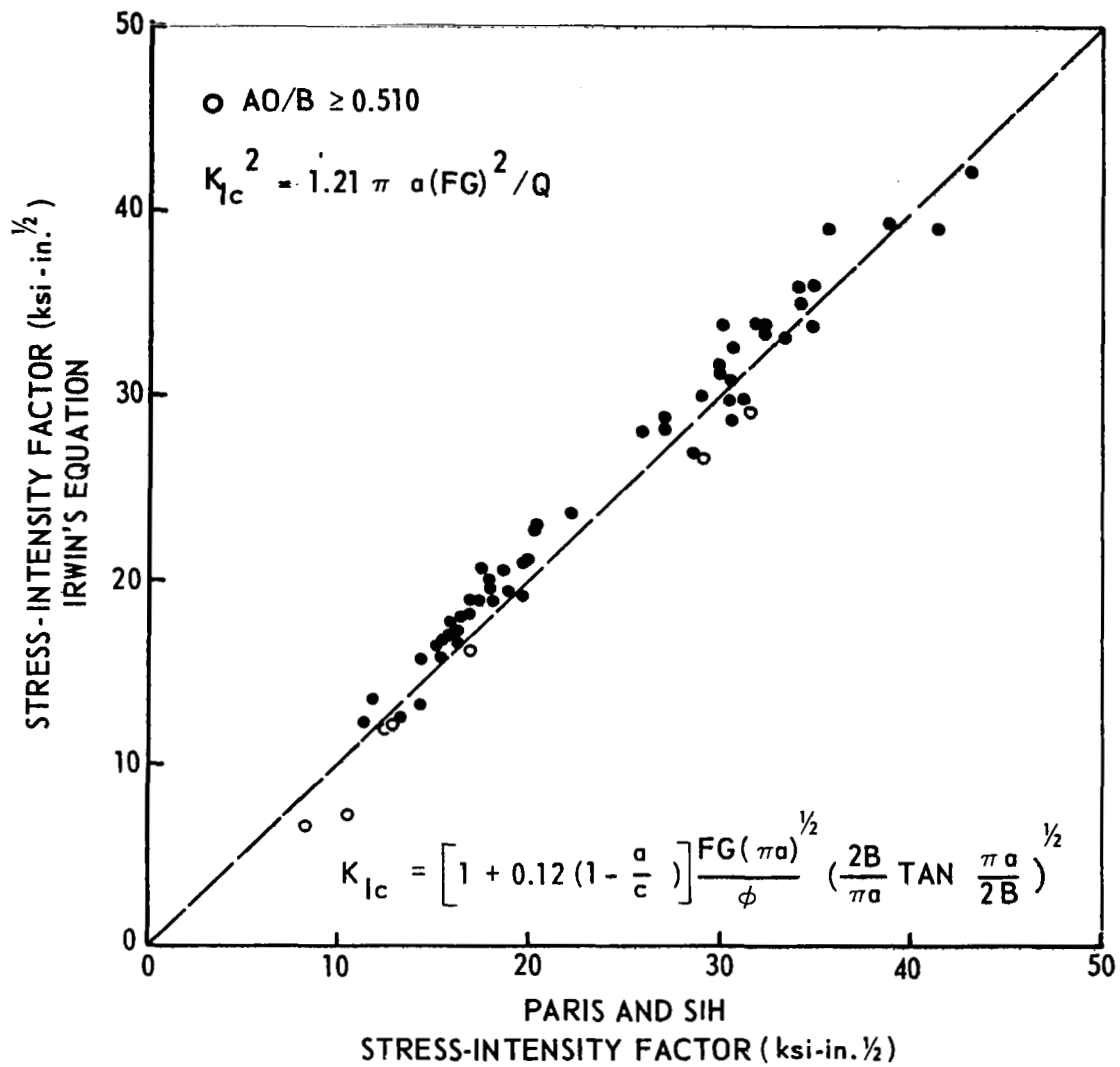
Figure 13. Comparison of the Irwin and Paris and Sih Approximations
for Calculating Stress-Intensity Factors for Surface Cracks

97
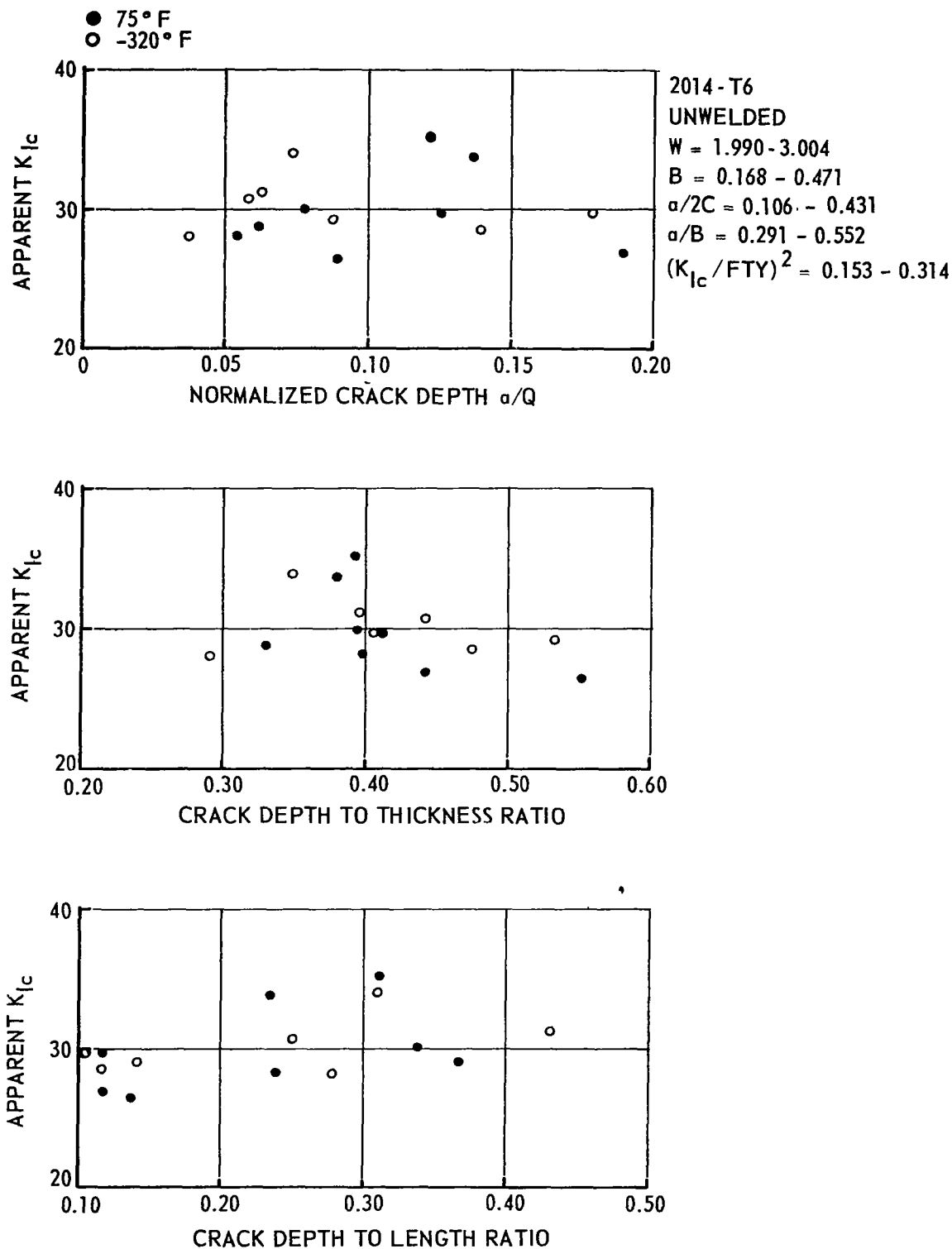
Figure 14. Effect of Crack Depth and Flaw Shape on the K_{Ic} Value
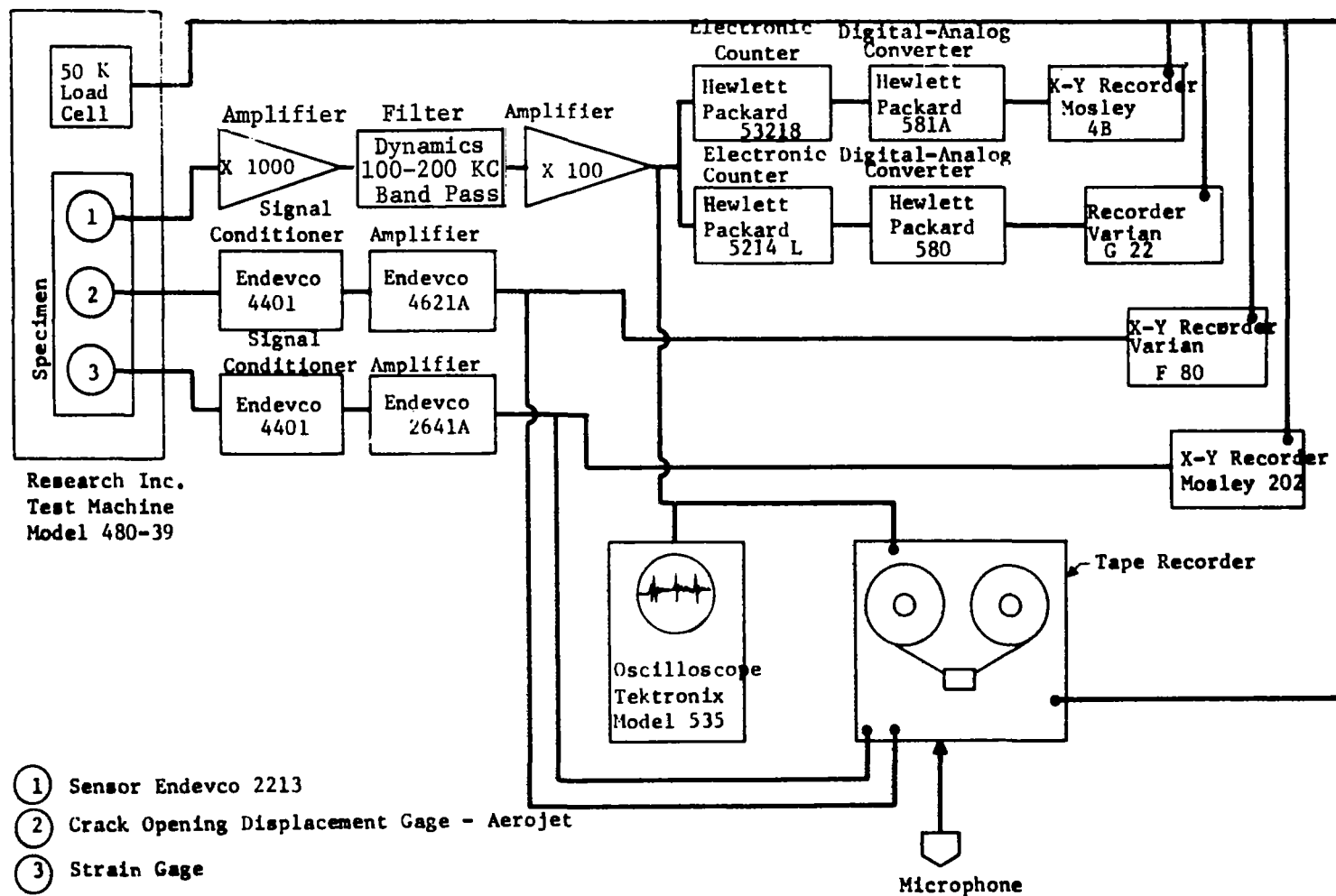
Figure 15. Schematic of Instrumentation Used for Tensile Specimens
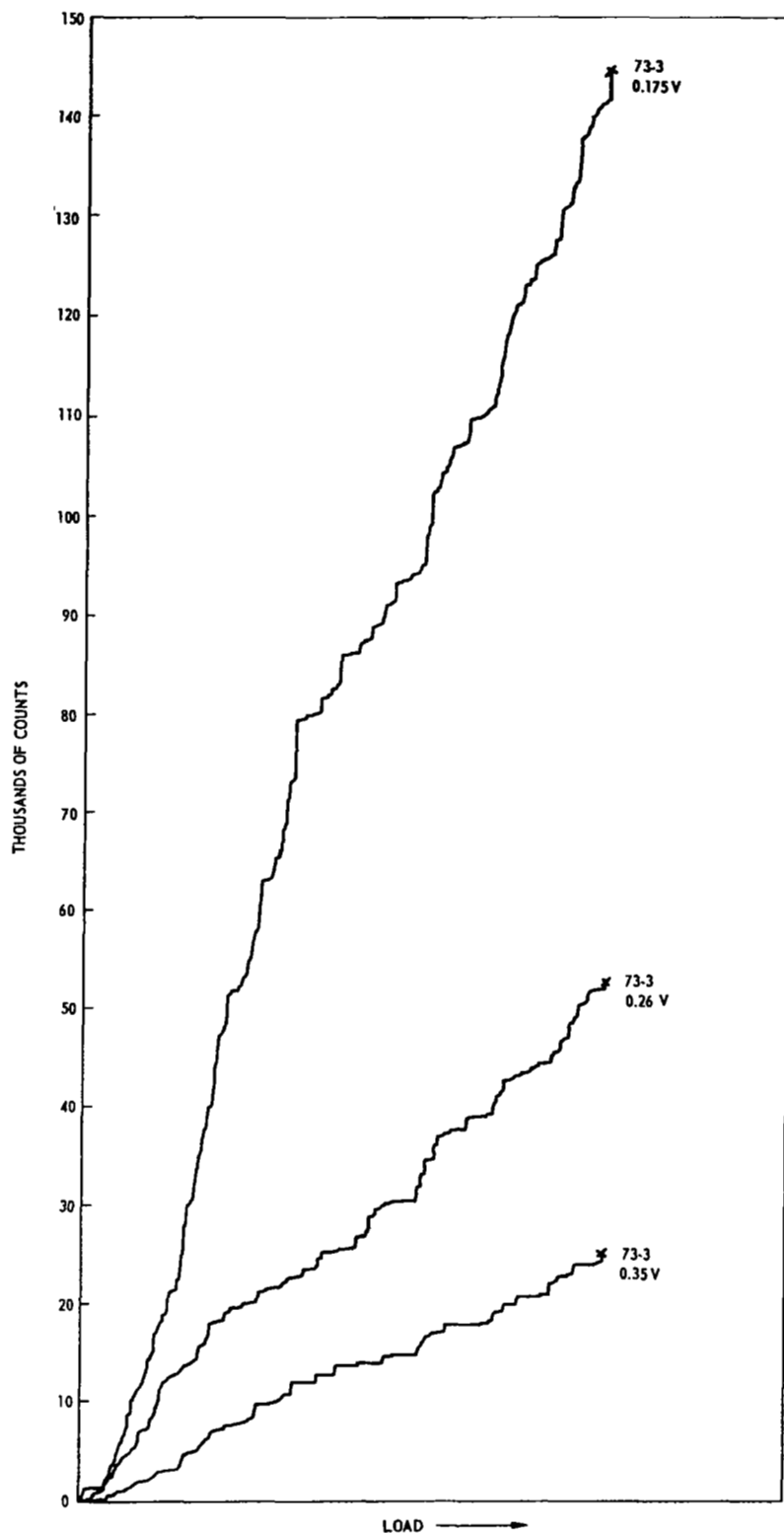
Figure 16. Effect of Counter Triggering Level on the Plot of SWE-Count vs Load. 7075-T73 Parent Metal Tested at −320°F

100
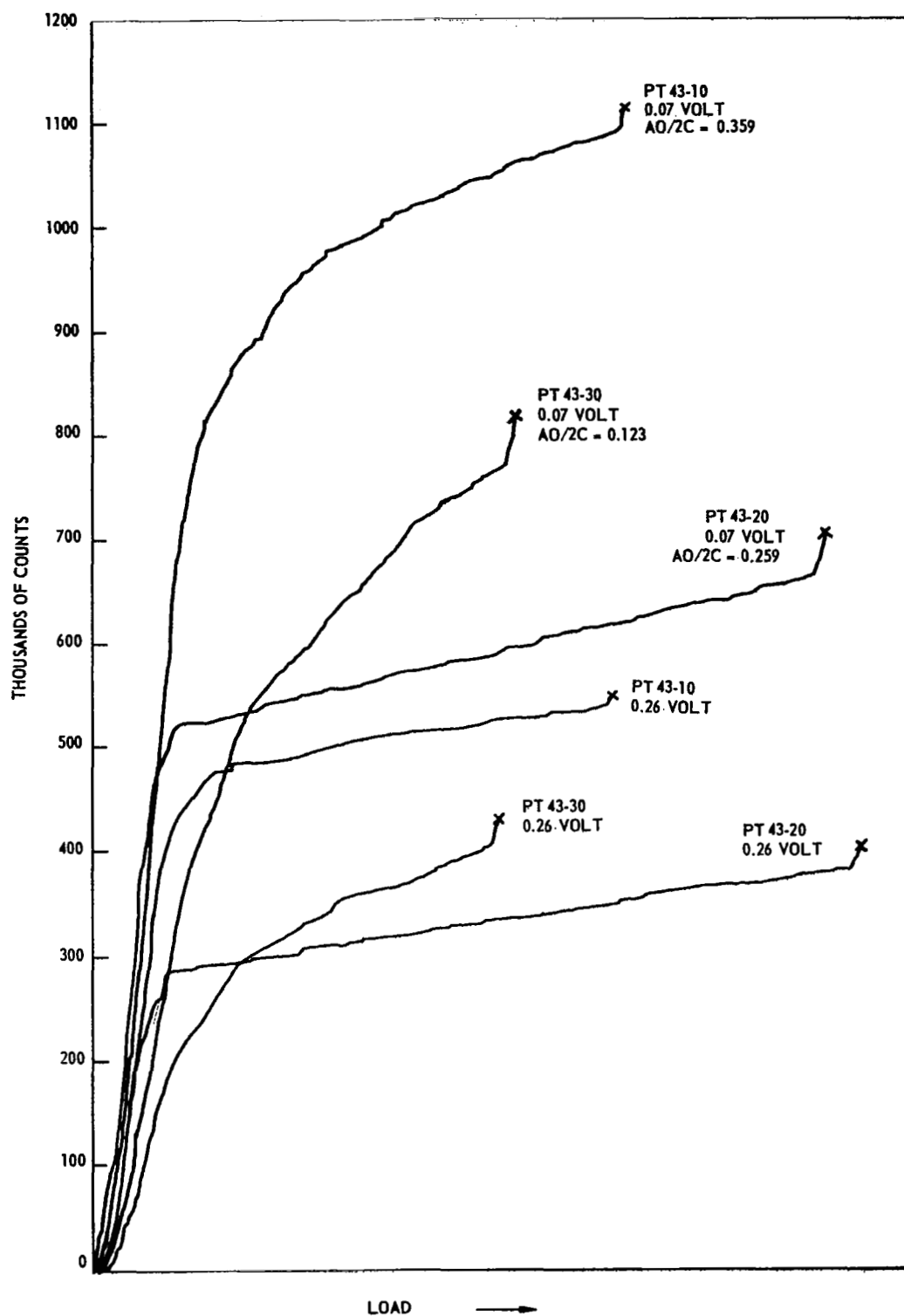
Figure 17. Effect of Triggering Level on the Plot of SWE-Count vs Load. 2014-T6 TIG-welded with 4043 Filler Wire and Tested at -423°F with Three Flaw Sizes

101
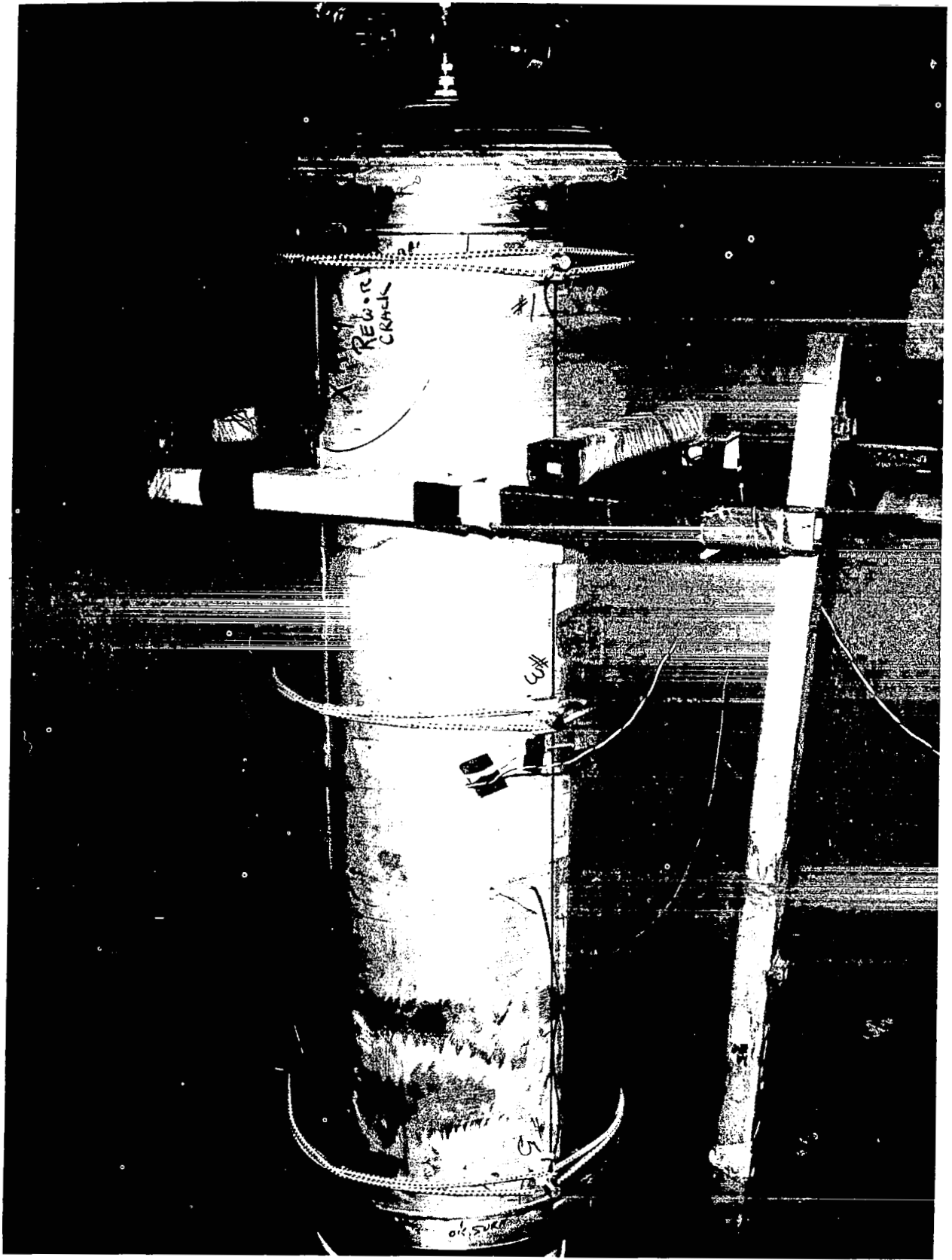
Figure 18. Pressure Vessel Test Set-up
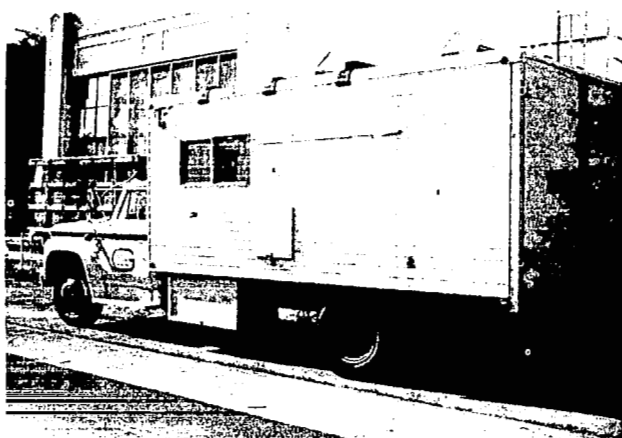
a. Truck
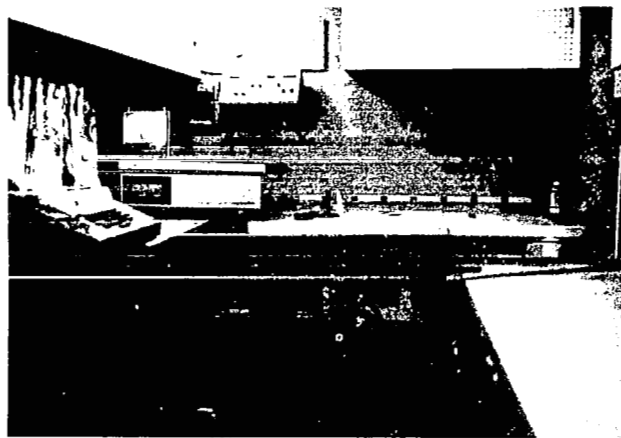
b. Forward Work Area, TV Display and Video Tape Recorder.
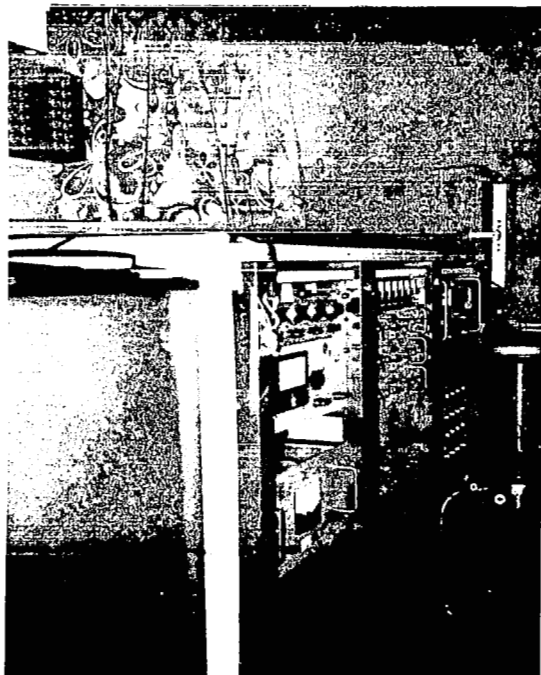
c. Rear Work Area and Instrument Racks.
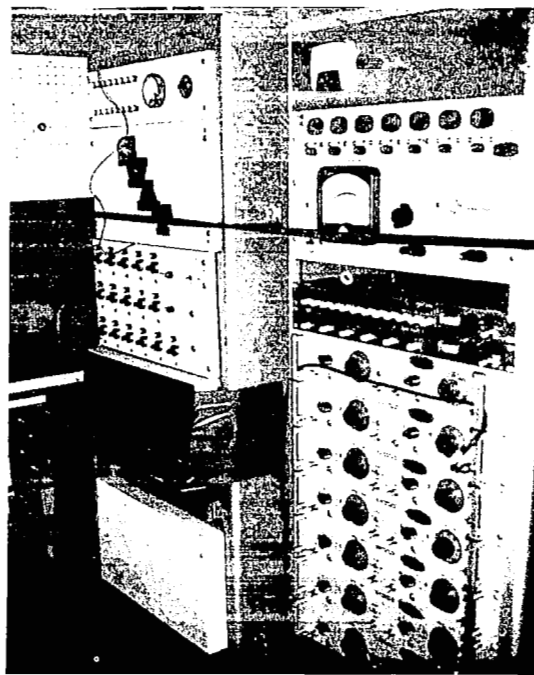
d. Computer, Data Display and Filters.

Figure 19. SWAT Mobile Test Laboratory
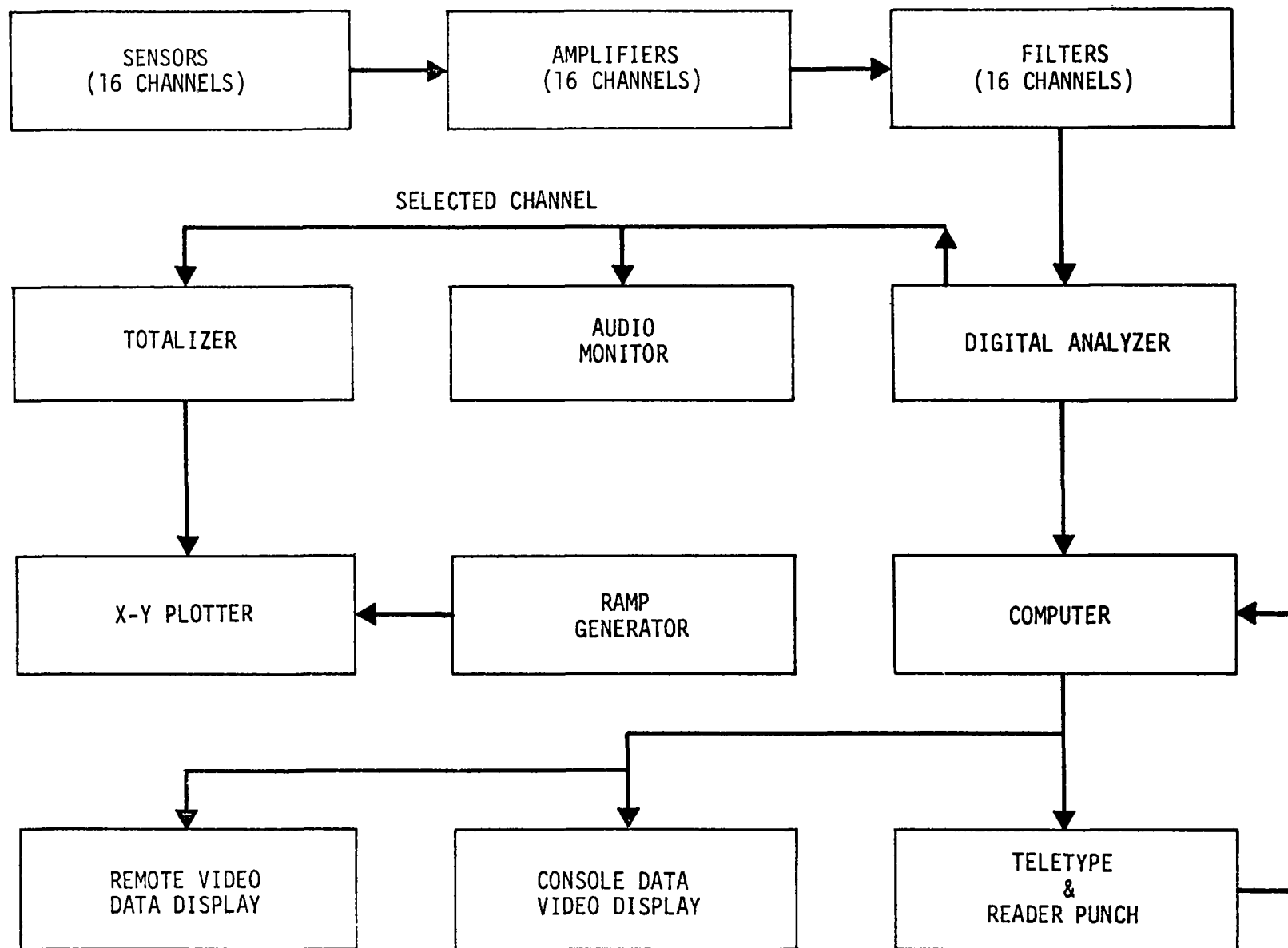
Figure 20. Schematic Diagram - Real Time Acoustic Emission Analysis and Triangulation System

OSCILLOGRAM AT 27.3 in./sec.
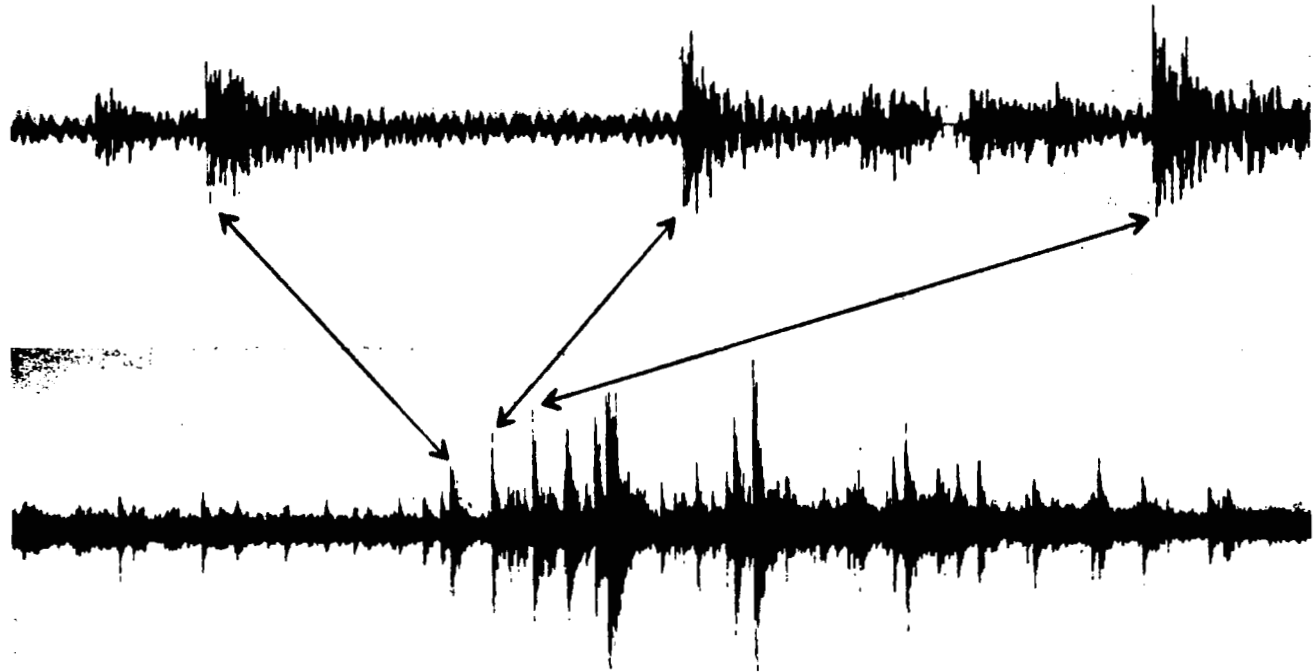
OSCILLOGRAM AT 2.5 in./sec.

NOTE: These photos illustrate typical sensor resonant ring down decay after receipt of burst type stress wave.

Figure 21. Burst Type Stress Wave Emissions
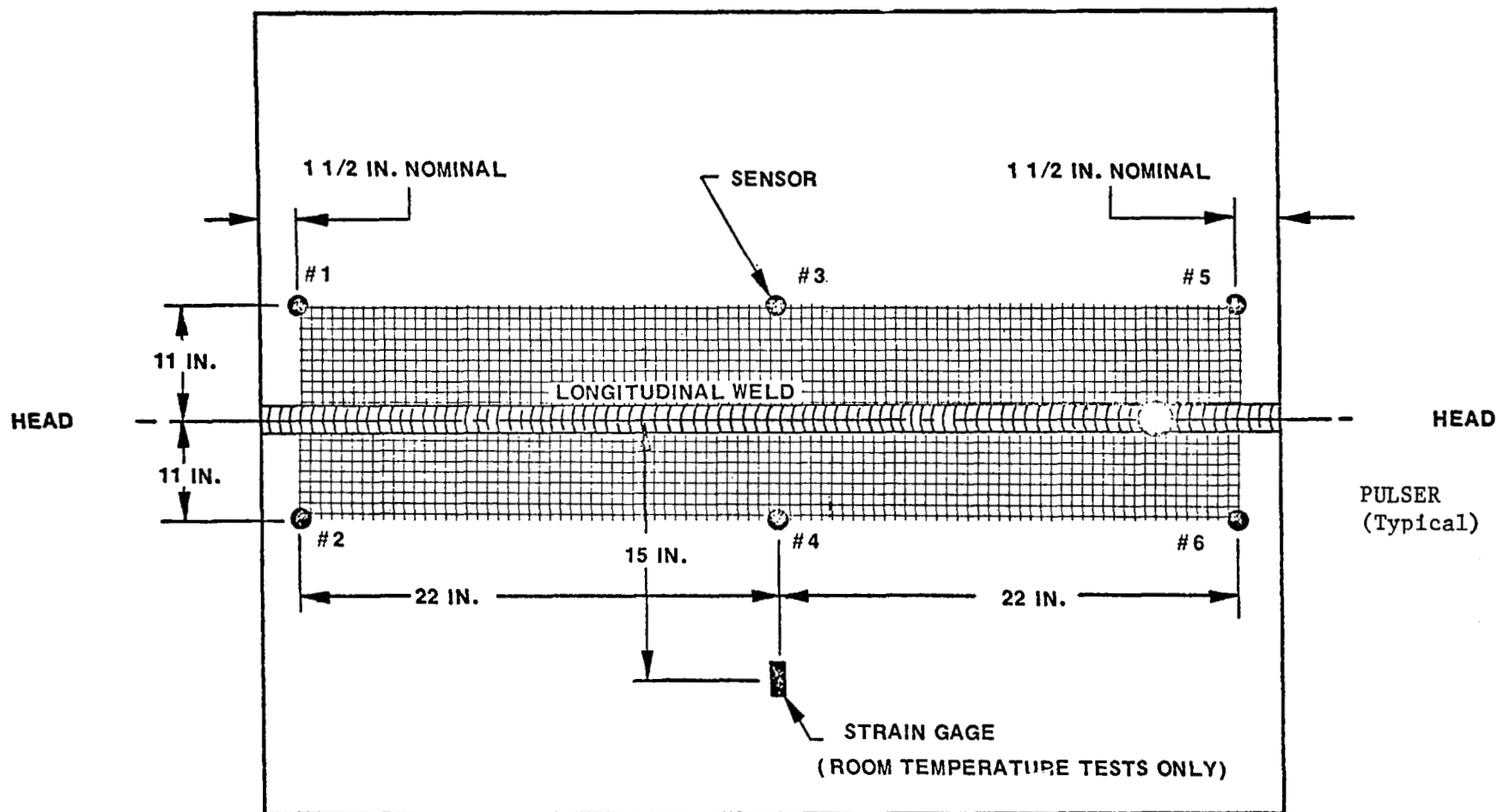
NOTE: 1. CROSSHATCHING INDICATES AREA MONITORED BY SWAT SYSTEM.

2. BECAUSE OF EXCESSIVE SENSOR DAMAGE DURING THE FIRST −320°F TEST, ONLY SENSORS 1 − 4 WERE USED FOR THE 2219 VESSEL TESTED AT −320°F. ALSO FOR THIS TEST SENSORS 1 AND 3 WERE OFFSET FROM THE WELD BY 8 INCHES AND SENSORS 2 AND 4 OFFSET FROM THE WELD BY 14 INCHES.

Figure 22. Location of Stress Wave Emission Monitoring Sensors, Strain Gage and Area Surrounding the Vessel Longitudinal Weld Which was Monitored During Hydrotest.

Figure 23.   Sensor Attached to the Pressure Vessel
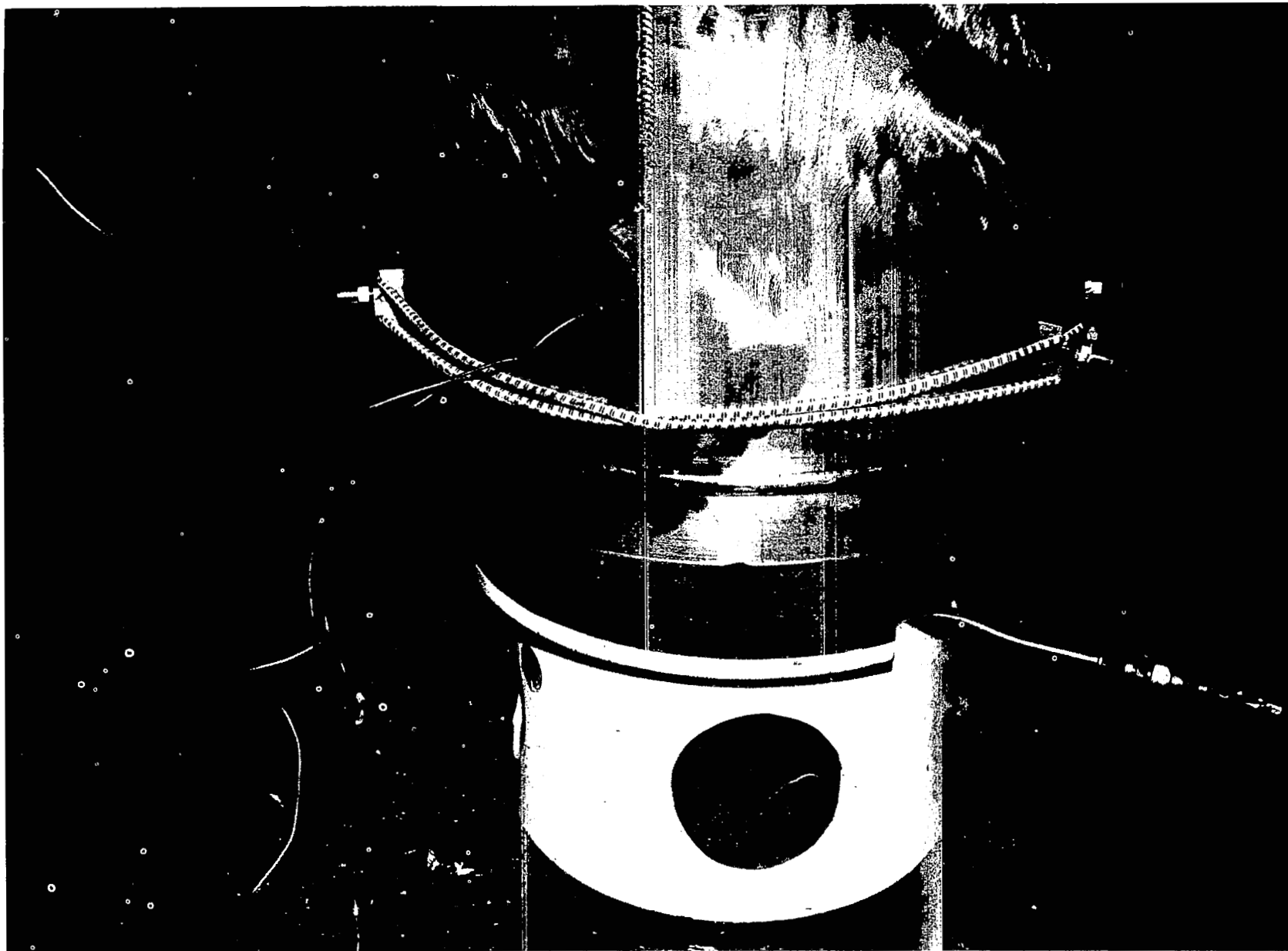
Figure 24.   Pulser Attached to the Pressure Vessel
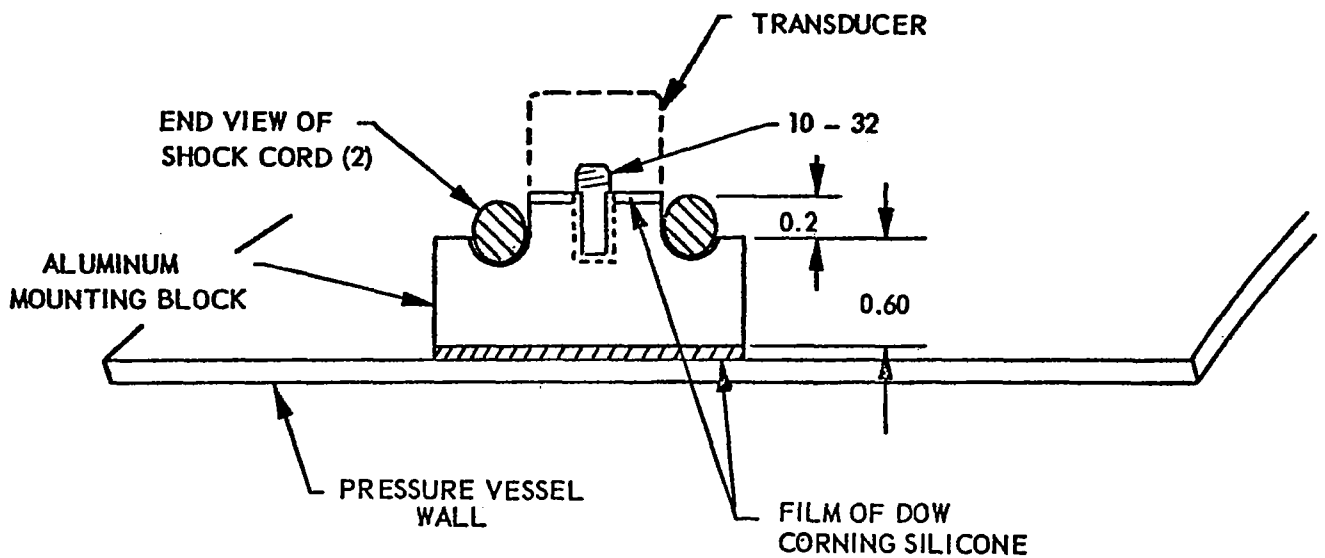
(a) SENSOR ATTACHMENT – ROOM TEMPERATURE
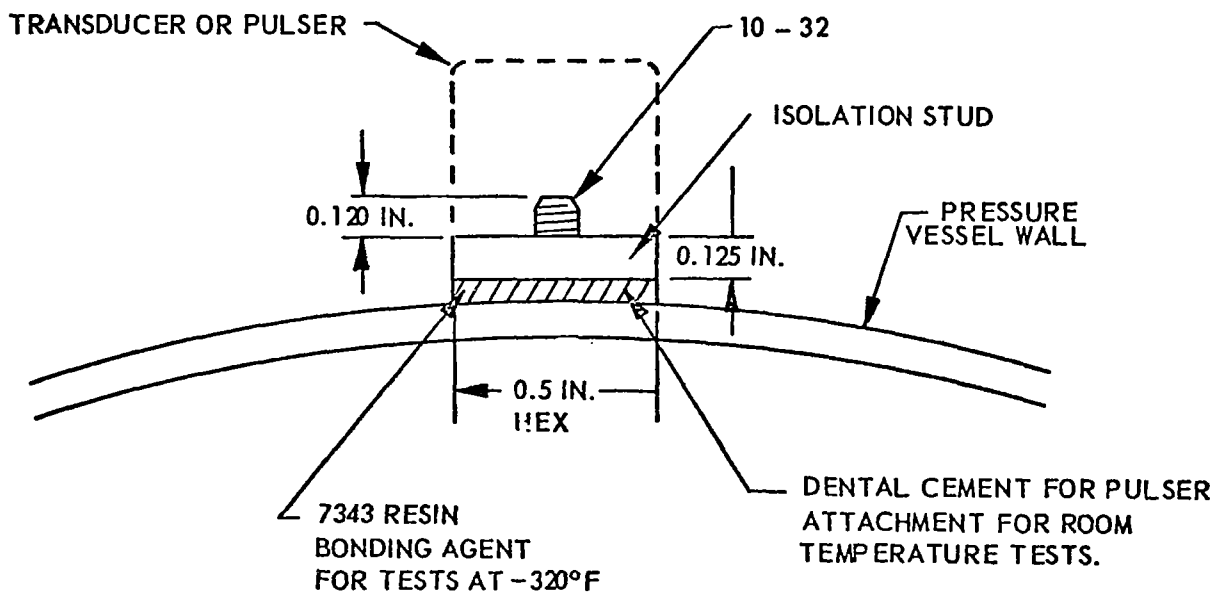
(b) SENSOR ATTACHMENT – 320°F
    PULSER ATTACHMENT – ROOM TEMPERATURE AND –320°F

Figure 25. Schematic Representation of Sensor and Pulser Mounting
Techniques Used for Vessel Hydrotest.

109
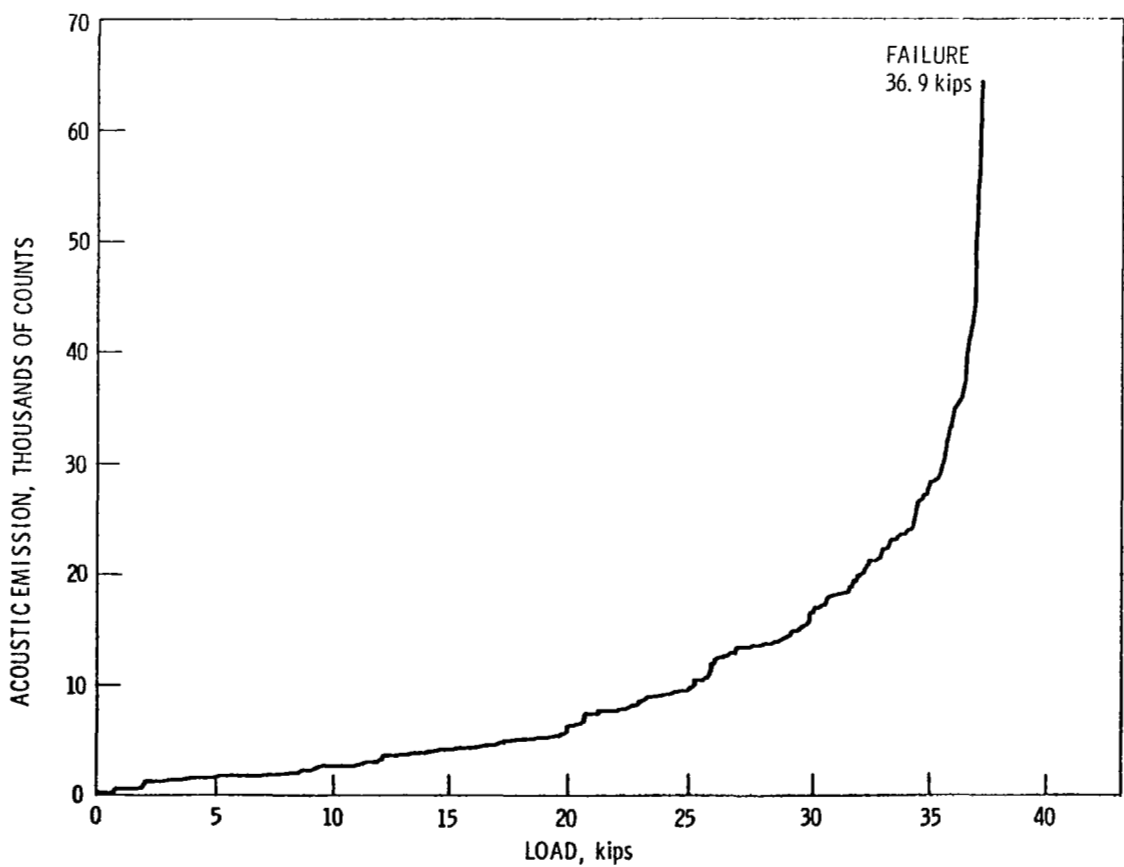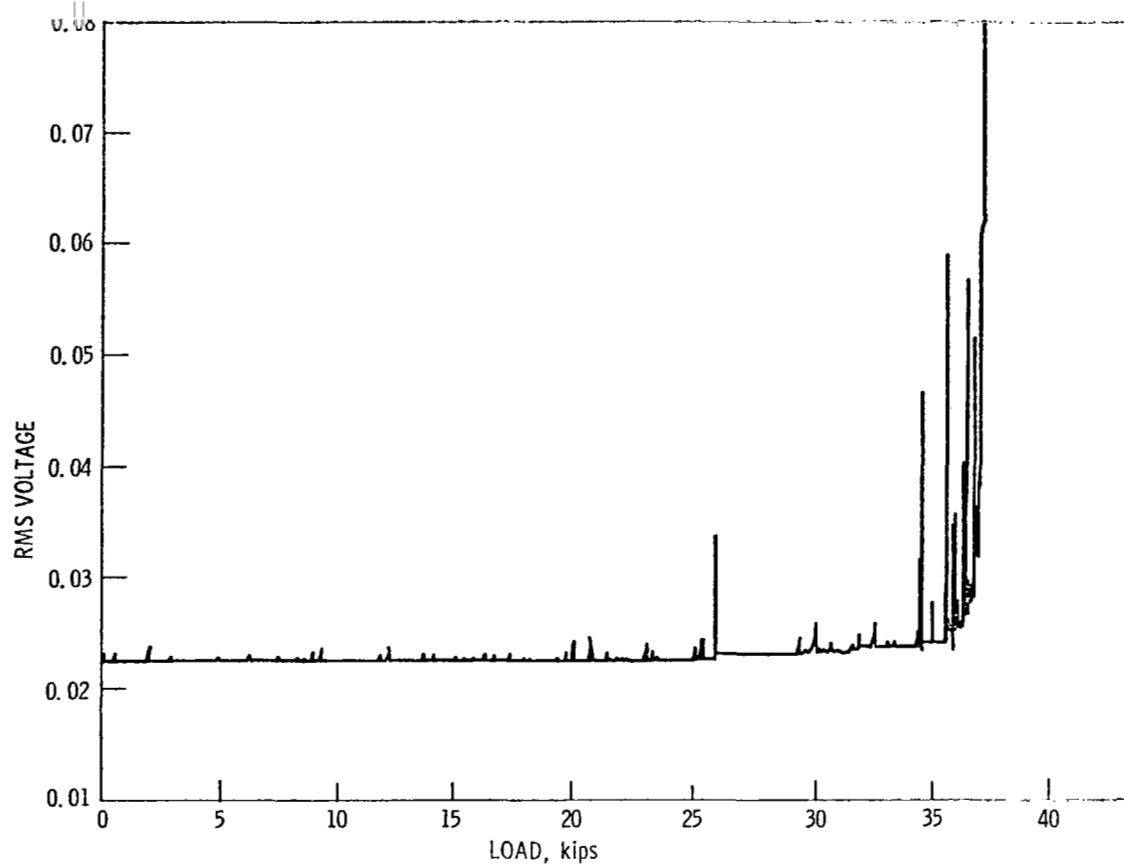
Figure 26.   Precursor of Plane Strain Fracture of 2014-T6 PTC-Tension
Specimen No. 2 Tested at Room Temperature.
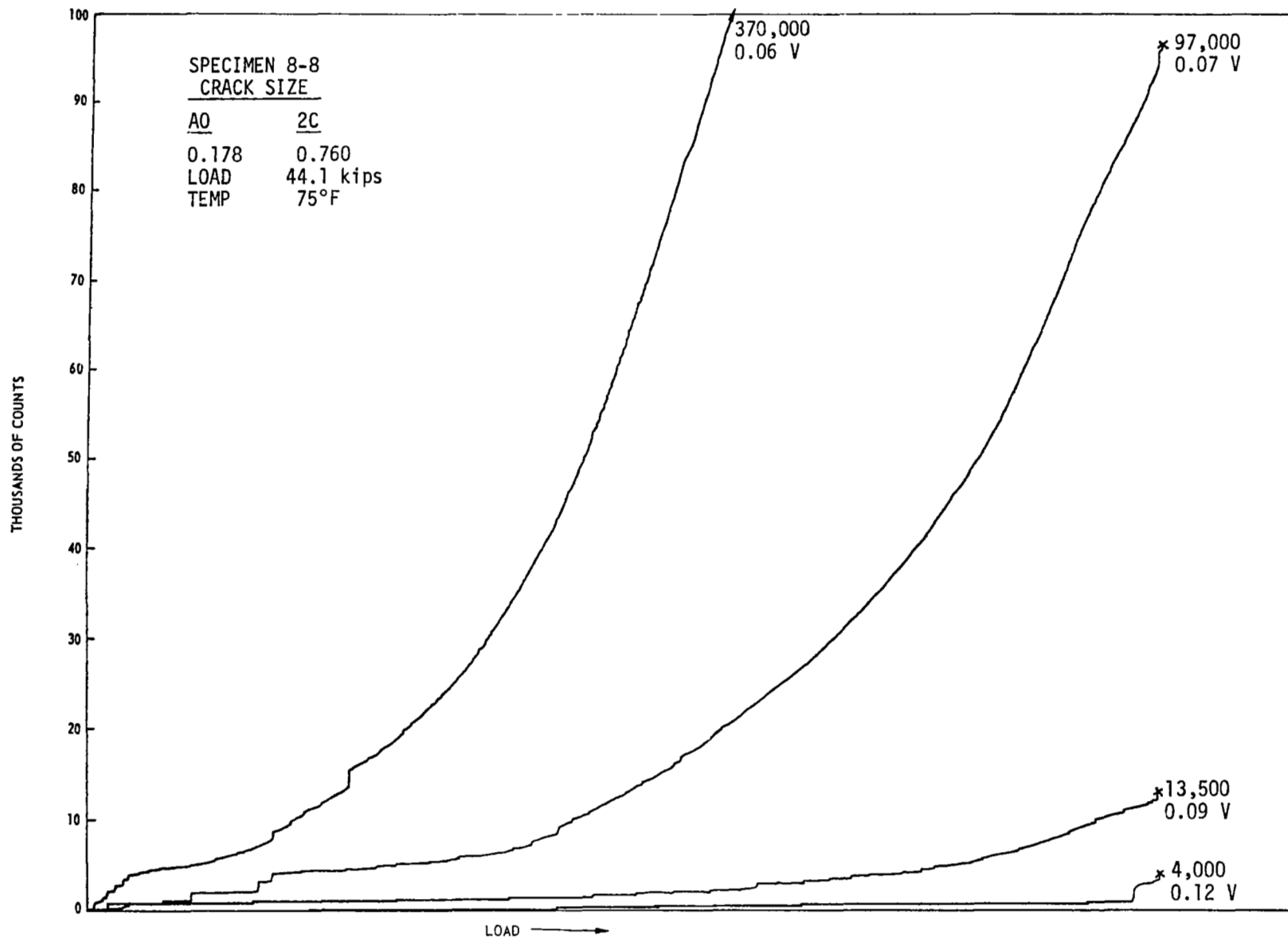
Figure 27. Effect of Trigger Level on SWE Precursor in 2014-T6 Tested at 75°F.

111
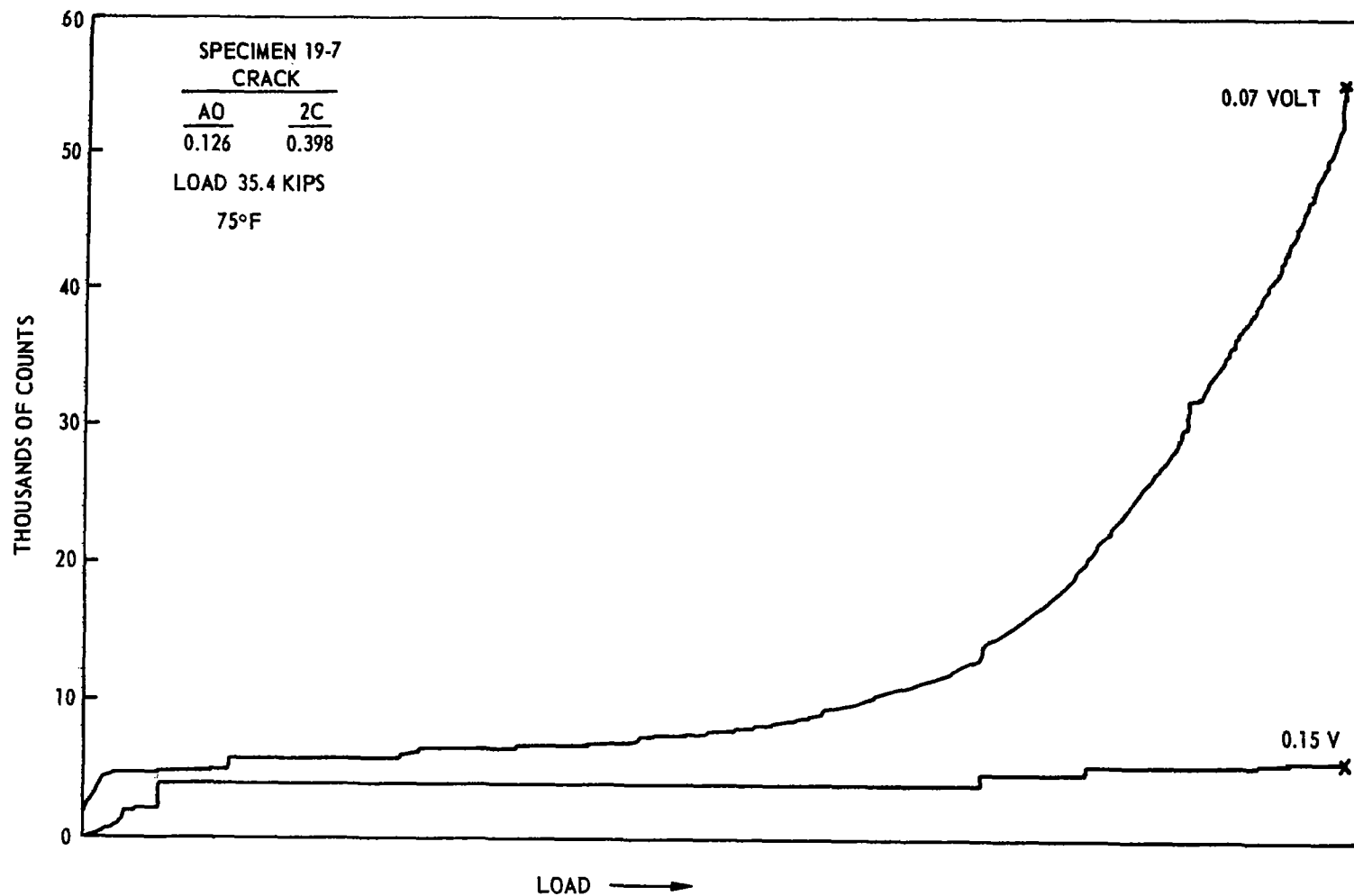
Figure 28. Effect of Trigger Level on SWE Precursor in 2219–T87
Tested at 75°F

NEAR START OF LOADING NEAR FAILURE

SPECIMEN 4-2

75°F

SPECIMEN 8-4

-320°F

113
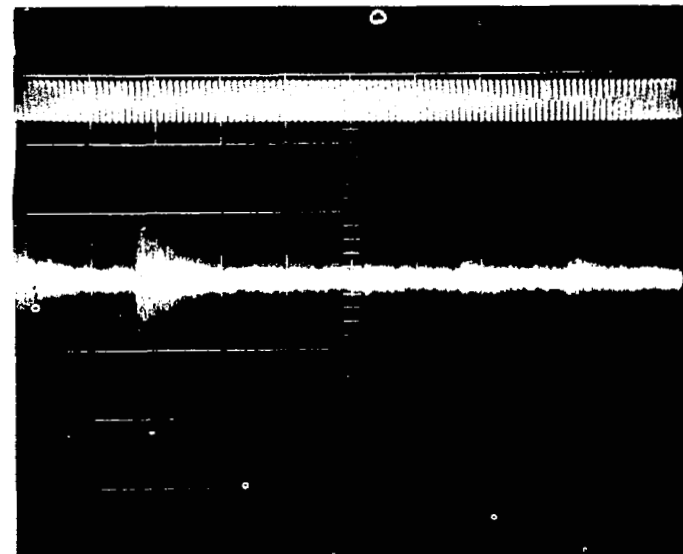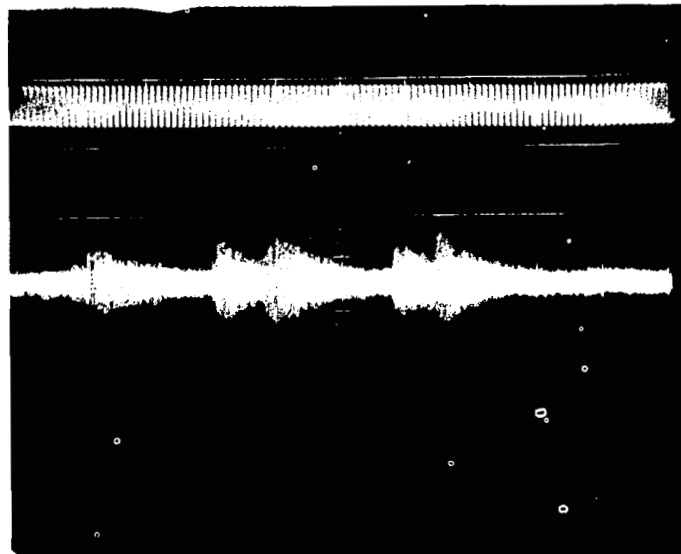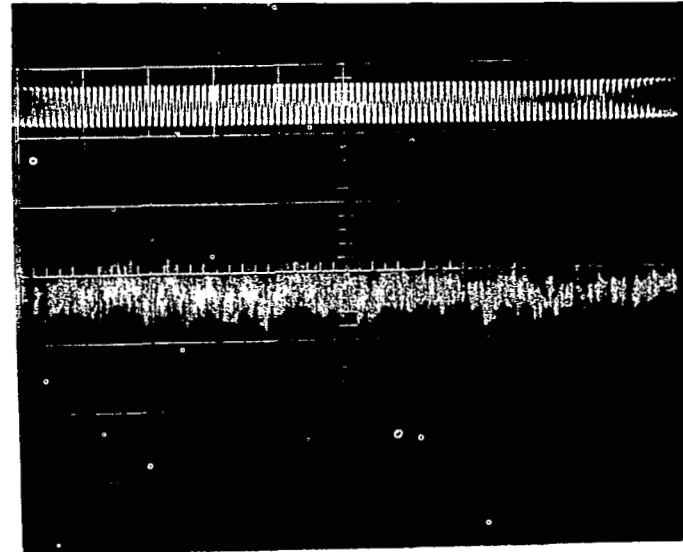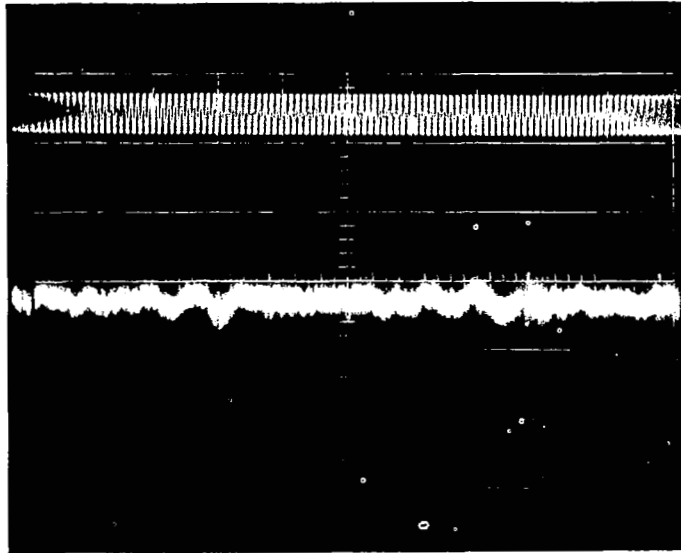
Figure 29. Background "Noise" Levels at the Start and End of PTC Tension
Tests at 75 and -320°F. 2014-T6 Parent Metal with Surface
Flaws.
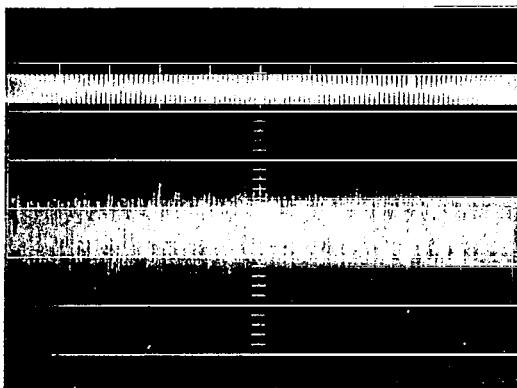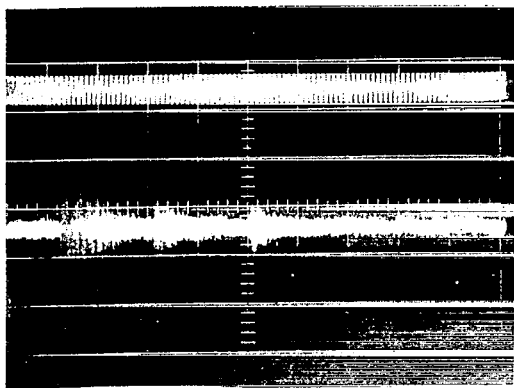
PT 43-23   75°F
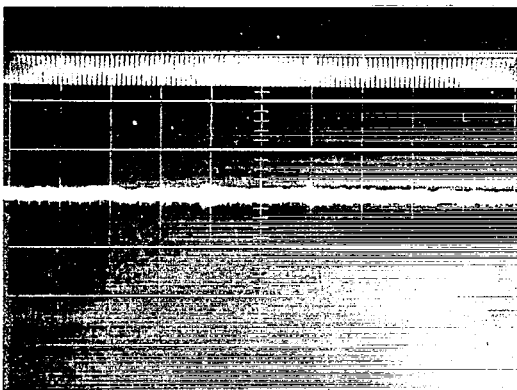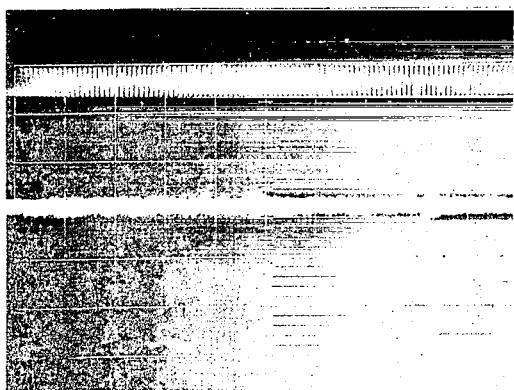
PT43-43   ~320°F
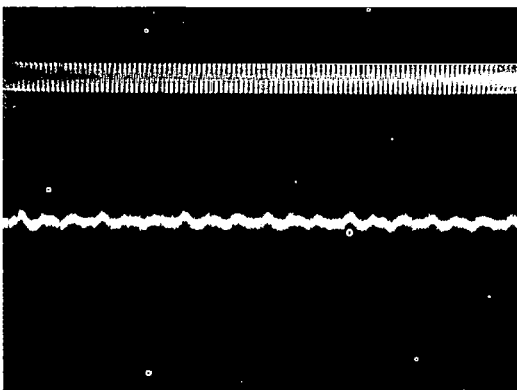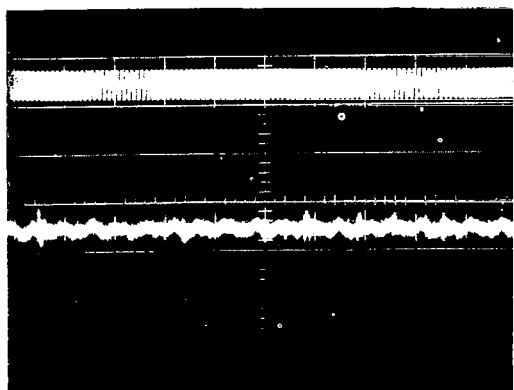
PT 43-10   -423°F

Figure 30.   Background "Noise" Levels at the Start and End of PTC Tension
             Tests at 75, -320 and 423°F.   2014-T6 TIG Welded with 4043 Wire.

114
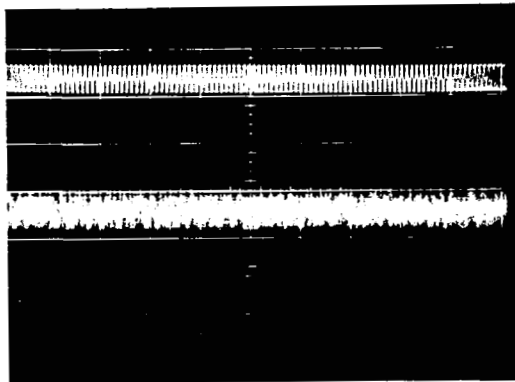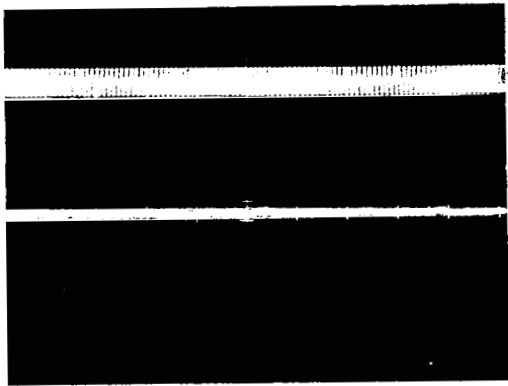
T43-2   75°F
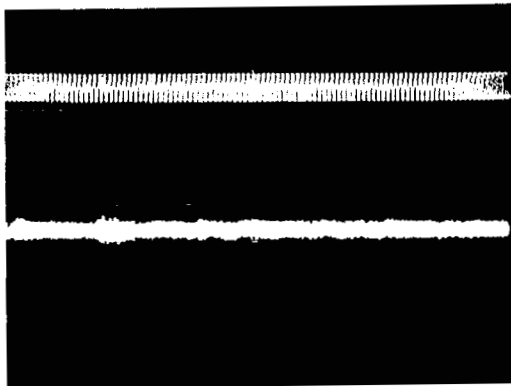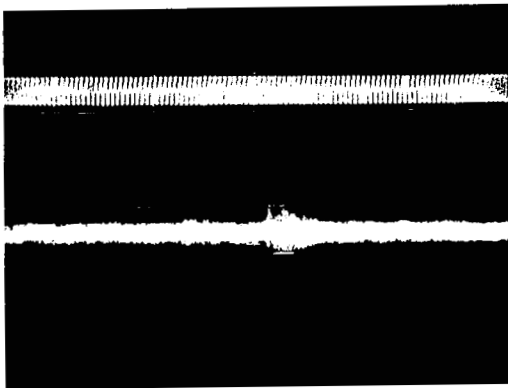
T43-4   -320°F
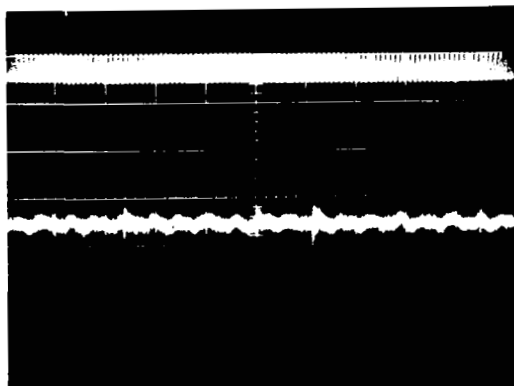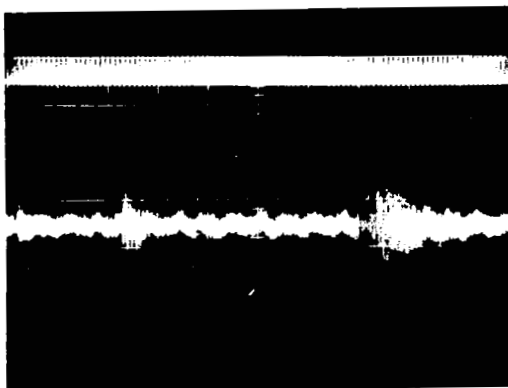
T43-5   -423°F

Figure 31.   Background "Noise" Levels at the Start and End of Tension
             Tests at 75, -320 and -423°F.   With no Deliberate Flaws.
             2014-T6 TIG Welded with 4043 Wire
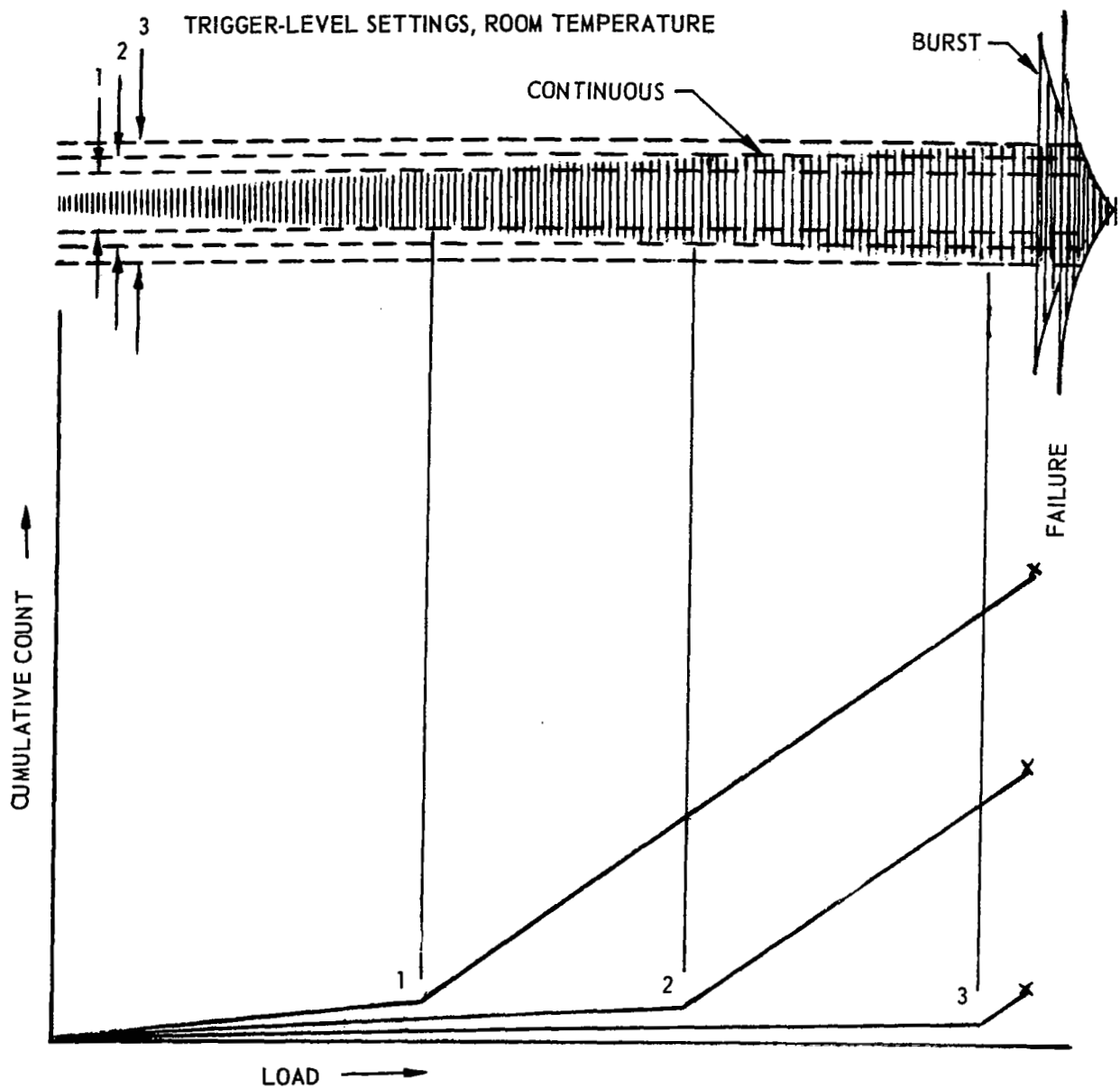
Figure 32. Schematic of the Effect of Trigger-Level Setting on the Precursor (Room-Temperature Test)

116
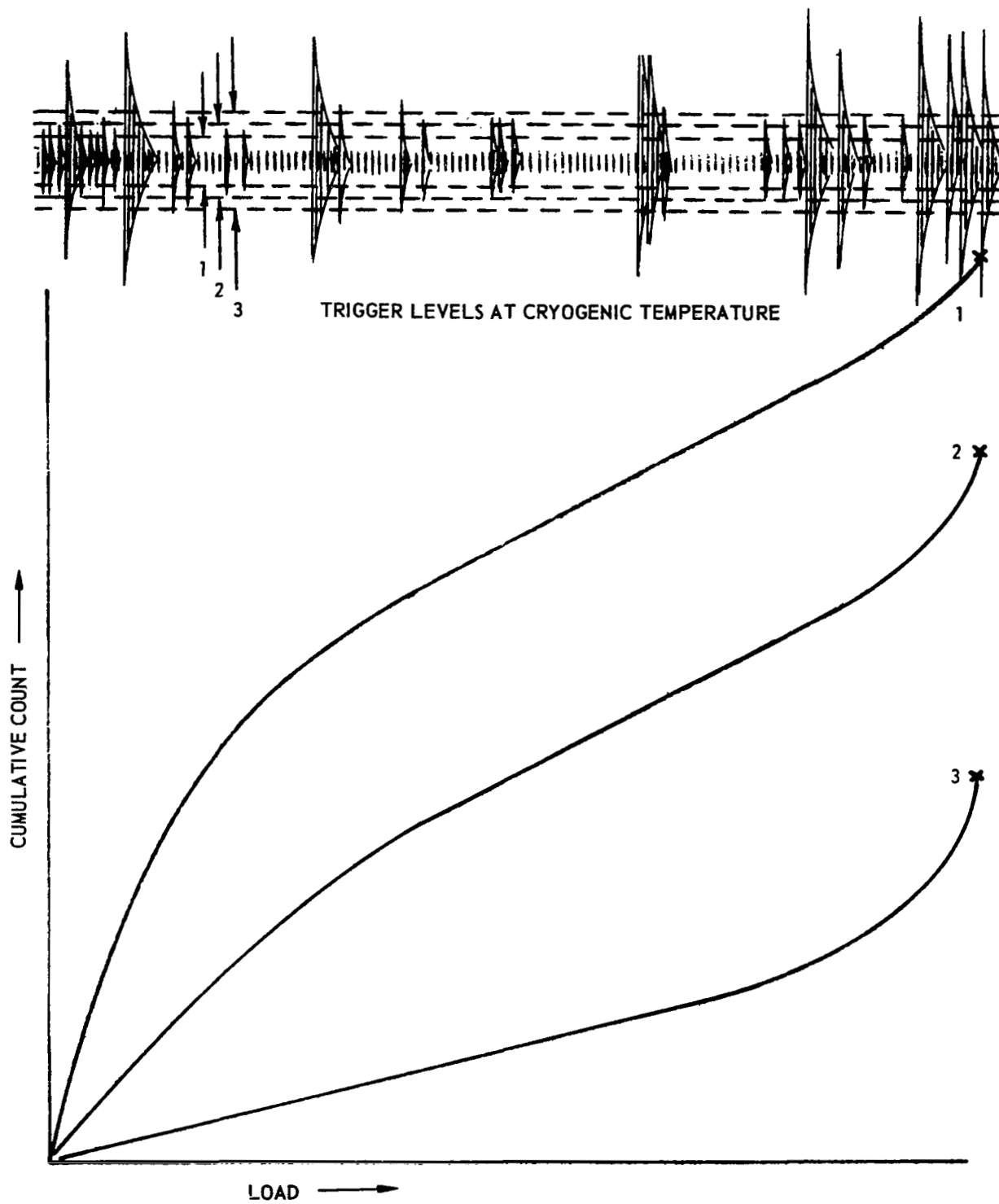
Figure 33. Schematic of the Effect of Trigger-Level Setting on the Precursor at Cryogenic Temperature.
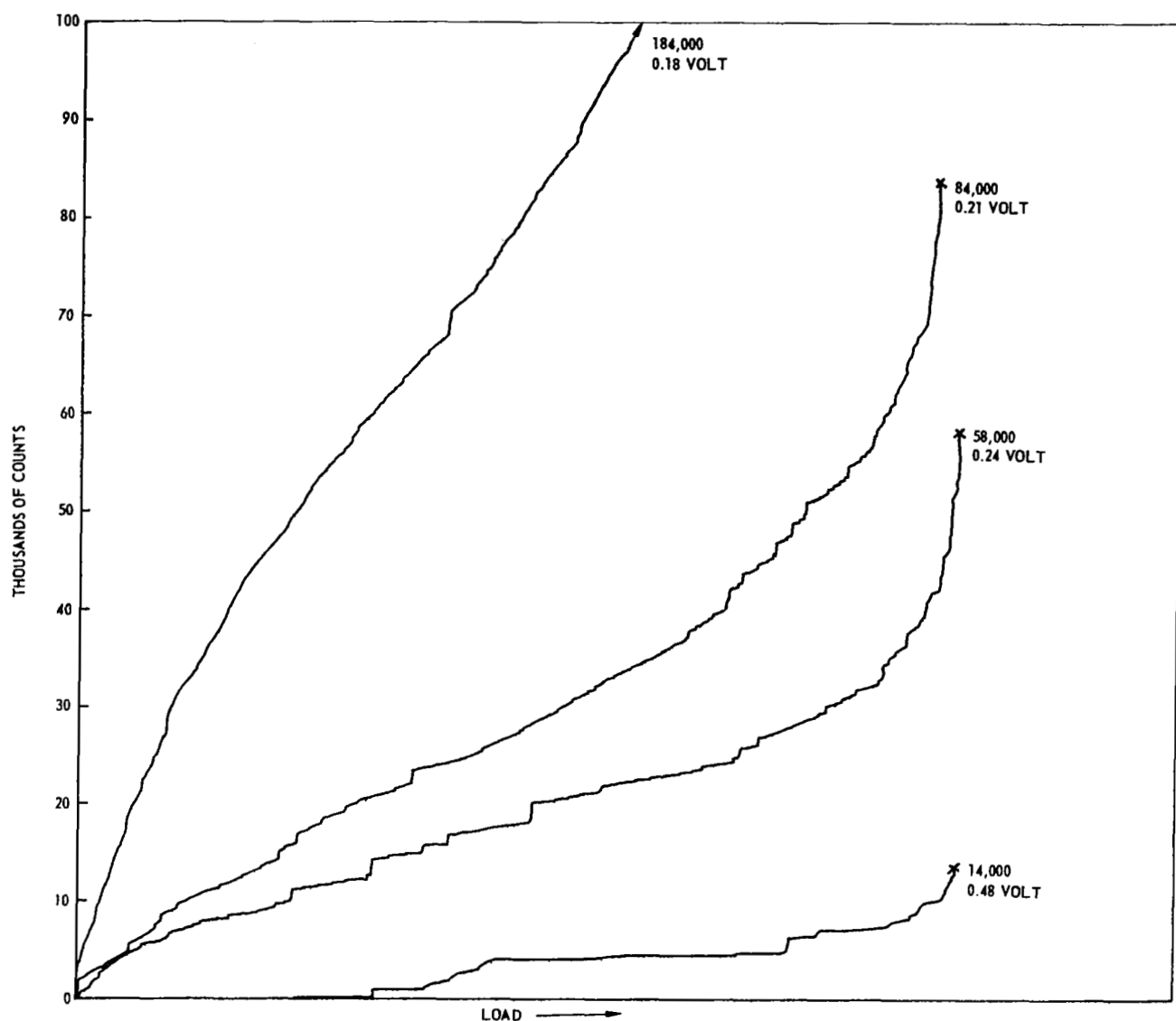
Figure 34. Effect of Trigger Level on Precursor at -320°F. 7075-T73 Unwelded

118
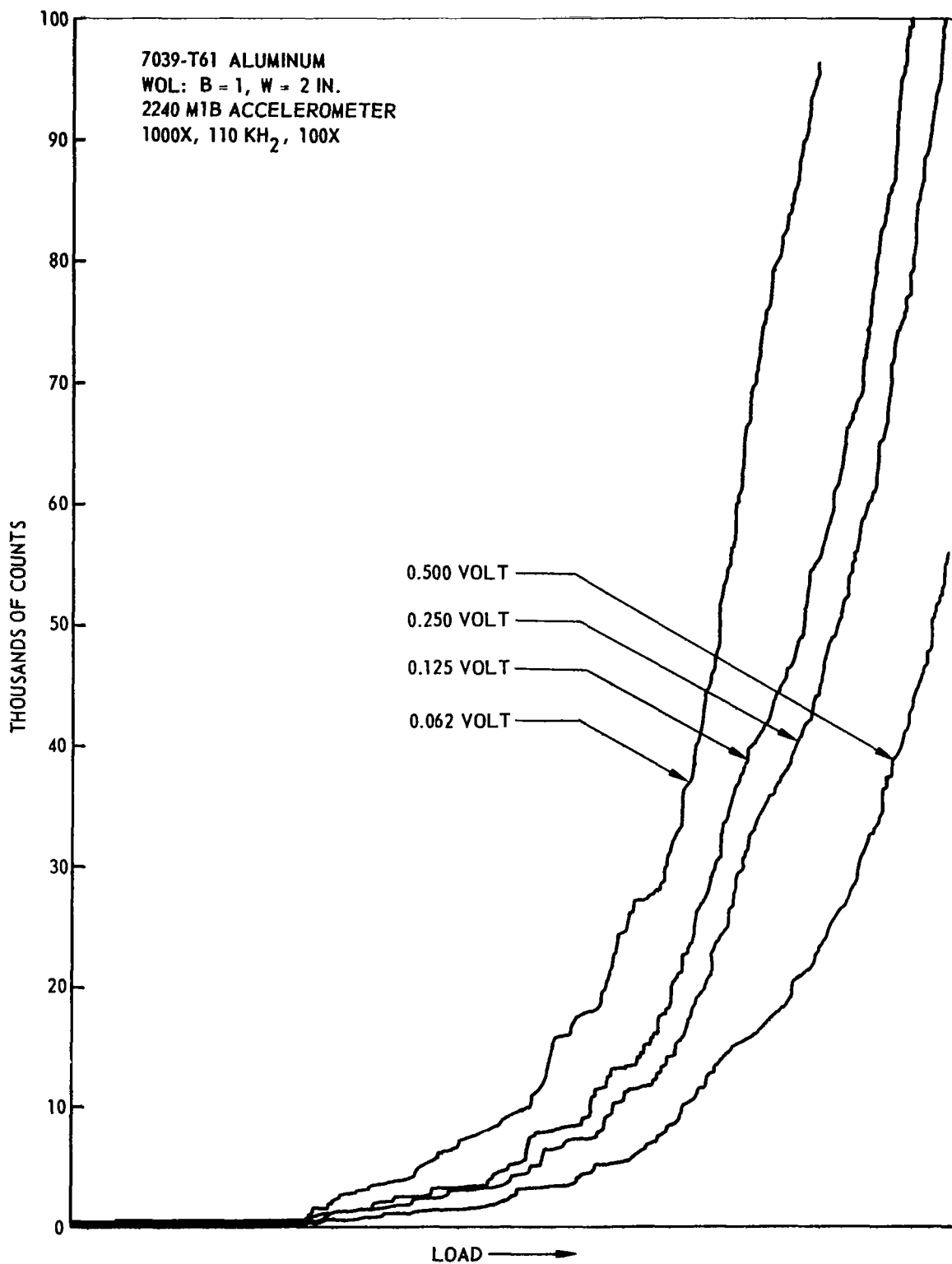
Figure 35. SWE Precursor in a 7039-T61 WOL Tension Specimen. Note the Effect of Trigger Level

119
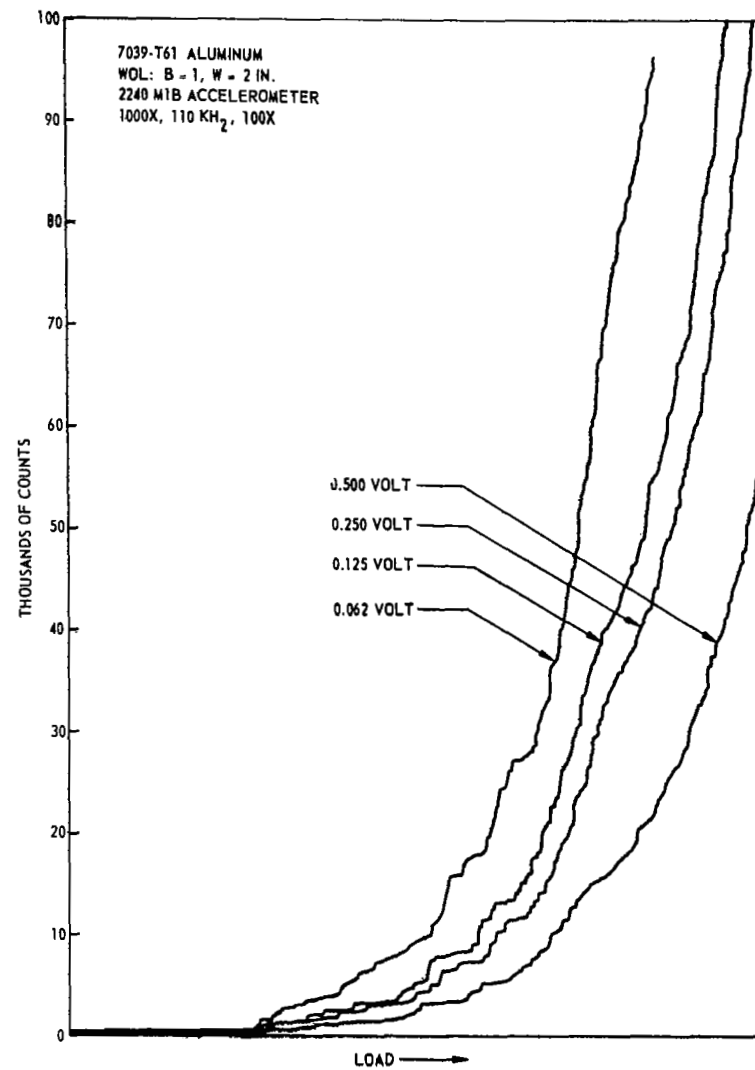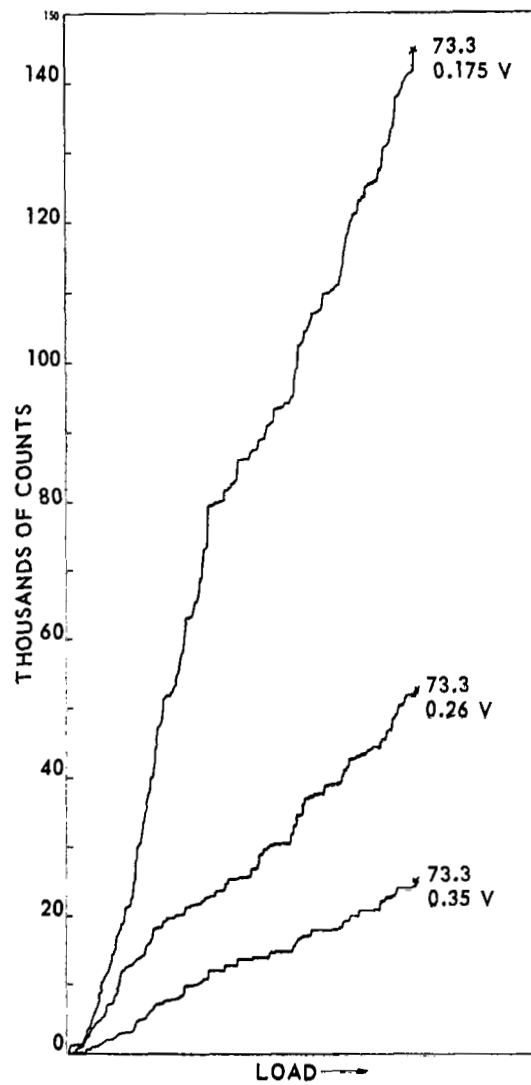
Figure 36. Comparison of PTC and WOL Tension Tests at -320°F
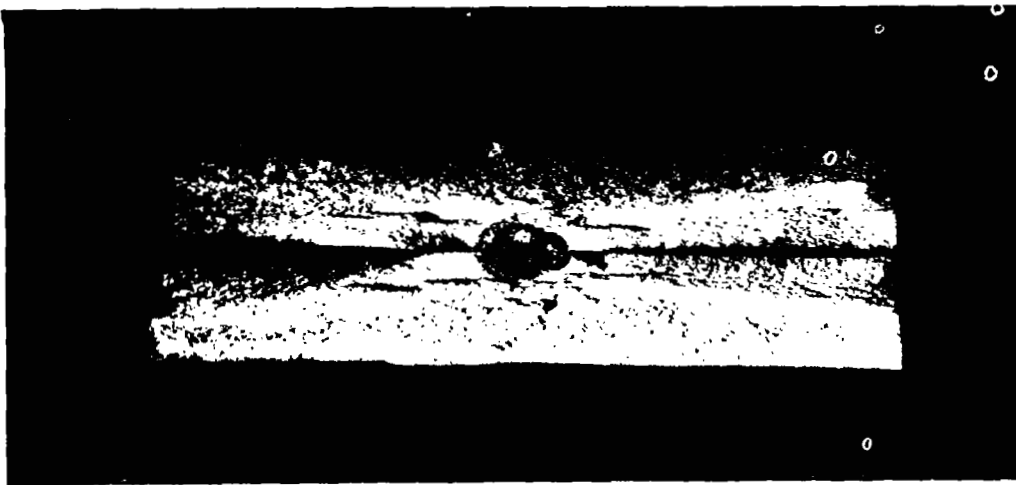
73-6
3,310,000
COUNT AT
0.32 VOLT.

SEVERE
TRANSVERSE
CRACKING
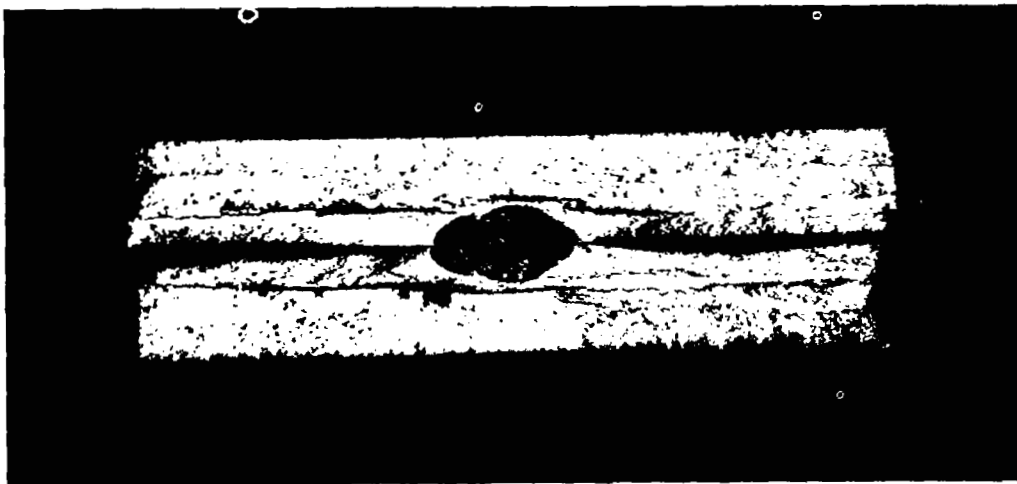
73-7
3,300,000
COUNT AT
0.32 VOLT.

SEVERE
TRANSVERSE
CRACKING
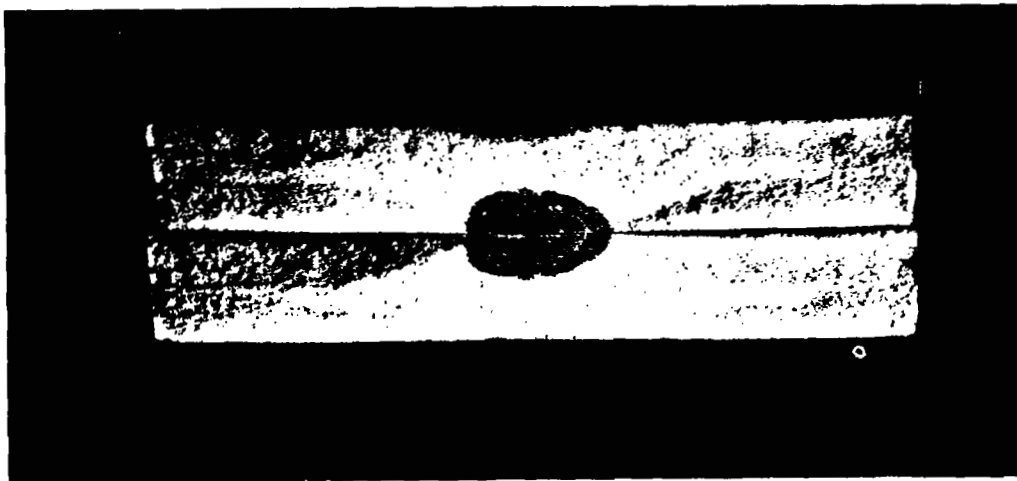
73-10
212,500
COUNT AT
0.07 VOLT.

NO
TRANSVERSE
CRACKING

Figure 37.   Effect of Delamination-Type Flaws on SWE Count for Tests
at 75°F.   7075-T73 Parent Metal Tested at -320°F.
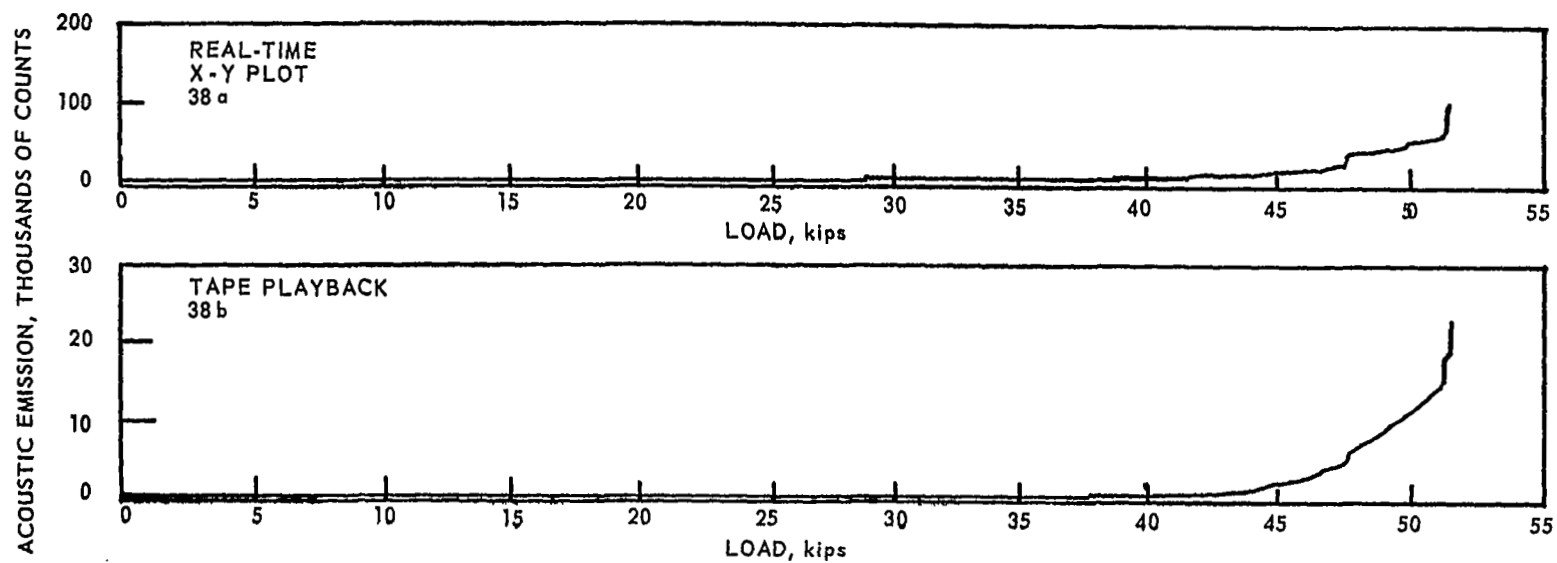
Figure 38. Effect of Tape Playback on Cumulative Count in 2219-T87 Specimen No. 32 Tested at -320°F.
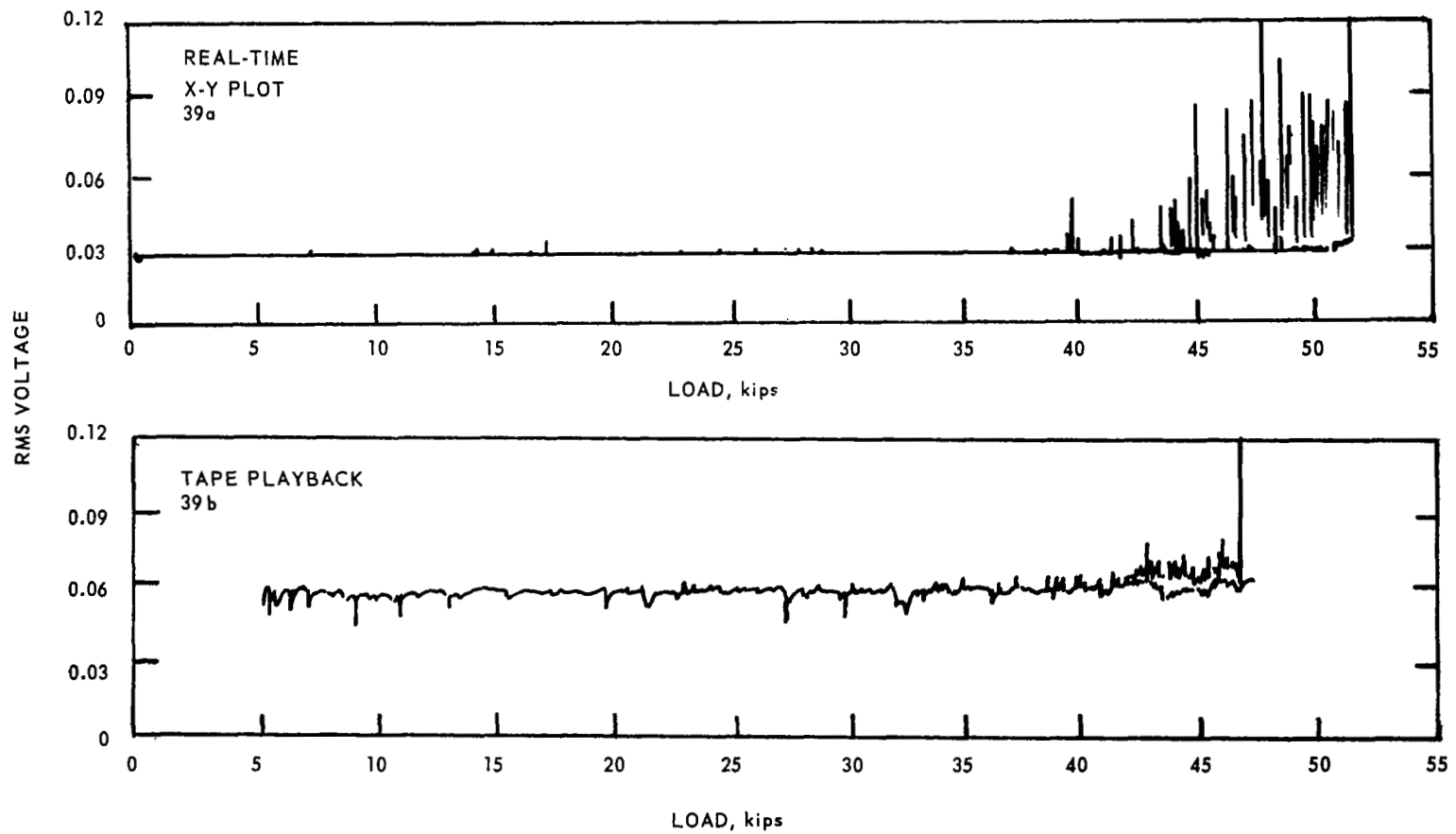
Figure 39. Effect of Tape Playback on the RMS-Voltage Precursor
(Same test as Figure 38).
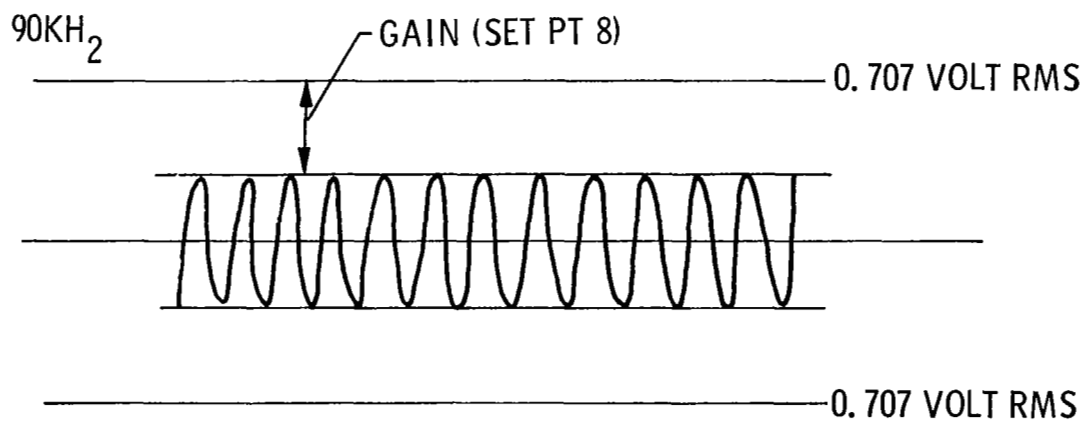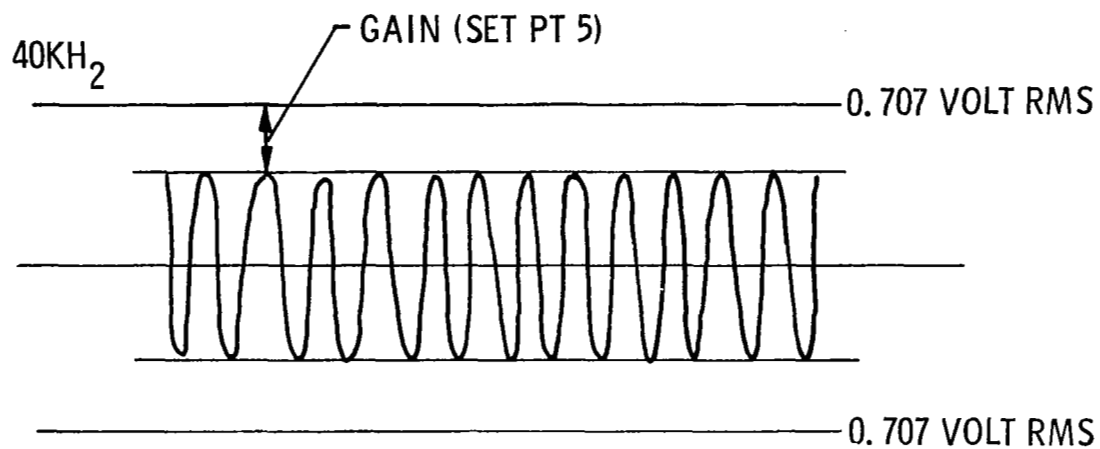
Figure 40. Dunegan System (Constant Trigger Level - 1 Volt)
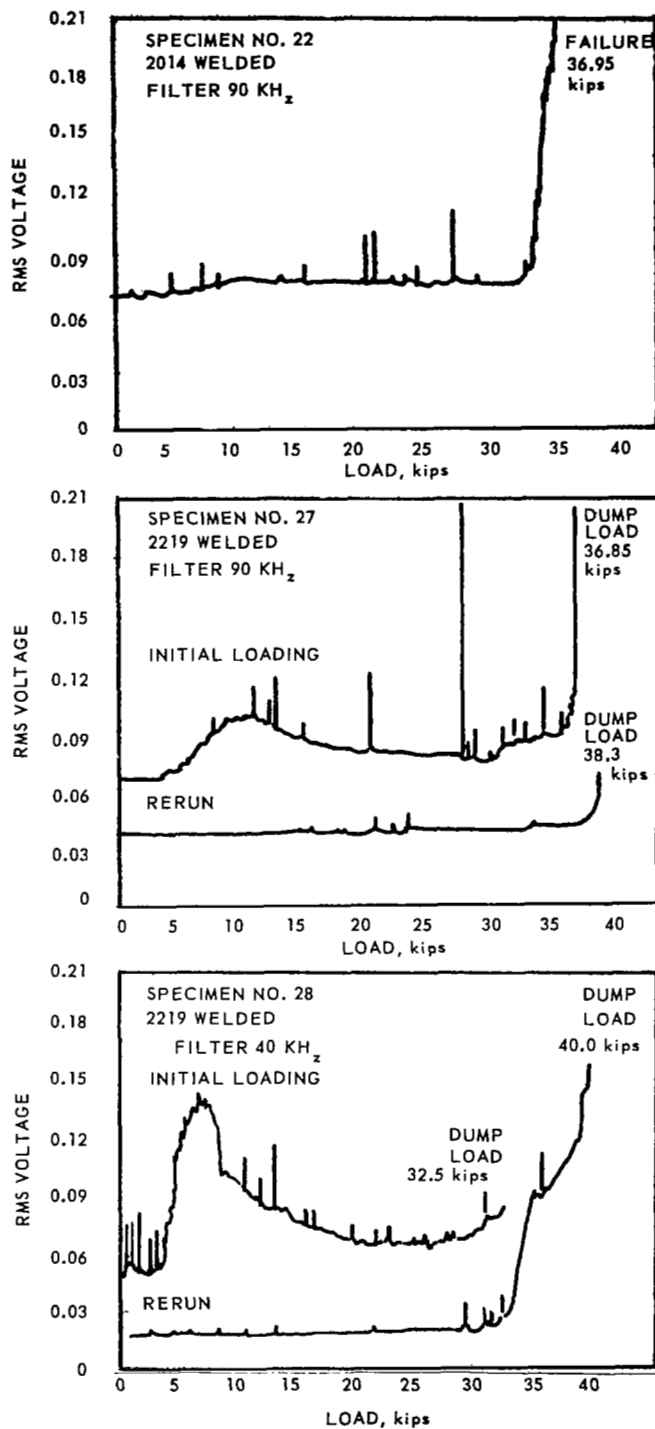
Figure 41. Kaiser Effect in Longitudinally Welded, Unnotched, Tension Specimen

125
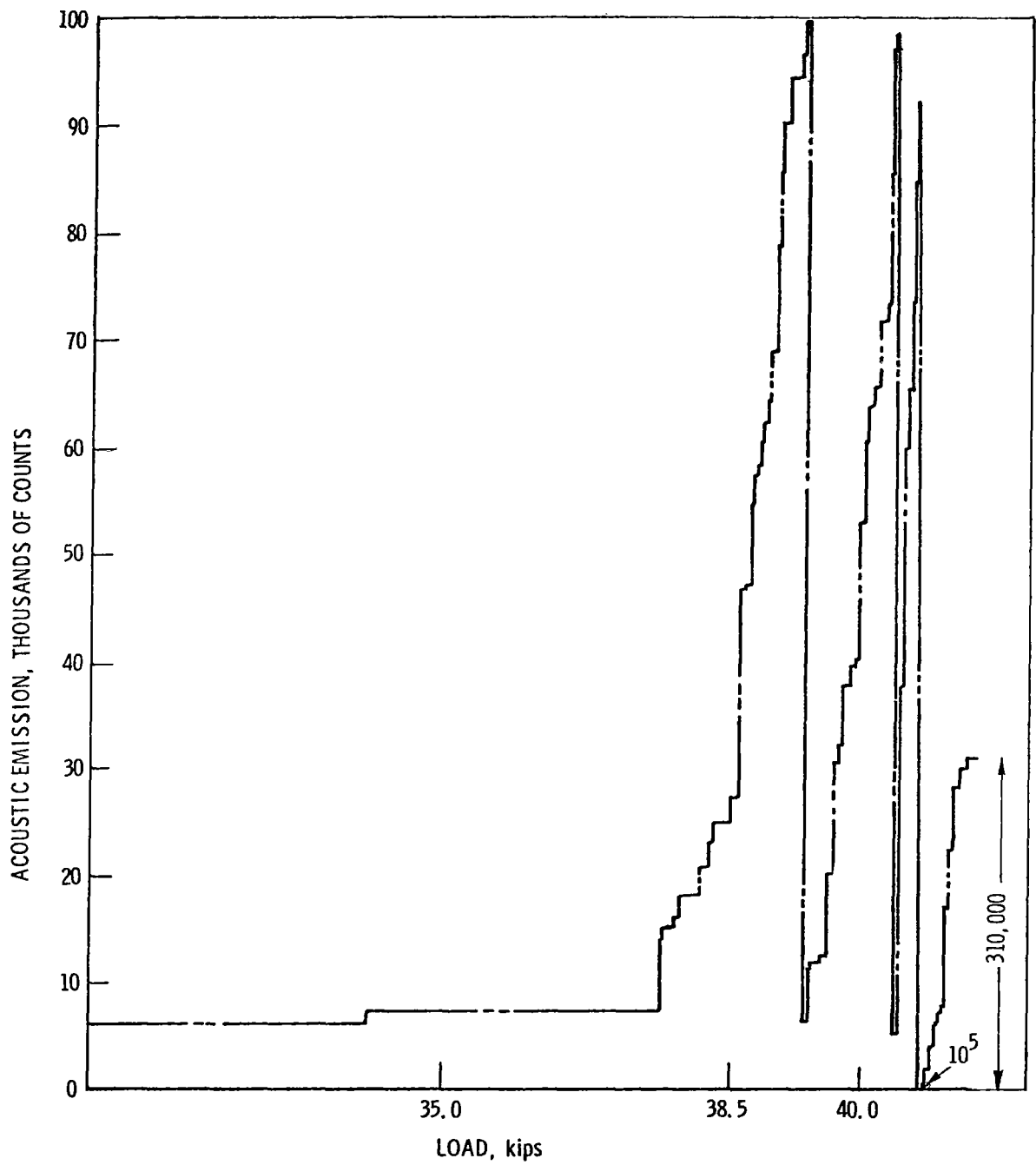
Figure 42. Kaiser Effect in Third Cycle of Specimen No. 27
(second cycle to 38 kips).

126
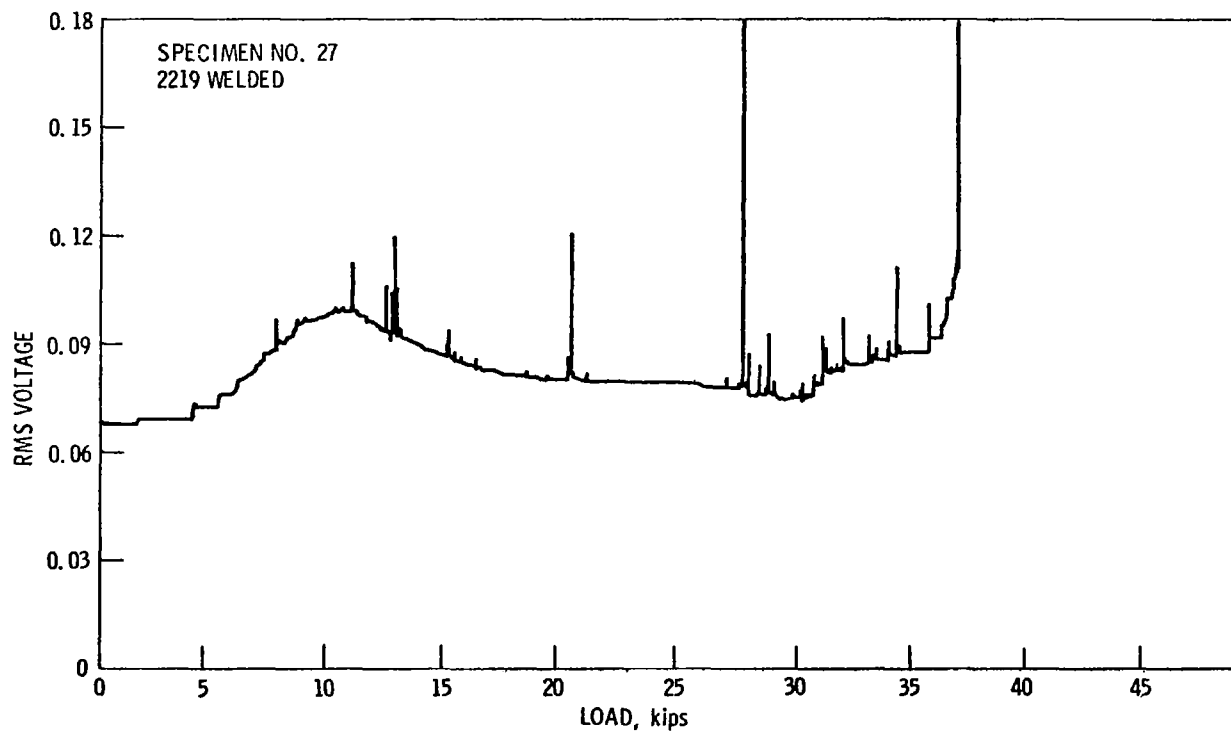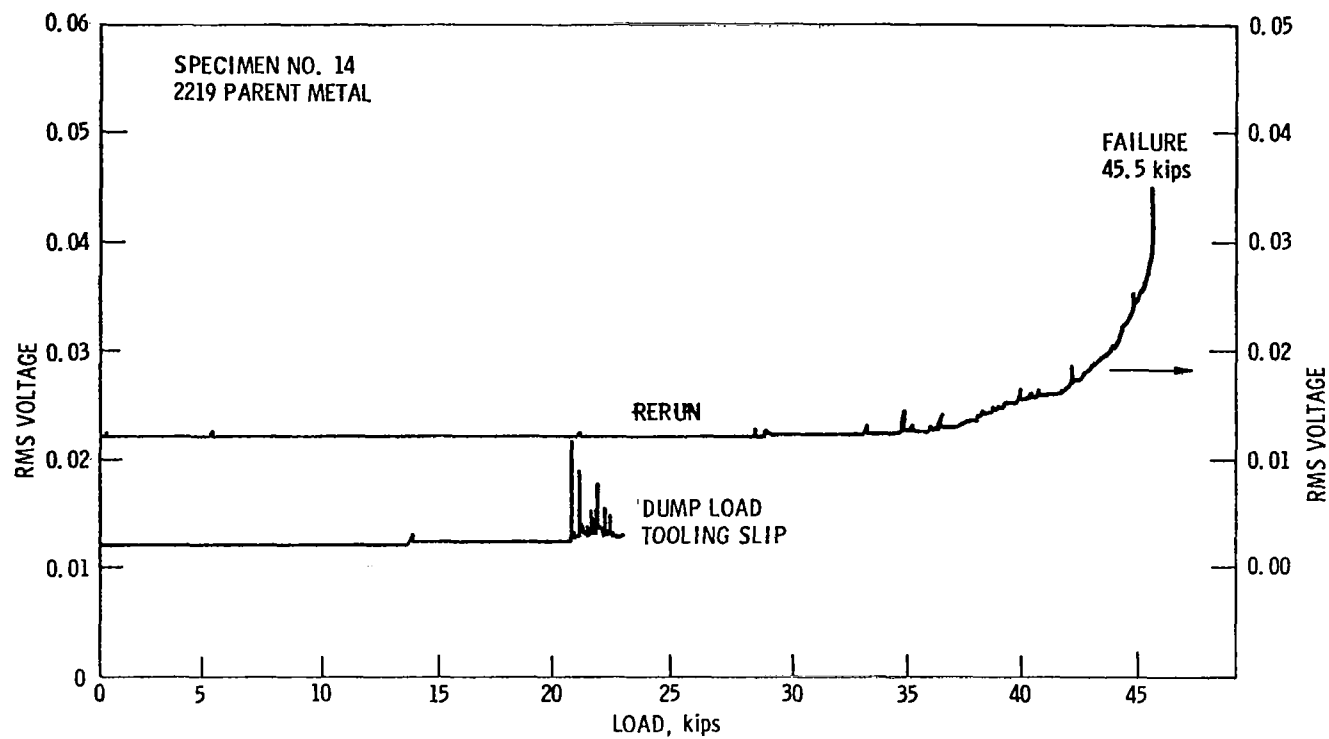
Figure 43. Comparison of Welded and Unwelded, Unnotched 2219 Specimens
Tested at Room Temperature.
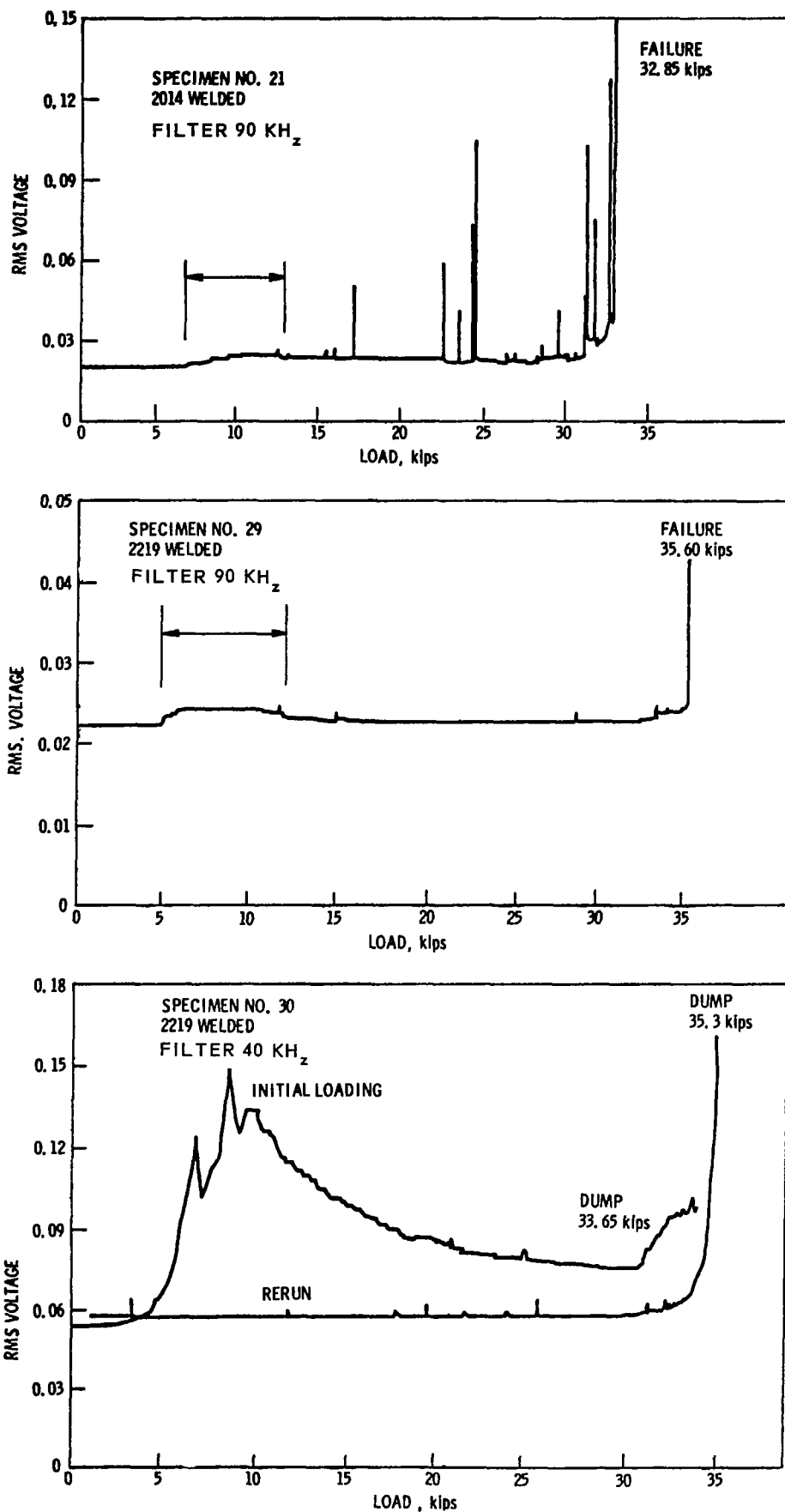
Figure 44. Kaiser Effect in Longitudinally Welded PTC-Tension Specimens.

128
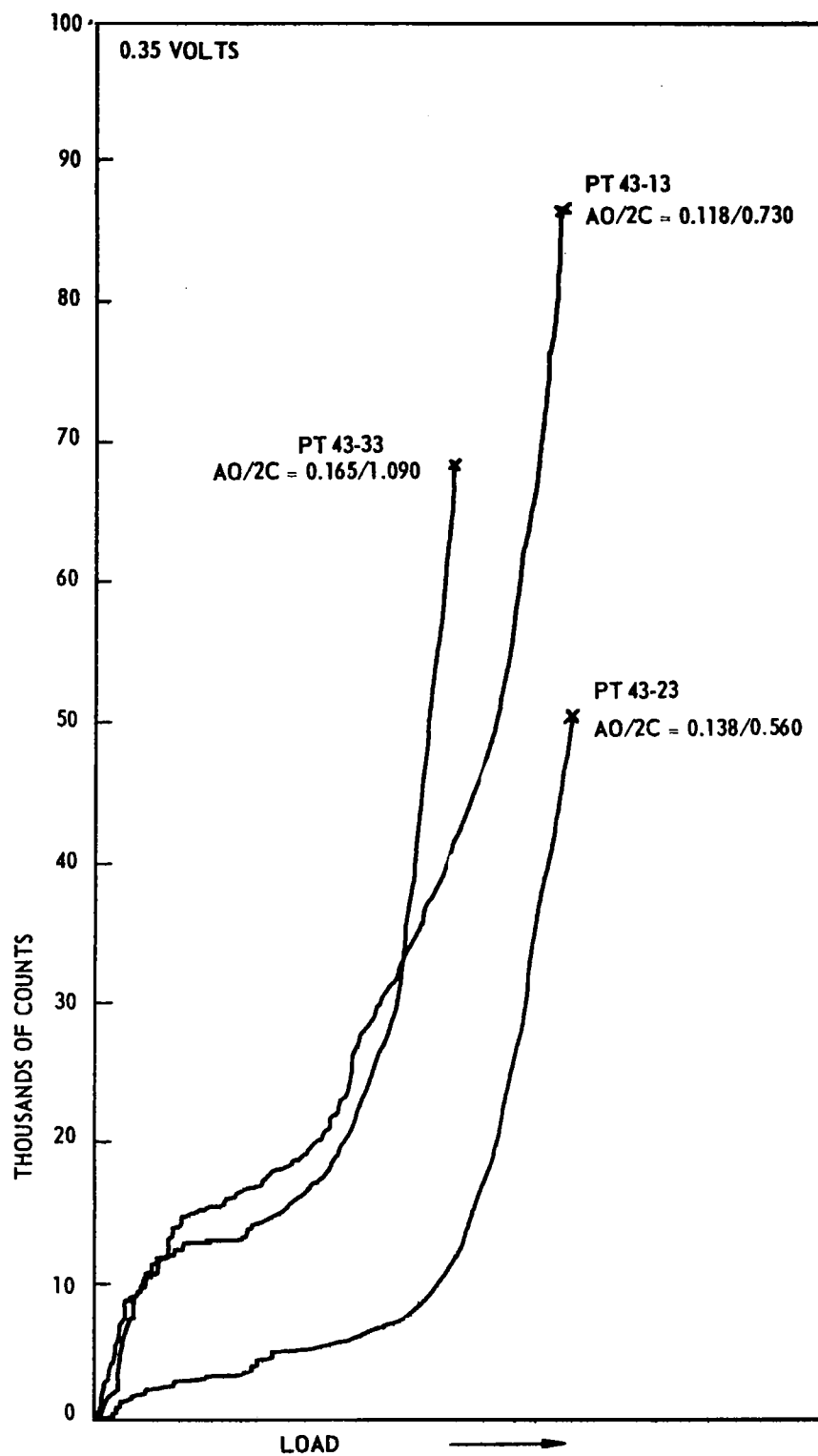
Figure 45. Cumulative SWE Count vs Load for Three Flaw Sizes.
2014-T6 TIG Welded with 4043 Wire, Specimens 0.30-in.
Thick, Tested at 75°F
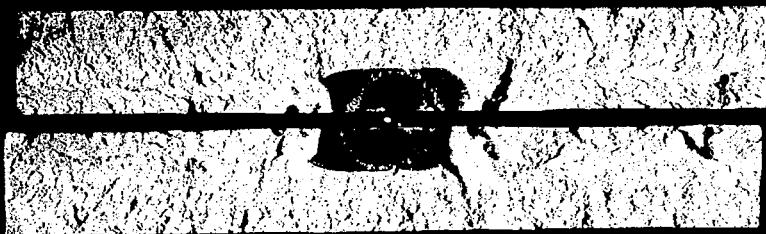
PT 43-13
86,500
COUNT

PT 43-23
50,500
COUNT

PT 43-33
68,500
COUNT

Figure 46.   Flaws in the Tension Specimens of Figure 45

130
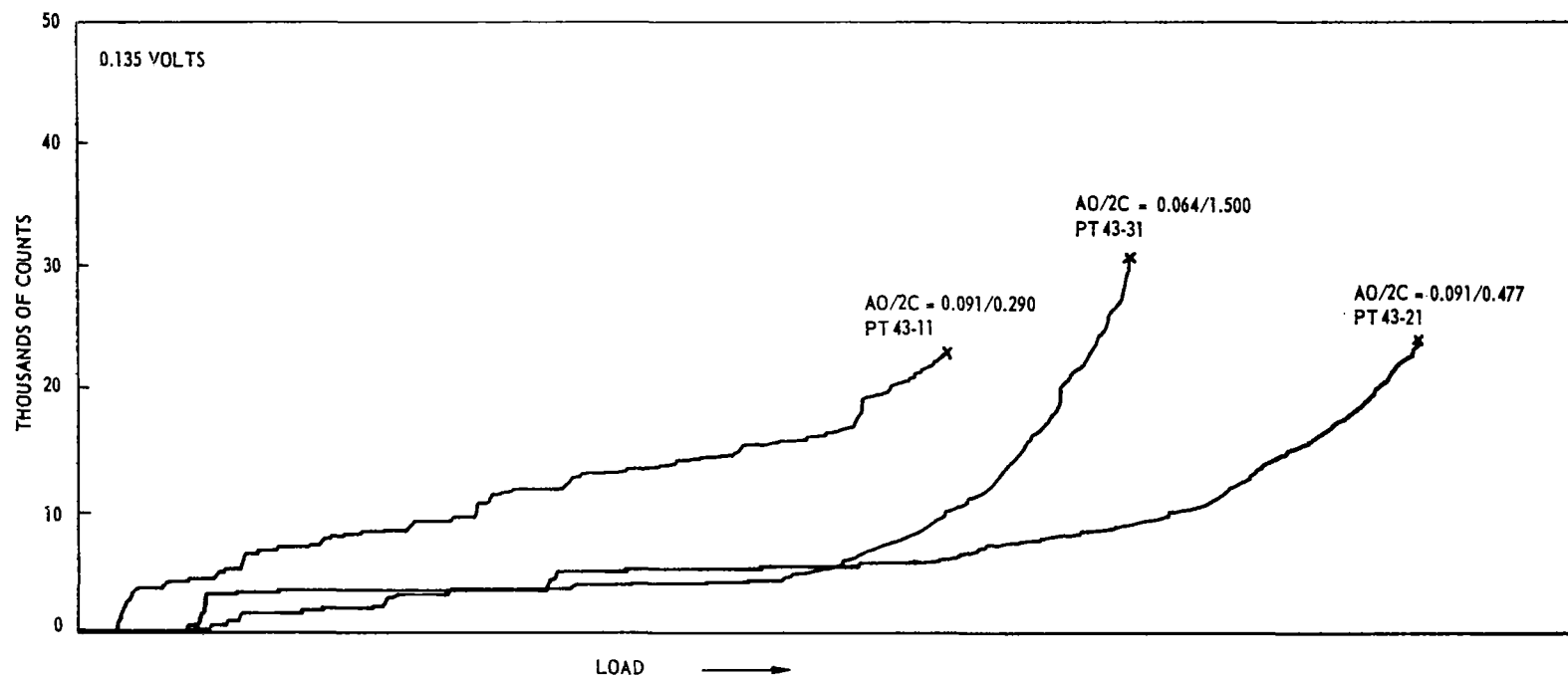
Figure 47. Cumulative SWE Count vs Load for Three Flaws. 2014-T6
TIG Welded with 4043 Wire, Specimens 0.18-in. Thick,
Tested at 75°F
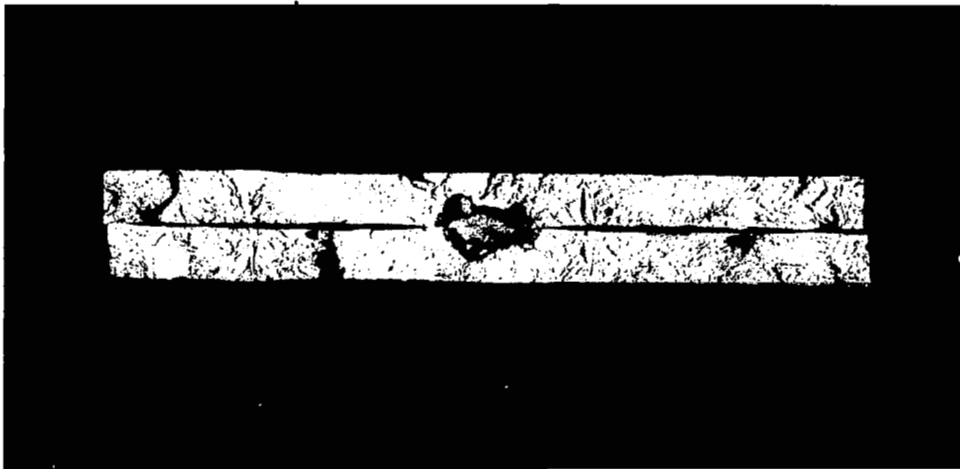
PT 43-11
22,500
COUNT
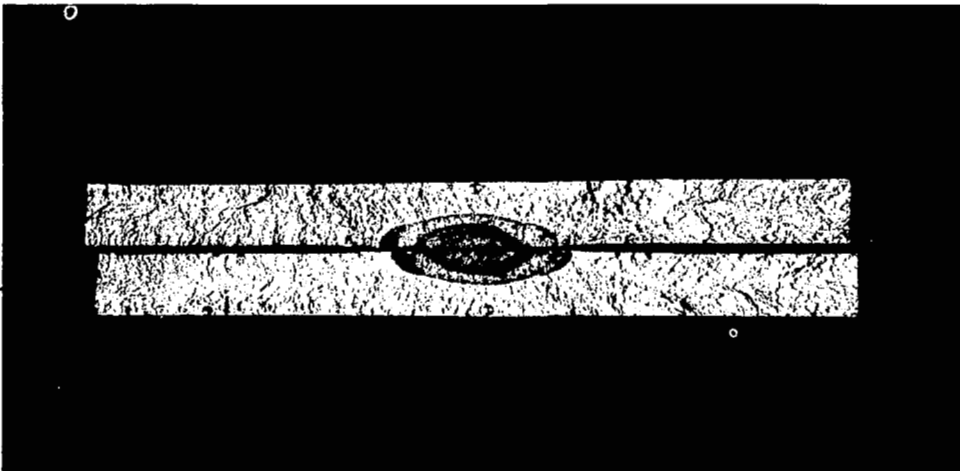
PT 43-21
23,500
COUNT
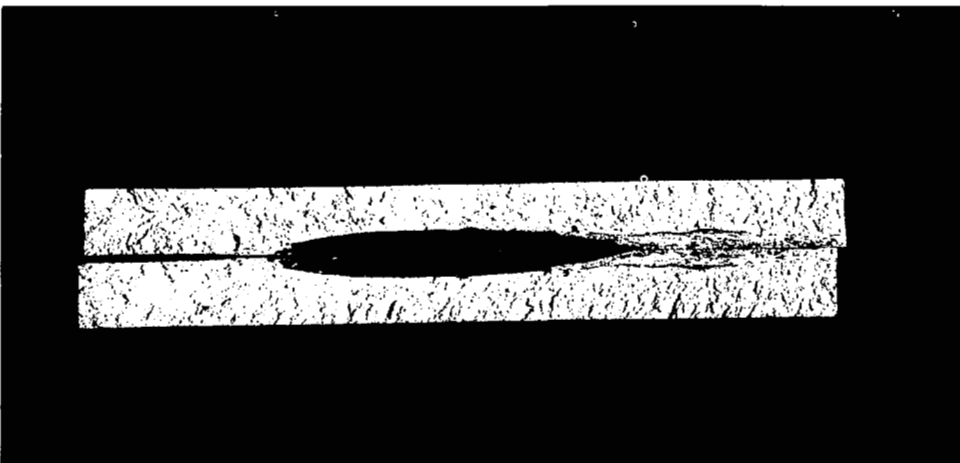
PT 43-31
30,500
COUNT

Figure 48.   Flaws in the Tension Specimens of Figure 47
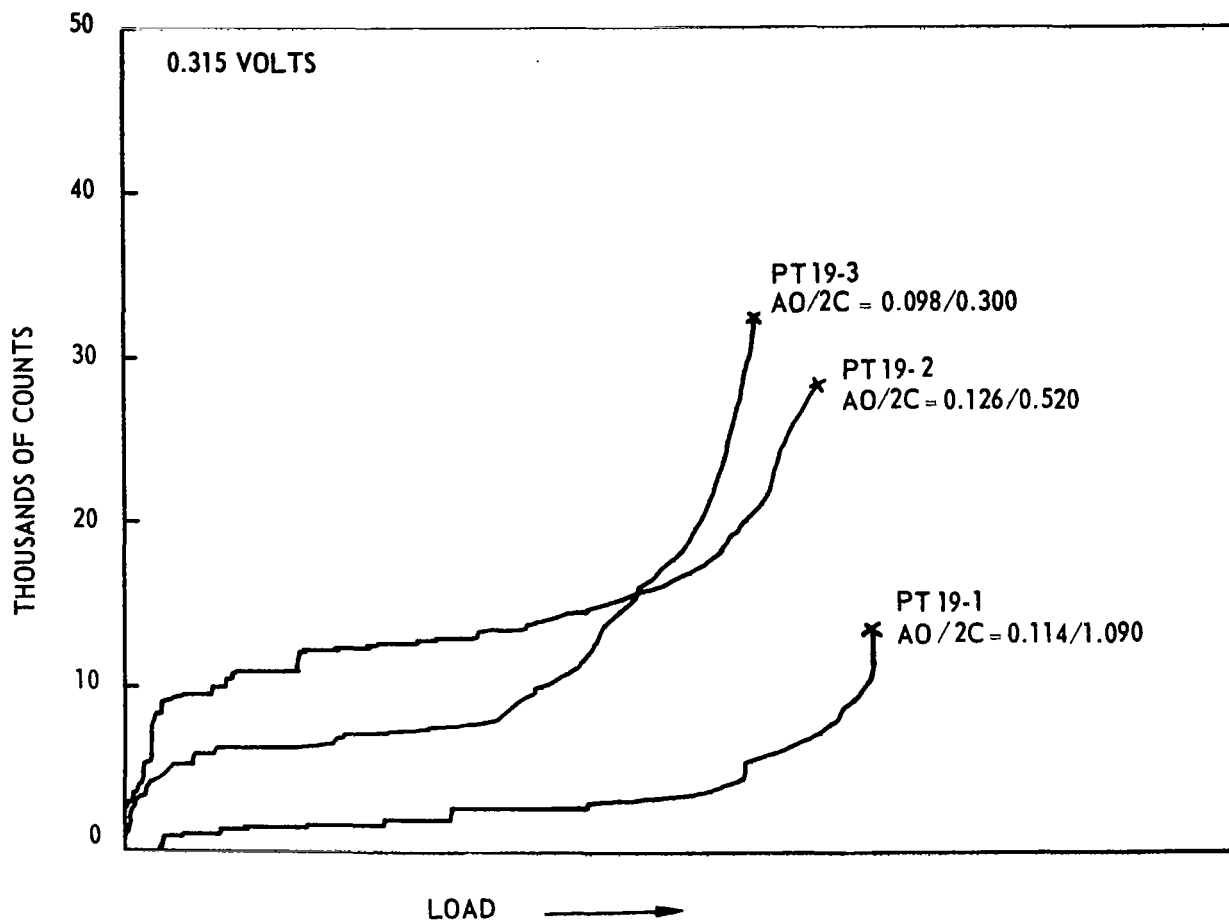
Figure 49. Effect of Flaw Size on SWE Count. 2014-T6 TIG Welded with 2319 Wire
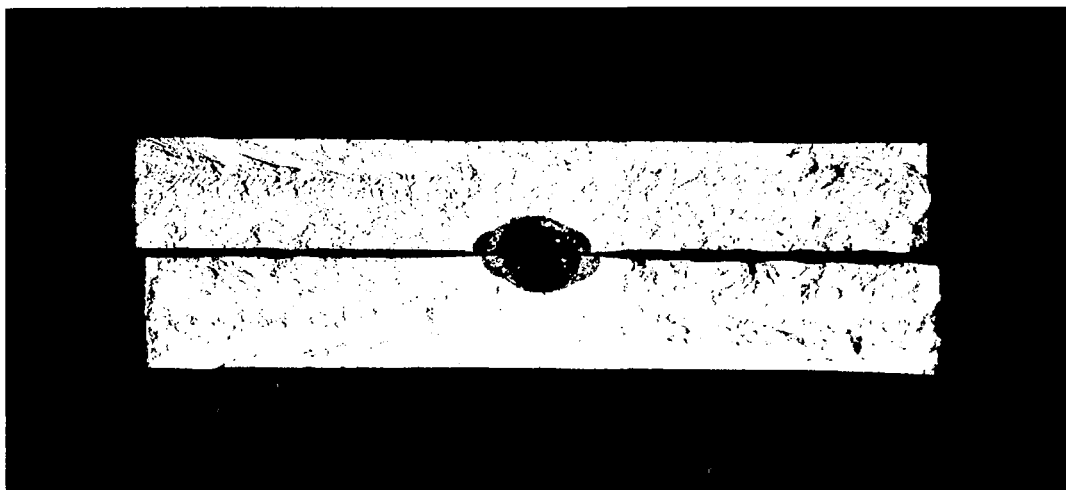
PT 19-1
13,500
COUNT
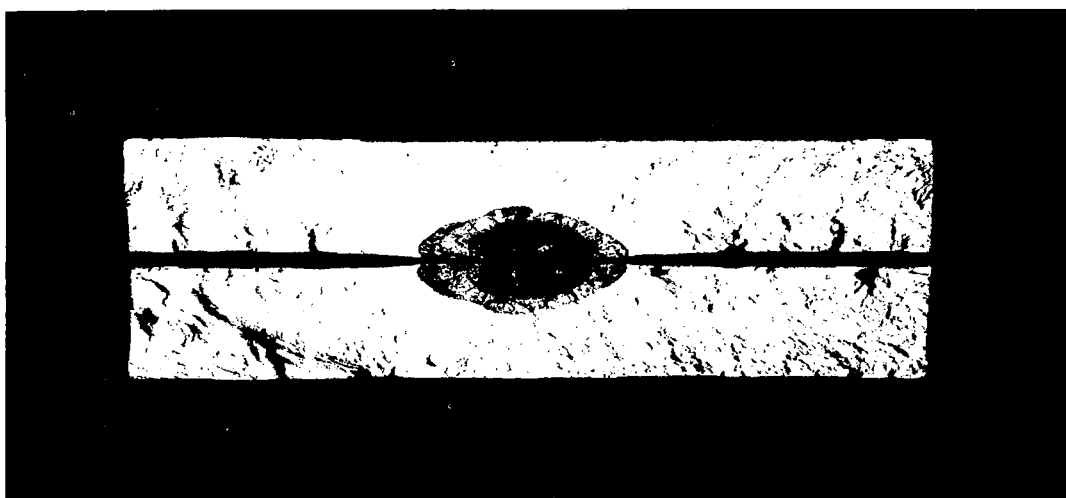
PT 19-2
28,500
COUNT

PT 19-3
32,500
COUNT

Figure 50.   Flaws in the Tension Specimens of Figure 49
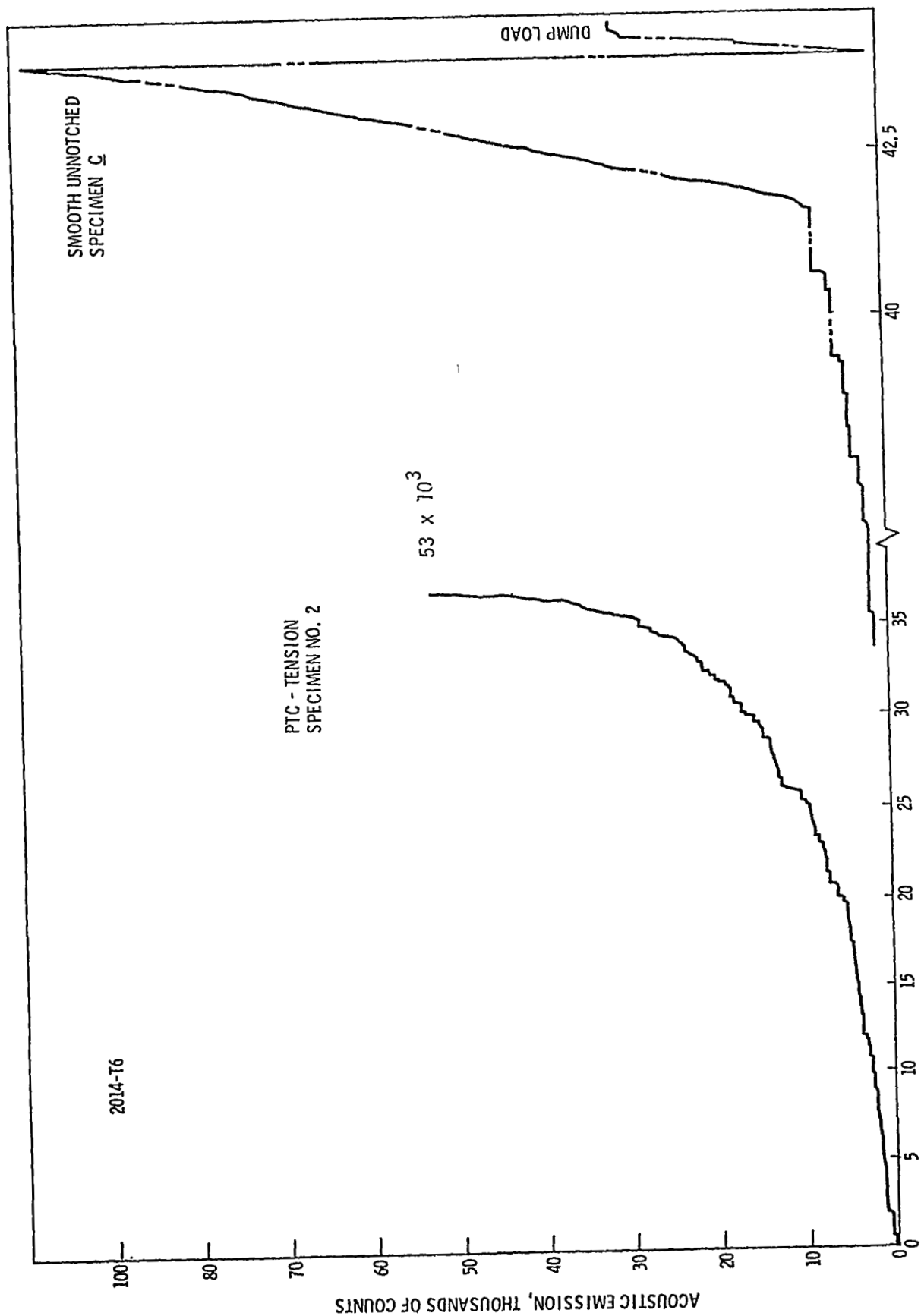
Figure 51. Comparison of Precursors in Notched (PTC) and Unnotched
Tension Tests (Specimen No. 2 and C)

135
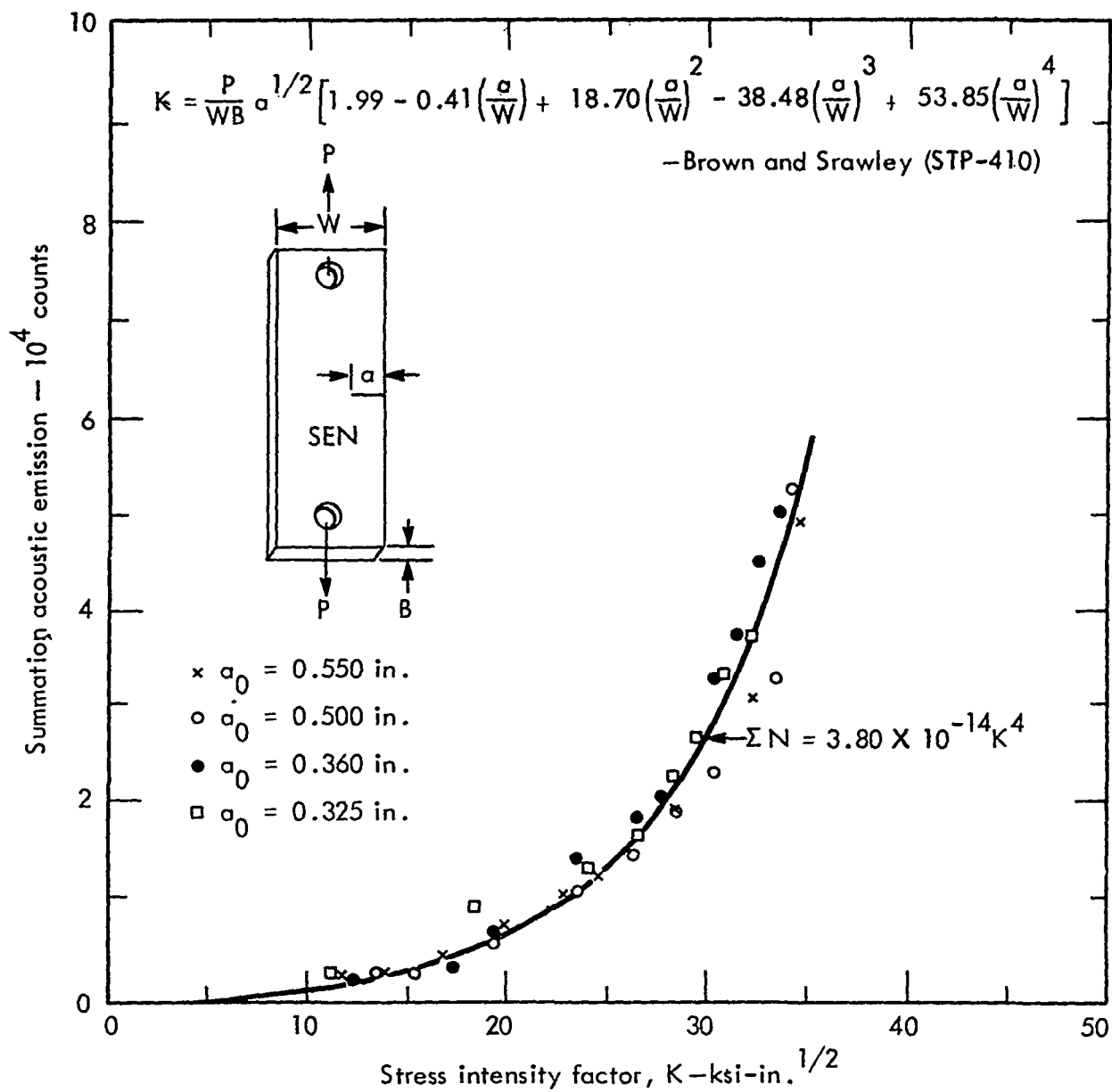
Figure 52. Summation of Acoustic Emission as a Function of
Stress-Intensity Factor - 7075-T6 Aluminum in
Air (Dunegan)
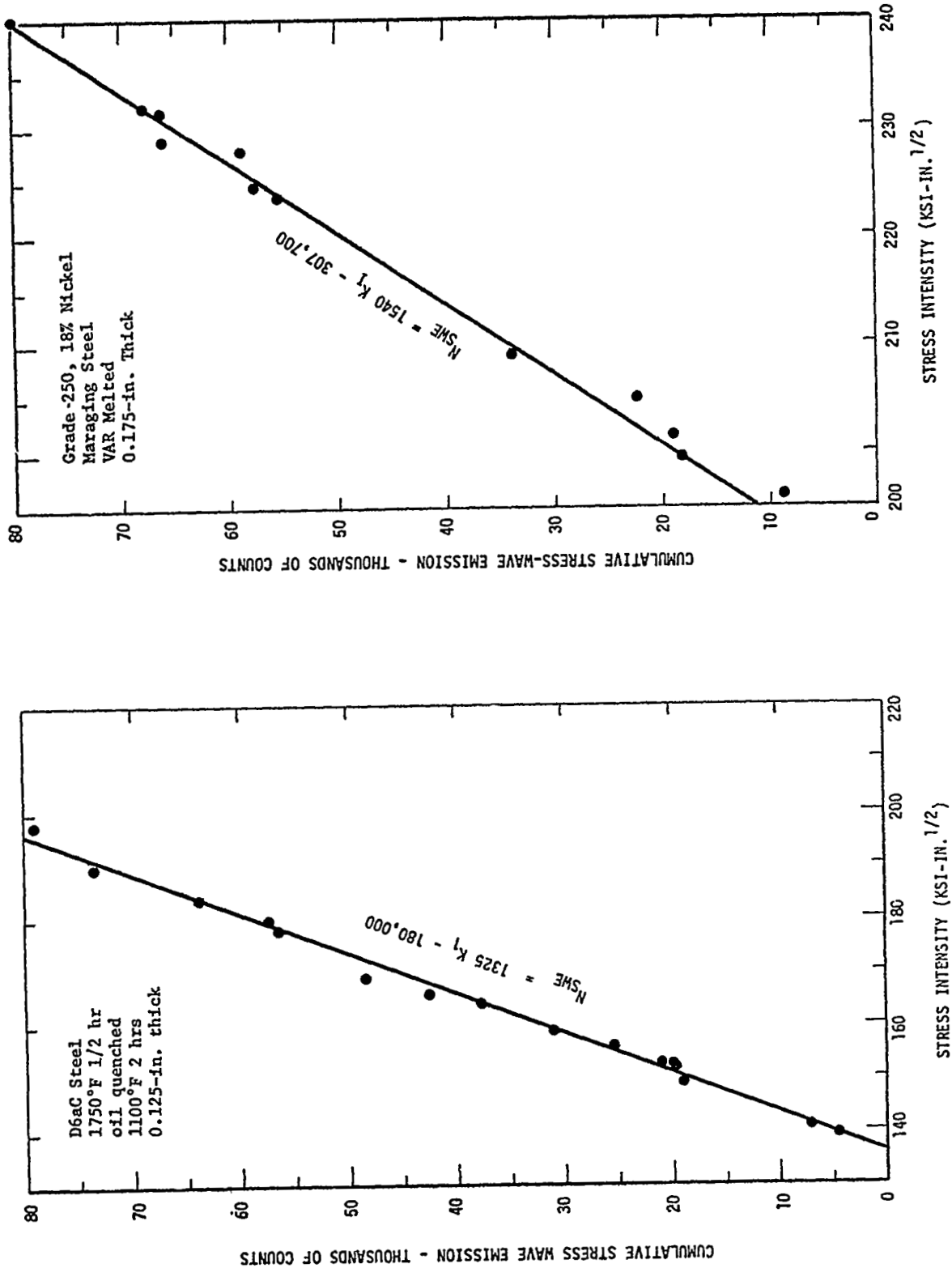
Figure 53. Relationship BEtween Stress Intensity and Cumulative Count for Materials Under Constant Load and Subjected to Stress-Corrosion Cracking in 70°F Water.

137
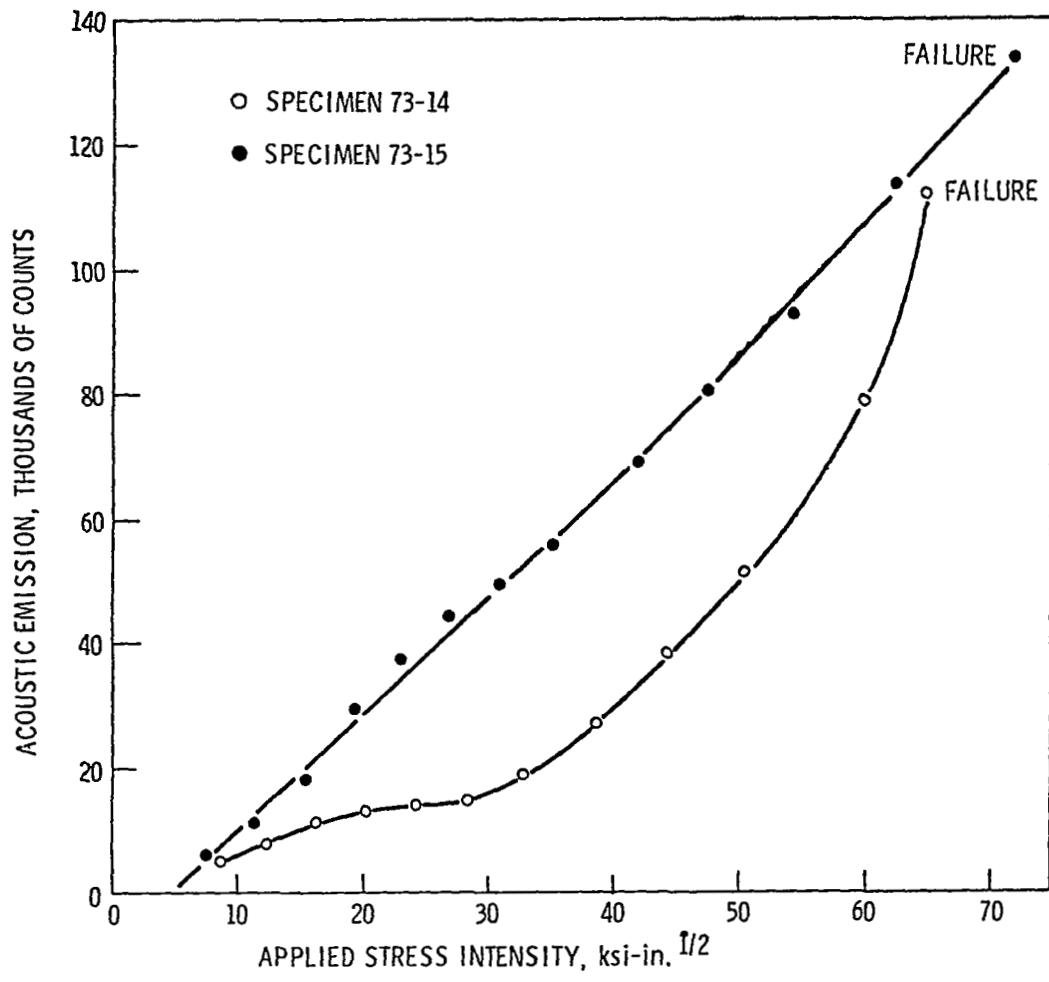
Figure 54. Relationship Between Cumulative Acoustic-Emission Count
and Stress Intensity Factor in SEN-Tension Tests of 7075-T6
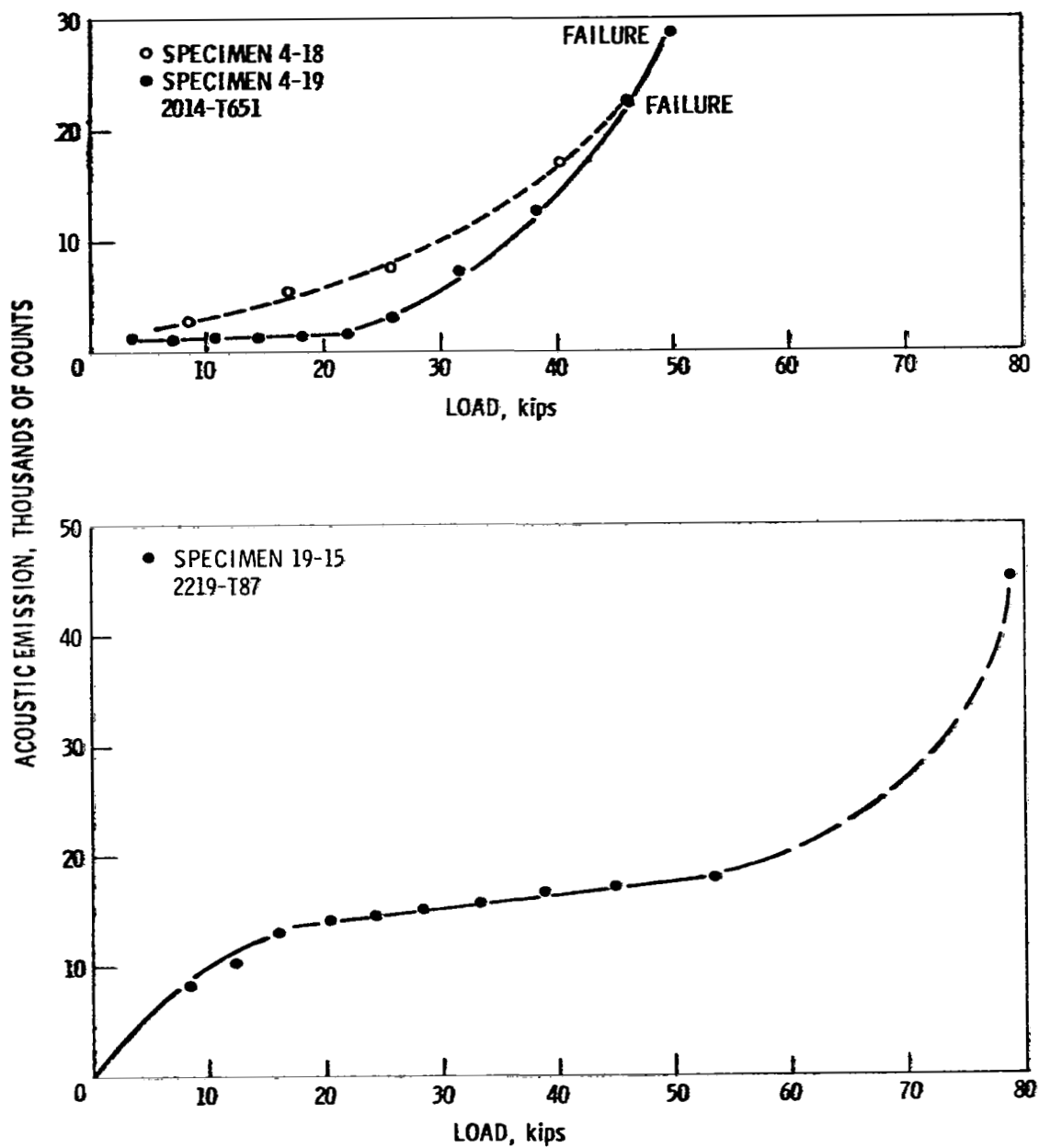
Figure 55. Relationship Between Cumulative Count and K in SEN-Tension Tests of 2014-T6 and 2219-T87.
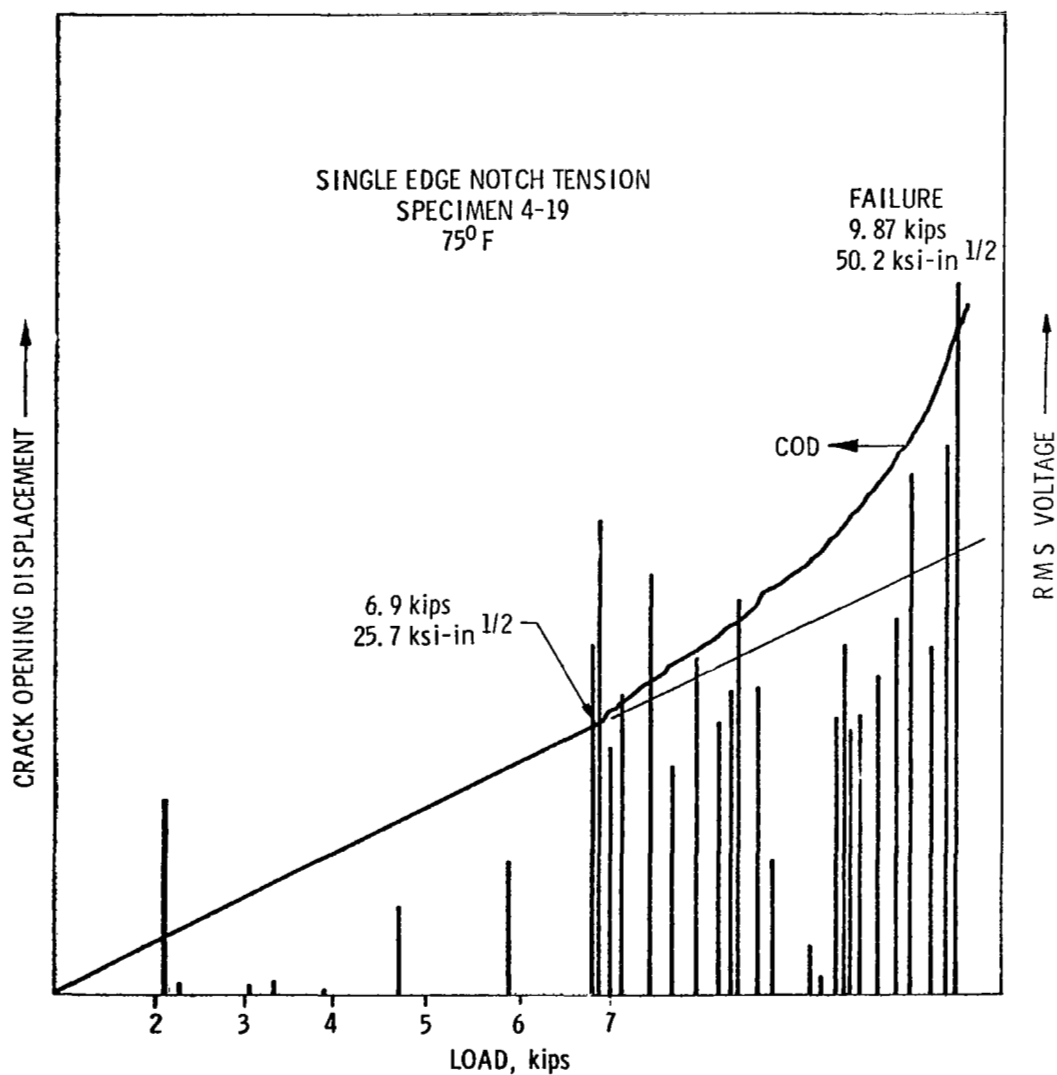
Figure 56. Correlation Between Crack–Opening–Displacement Measurement and Acoustic Emission in a SEN–Tension Test of 2014–T651 (see Table XI).
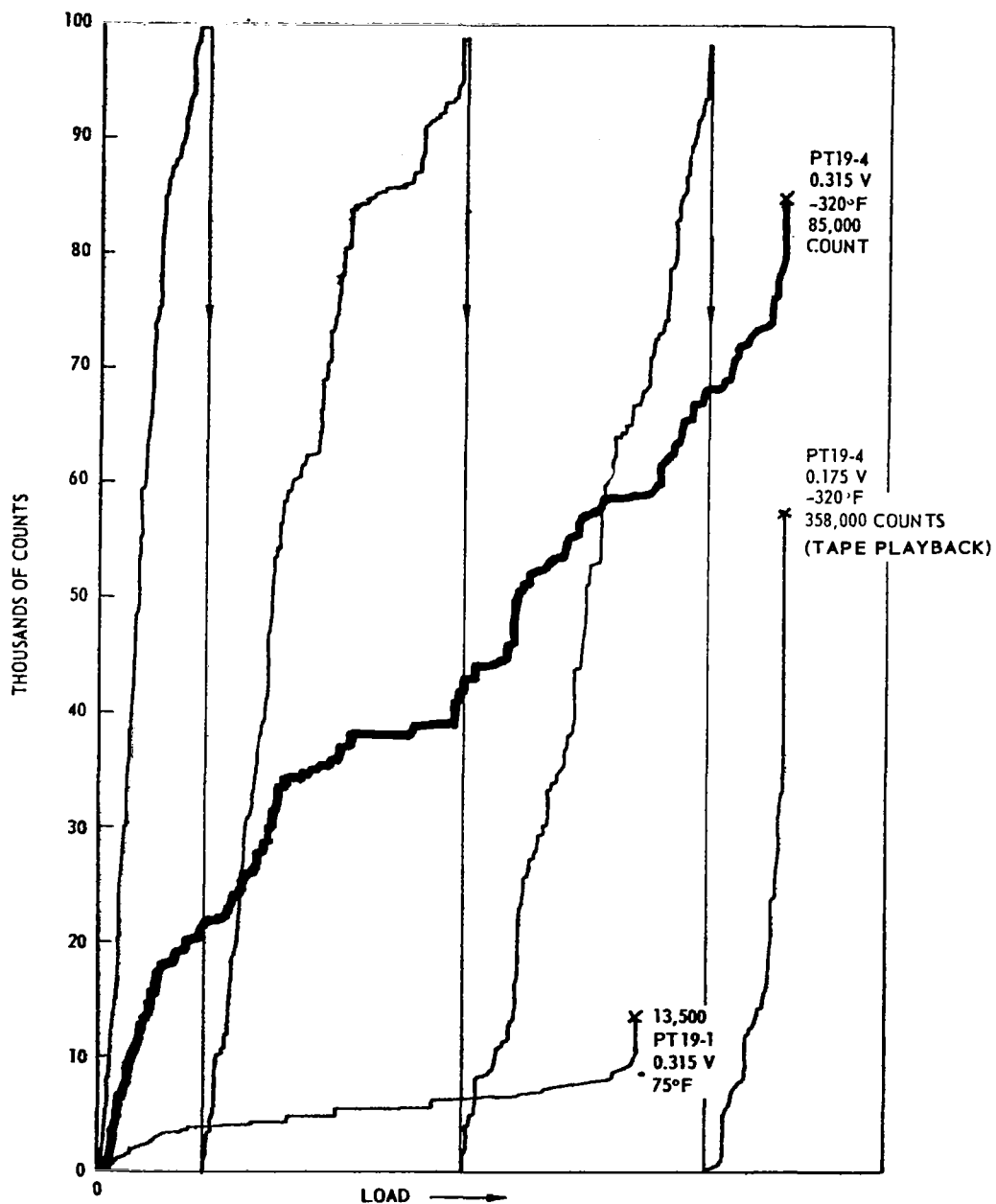
Figure 57. Effect of Temperature on SWE Count. 2014-T6
TIG Welded with 2319 Wire; Nearly Identical
Flaws.

141
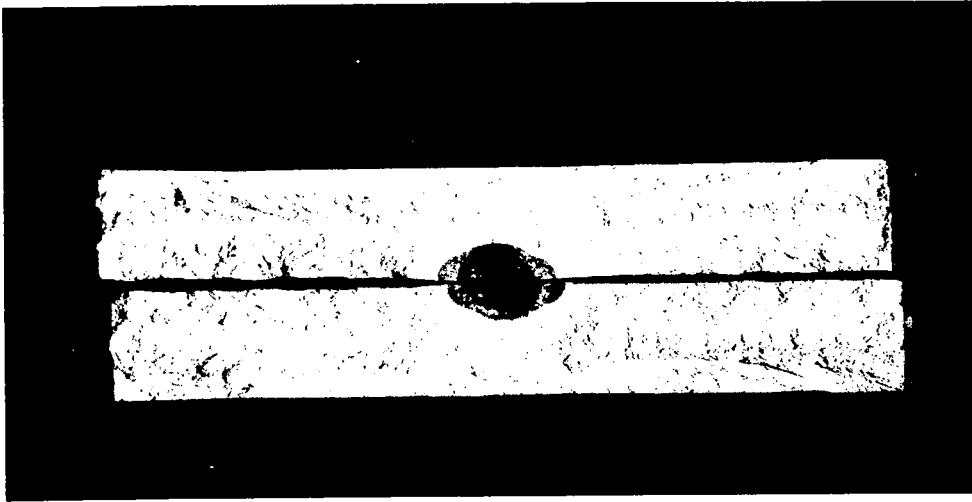
PT 19-1
75°F
13,500
COUNT
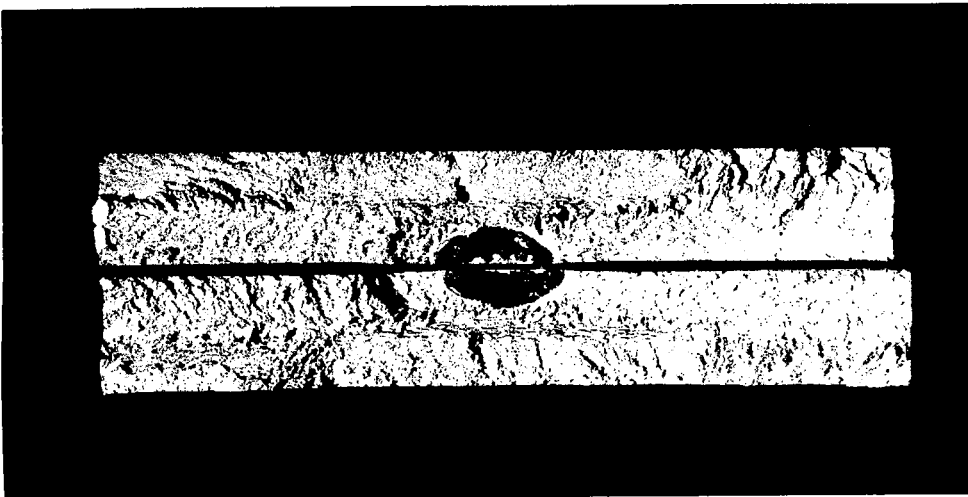
PT 19-4
-320°F
358,000
COUNT

Figure 58.   Flaws in the Tension Specimens of Figure 57

142

Figure 59. Effect of Temperature on SWE Count. 2014–T6 TIG Welded with 4043 Wire; Nearly Identical Flaws

143
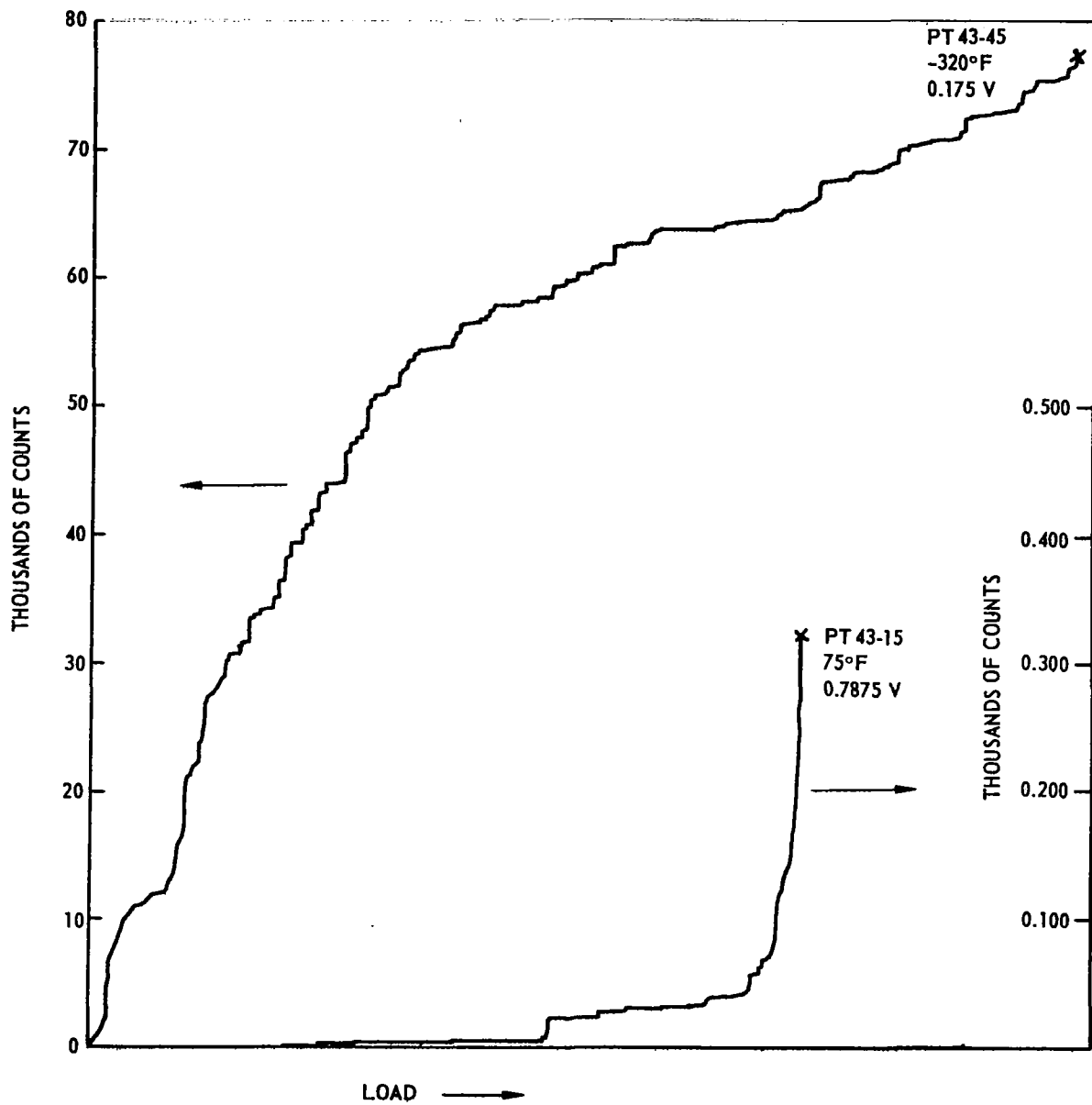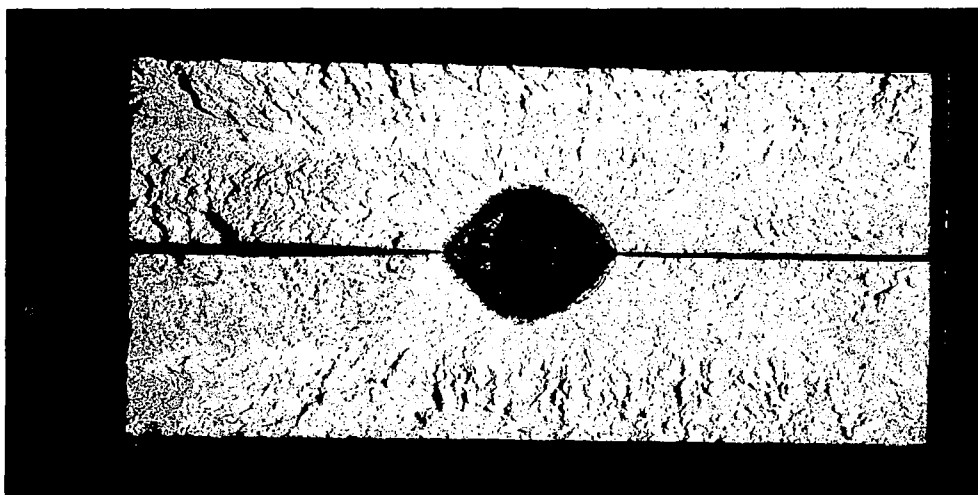
PT 43-15
75°F
325 COUNT
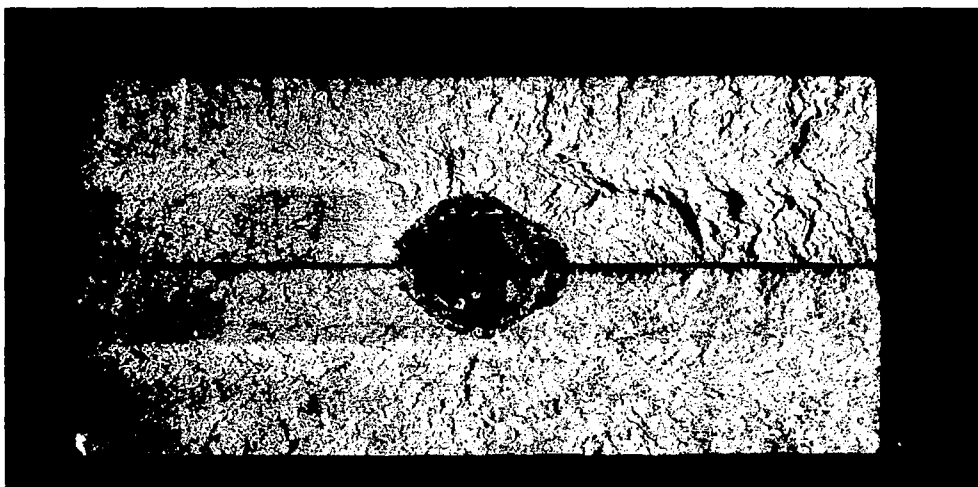
PT 43-45
–320°F
77,500
COUNT

Figure 60.   Flaws in the Tension Specimens of Figure 59

144
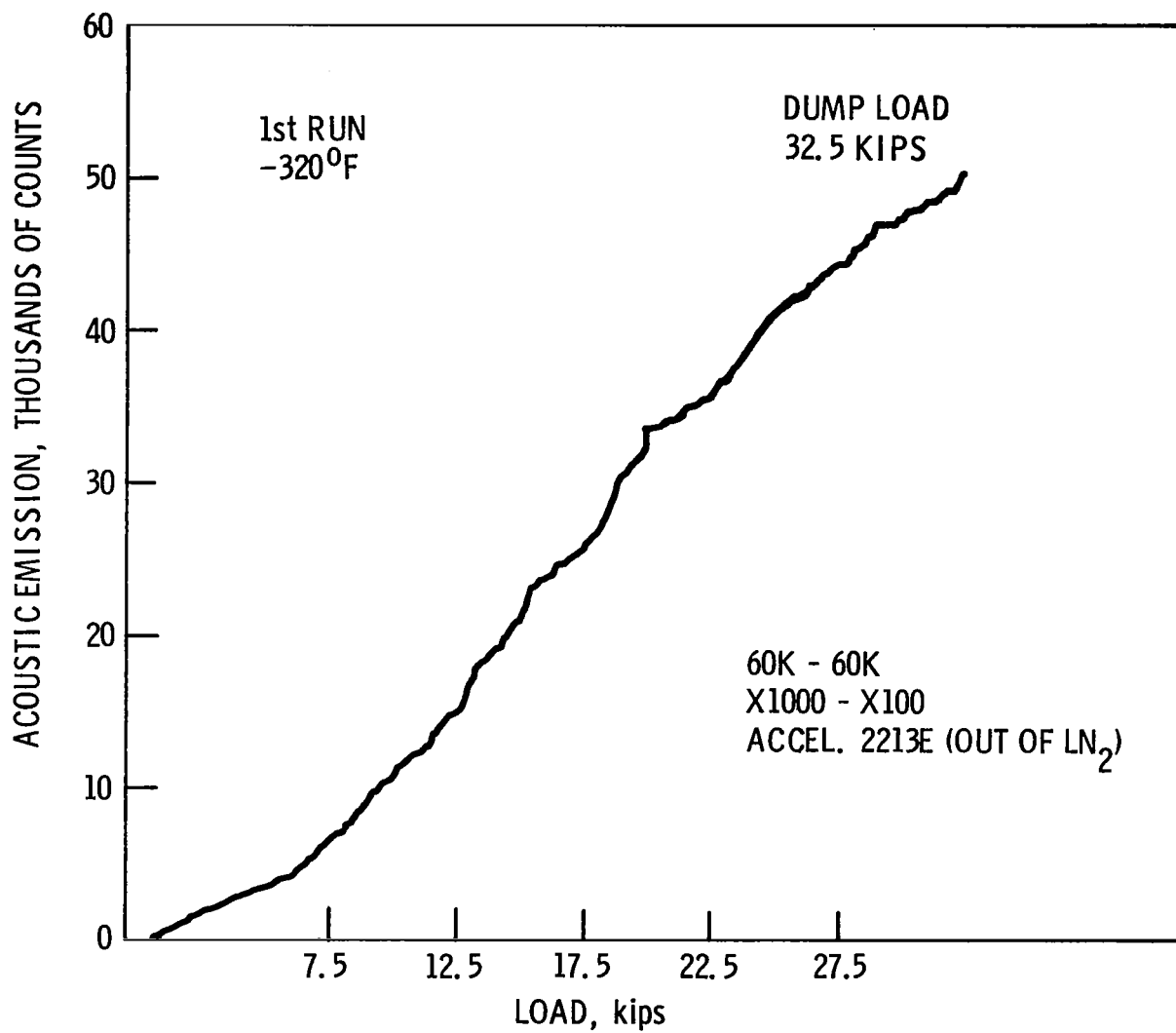
Figure 61. First Load Cycle for 2219 Specimen I at -320°F (32.5 Kips maximum load, 500,000 counts).
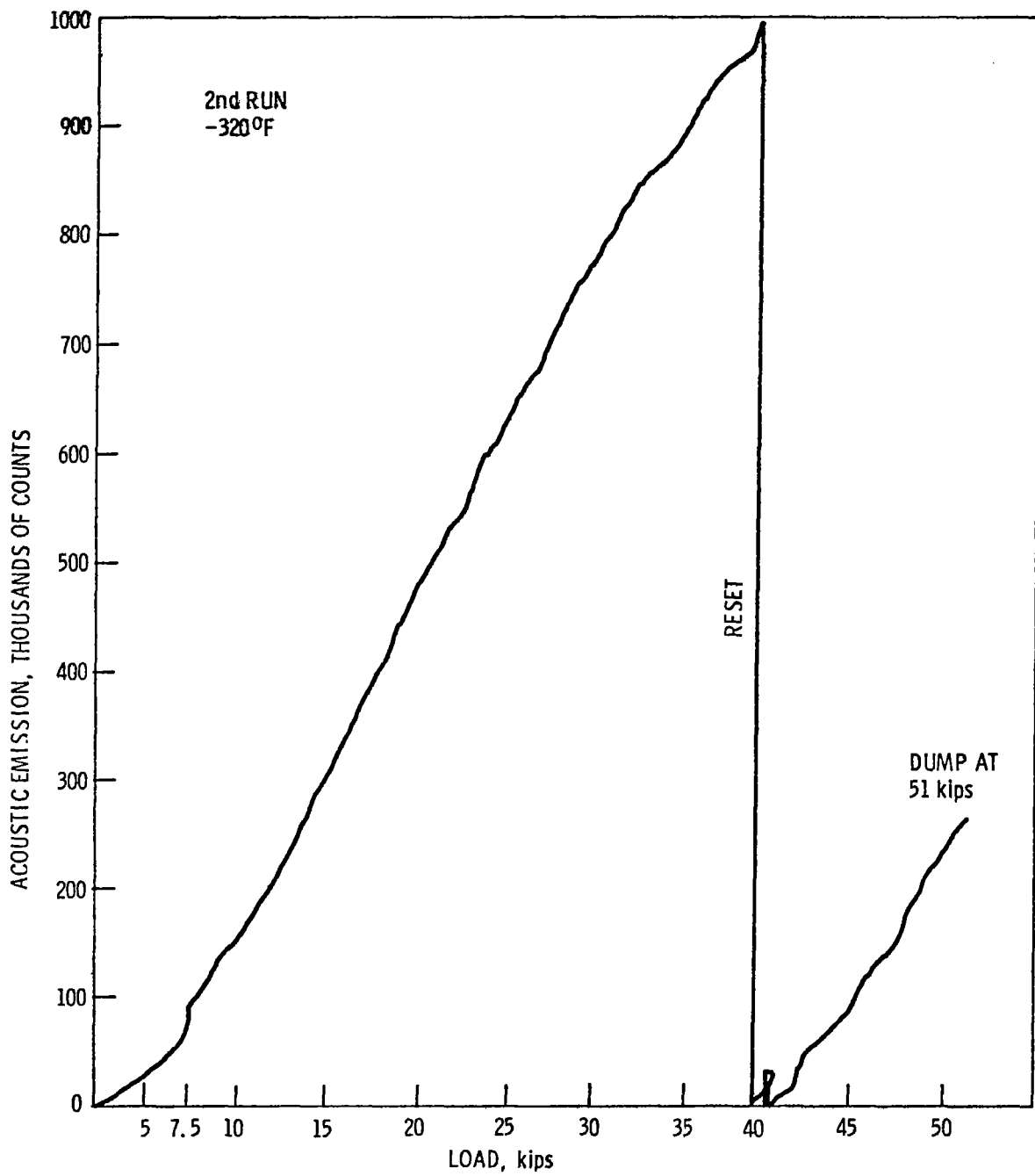
Figure 62. Second Load Cycle for 2119 Specimen I at -320°F
at 32.5 kips, 850,000 counts .

146
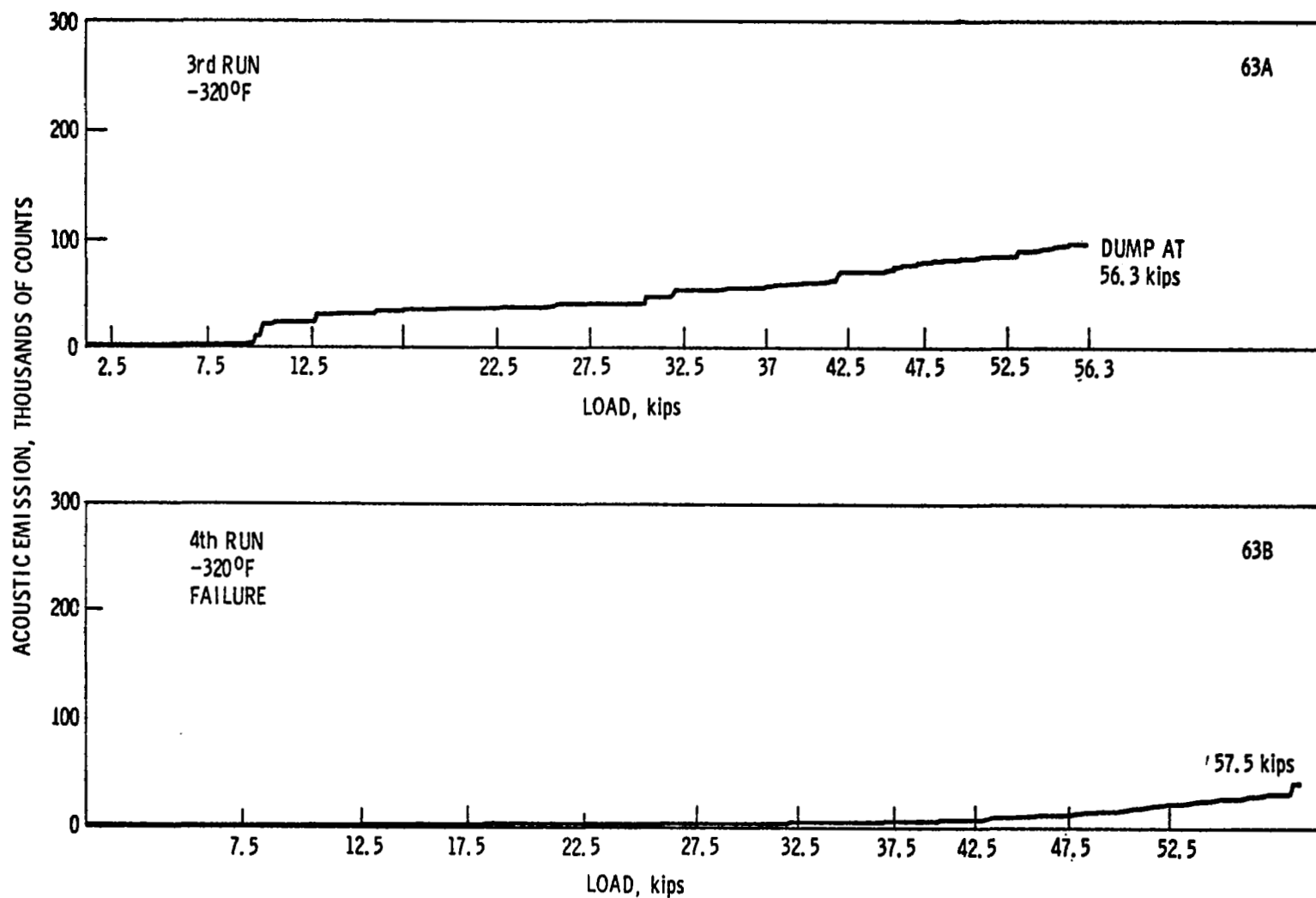
Figure 63. Third and Fourth Load Cycle for 2219 Specimen I at -320°F (in the 3rd and 4th Cycles, the count at 32.5 kips was 55,000 and 5,000, respectively.
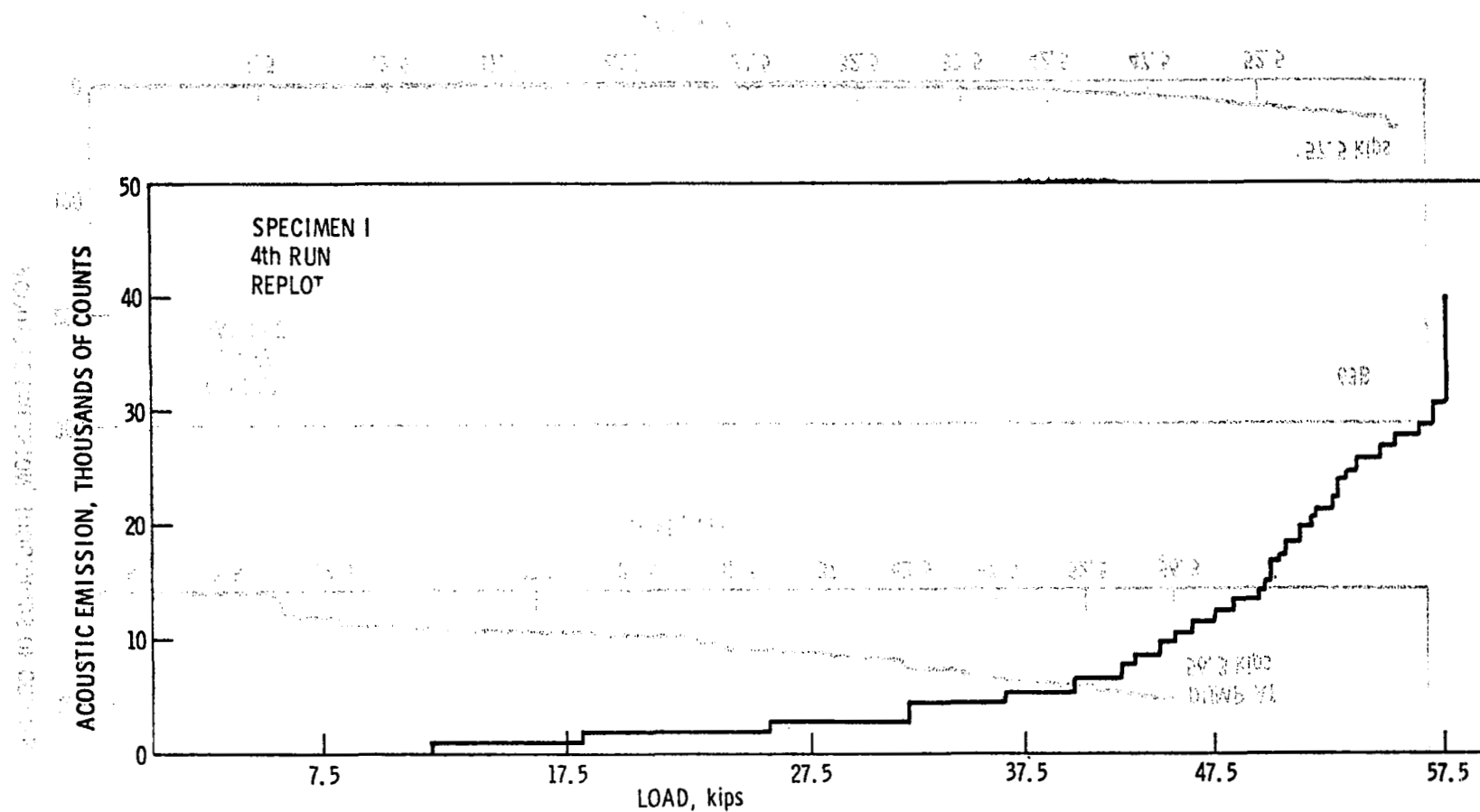
Figure 64. Effect of X-Y Plot Scale Factor on the Precursor of Failure for 2219 Specimen I at -320°F.
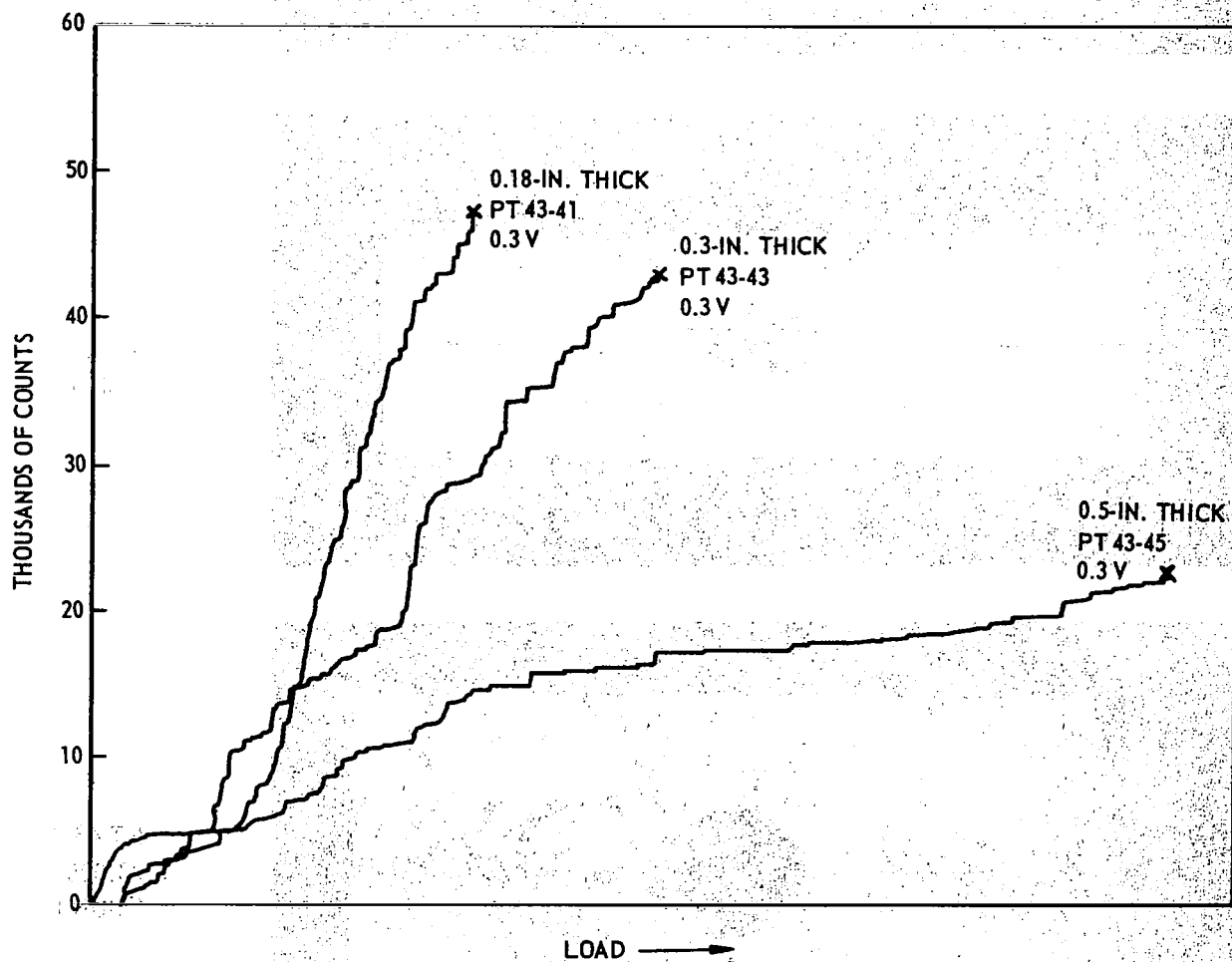
Figure 65. Effect of Specimen Thickness on SWE Count. 2014-T6 TIG
Welded with 4043 Wire; Tested at -320°F

149
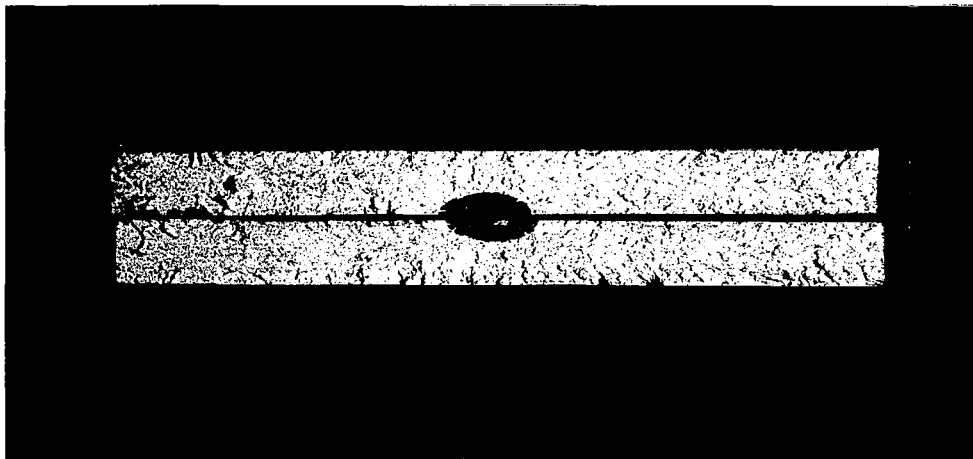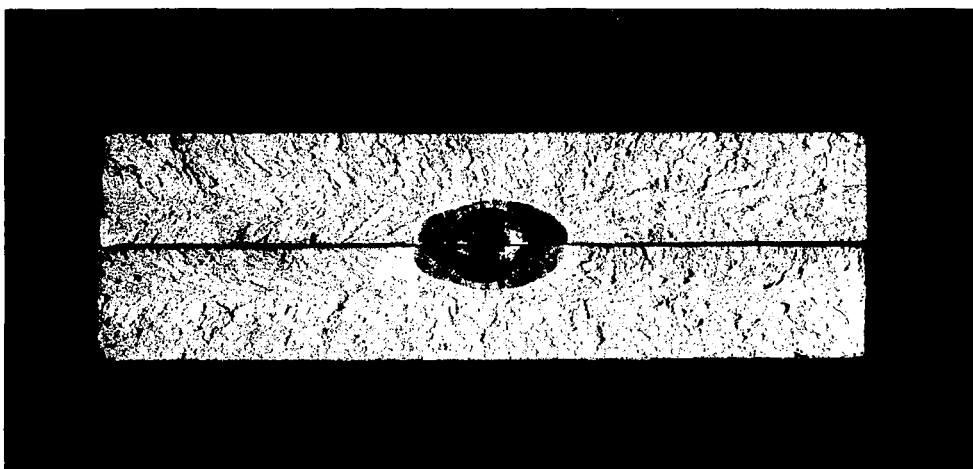
PT 43-41
47,500
COUNT

PT 43-43
43,000
COUNT
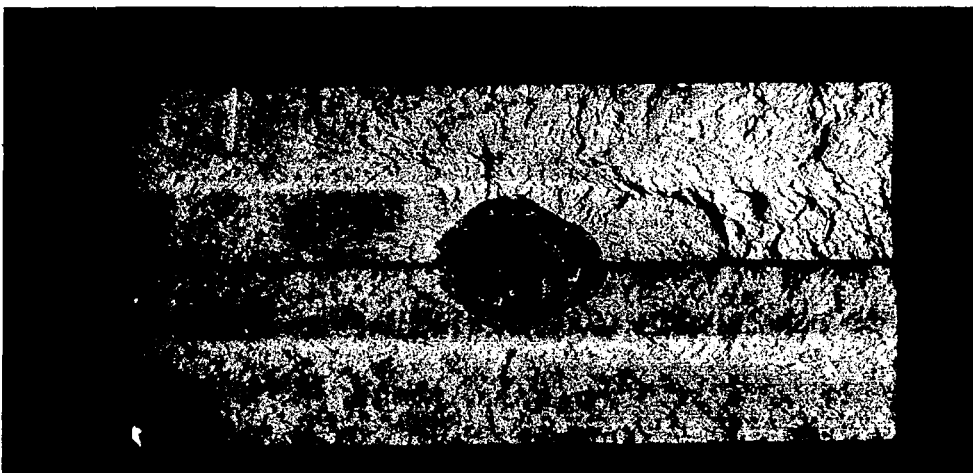
PT 43-45
23,000
COUNT

Figure 66.   Flaws in the Tension Specimens of Figure 65
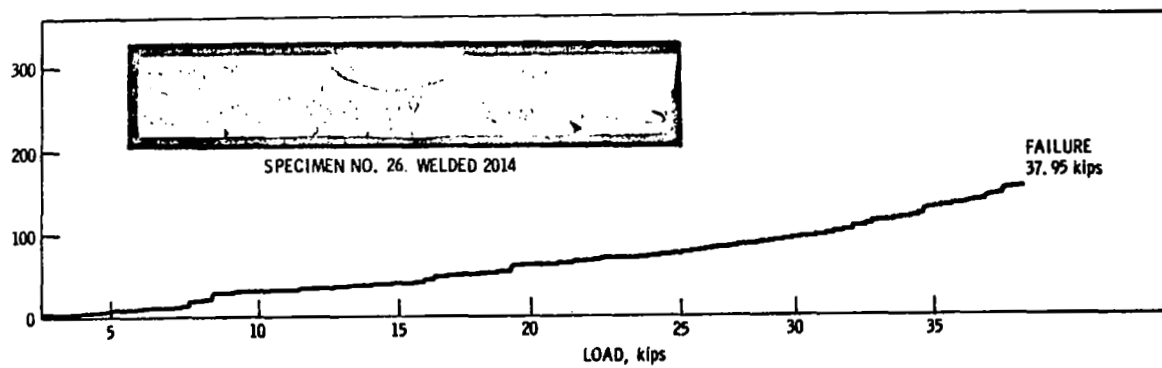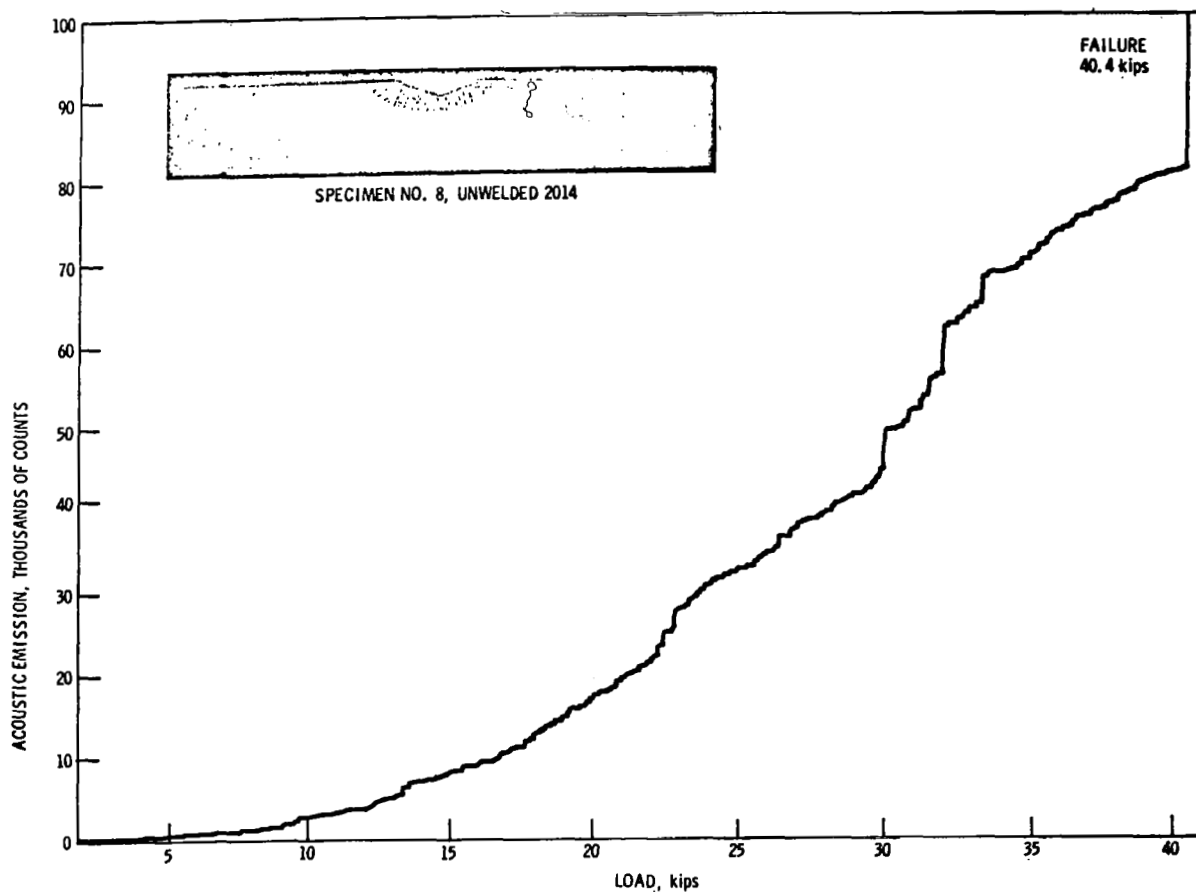
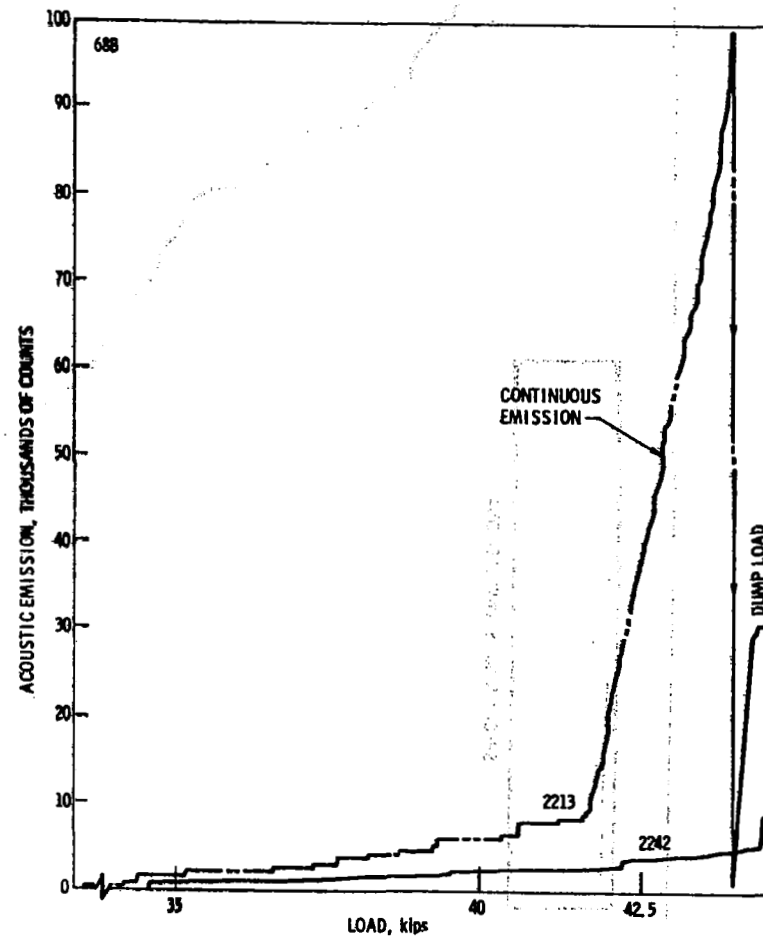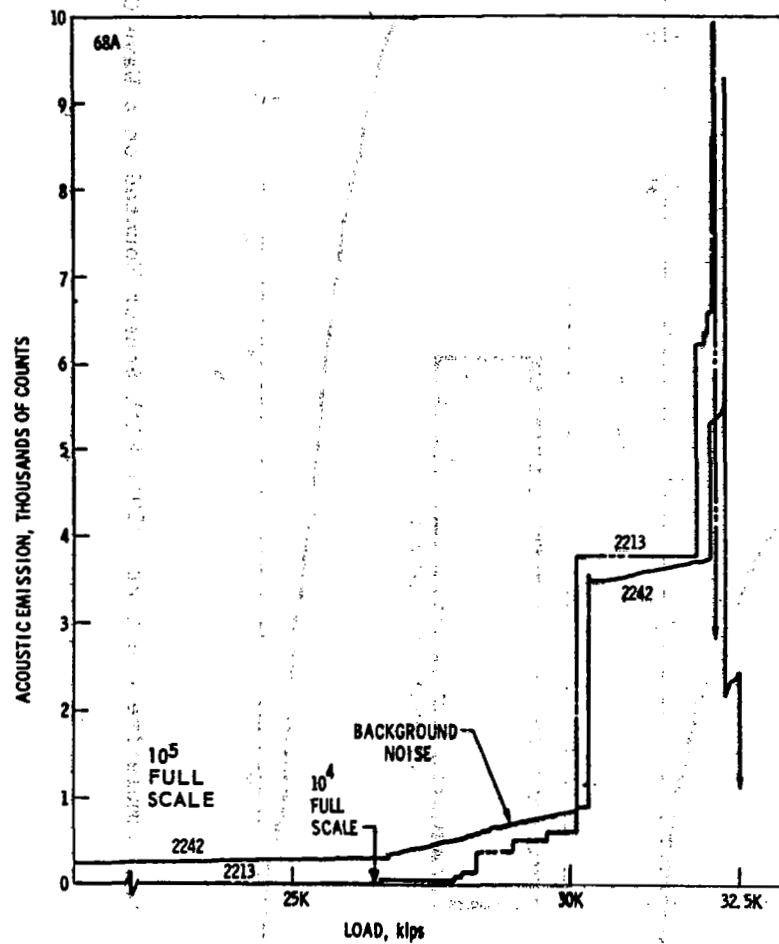Figure 67. Cumulative Count at -320°F With Sensor Mounted on a Wave Guide.

151

Figure 68. Comparison of Two Transducers Mounted on 2014-T6 Unnotched Tension Specimen No. C.
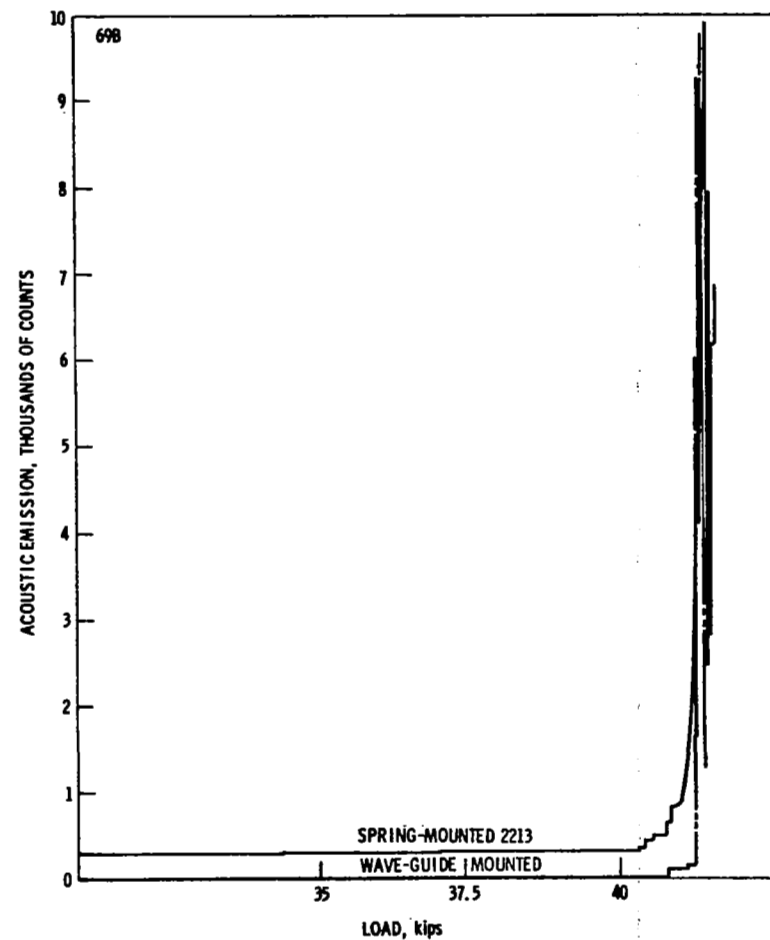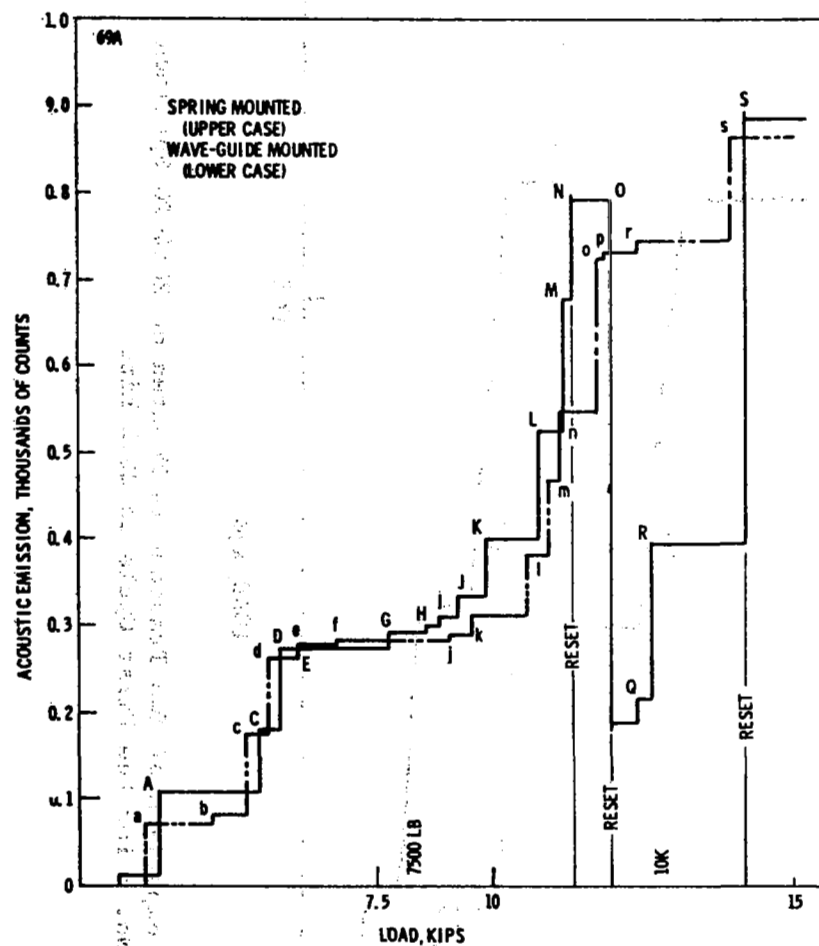
152

Figure 69.   Comparison of the Output from Spring-Mounted and Wave-Guide-Mounted
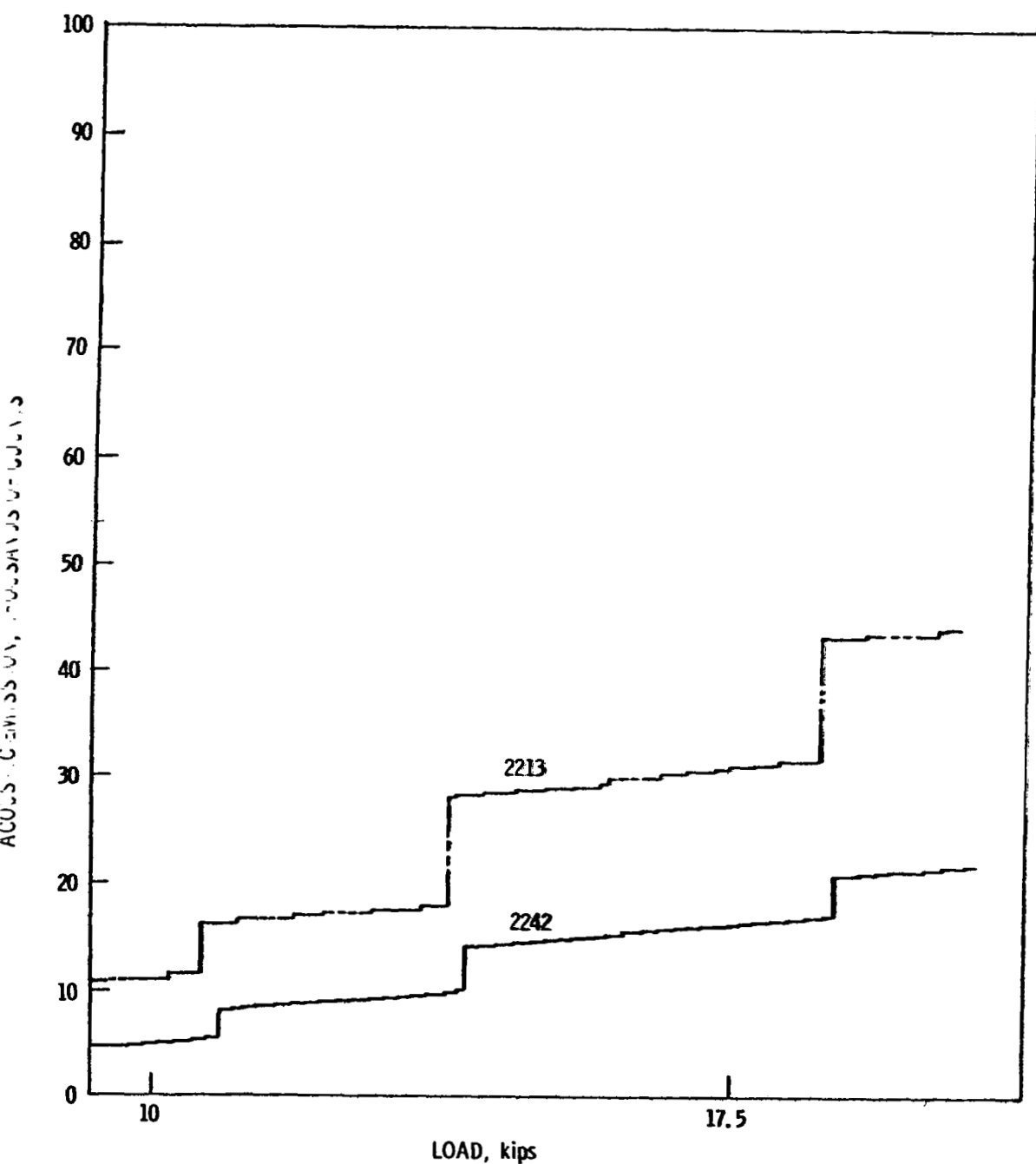2213 Accelerometers on 2219-T87 Specimen No. 28.

Figure 70. Comparison of Two Transducers Mounted on 2014-T6 Specimen
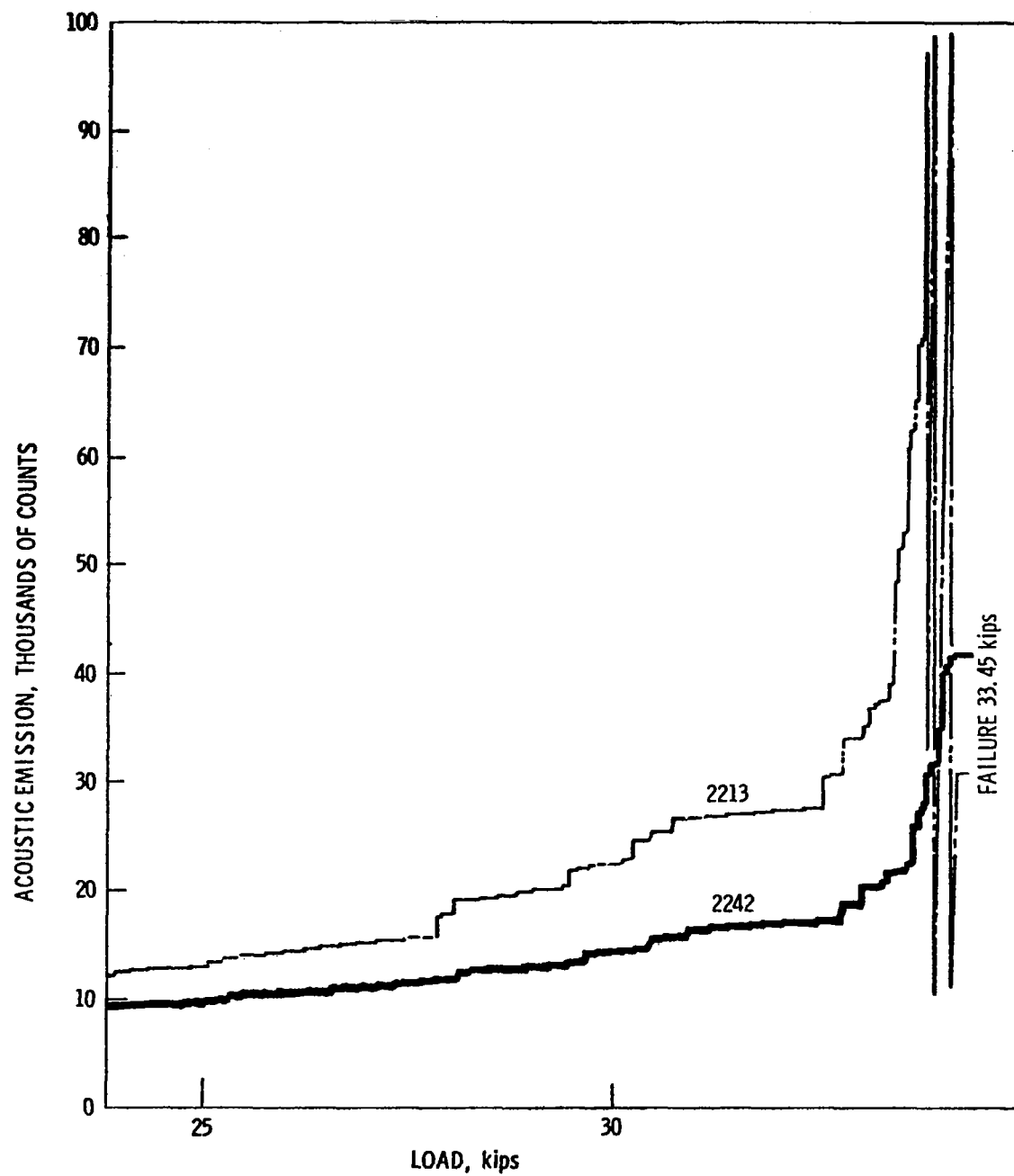No. 3 for the First Cycle to 20.2 kips.

154

Figure 71.   Comparison of Two Transducers Mounted on 2014-T6 Specimen
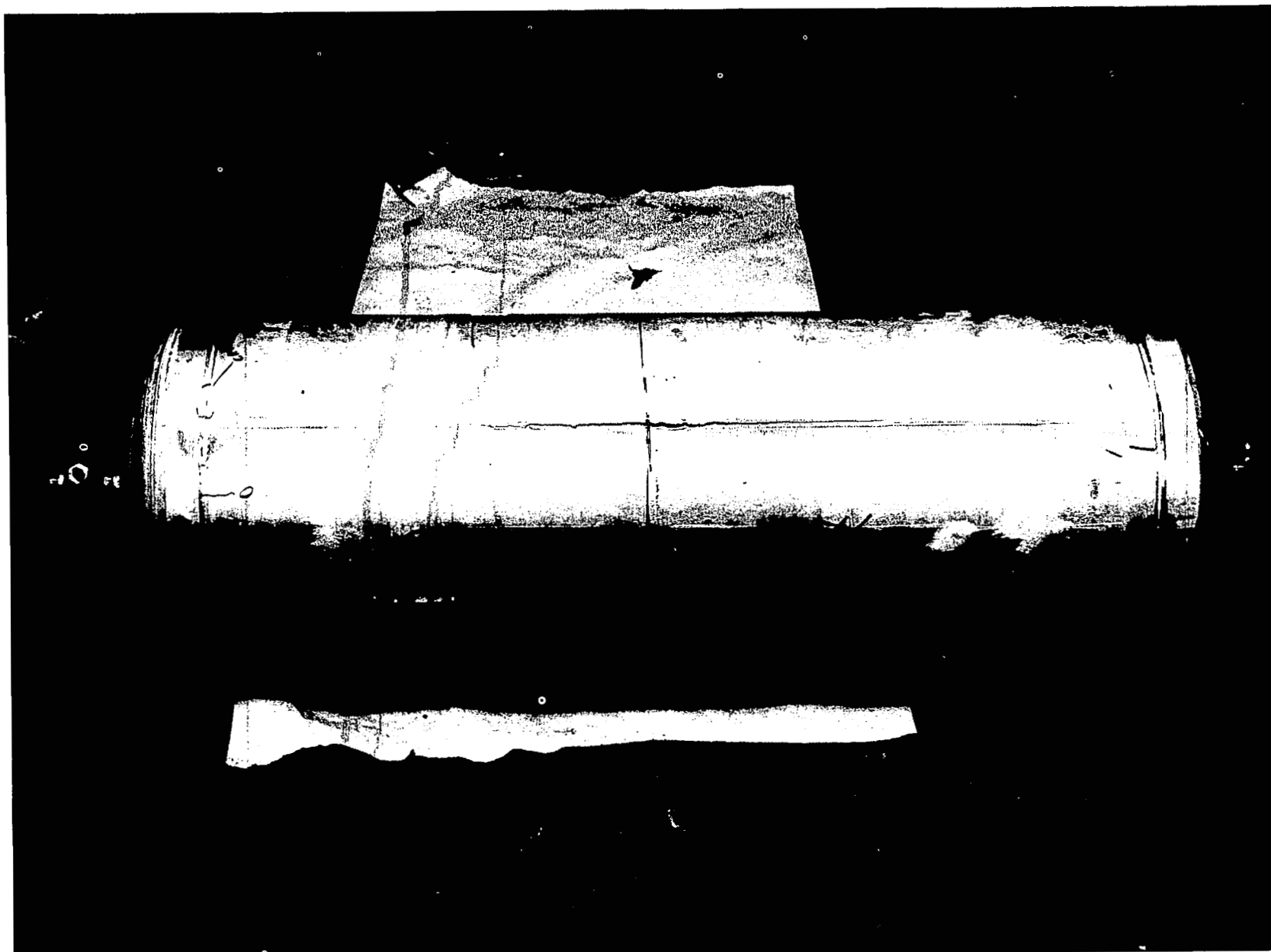No. 3 for the Second Cycle to Failure.

Figure 72.   2014-T6 Aluminum Vessel Hydroburst at Room Temperature

Figure 73. Close-up Views of the Failure Origin of the 2014-T6 Aluminum
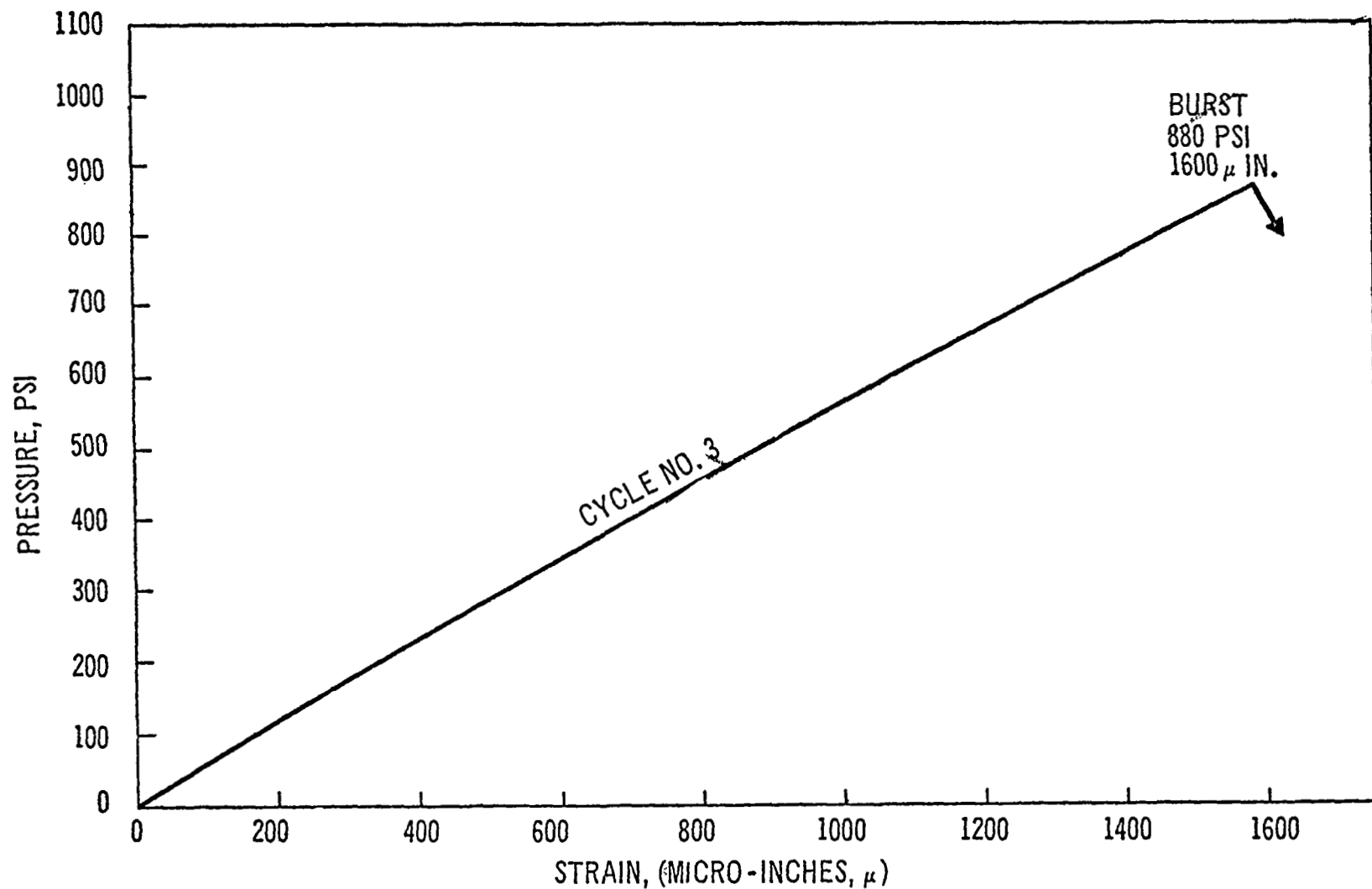Vessel Hydroburst at Room Temperature

Figure 74. Strain Gage Data (Hoop Orientation) for Final Pressure Cycle of the 2014-T6 Aluminum Vessel Tested at Room Temperature. Note Elastic Behavior of the Parent Metal Cylinder Section Where the Gage was Mounted.
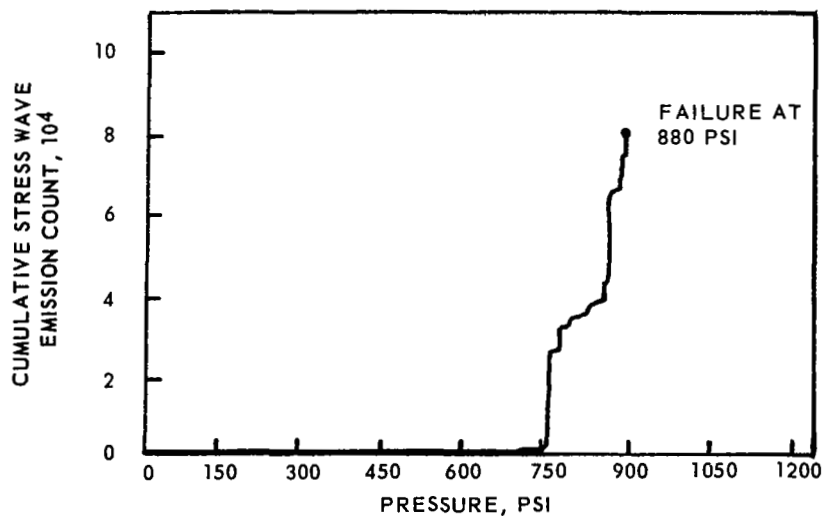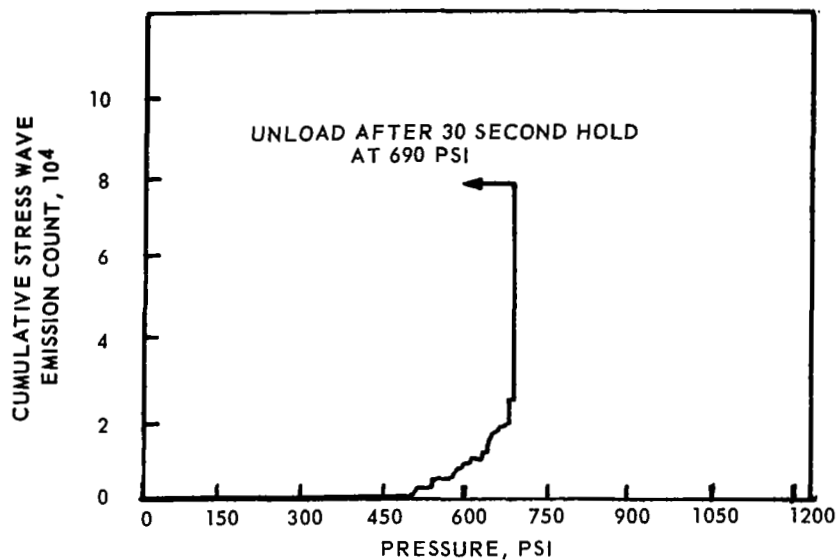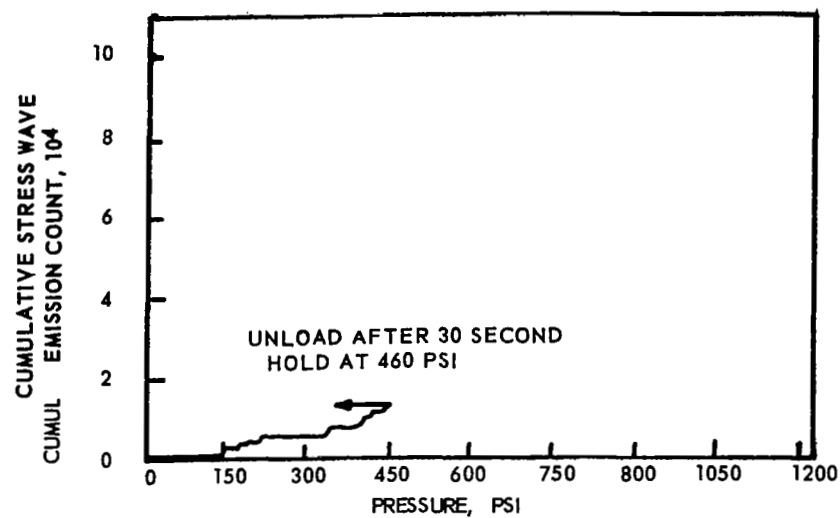
Figure 75. Cumulative Stress Wave Emission vs Pressure for the 2014-T6 Aluminum Vessel Hydroburst at Room Temperature (3 pages)

159
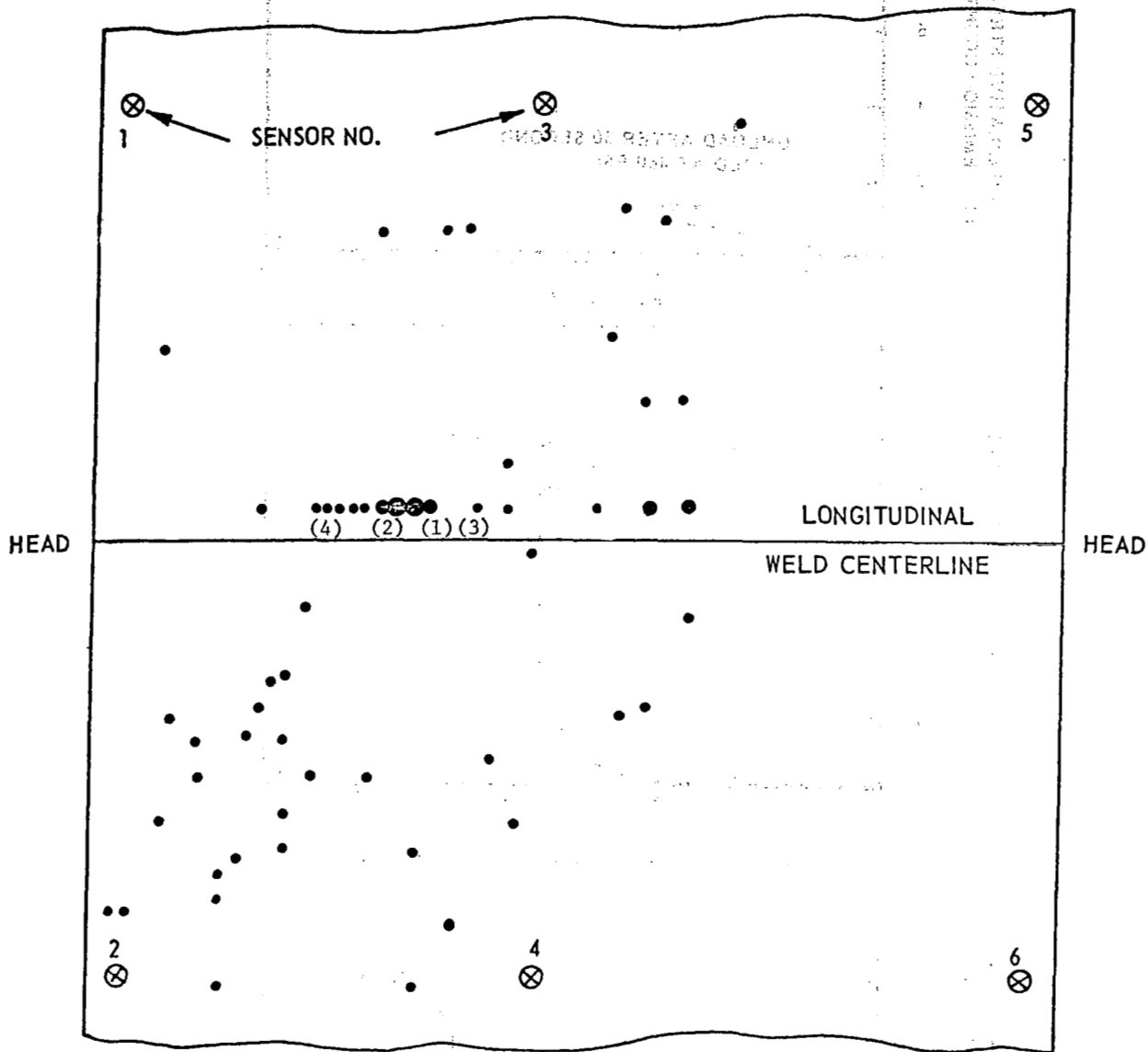
NOTE: Numbers in ( ) indicate fracture surface defects shown in Figure 80 .

Figure 76 . Location of SWE Sources Detected When Pressurizing 2014-T6 Aluminum Vessel to 460 psi at Room Temperature.
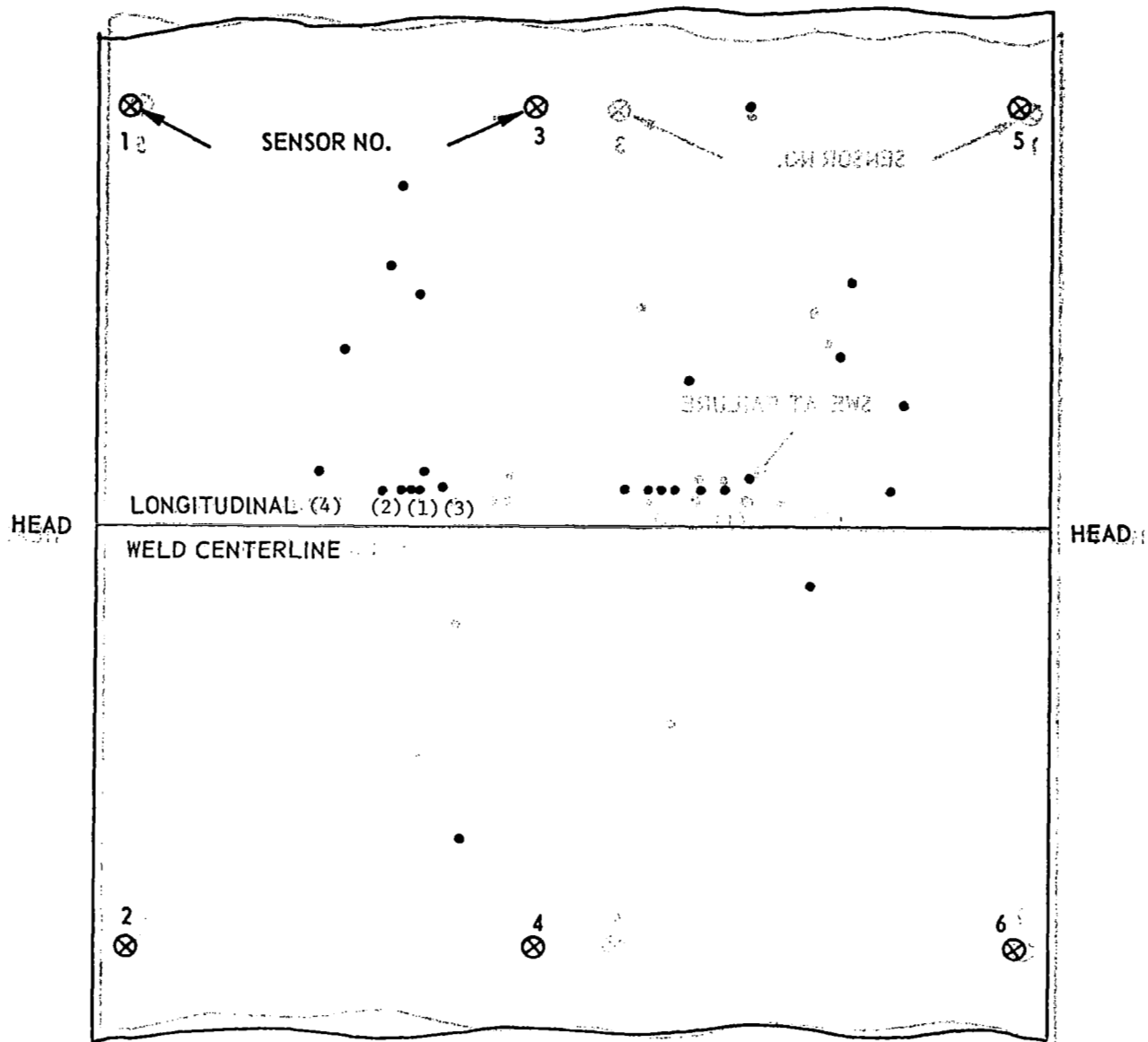
NOTE: Numbers in ( ) indicate fracture surface defects shown in
Figure 80 .

Figure 77. Location of SWE Sources Detected When Pressurizing the
2014-T6 Aluminum Vessel to 690 psi at Room Temperature.

NOTE: Numbers in ( ) indicate fracture surface defects shown in
Figure 80 .

Figure 78 .   Location of SWE Sources Detected When Pressurizing the
2014-T6 Aluminum Vessel to Failure at 880 psi at
Room Temperature.
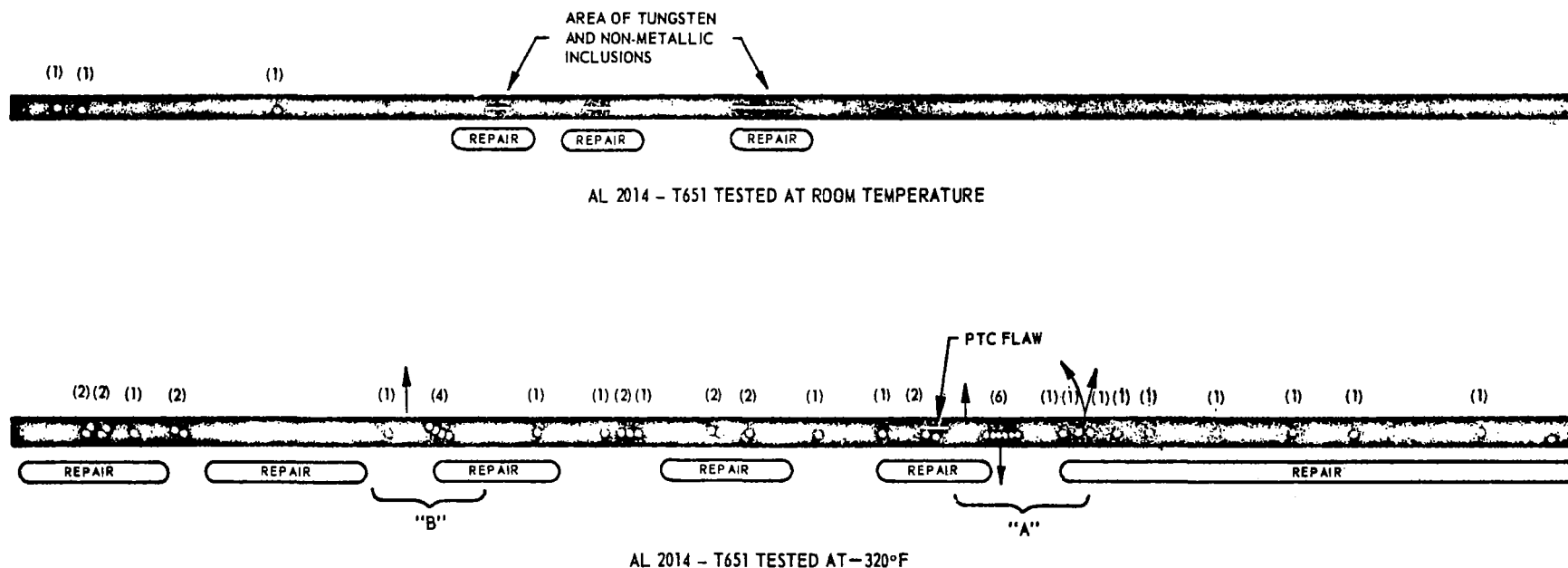
AREA OF TUNGSTEN
AND NON-METALLIC
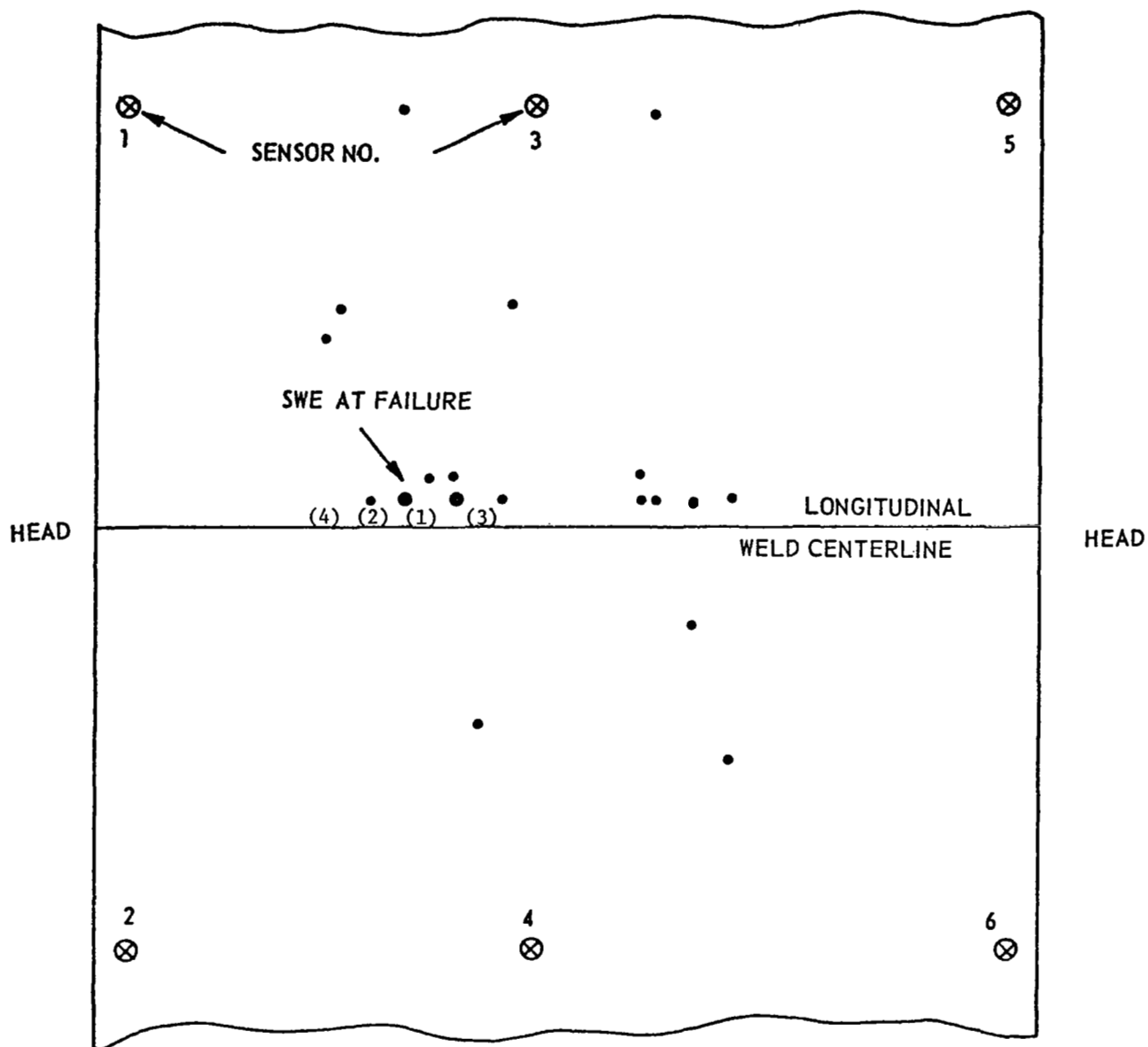INCLUSIONS

(1) (1)   (1)

REPAIR   REPAIR   REPAIR

AL 2014 – T651 TESTED AT ROOM TEMPERATURE

PTC FLAW

(2)(2) (1) (2)   (1)   (4)   (1)   (1)(2)(1)   (2) (2)   (1)   (1) (2)   (6)   (1)(1) (1)(1) (1)   (1)   (1)   (1)   (1)

REPAIR   REPAIR   REPAIR   REPAIR   REPAIR   REPAIR

"B"   "A"

AL 2014 – T651 TESTED AT–320°F

NOTE: NUMBERS IN ( ) INDICATE NUMBER OF PORES DETECTED AT EACH LOCATION.
INITIAL WELD AREAS REQUIRING REPAIR ARE SHOWN ADJACENT TO WELD.
ARROWS FROM WELD OF -320°F TEST INDICATE FRACTURE BRANCHING.
"A" AND "B" INDICATE PRIMARY AND POSSIBLE SECONDARY FAILURE ORIGIN.

Figure 79. Longitudinal Weld Defects - 2014-T6 Aluminum Pressure Vessels

FAILURE ORIGIN
AT ROOT OF REPAIR WELD

FAILURE ORIGIN

Non Fusion
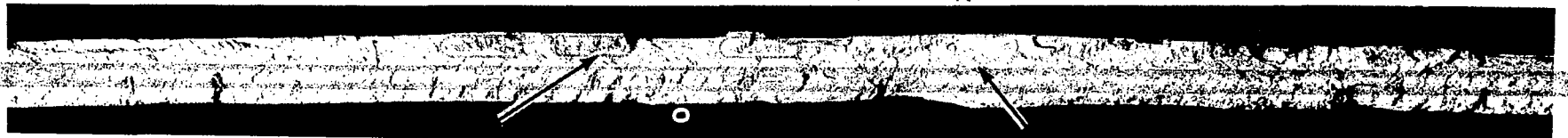
Figure 80. Longitudinal Weld Fracture Faces –2014–T6 Aluminum Vessel Hydroburst at Room Temperature.
Note Repair Weld Area from which Failure Occurred and Other Weld Defects Indicated by Arrows.
(Striations on Surface are Due to Weld Head Oscillation).
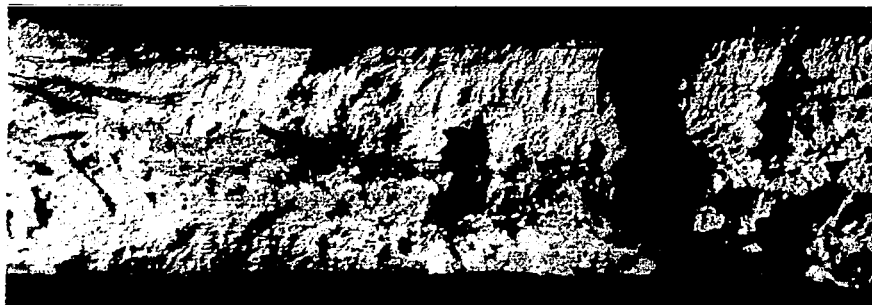
(1)

(2)

(3)
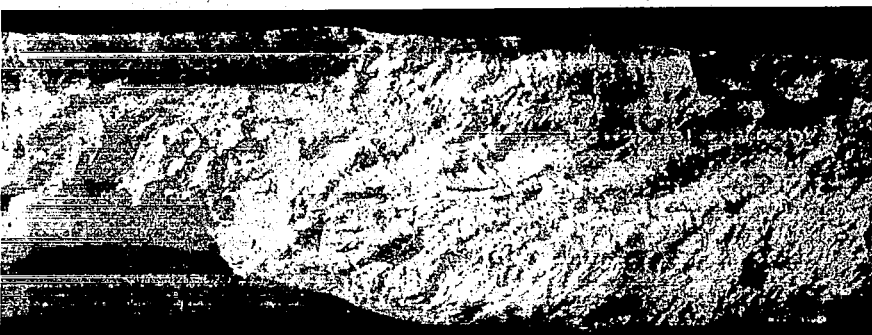
(4)

Figure 81. Areas of Longitudinal Weld Non-Fusion, Inclusions and Porosity on the Fracture Surface of the 2014-T6 Aluminum Vessel Burst at Room Temperature. Figure 78 shows the location of these defects in the longitudinal weld. (Magnification approximately 4X)

165
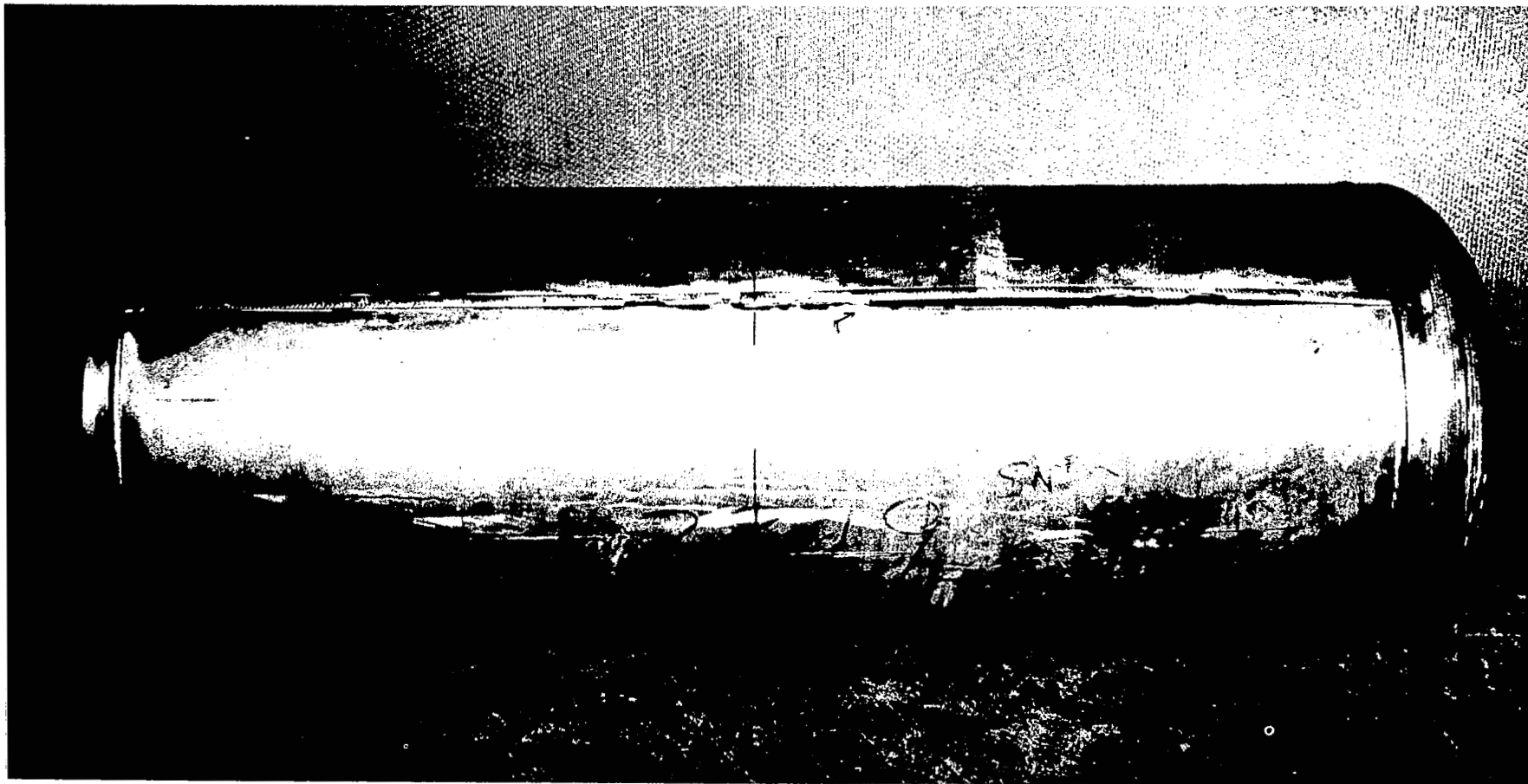
Figure 82.   2219-T87 Aluminum Vessel Hydroburst at Room Temperature.
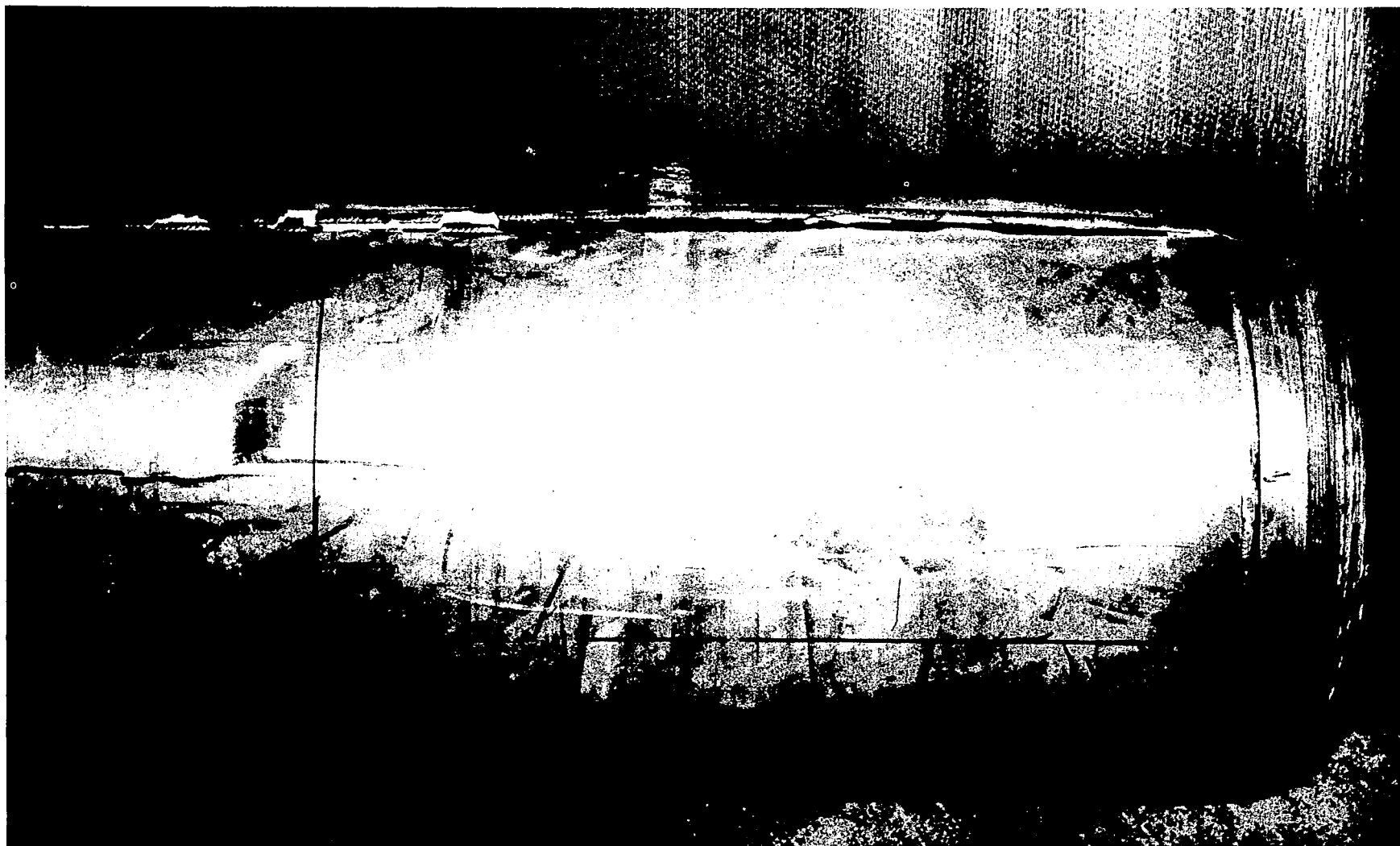
Figure 83. Close-up View of 2219-T87 Aluminum Vessel Fracture After Hydroburst
at Room Temperature.
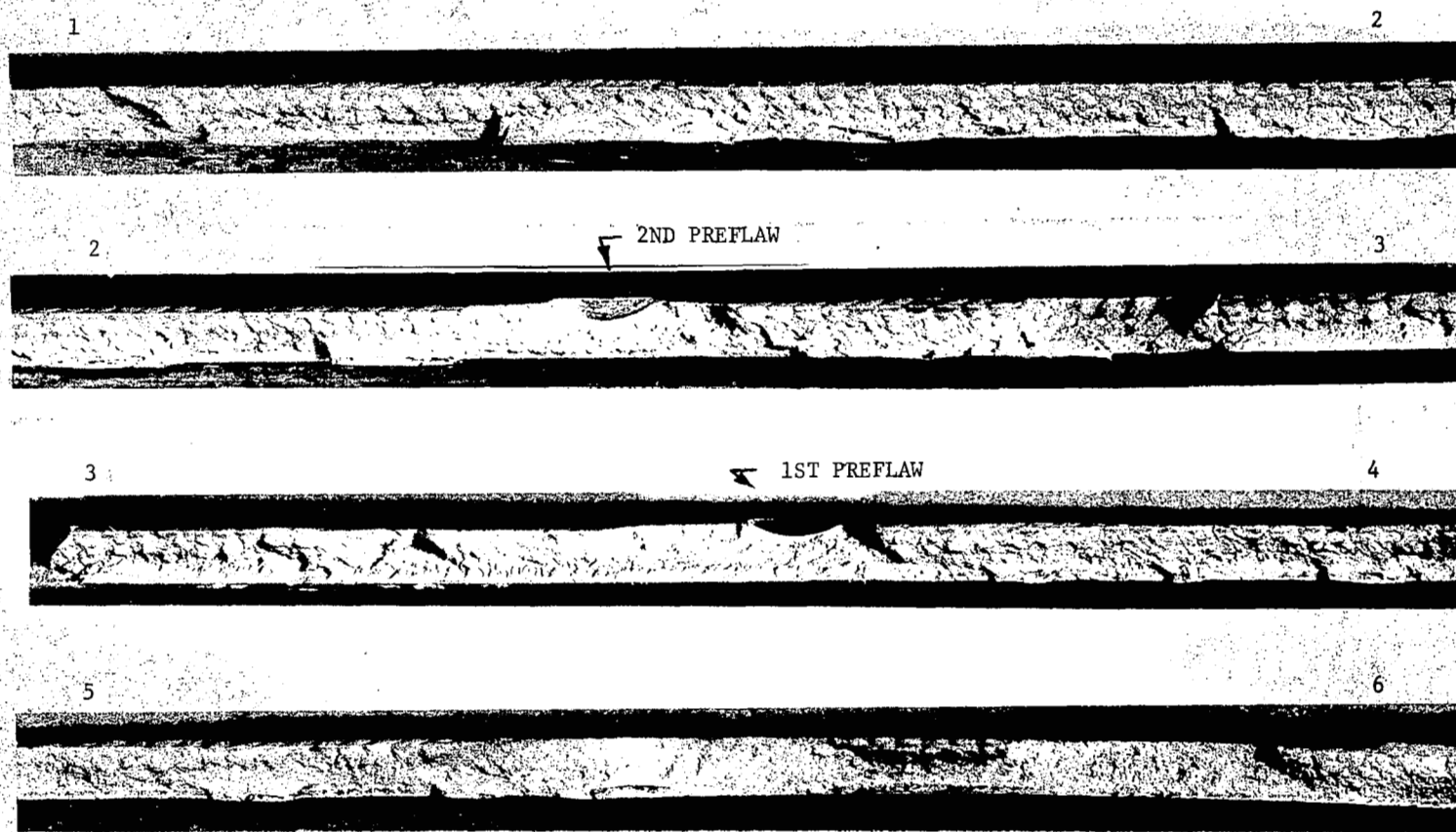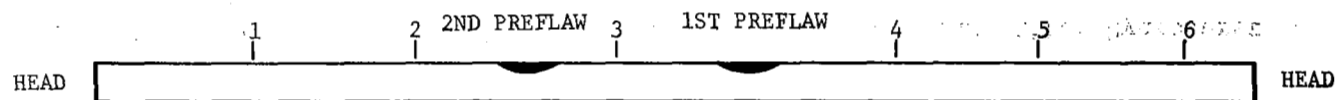
Figure 84. Longitudinal Weld Fracture Faces –2219-T87 Aluminum Vessel Hydroburst at Room Temperature. Note Preflaws and Fracture Propagation Through these Defects. Failure Origin was at the 1st Preflaw Introduced into the Weld. (Striations on Surface are Due to Weld Head Oscillation).

168
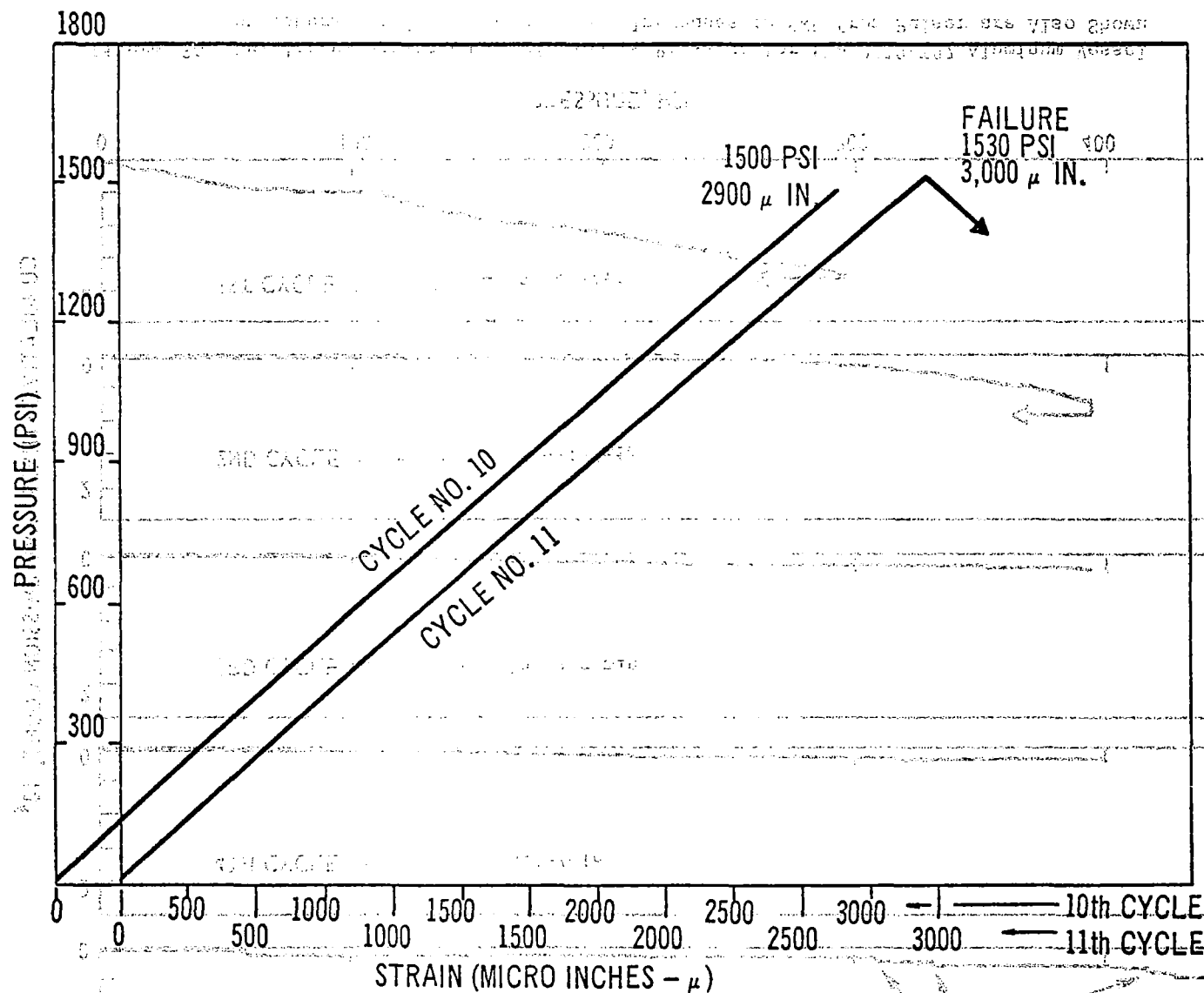
Figure 85. Strain Gage Data (Hoop Orientation) for Final Pressure Cycles of the 2219-T87 Aluminum Vessel Tested at Room Temperature. Note Elastic Behavior of the Parent Metal Cylinder Section Where the Gage was Mounted.
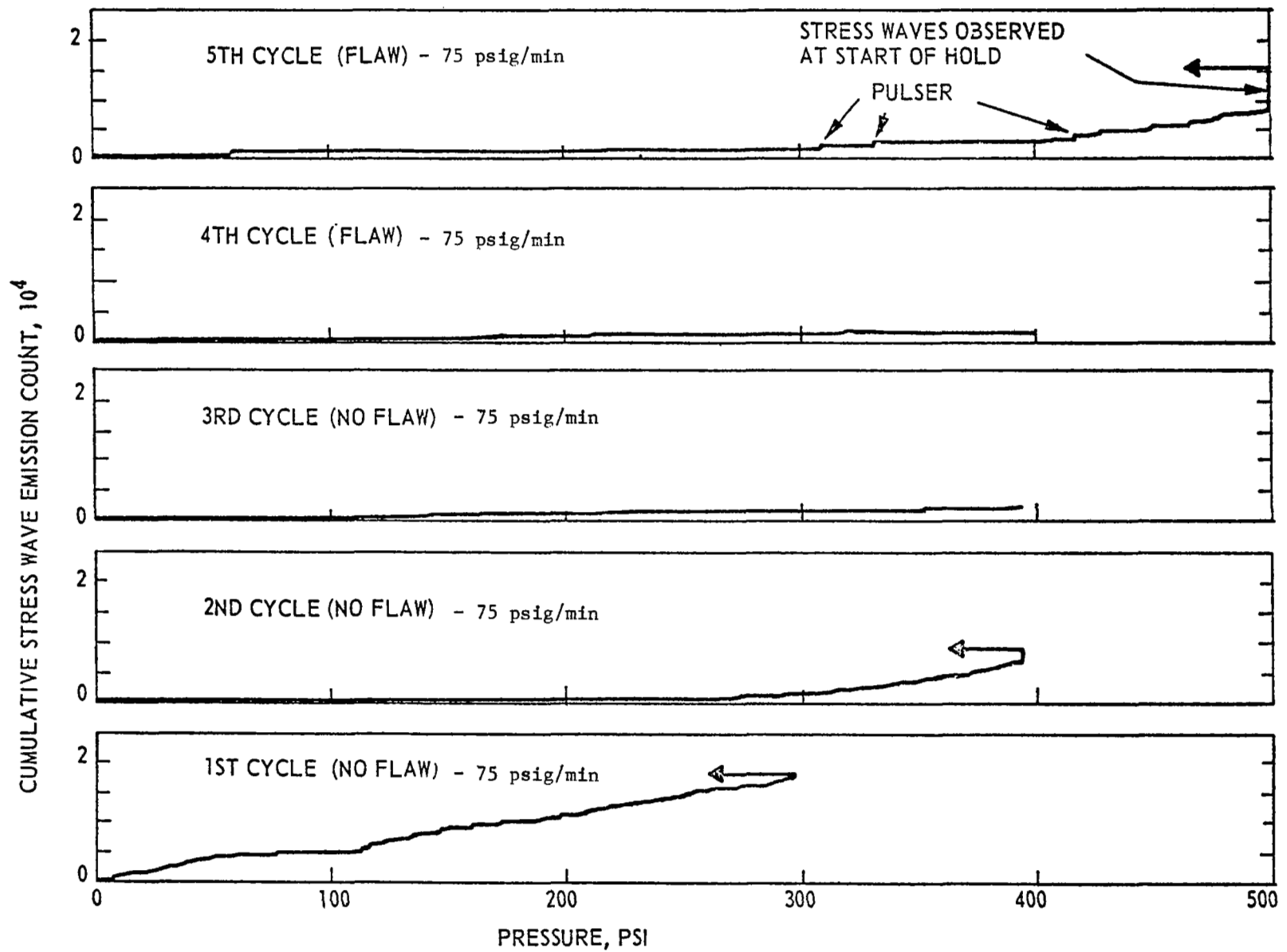
Figure 86. Cumulative Stress Wave Emission vs Pressure for the 2219-T87 Aluminum Vessel Hydroburst at Room Temperature. Increases in SWE from Pulser are Also Shown
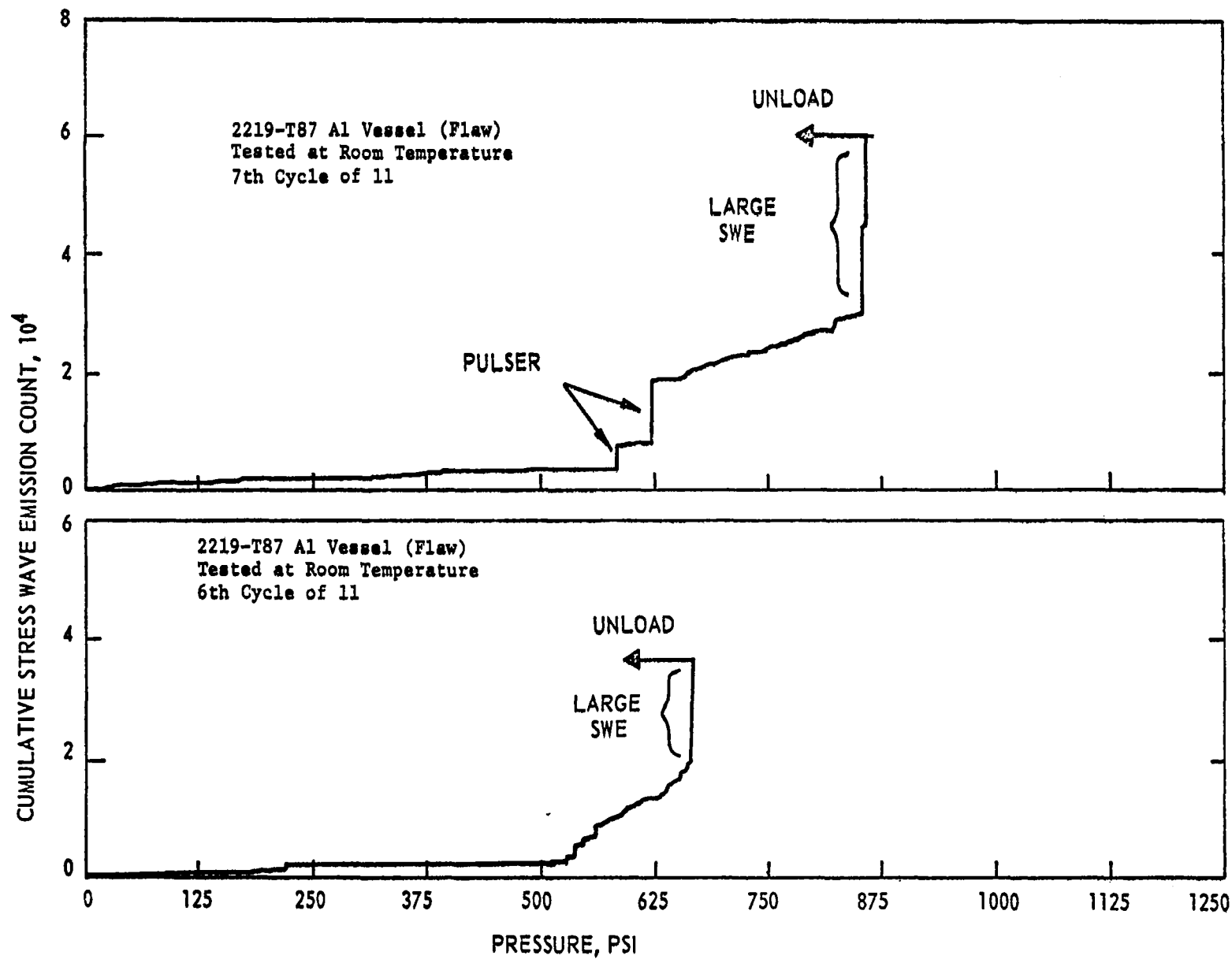
Figure 86. Continued (Page 2 of 4)
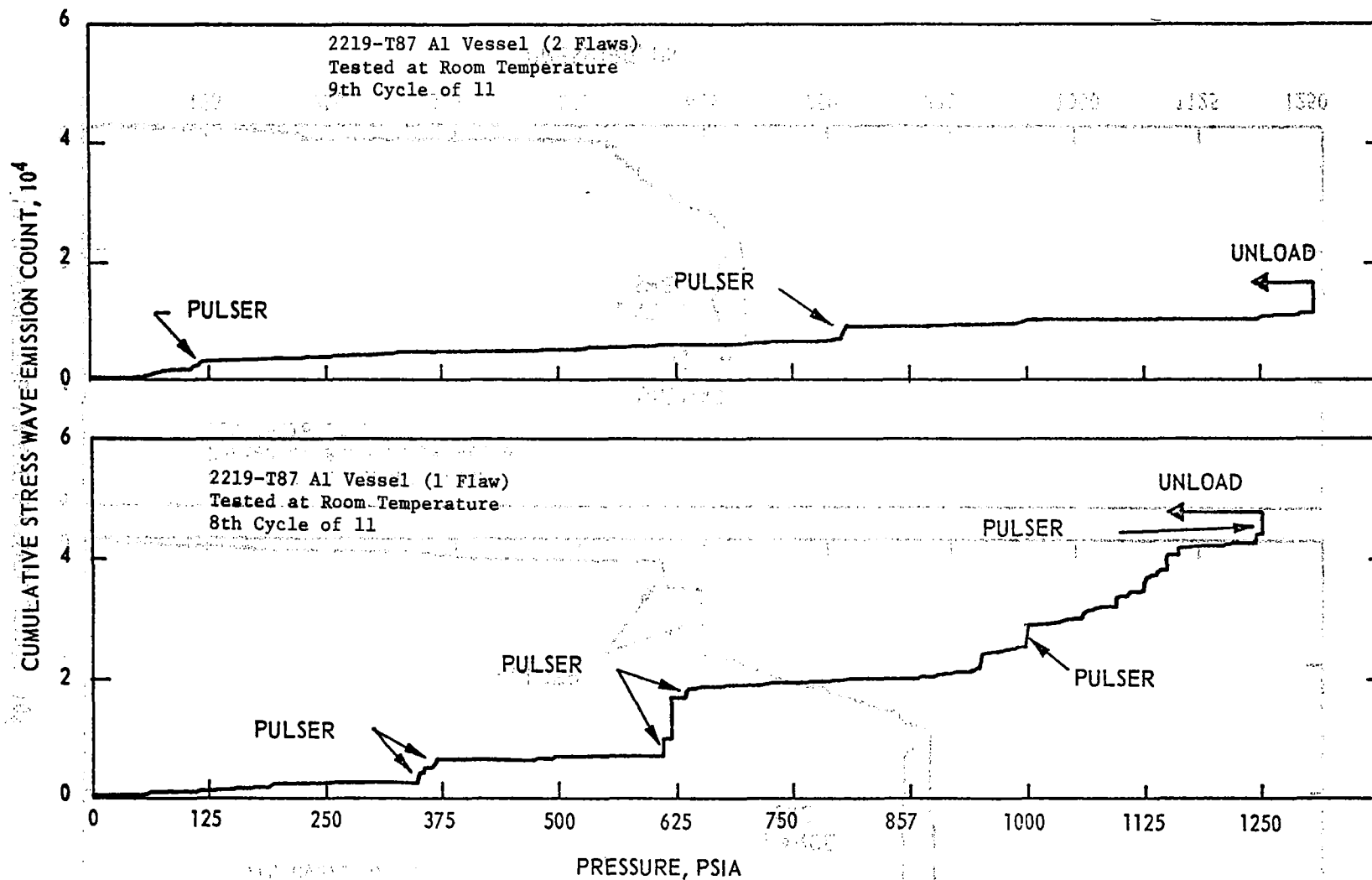
Figure 86. Continued (Page 3 of 4)
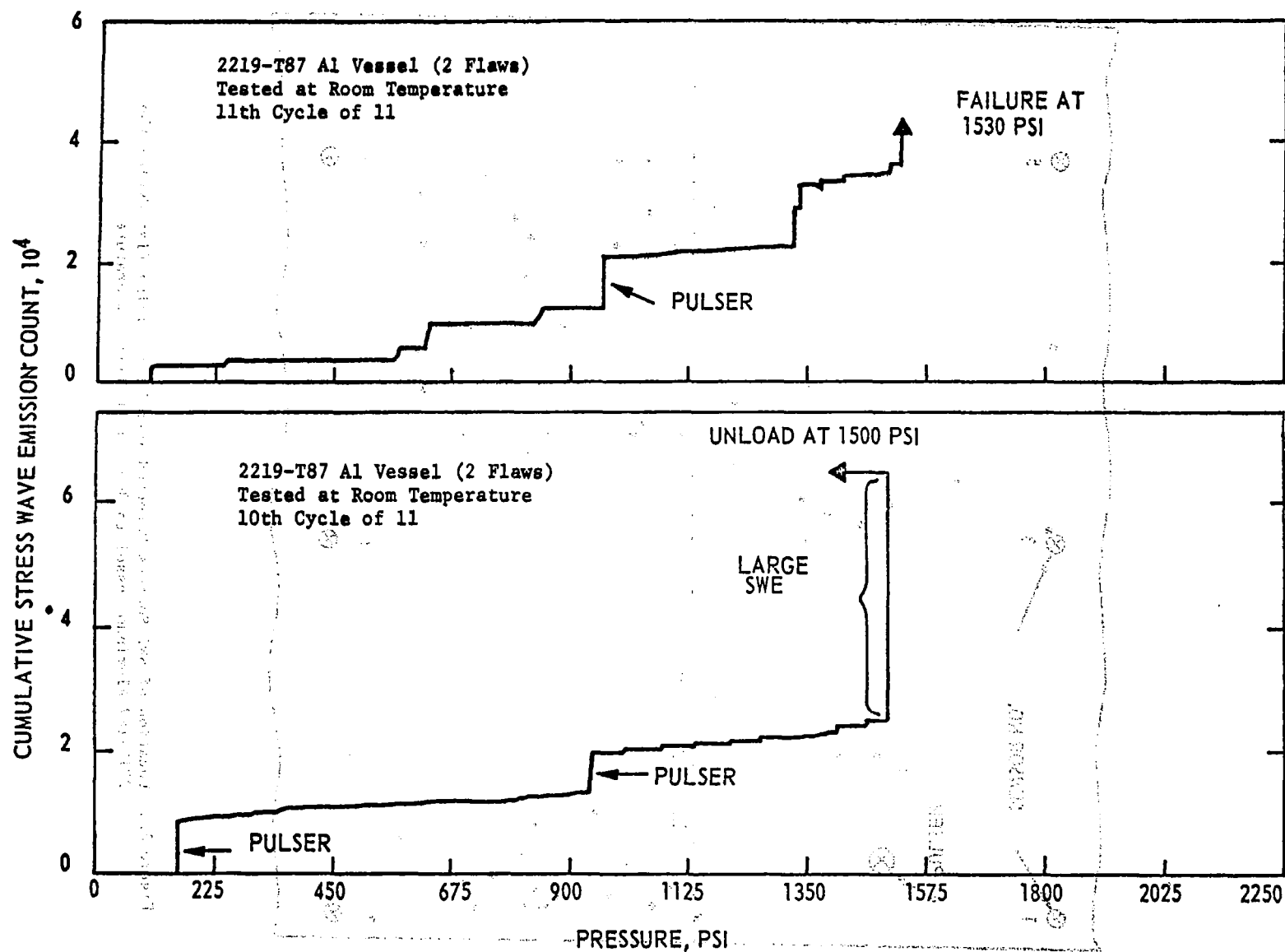
Figure 86. Continued (Page 4 of 4)
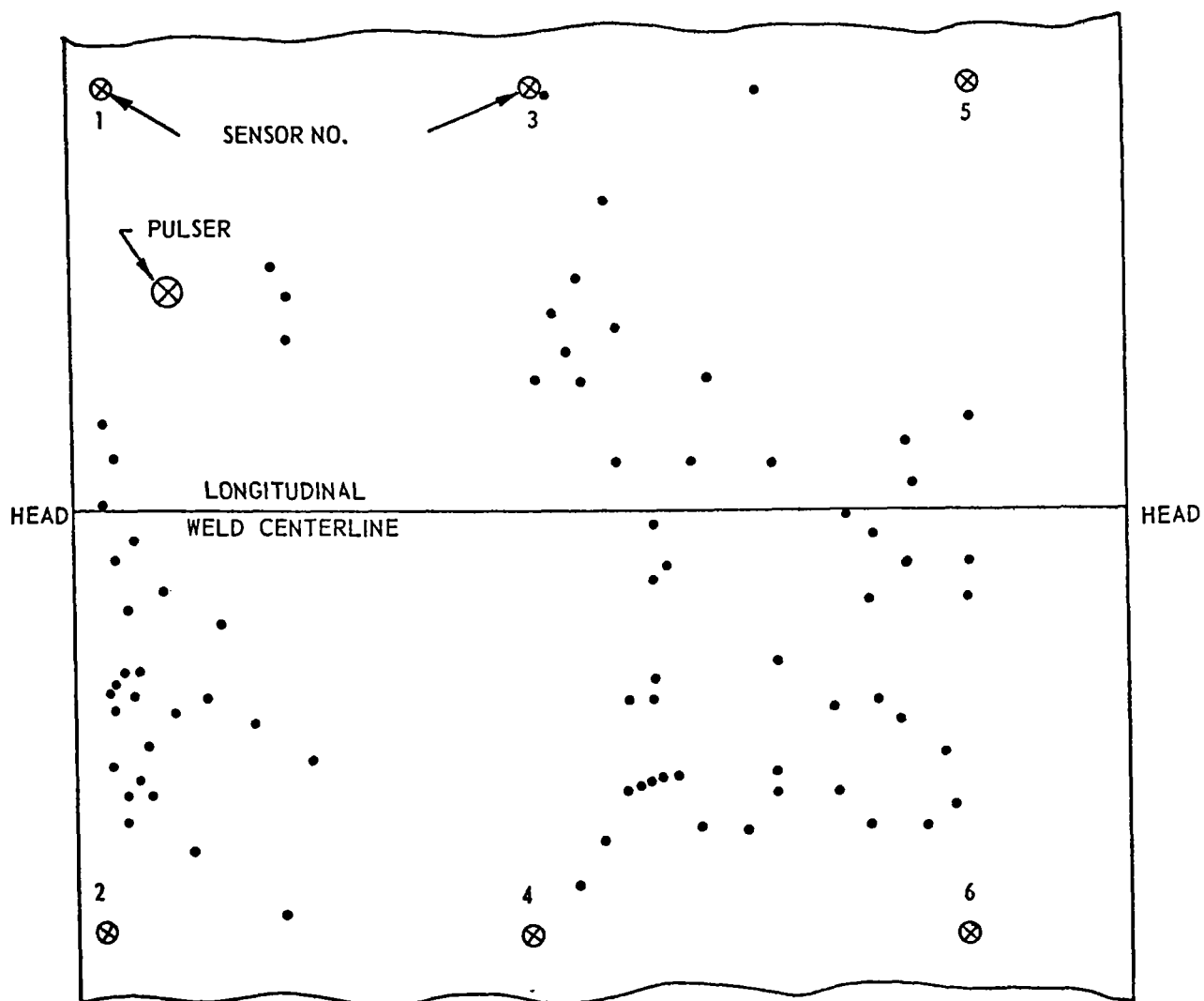
Figure 87. Location of SWE Sources Detected When Pressurizing (1st Cycle) the 2219-T87 Aluminum Vessel to 300 psi at Room Temperature.

174

Figure 88. Location of SWE Sources Detected When Pressurizing (2nd Cycle) the 2219-T87 Aluminum Vessel to 400 psi at Room Temperature.
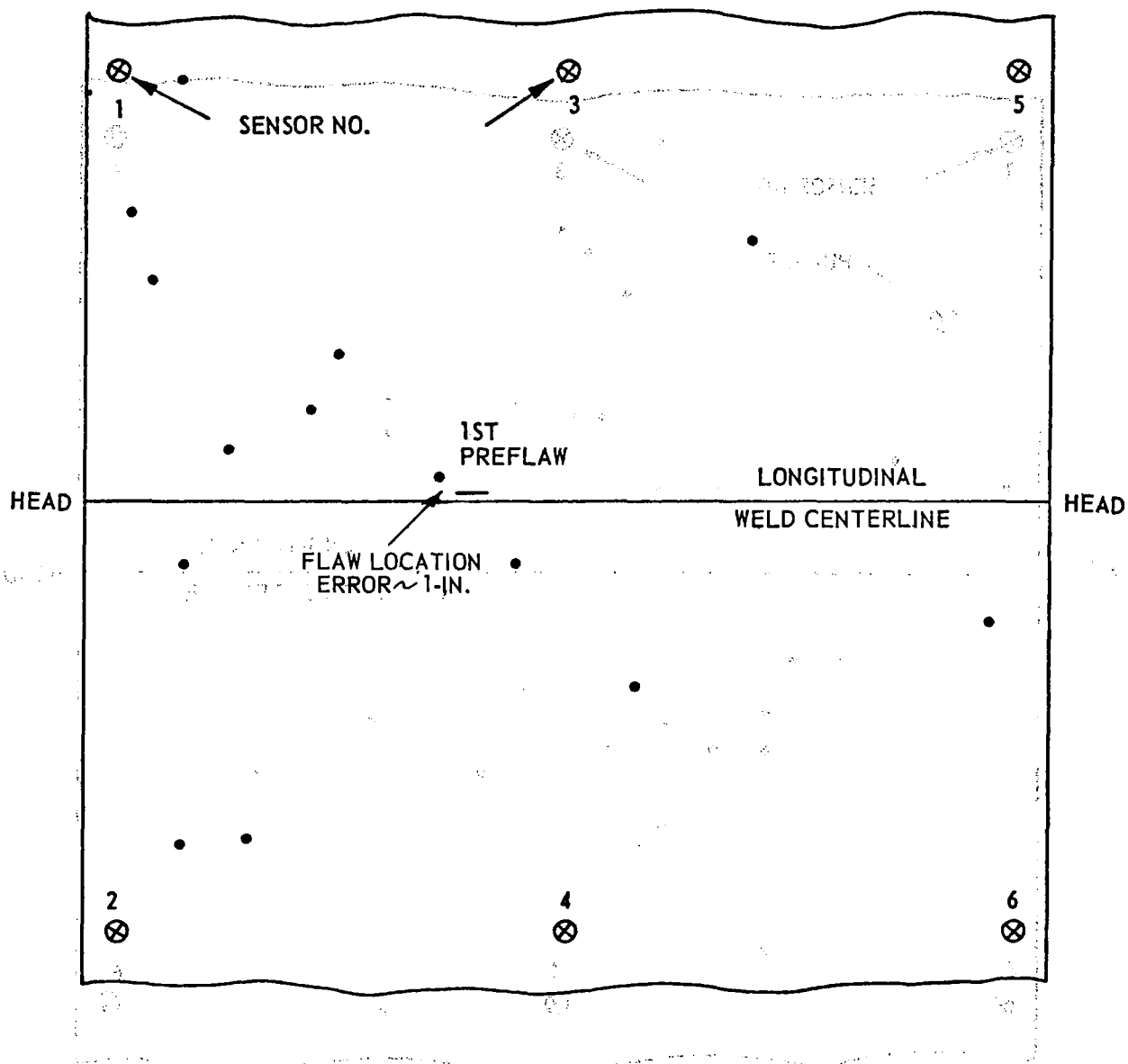
Figure 89. Location of SWE Sources Detected When Pressurizing (4th Cycle)
the 2219-T87 Aluminum Vessel to 400 psi at Room Temperature.
Location of the 1st Preflaw Inserted in the Longitudinal Weld
is Shown.
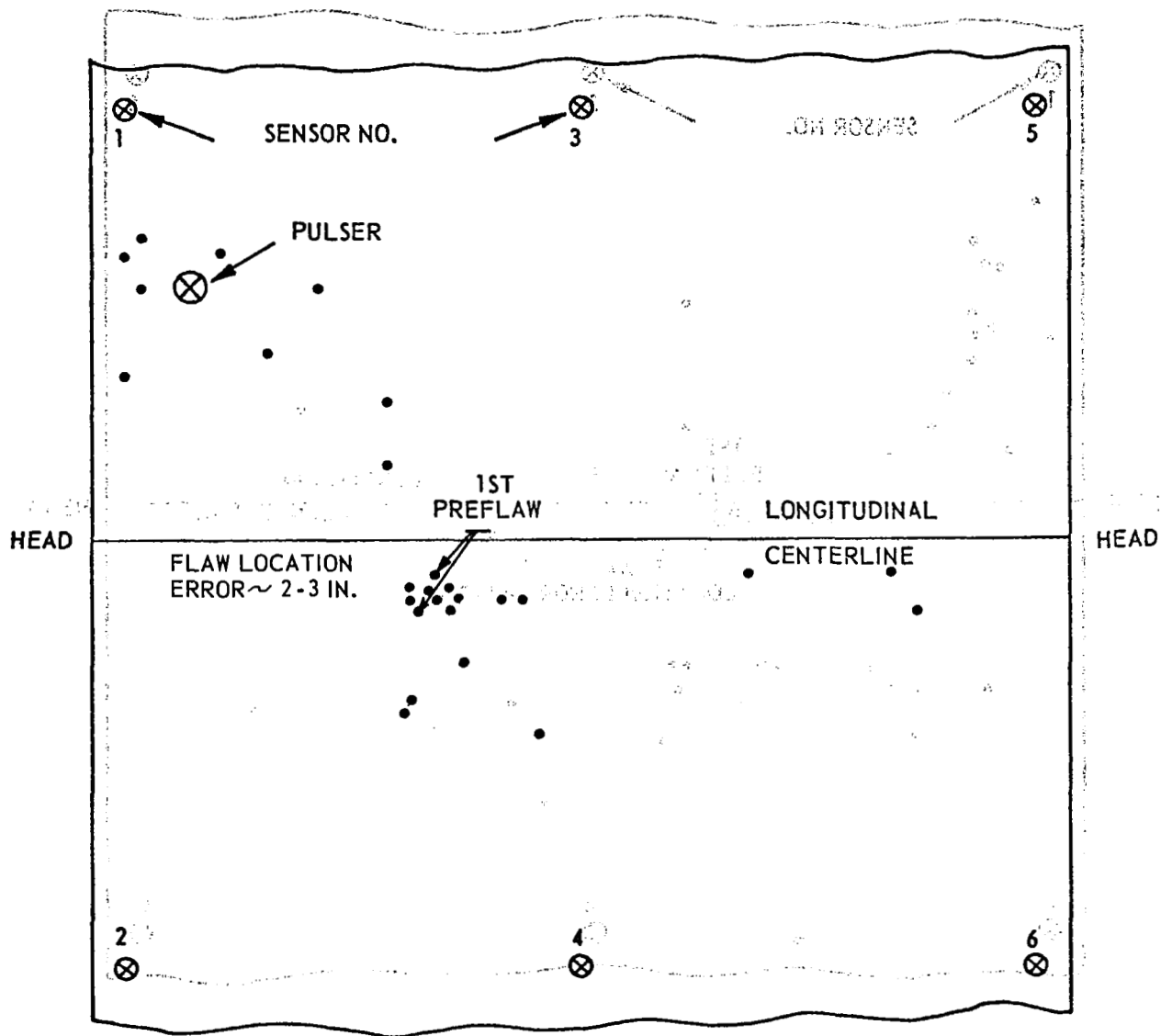
Figure 90. Location of SWE Sources Detected When Pressurizing (5th Cycle)
the 2219-T87 Aluminum Vessel to 500 psi at Room Temperature.
Weld Preflaw Location also Shown.

177
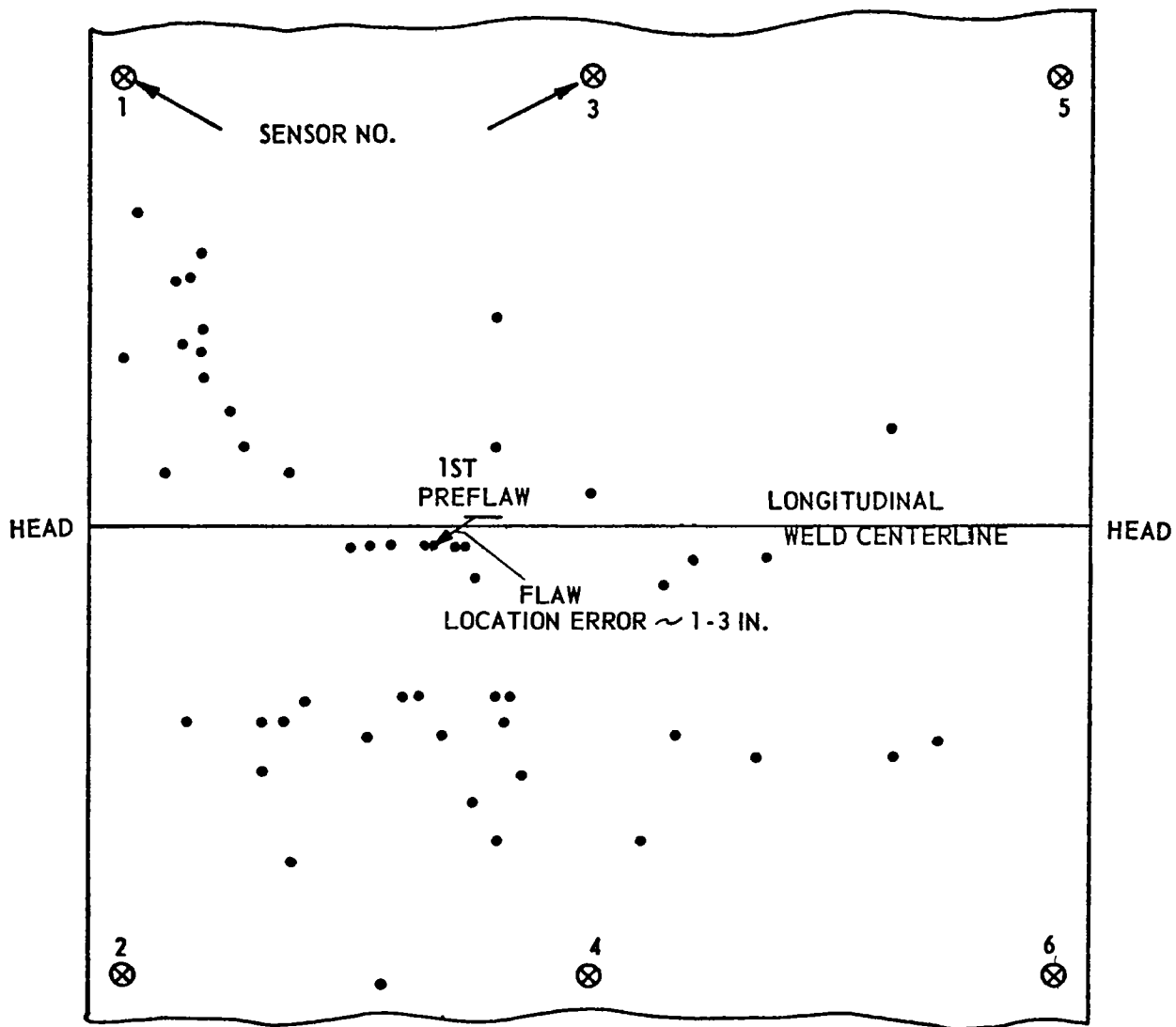
Figure 91. Location of SWE Sources Detected When Pressurizing (6th Cycle)
the 2219-T87 Aluminum Vessel to 680 psi at Room Temperature.
Weld Preflaw Location also Shown.
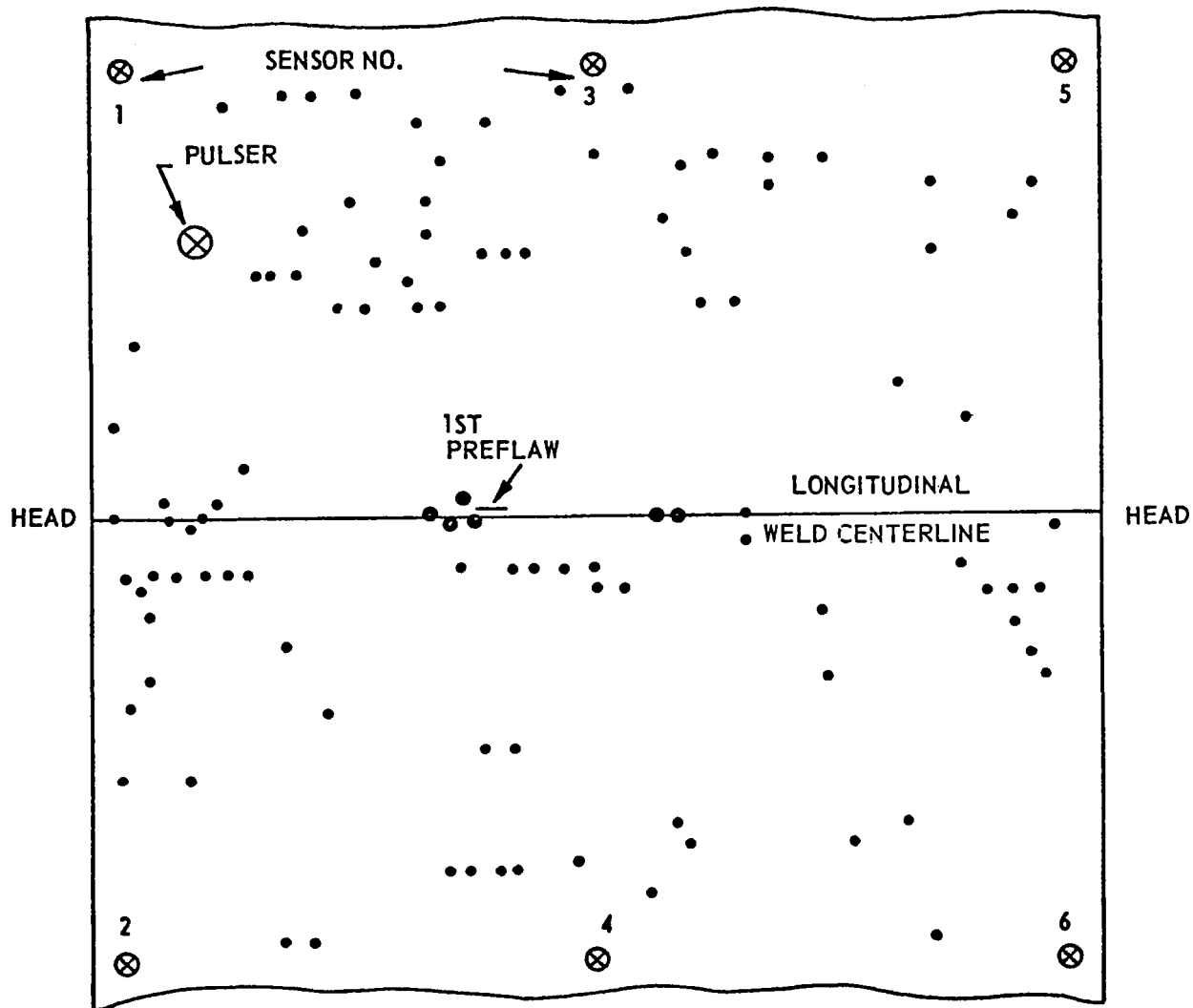
Figure 92. Location of SWE Sources Detected When Pressurizing (7th Cycle)
the 2219-T87 Aluminum Vessel to 860 psi at Room Temperature.
Weld Preflaw Location also Shown.

179
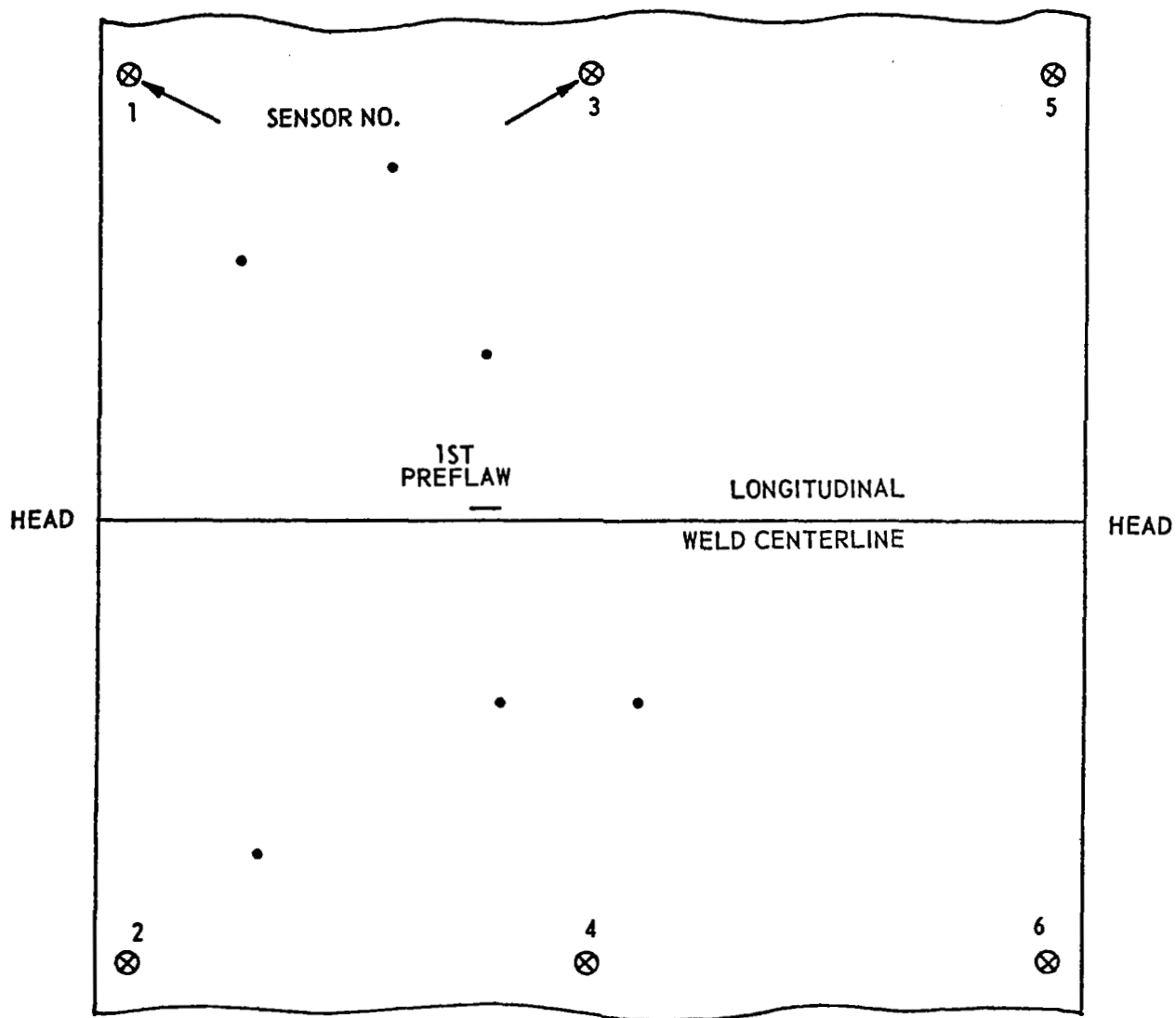
Figure 93. Location of SWE Sources Detected When Pressurizing (8th Cycle) the 2219-T87 Aluminum Vessel to 1250 psi at Room Temperature. Weld Preflaw Location also Shown.

Figure 94. Location of SWE Sources Detected When Pressurizing
(10th and 11th Cycles) The 2219-T87 Aluminum Vessel
to 1500 and 1530 psi (failure) at Room Temperature.
Weld Preflaw Locations also Shown.

181

2ND PTC FLAW   1ST PTC FLAW

(1)   (1)   (1)   (2)   (1)   (1)   (1) (1)
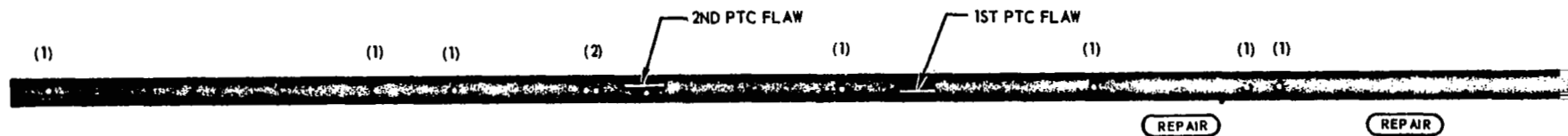
(REPAIR)   (REPAIR)

AL 2219 – T87 TESTED AT ROOM TEMPERATURE

PTC FLAW

(2)   (1)

(REPAIR)   (REPAIR)   (REPAIR)

AL 2219 – T87 TESTED AT –320°F

NOTE: NUMBERS IN ( ) INDICATE NUMBER OF PORES DETECTED AT EACH LOCATION.
INITIAL WELD AREAS REQUIRING REPAIR ARE SHOWN ADJACENT TO WELD.

Figure 95. Longitudinal Weld Defects – 2219-T87 Aluminum Pressure Vessels
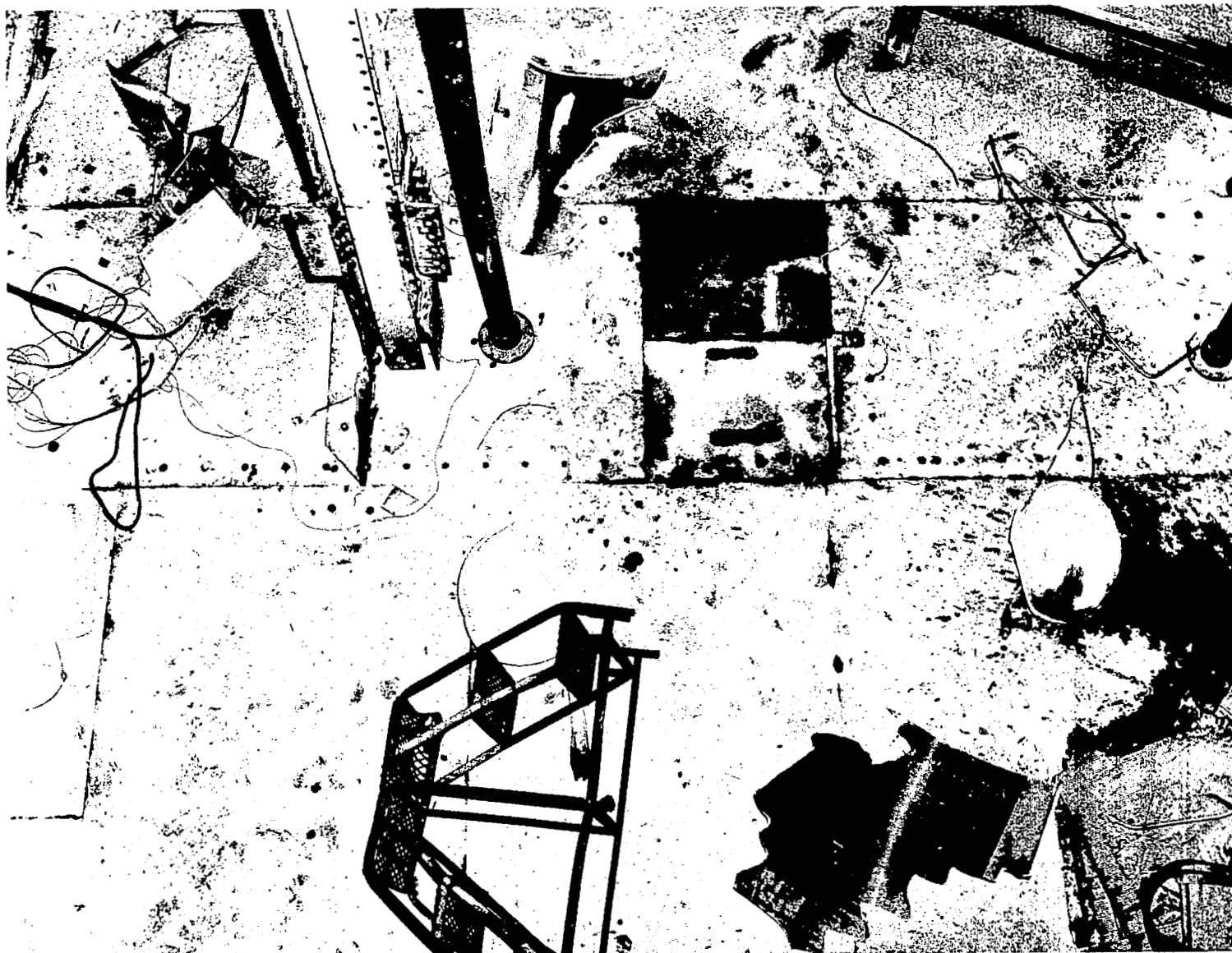
Figure 96. 2014-T6 Aluminum Vessel after Burst at -320°F

Figure 97.   2014-T6 Aluminum Vessel After Burst at -320°F and Reassembly on Floor of Test Cell

HEAD

"B"

PTC
FLAW

"A"

HEAD

LONGITUDINAL
WELD

"A" – PRIMARY FAILURE ORIGIN   "B" – POSSIBLE SECONDARY FAILURE ORIGIN
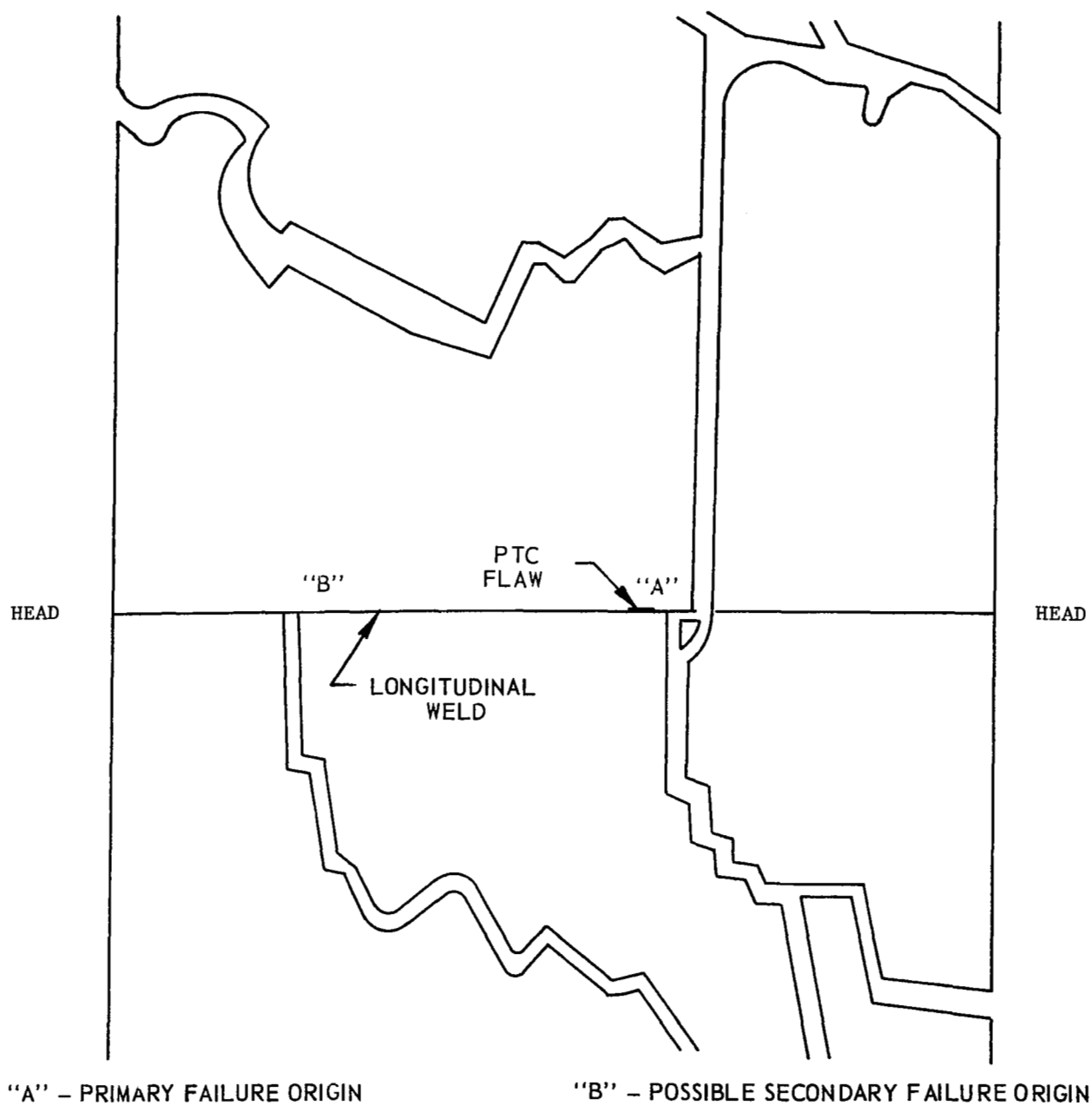
Figure 98.   Fracture Surfaces in the Cylinder Section Near the
Longitudinal Weld.   2014-T6 Vessel Tested at –320°F.

185
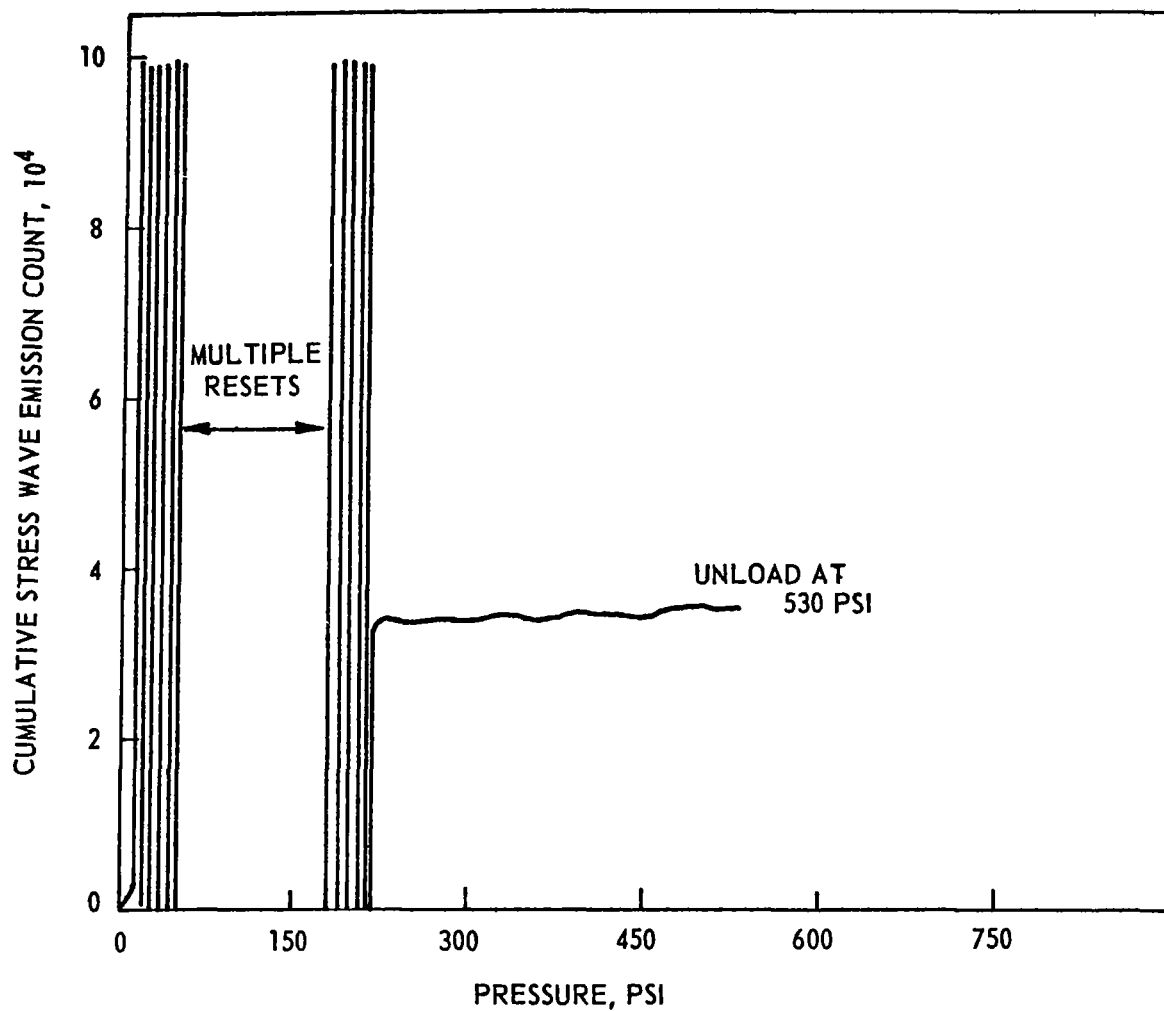
Figure 99. Cumulative Stress Wave Emission vs Pressure for the 2014-T6 Vessel Tested at -320°F. Cycle No. 1 of a Two Cycle Test Series (Page 1 of 2)

186
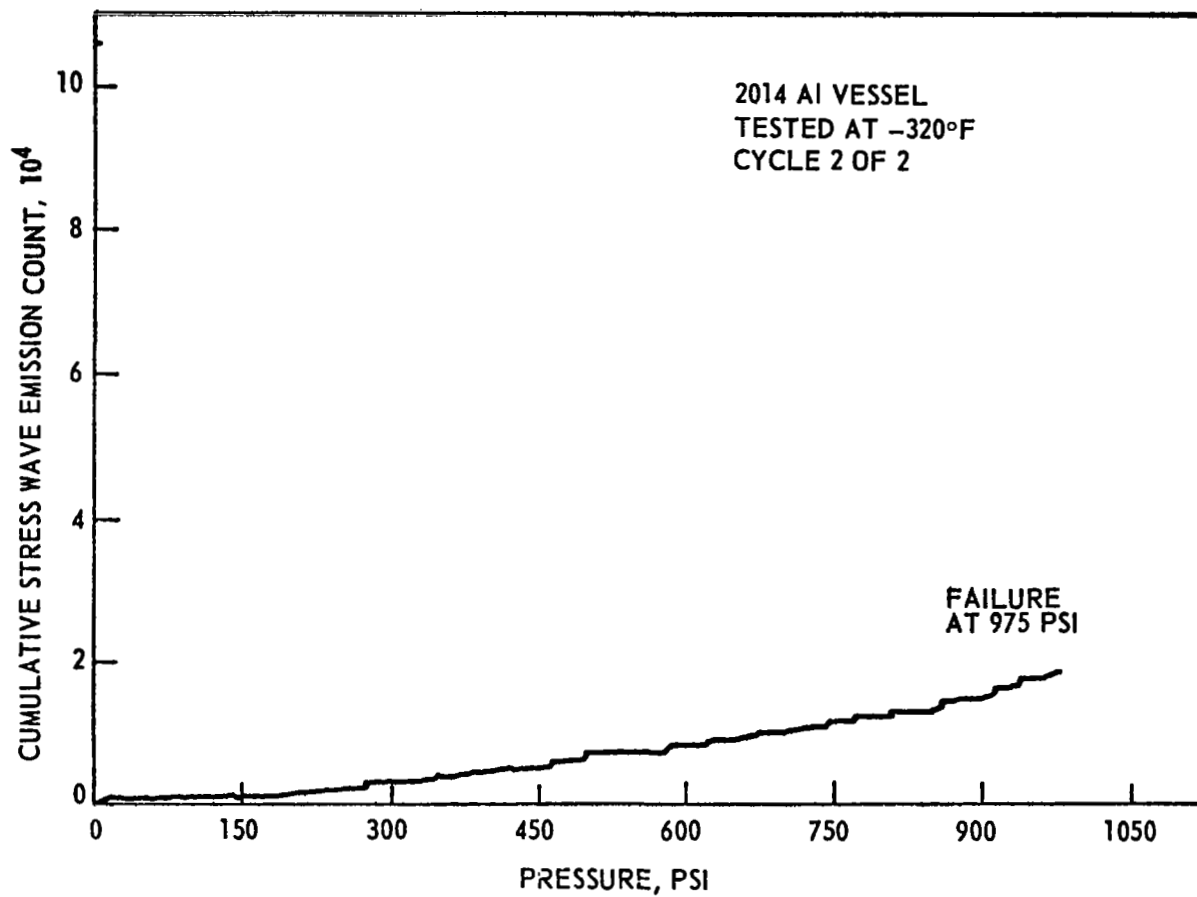
Figure 99.   Continued (Page 2 of 2)
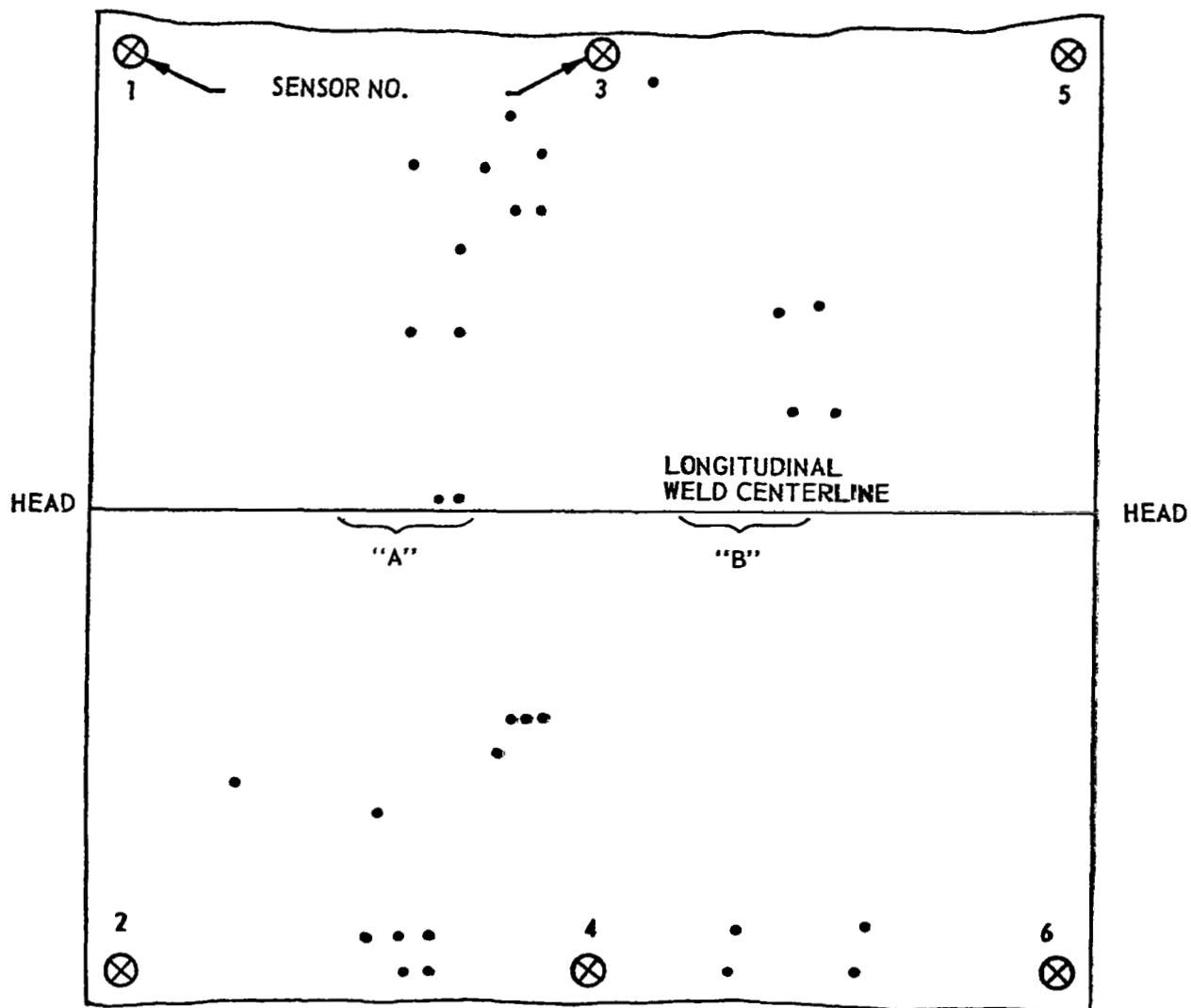
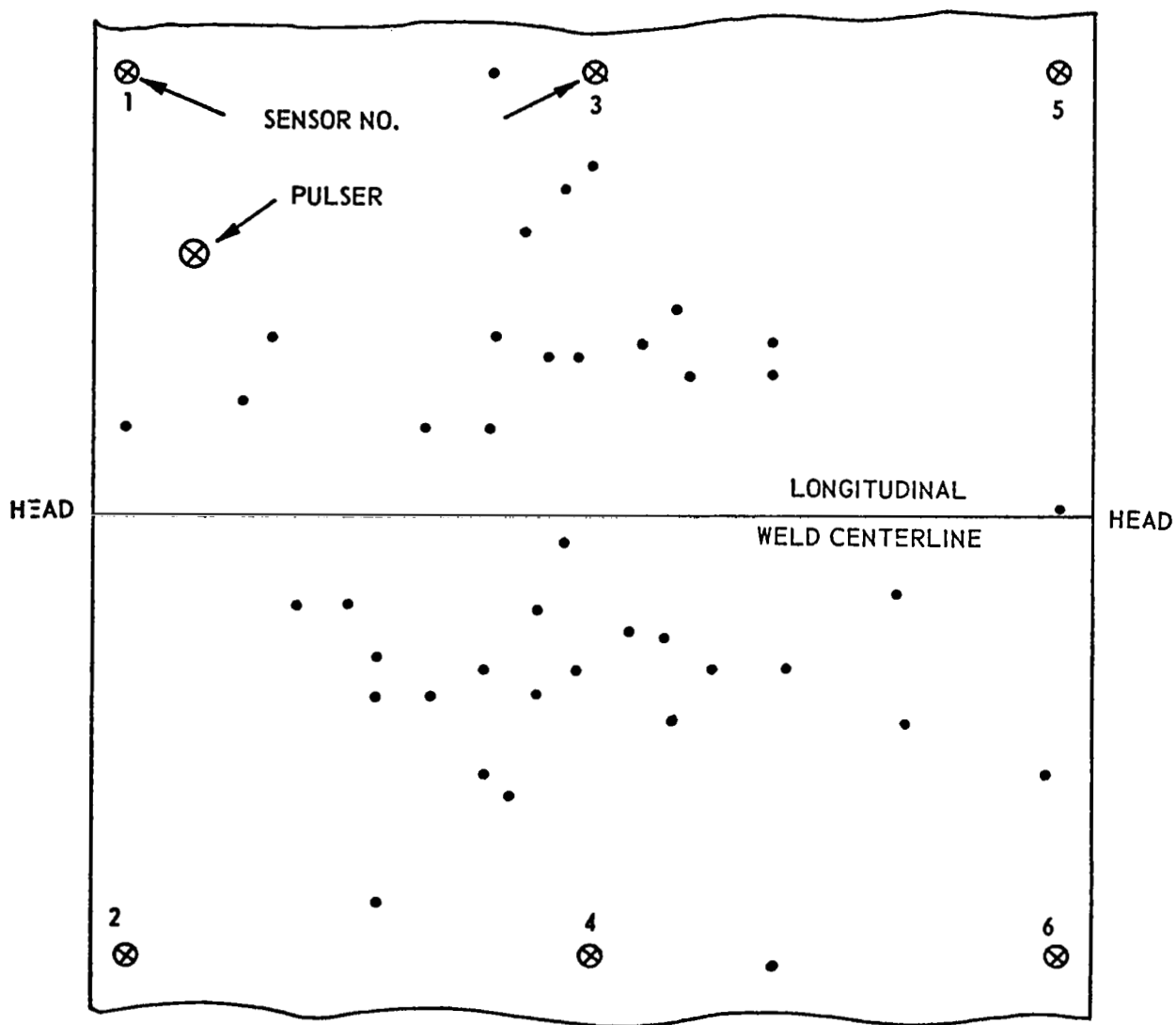Figure 100. Location of SWE Sources Detected When Pressurizing (1st Cycle) the 2014-T6 Aluminum Vessel to 550 psi at -320°F. "A" and "B" indicate primary and secondary (possible) failure origins.
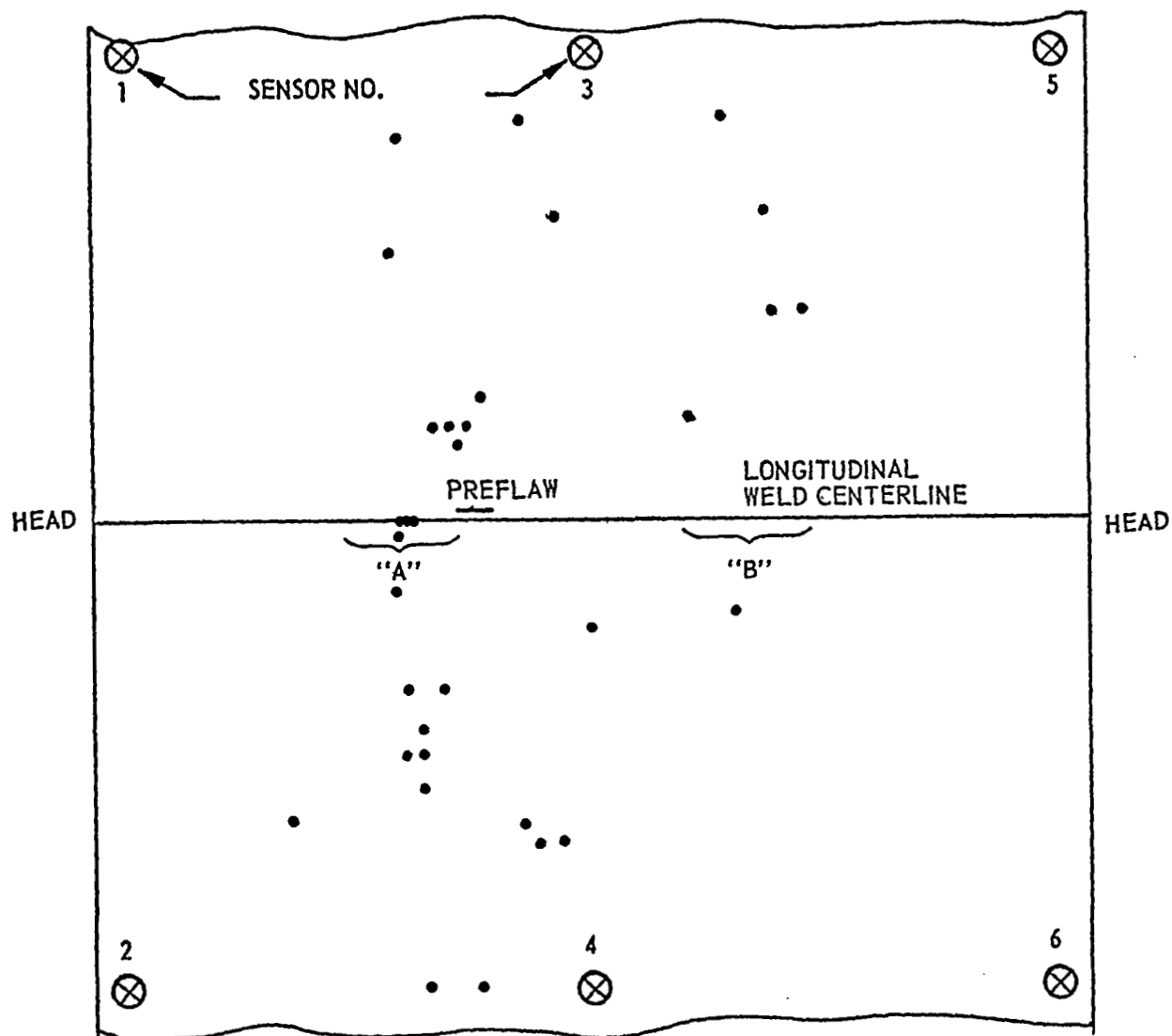
Figure 101. Location of SWE Sources Detected When Pressurizing the 2014-T6 Aluminum Vessel to Failure (2nd Cycle) at -320°F. Weld Preflaw Location also Shown. "A" and "B" indicate primary and secondary (possible) failure origins.

189
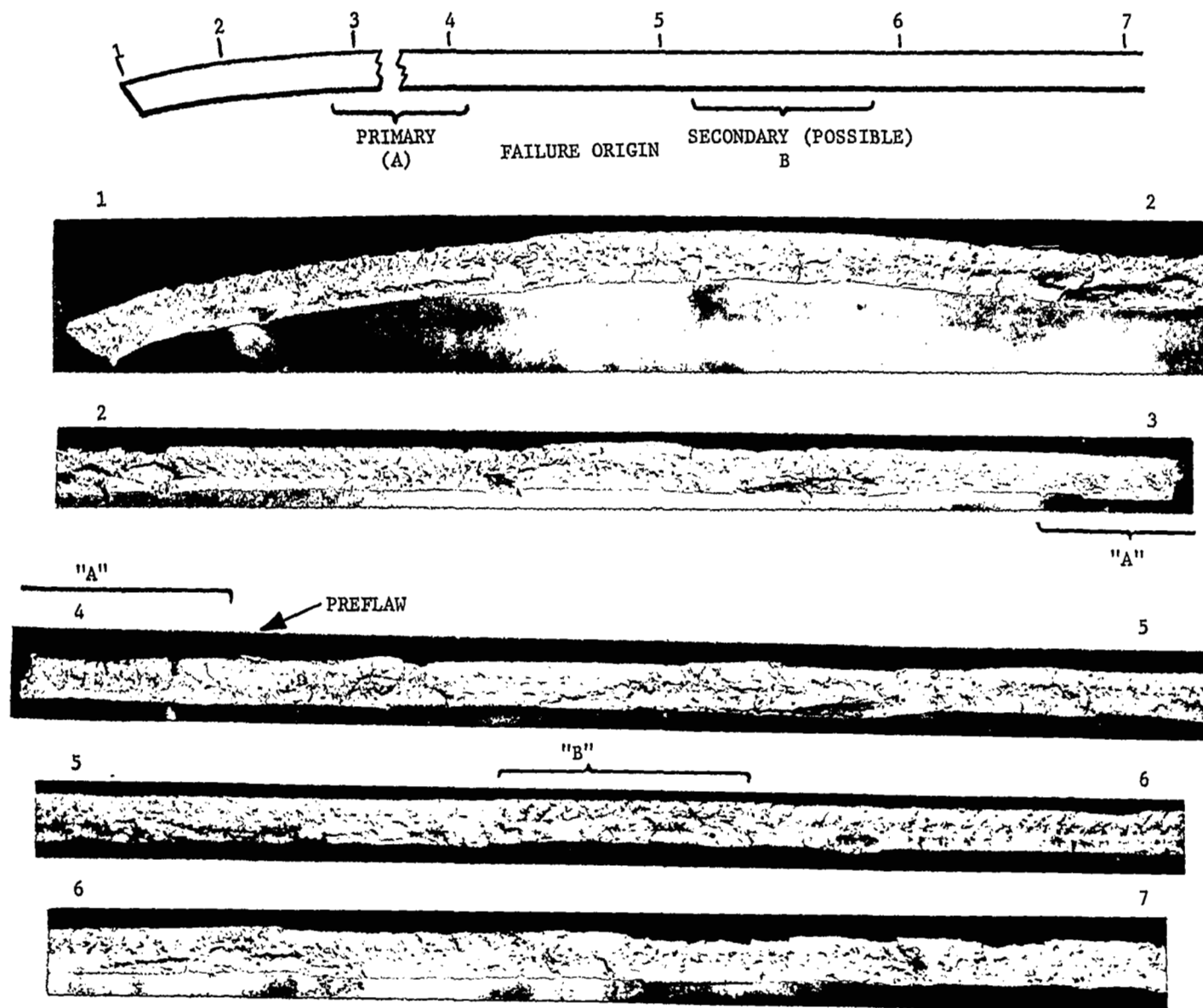
Figure 102. Longitudinal Weld Fracture Faces -2014-T6 Aluminum Vessel Hydroburst at -320°F. Note Preflaw (arrow) and that the Fracture Did Not Propagate Through This Defect. (Striations on Surface are Due to Welding Head Oscillation)

(1)

(2)

PTC Flaw
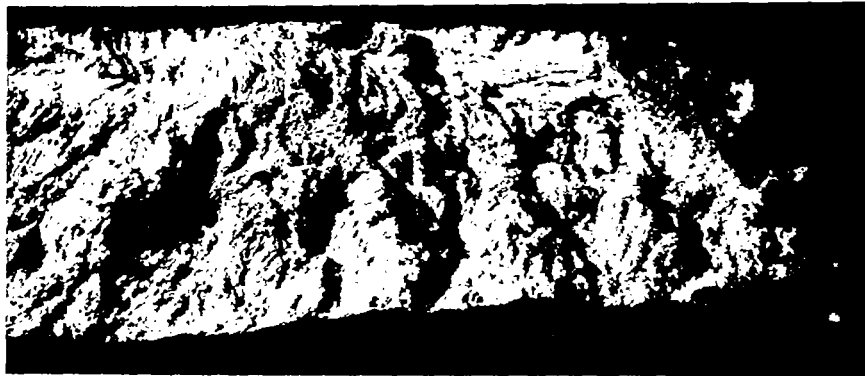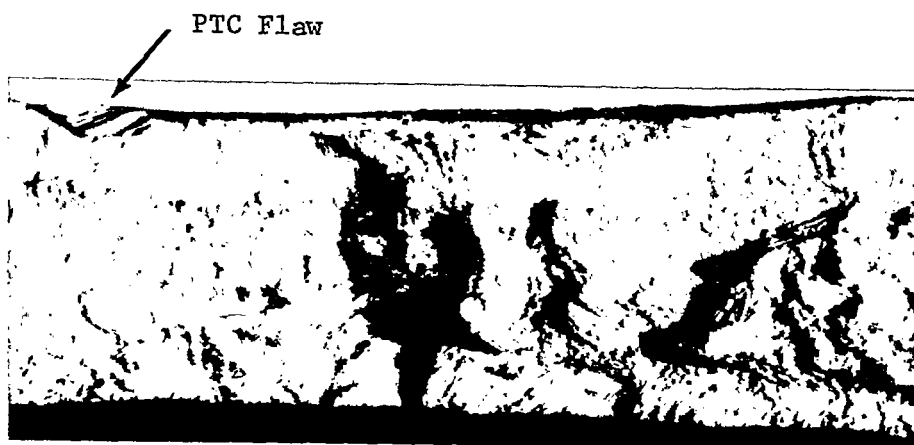
(3)

Figure 103. Areas of Longitudinal Weld Non-Fusion, Inclusions
and Porosity on the Fracture Surface of the 2014-T6
Aluminum Vessel Burst at -320°F. Figure 102 shows the
location area "A" of these defects in the longitudinal
weld. Note - the end of the PTC flaw in (3) and that
the fracture surface did not propagate through this
defect. (Magnification approximately 4X)

191

(1)

(2)

(3)

Figure 104. Areas (other than primary fracture Area A) of
longitudinal weld non-fusion, inclusions and porosity
on the fracture surface of the 2014-T6 aluminum vessel
tested at -320°F. Figure 102 shows the location ("B") of
these defects in the longitudinal weld.
(Magnification approximately 4X)
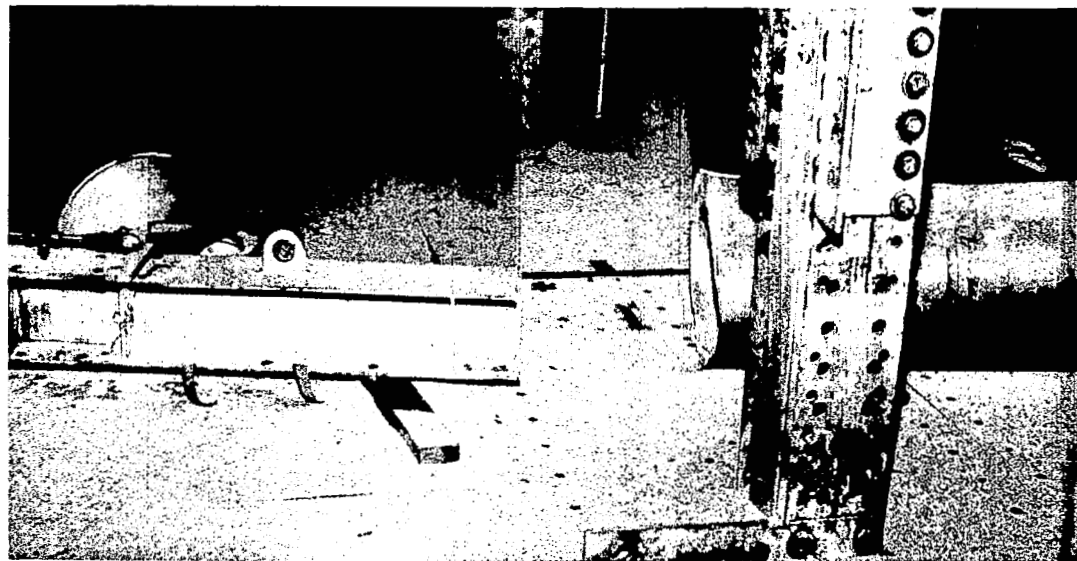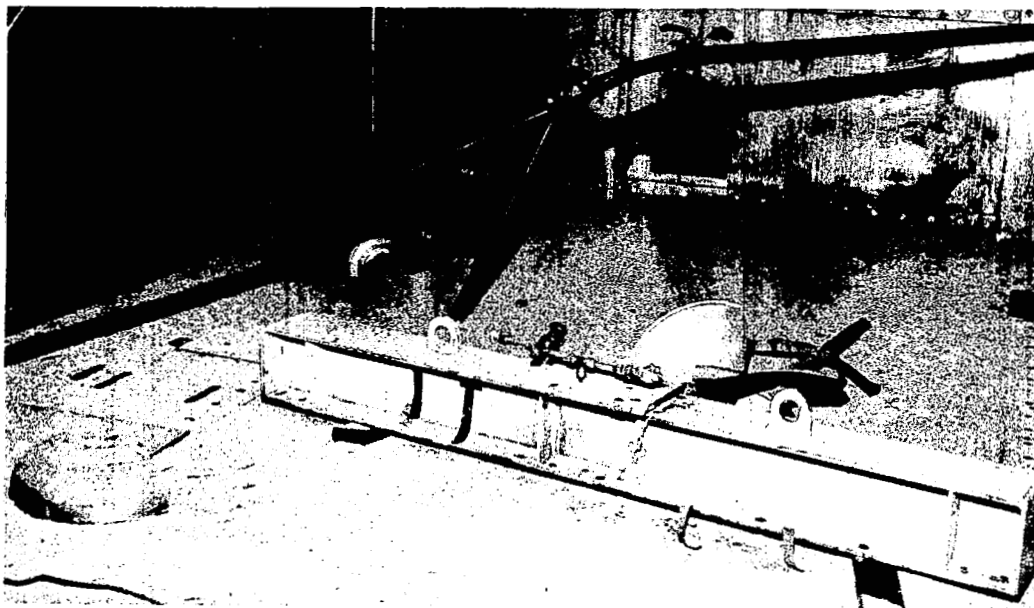
Figure 105.   Fractured 2219-T87 Aluminum Chamber in Test Cell After
Testing at -320°F.
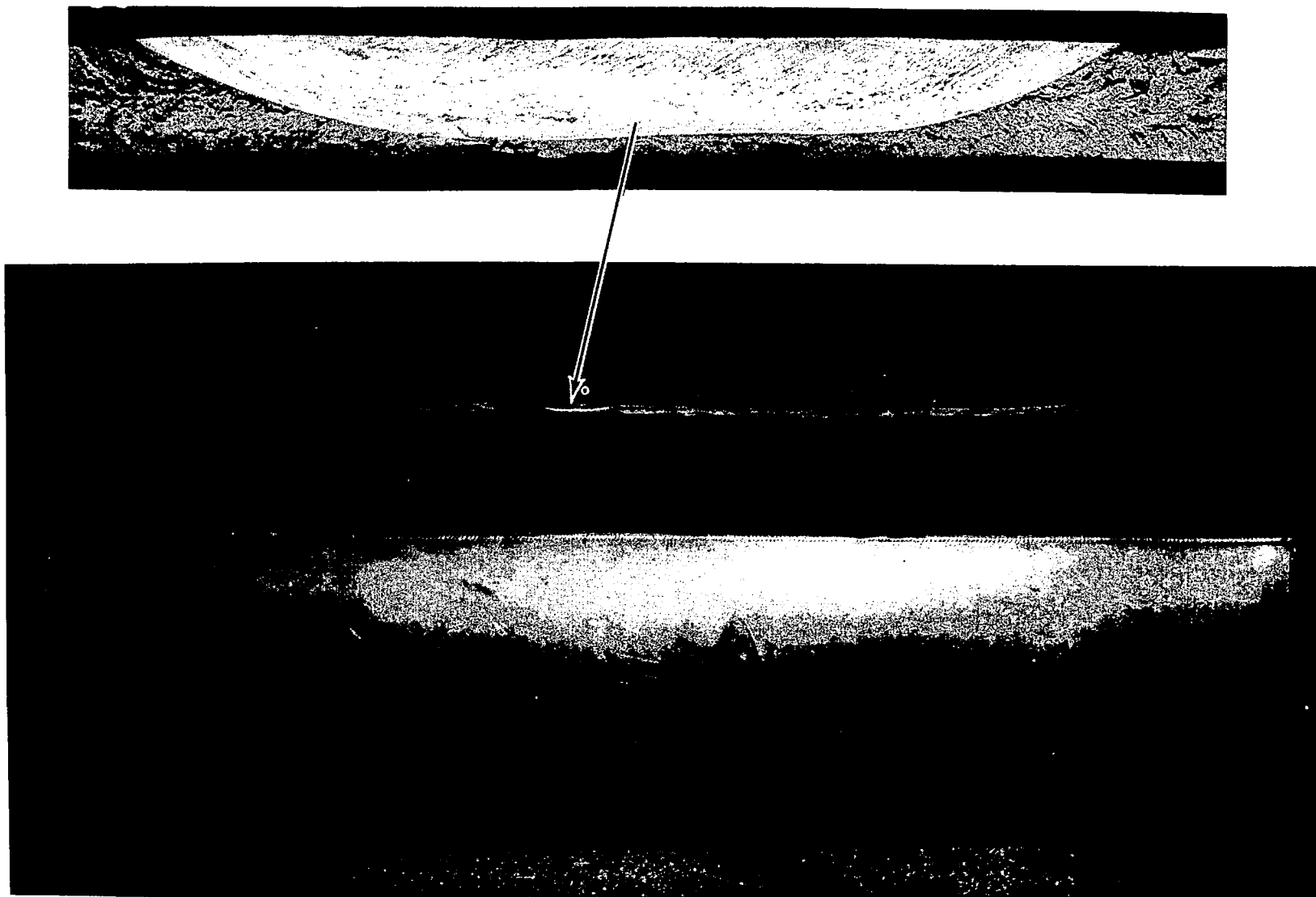
Figure 106.   Fracture Cylinder Section and Close-up View of the Longitudinal Weld
PTC Flaw for the 2219-T87 Aluminum Vessel Hydroburst at -320°F.
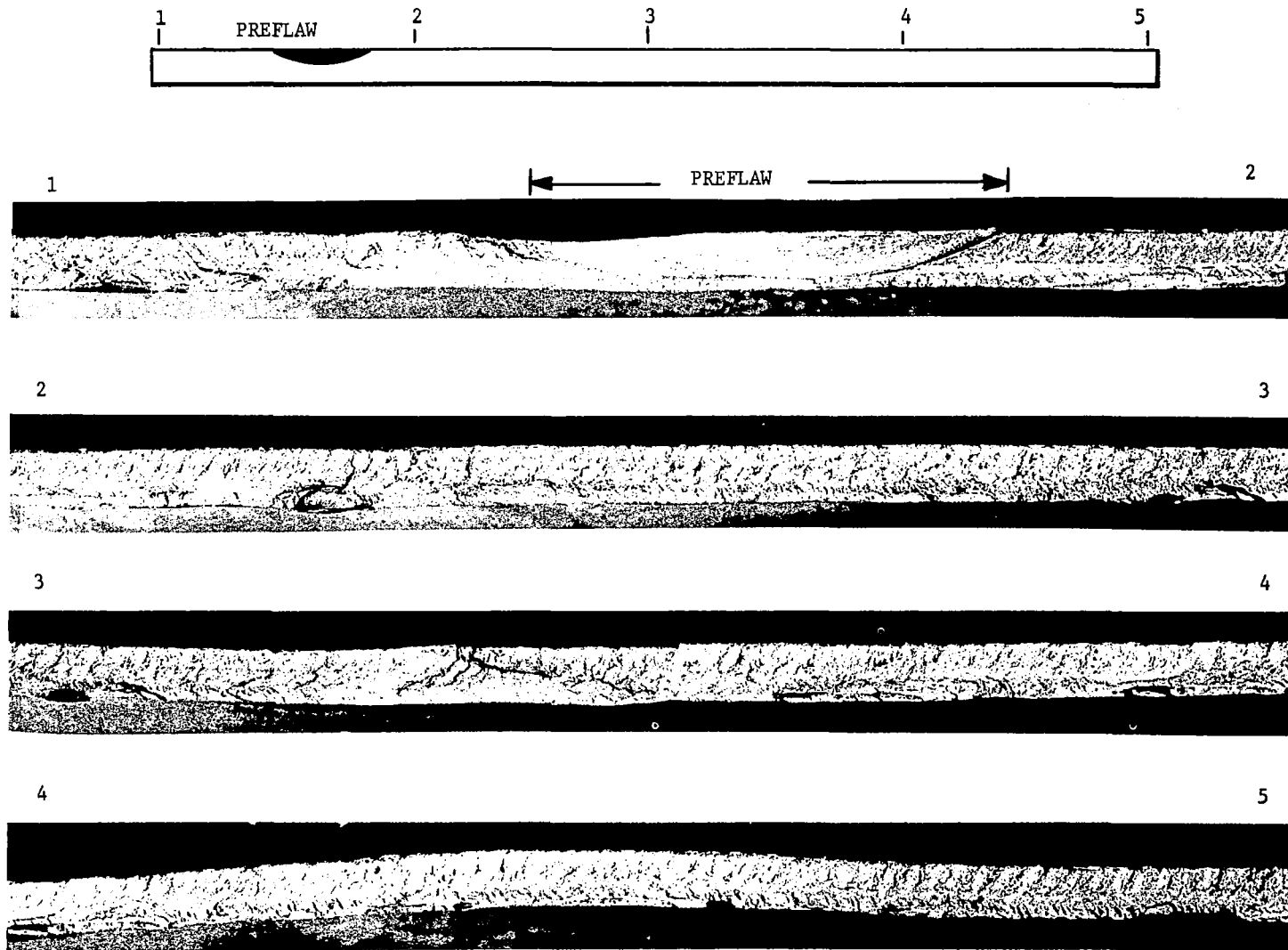
Figure 107. Longitudinal Weld Fracture Faces -2219-T87 Aluminum Vessel Hydroburst at -320°F. Note Preflaw - Failure Originated from this Defect. (Striations on Surfaces are due to Weld Head Oscillation).
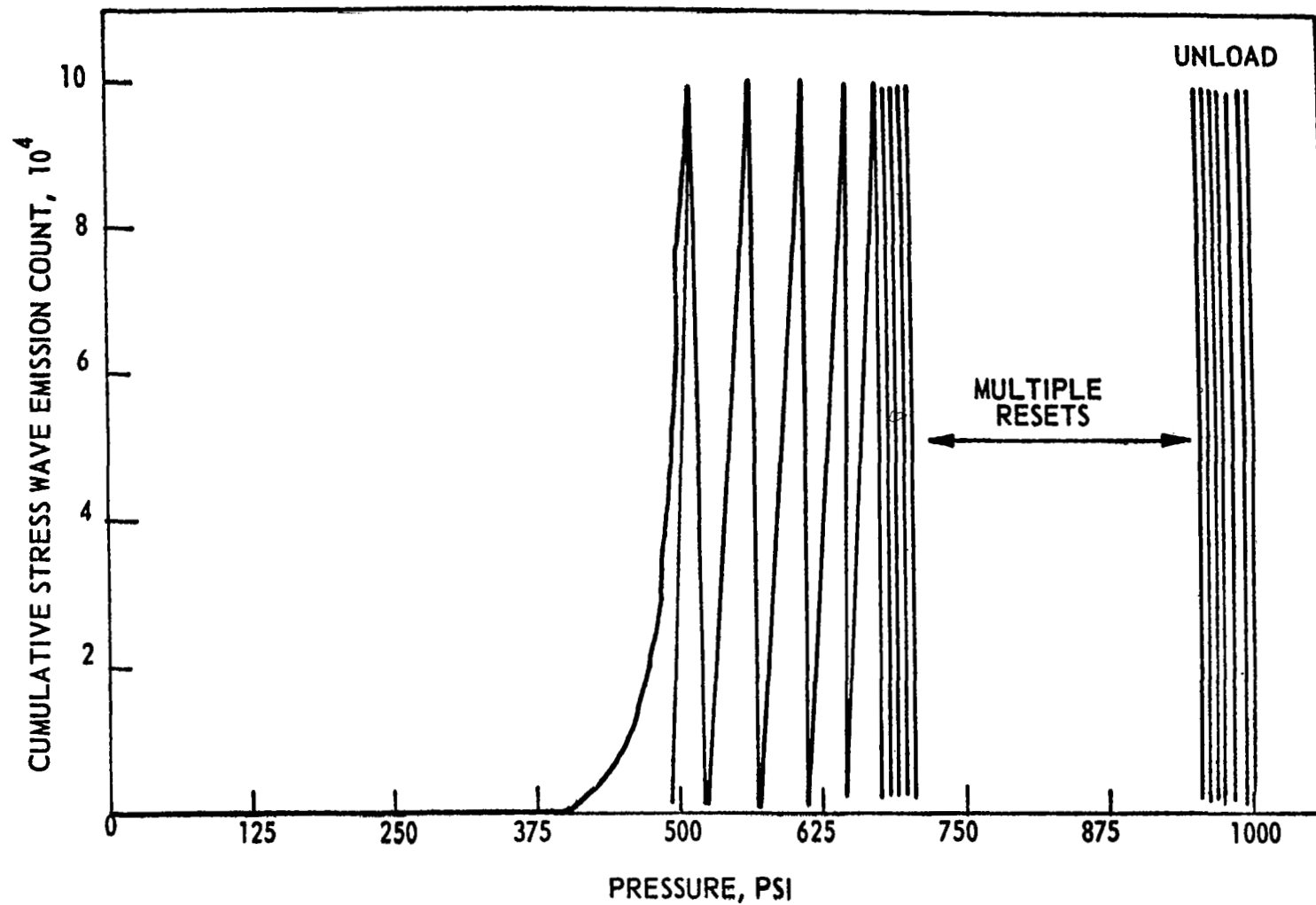
Figure 108. Cumulative Stress Wave Emission vs Pressure for the 2219-T87 Vessel
Tested at -320°F. Cycle No. 3 of a five cycle test series (Page 1 of 3)
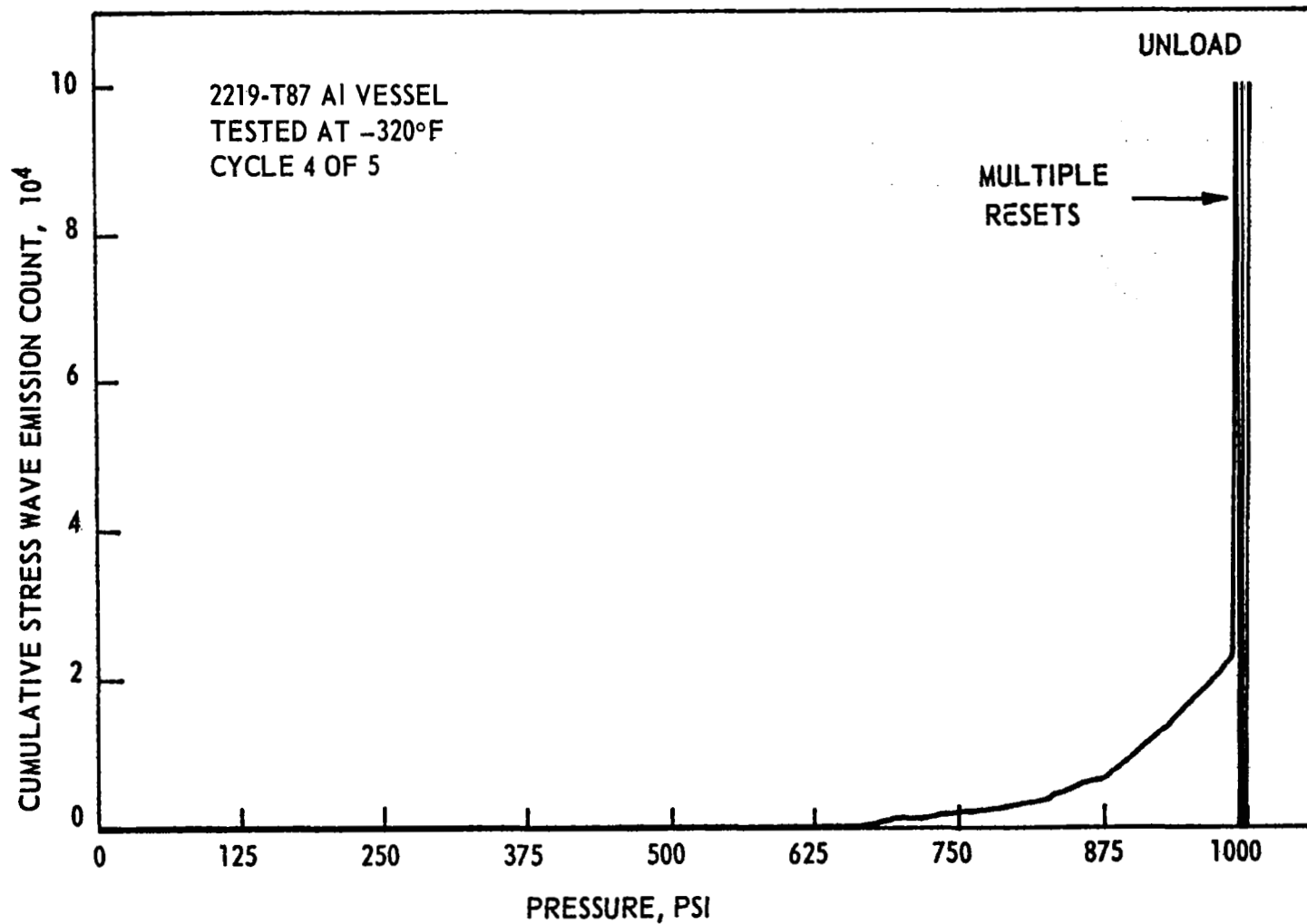
Figure 108. Continued (Page 2 of 3)
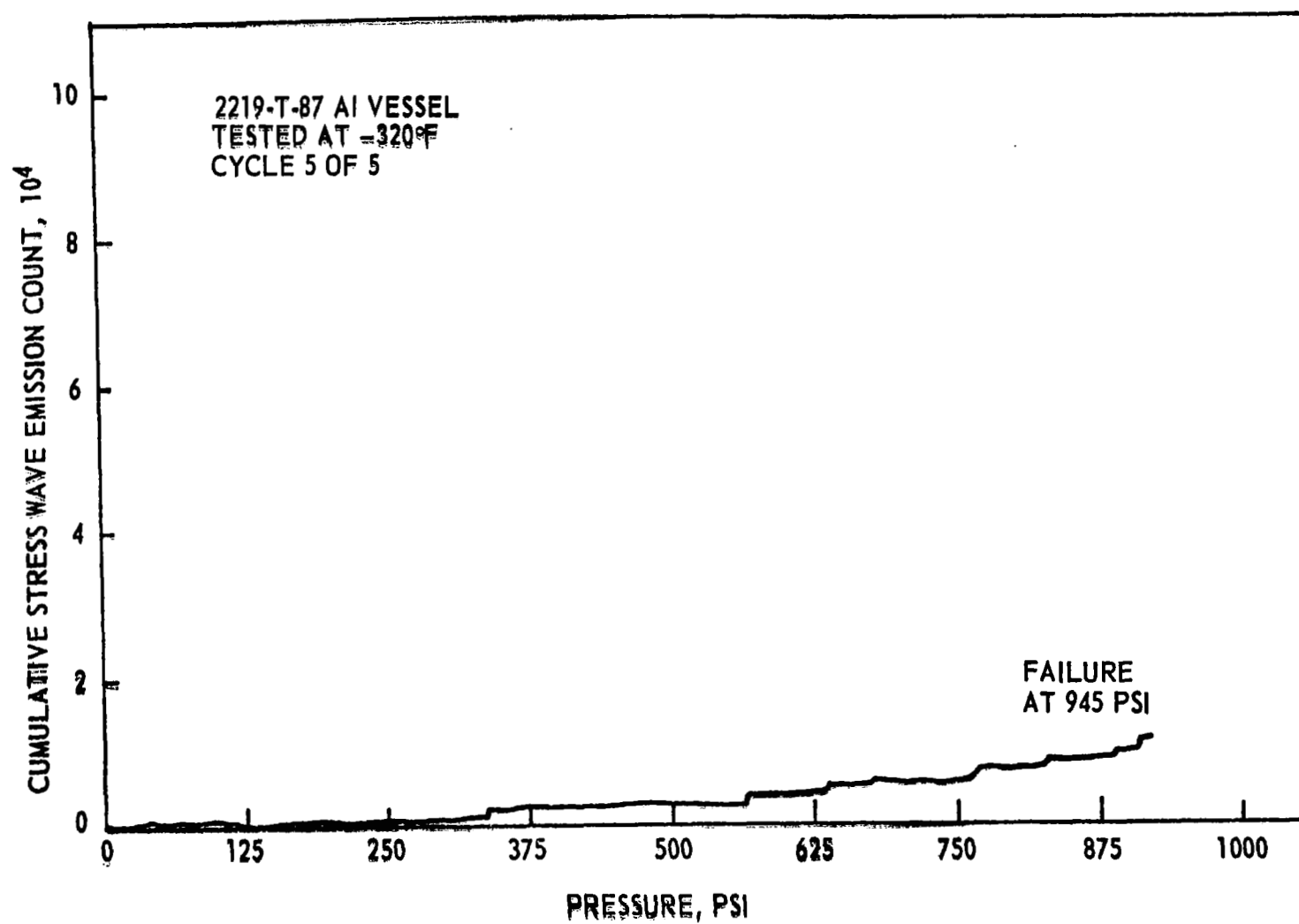
Figure 108. Continued (Page 3 of 3)
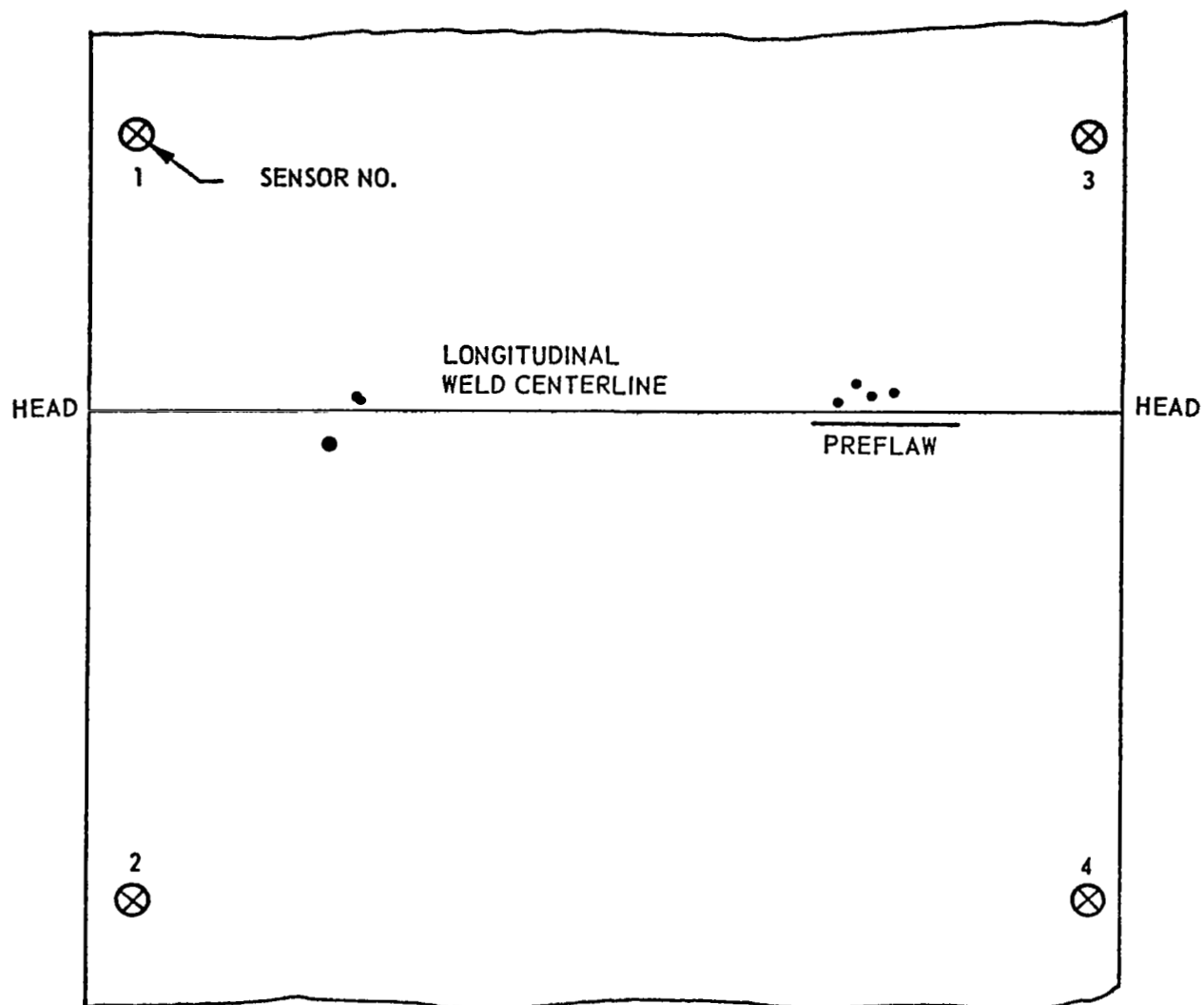
Figure 109.   Location of SWE Sources Detected When Pressurizing (3rd Cycle)
the 2219-T87 Aluminum Vessel to 1000 psi at -320°F. Weld
Preflaw Location also Shown.
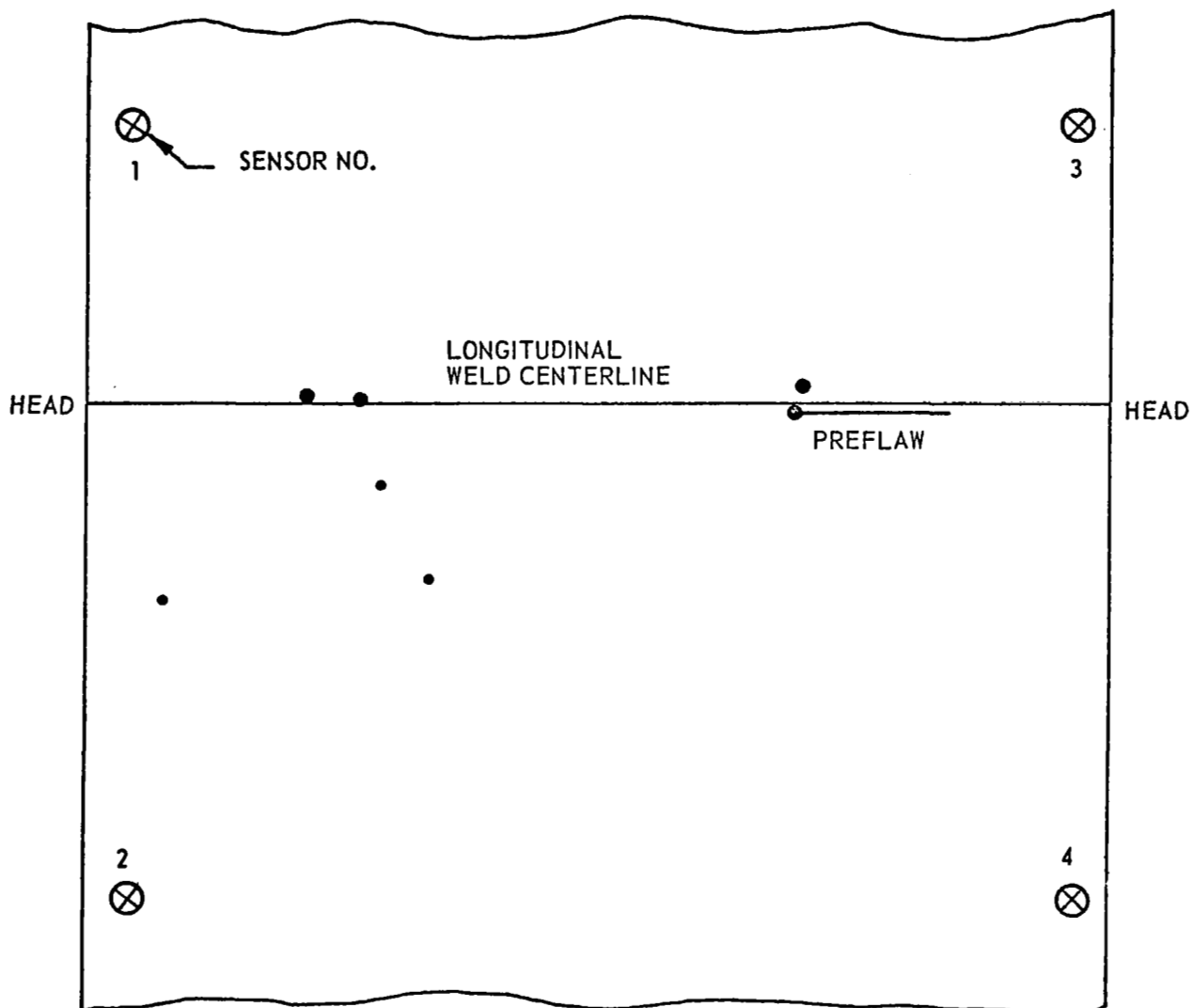
Figure 110. Location of SWE Sources Detected When Pressurizing (4th Cycle) the 2219-T87 Aluminum Vessel to 1000 psi at -320°F. Weld Preflaw Location also Shown.
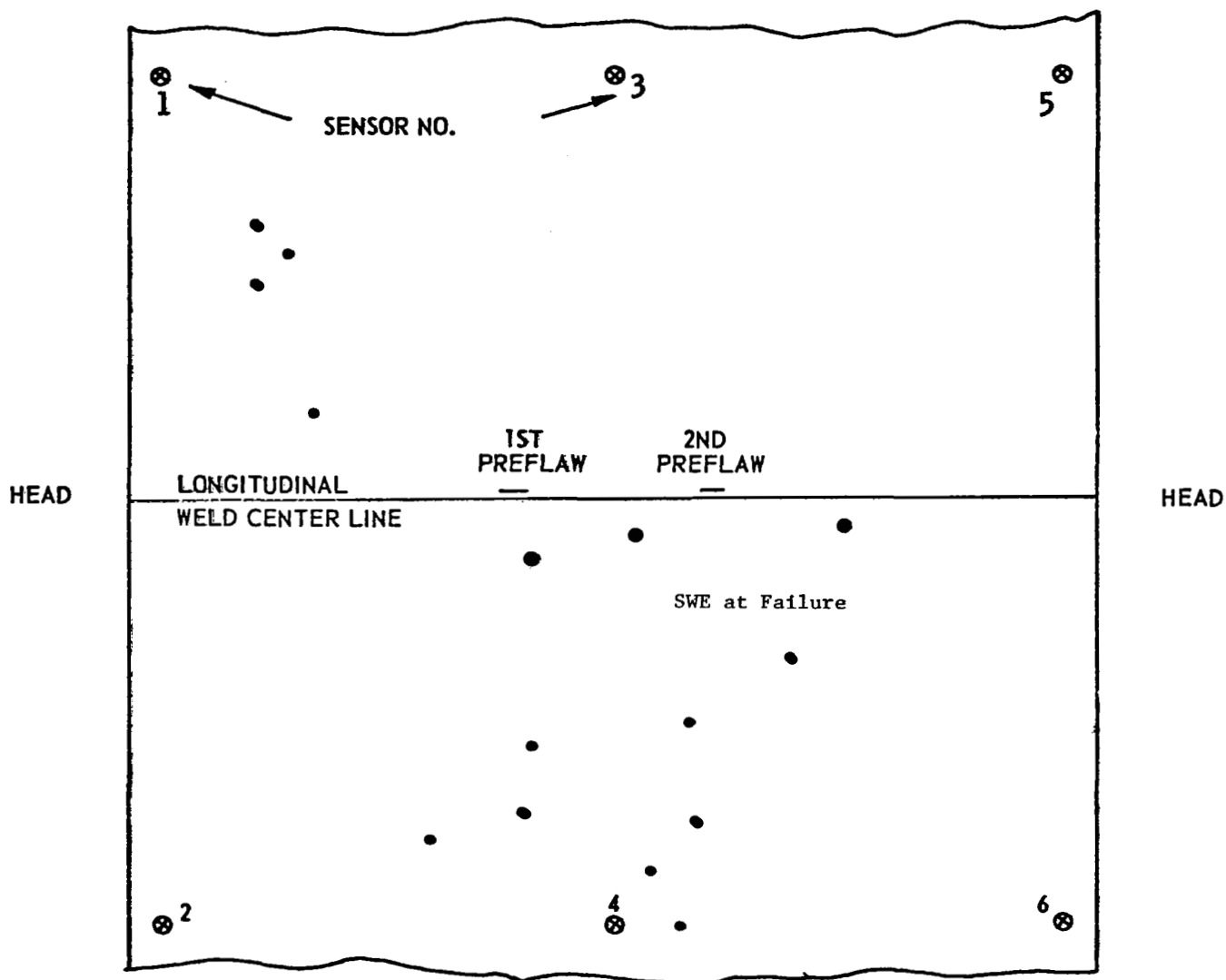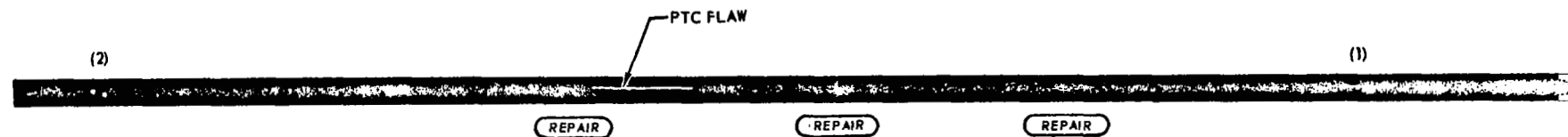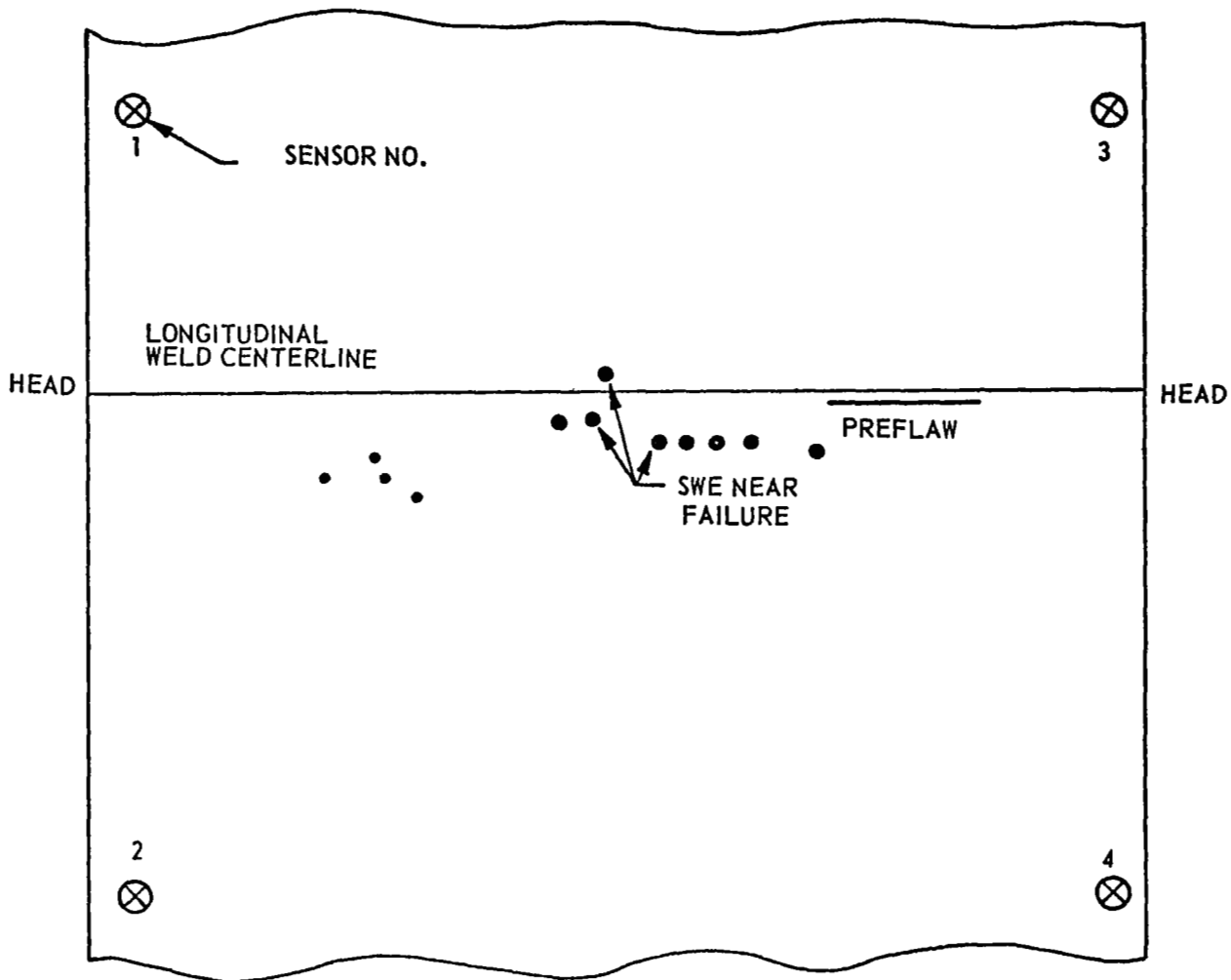
Figure 111. Location of SWE Sources Detected When Pressurizing (5th Cycle) the 2219-T87 Aluminum Vessel to Failure (945 psi) at -320°F. Weld Preflaw Location from Which Failure Initiated is also Shown.

201

BIBLIOGRAPHY

1971

Hartbower, C.E. and Reuter, W.G., "Stress Corrosion Cracking in 6Al-4V Titanium in Water and Methyl Alcohol", presented by Hartbower at the International Symposium on Stress Corrosion Mechanisms in Titanium Alloys, Georgia Institute of Technology, Atlanta, Georgia, Jan. 27-29, 1971.

Hartbower, C.E., Morais, C.F., Reuter, W.G. and Crimmins, P.P., "Detection of Weld Cracking on HY-80, HY-100 and HY-130 Steels by Stress Wave Emission", final report on Navy Contract N00024-70-C-5215, Project Ser. No. SF51541009, Task 12445, March 1971.

Hartbower, C.E., "Acoustic-Emission Measurements in the Ocean Engineering Program", for the Naval Civil Engineering Laboratory, Port Hueneme, Calif. 93043, 15 May 1971.

Hartbower, C.E., Morais, C.F., Reuter, W.G., and Crimmins, P.P., "Development of a Nondestructive Testing Technique to Determine Flaw Criticality", final Technical Report on Contract F33615-68-C-1705, ARPA Order No. 1244, Program Code 8D10, August 1971.

Hartbower, C.E., Reuter, W.G., Morais, C.F. and Crimmins, P.P., "Use of Acoustic Emission for the Detection of Weld and Stress-Corrosion Cracking", prepared for an ASTM Symposium on Acoustic Emission, Bal Harbour, Florida (Miami) Dec 7-8, 1971 and publication in an ASTM STP (Proceedings of Symposium).

Mow, Chao-Chow; Pao, Yih-Hsing, "The Diffraction of Elastic Waves and Dynamic Stress Concentrations", Rand Corp., Santa Monica, Calif., Report No. R-482-PR on Contract F44620-67-C-0045, AD-724 893, April 1971.

Martin, S.E., "Steady State Stress Wave Propagation in Fiber-Reinforced Elastic Materials", Texas University, Austin Engineering Mechanics Research Lab., Contract DAAD05-69-C-0241, NSF-GK-4712, AD-723 390, Feb. 1971, 43P

Waite, E.V., Parry, D.L., "Field Evaluation of Heavy-Walled Pressure Vessels Using Acoustic Emission Analysis", (Idaho Nuclear Corp., Idaho Falls), Mater. Eval., 29, No. 6, 117-24, June 1971.

1970

Bailey, Eugene C., "Industry Sponsored Programs", (Commonwealth Edison Co., Chicago), Nucl. Met., Met. Soc. AIME, 16, 39-47, 1970, (NMAIA). From Symposium on the Technology of Pressure-Retaining Steel Components, Vail Village, Colo.

Barkhoudarian, S., Scott, C.C., "Preliminary Study of Feasibility of Acoustic Detection of Small Sodium-Water Reactions in LMFBR Steam Generators", (Atomic Power Development Associates, Inc., Detroit, Mich.), Contract AT(11-1)-865, 79p, May 1970.

Bell, James F., "Finite Amplitude Wave Propagation in Solids", Johns Hopkins University, Baltimore, Md., Depart. of Mechanics, Final Report 1 Jan 64 - 31 Jan 69, Contract DA-31-124-ARO(D)-154, DA-ORD-31-124-G8, Proj. DA-2-0-061102-B-33-G, AD-704, 367, Mar. 1970, 37P.

Bill, R.C., Frederick, J., "Use of Acoustic Emission in Nondestructive Testing", Michigan Univ., Ann Arbor, Dept. of Mechanical Engineering, Semi Annual Report No. 4, 1 Mar. - 31 Aug. 1970, Report No. 01971-4-P, Contract F33615-68-C-1703, ARPA Order 1244, Project ORA-01971, AD-879 708, Dec. 1970, 66P.

(BNWL-1315-1) "Nuclear Safety Quarterly Report for USAEC Division of Reactor Development and Technology, November, December 1969 - January 1970", Battelle-Northwest, Richland, Wash. Pacific Northwest Lab, Contract AT(45-1)-1830, March 1970, 148p.

Crowe, J.C., "Techniques for Nondestructive Evaluation of Radioactive Waste Capsule End Cap Welds", (Battelle-Northwest, Richland, Wash. Pacific Northwest Lab) (nd) 20p.

Dunegan, H.L., Harris, D.O., and Tetelman, A.S., Materials Evaluation Journal, MAEVA Vol. 28, No. 10, Oct. 1970, pp. 221-227.

Frederick, J.R., "Use of Acoustic Emission in Nondestructive Testing", Michigan Univ., Ann Arbor, Dept. of Mechanical Engineering, Semi Annual Report No. 3, 1 Sept 69 - 28 Feb 70, Report No. 01971-3-P, Contract F33615-68-C-1703, ARPA Order-1244, Project ORA-01971, AD-872 256, June 1970, 32P.

Green, A.T. and Hartbower, C.E., "Detection of Incipient Failure in Pressure Vessels by Stress Wave Emission", paper presented by Hartbower at the International Sympsoium on Nondestructive Testing of Nuclear-Power-Reactor Components:, Rotterdam, The Netherlands, Feb 26-27, 1970.

Green, A.T. and Hartbower, C.E., "Development of a Nondestructive Testing Technique to Determine Flaw Criticality", Interim Technical Report on Contract F33615-68-C-1705 to the Advanced REsearch Projects Agency (ARPA Order No. 1244, Code 8D10), May 1970.

Green, A.T., Hartbower, C.E. and Crimmins, P.P., "Subcritical Crack Growth in Beryllium at $-320°F$", presented by Green at the ASTM Annual Meeting in Toronto, Canada, June 1970.

Harris, D.O. and Dunegan, H.L., "Verification of Structural Integrity of Pressure Vessels by Acoustic Emission and Periodic Proof Testing", Report UCRL-72783, Lawrence Radiation Laboratory, Livermore, 1970.

Hartbower, C.E., "Technical Note: Application of SWAT to the Nondestructive Inspection of Welds", The WELDING JOURNAL, Vol 35(2), p. 54-s, Feb 1970.

Hartbower, C.E. and Reuter, W.G., "Stress Corrosion Cracking in 6A1-4V Titanium in Water and Methyl Alcohol", presented by Reuter at the 7th Annual Western Metal and Tool Conference and Exposition, March 9-13, 1970, Los Angeles.

Hartbower, C.E., Reuter and Crimmins, P.P., "Stress-Wave Characteristics of Fracture Instability in Constructional Alloys", presented by Hartbower at the Joint Meeting of Commissions IX & X of the International Institute of Welding, Lausanne, Switzerland, July 1970.

Hutton, P.H., Acoustic Emission-What It Is and Its Application to Evaluate Structural Soundness of Solids, BNWL-SA-2983, Battelle-Northwest, Richland, Washington, February 1970.

Isbell, William M., Christman, Douglas R., "Whock Propagation and Fracture in 6061-T6 Aluminum From Wave Profile Measurements", General Motors Technical Center, Warren, Mich., Materials and Structures Lab., Interim Technical Report, Report No. MSL-69-60, Contract DASA01-68-C-0114, Project DASA-NWER-AA-106, AD-705 536, 42P, April 1970.

Isono, Eiji, "History of the Acoustic Emission Method - A New Tool for NDT", translated from Hihakai Kensa, No. 11, 579-985, 32P, 1970.

Jones, John P., "Stress Wave Dispersion Rod - Reinforced Composites", Aerospace Corp., El Segundo, Calif., Lab Operations, Descriptive Note: Report for Jan-Jul 69, Report No. TR-0066(6240-30)-3, Contract F04701-69-C-0066, AD-702 801, 37P, Jan. 1970.

Keck, Henry E., Armenakas, Anthony E., "Wave Propagation in Transversely Isotropic, Layered Cylinders", Polytechnic Inst. of Brooklyn, N.Y., Dept. of Aerospace Engineering and Applied Mechanics, Report No. PIBAL-70-9, Contract F44620-69-C-0072, Project AF-9782, Task 978201, 38P, Mar. 1970.

Liptai, R.G., Harris, D.O., Engle, R.B., Tatro, C.A., "Acoustic Emission Techniques in Materials Research", California Univ., Livermore, Lawrence Radiation Lab., from Symposium on Advanced Experimental Techniques in the Mechanics of Materials, San Antonio, Tex., 97p, 9 July 1970.

Liptai, R.G., Harris, D.O., Engle, R.B., and Tatro, C.A., "Acoustic Emission Techniques in Materials Research", to be published in International Journal of Nondestructive Testing and in Proceedings of the Symposium on Advanced Experimental Techniques in the Mechanics of Materials, San Antonio, Tex., Sept. 1970.

Liptai, R.G., Harris, D.O., Engle, R.B., and Tatro, C.A., "Acoustic Emission Techniques in Materials Research," Rept. UCRL-72582, Lawrence Radiation Laboratory, Livermore, 1970.

Liptai, R.G., "Acoustic Emission from Composite Materials", Rept. UCRL-72657, Lawrence Radiation Laboratory, Livermore, 1970.

Nielsen, A., Latham, F.G., Kirby, N., "Acoustic Emission from Steel Pressure Vessels", United Kingdom Atomic Energy Authority, Risley, England, Reactor Group (832 9530), 13P, April 1970.

Parry, D.L., Robinson, D.L., "Incipient Failure Detection by Acoustic Emission - A Development and Status Report", Report IN-1398, Idaho Nuclear Corp., Idaho Falls, 111P, July 1970.

Pottinger, Marion G., "The Anisotropic Equivalent of the Love Longitudinal Wave Propagation Approximation", Final Report, Aerospace Research Labs, Wright-Patterson AFB, Ohio, Report No. ARL-70-0064, Project AF-7065, Task 706500, AD-710 596, 28P, April 1970.

Reinhart, Eugene R., Wylie, Robert D., "Nondestructive Testing Techniques Applied to In-Service Inspection", Southwest Research Inst., San Antonio, from Symposium on the Technology of Pressure-Retaining Steel Components, Vail Village, Colo., Nucl. Met., Met. Soc. AIME, 16, 199-217, 1970.

Reitz, Edward S., Armenakas, Anthony E., "Propagation of Harmonic Waves in Orthotropic Circular Cylindrical Shells, Part I, Theoretical Investigation", Polytechnic Inst. of Brooklyn, N.Y., Dept. of Aerospace Engineering and Applied Mechanics, Report No. PIBAL-70-18, Contract NONR-839(40), Project NR-064-427, AD-706 749, 31P, Mar. 1970.

Romrell, D.M. and Bunnell, R.A., "Acoustic Emission Monitors Crack Growth in Ceramics, BNWL-SA-3064, Battelle-Northwest, Richland, Wash., March 1970.

Spanner, J.C., "A selective Review on the Utilization of Acoustic Emission Techniques for Materials Research and Structural Integrity Analysis (A LiteratureSurvey)", MS thesis, Washington State University, Department of Metallurgy, 1970.

Tinder, Richard F., "Flow Mechanisms and Acoustical Emission During Initial Yielding in Crystals", Final Report, Washington State Univ., Pullman, Contract AF-AFOSR-1449-68, Project AF-9763, Task 976301, AD-705 686, 3P, April 1970.

Waite, E.V., "Acoust-s- A Digital Program for Acoustic Triangulation of Spherical Vessels", Idaho Nuclear Corp., Idaho Falls, 22P, March 1970.

1969

Adams, K.H., Bass, B.R., Borhaug, J.E., Goodman, C.H., Thompson, H.A., "Experimental Investigation of Delayed Acoustic Emission in Beryllium", Tulane Univ., New Orleans, La., Dept. of Mechanical Engineering, Mar. 1969.

(BNWL-1266), "Nuclear Safety Quarterly Report, August-October 1969 for Nuclear Safety Branch of USAEC Division of Reactor Development and Technology", Battelle-Northwest, Richland, Wash., Pacific Northwest Lab., Contract AT(45-1)-1830, 117p, December 1969. Also, Nuclear Safety Quarterly Reports for November, December 1968, and January 1969, AEC Research and Development Report, Battelle-Northwest, March 1969.

Chambers, R.H.,"New Techniques in Nondestructive Testing by Acoustical and Exo-electron Emission", AD-691-230, Arizona University, Tuscon, Arizona, July 1969.

Day, C.K., "An Investigation of Acoustic Emission from Defect Formation in Stainless Steel Weld Coupons", BNWL-902, Battelle-Northwest, Richland, Washington, January 1969.

Day, C.K., "An Investigation of the Plastic Bursts of Microstrain in Zinc as Sources for Acoustic Emission", M.S. Thesis, Washington State University, Pullman, Washington, 1969.

Dunegan, H.L., Harris, D.O., Tetelman, A.S., "Detection of Fatigue Crack Growth by Acoustic Emission Techniques", Univ. of California, Livermore, Proceedings of the Seventh Symposium on Nondestructive Evaluation of Components and Materials in Aerospace, Weapons Systems, and Nuclear Applications, San Antonio, Texas, pp. 20-31, April 23-25, 1969, North Hollywood, Calif. Western Periodicals Company, 1969.

Dunegan, H. and Harris, D., "Acoustic Emission – A New Nondestructive Testing Tool", Ultrasonics, 7, 160-166, July 1969.

Dunegan, H.L. and Tetelman, A.S., "Non-Destructive Characterization of Hydrogen-Embrittlement Cracking by Acoustic Emission Techniques", UCRL-71654, Lawrence Radiation Laboratory, November 1969.

Engle, Robert B., Dunegan, Harold L., "Acoustic Emission: Stress Wave Detection as a Tool for Nondestructive Testing and Material Evaluation", Univ. of California, Livermore, Int. J. Non-Destruct. Test.; 1: 109-25 June 1969.

Fitch, C.E., Jr., "Acoustic Emission Signal Analysis in Flat Plates", BNWL-1008, Battelle-Northwest, Richland, Washington, April 1969.

Frederick, J.R., "Use of Acoustic Emission in Nondestructive Testing", Semi-Annual Report 01971-1P, July 1968-February 1969, University of Michigan, Ann Arbor, Michigan, May 1969.

Frederick, J.R., "Use of Acoustic in Nondestructive Testing", Semi-Annual Report 01971-2-T, March-August 1969, University of Michigan, Ann Arbor, Michigan, November 1969.

Gerberich, W.W. and Reuter, W.G., "Theoretical Model of Ductile Fracture Instability Based on Stress-Wave Emission", ONR Contract Report N00014-66-C0340, Aerojet-General Corp., Sacramento, California, February 1969.

Green, A.T., "Detection of Incipient Failures in Pressure Vessels by Stress-Wave Emission", Nuclear Safety, 10, 4-18, January-February 1969.

Green, A.T., "Stress-Wave Emission Generated During the Hydrostatic Compression Testing of Glass Spheres", Final Report on Contract N00014-67-C0333, April 1969.

Green, A.T., "Development of a Nondestructive Testing Technique to Determine Flaw Criticality, ARPA Contract F33615-68-C-1705, Aerojet-General Corp., Sacramento, California, August 1969.

Green, A.T., "Stress Wave Emission and Fracture of Prestressed Concrete Reactor Vessel Materials", report for Oak Ridge National Laboratory, Subcontract No. 3118, Contract No. W-7405-eng-26, June 1969.

Hardy, H.R., Jr., "Applications of Acoustic Emissions in Rock Mechanics", presented at the Acoustic Emission Working Group Meeting, Philadelphia, Pennsylvania, October 1969.

Harris, D.O., Dunegan, H.L. and Tetelman, A.S., "Detection of Fatigue Crack Growth by Acoustic Emission Techniques," UCRL-71457, Lawrence Radiation Laboratory, March 1969.

Harris, D.O., Dunegan, H.L. and Tetelman, A.S., "Detection of Fatigue Lifetime by Combined Fracture Mechanics and Acoustic Emission Techniques, UCRL-71760, Lawrence Radiation Lab. (Oct. 1969) and Air Force Conference on Fatigue and Fracture of Aircraft Structures and Material, Miami Beach, Fla., 15-18 Dec. 1969.

Hartbower, C.E., Reuter, W.G. and Crimmins, P.P., "Tensile Properties and Fracture Toughness of 6Al-4V Titanium", AFML-TR-68-163, Vol. II, Aerojet-General Corp., Sacramento, California, March 1969.

Hartbower, C.E., Reuter, W.G. and Crimmins, P.P., "Mechanisms of Slow Crack Growth in High-Strength Steels and Titanium", Final Technical Report AFML-TR-67-26, Vol. II, June 1969 on Contract AF 33(615)-2788 for the period April 1967-April 1969, 199 pages.

Hartbower, C.E., "Application of SWAT to the Nondestructive INspection of Welds", Technical Note, Aerojet-General Corp., Sacramento, California, The WELDING JOURNAL, Vol. 35(2), Feb. 1970, September 1969.

Hartbower, C.E., Green, A.T. and Crimmins, P.P., "Correlation of Stress Wave Emission Characteristics with Fracture in Aluminum Alloys", Quarterly Progress Report on Contract NAS 8-21405 to NASA Huntsville, dated July 1969.

Hartbower, C.E., Green, A.T. and Crimmins, P.P., "Correlation of Stress Wave Emission Characteristics with Fracture in Aluminum Alloys", Quarterly Progress Report on Contract NAS 8-21405 to NASA Huntsville, dated December 1969.

Hartbower, C.E., Climent, F.J., Morais, C. and Crimmins, P.P., "Stress-Wave Analysis Technique Study on Thick Walled, Type A302B Steel Pressure Vessels", Final Report on Contract NAS 9-7759 (Mod. 1), July 1969.

Hutton, P.H., "Use of Acoustic Emission to Study Failure Mechanisms in Metal", presented at the Metals Engineering Pressure Vessels and Piping Conference, Washington, D.C., April 1969.

Hutton, P.H., "Acoustic Emission Detection in the Presence of Hydraulic Noise", Non-Destructive Testing, 2, 111-115, May 1969.

Hutton, P.H., "Detection of Incipient Failure in Nuclear Reactor Pressure Systems Using Acoustic Emission," BNWL-997, Battelle-Northwest, Richland, Washington, April 1969.

Hutton, Philip H., "Acoustic Emission - A New Tool for Evaluating Structural Soundness", (Battelle-Northwest, Richland, Wash.), BNWL-SA-2449, pp 165-79 of Proceedings of the Seventh Symposium on Nondestructive Evaluation of Components and Materials in Aerospace, Weapons Systems, and Nuclear Applications, April 23-25, 1969, San Antonio, Texas. North Hollywood, Calif., Western Periodicals Company, 1969.

Hutton, P.H., "Detecting Acoustic Emission in the Presence of Hydraulic Noise", Battelle-Northwest, Richland, Wash., Non-Destruct. Test., 2- 111-15, May 1969.

Hutton, P.H., "Integrity Surveillance of Pressure Systems by Means of Acoustic Emission", Battelle Northwest Labs., Richland, Wash., pp 1017-32 of Pressure Vessel Technology, Pt. II, New York; American Society of Mechanical Engineers, 1969. From 1st International Conference on Pressure Vessel Technology, Delft, Netherlands.

Hutton, P.H., "Integrity Surveillance of Pressure Systems by Means of Acoustic Emission", BNWL-SA-2194, Battelle-Northwest, Richland, Washington, presented at the International Conference on Pressure Vessel Technology, Delft, Holland, October 1969.

Hutton, P.H. and Pedersen, H.N., "Crack Detection in Pressure Piping by Acoustic Emission", Nuclear Safety Quarterly Progress Report, May-July 1969, BNWL-1187, pp. 3.1-3.18, Battelle-Northwest, Richland, Washington, (September 1969).

Jolly, W.D., "The Use of Acoustic Emission as a Weld Quality Monitor", BNWL-SA-2727, Battelle-Northwest, Richland, Washington, presented at the 24th Annual Petroleum Mechanical Engineering Conference, Tulsa, Oklahoma, September 1969.

Jolly, W.D., "The Application of Acoustic Emission to In-Process Weld Inspection", BNWL-SA-2212, Battelle-Northwest, Richland, Wash., March 1969.

Jolly, W.D., "Acoustic Emission Exposes Cracks During Welding Process", The Welding Journal, 35(1), 21-29, January 1969.

Liptai, R.G., Dunegan, H.L. and Tatro, C.A., International Journal of Non-destructive Testing, IJNTA, Vol. 1, No. 3, pp. 213-221, Aug 1969.

Moyer, M.W., "Acoustic Emission for Nondestructive Testing and Certification", Y-12 Plant Report Y-DA-2855, Union Carbide Corp., Oak Ridge, Tennessee, Feb. 20, 1969. 10 p. (from Acoustic Emission Working Group Conference, New Orleans, La.).

Nielsen, A.,"Acoustic Emission Investigations During Pressure Vessel Testing at Reactor Materials Laboratory, Culcheth (United Kingdom Atomic Energy Authority), (Danish Central Welding Inst., Copenhagen), pp 01-10 of Practical Fracture Mechanics for Structural Steel. Dobson, M.O. (Ed.). London-Chapman and Hall, Ltd.,1969. From Symposium on Fracture Toughness Concepts for Weldable Structural Steel, Risley, England.

Pollock, A.A., "Stress-Wave Emission in NDT", Non-Destruct. Test., 2- 178-82, Aug. 1969.

Sankar, N.G., "Unload Emission Behavior of Material and Its Relation to the Bauschinger Effect", Ph.D. Thesis, University of Michigan, Ann Arbor, Michigan, 1969.

Steele, R.K., Morais, C.F., Briar, H.P. and Stanfield, J., "Design of a System to Detect and Locate the Incipient Development of Flaws in Materials", Milestone Report No. 2, March 1969; Final Report on Contract N00600-C-0308, May 1969.

Tietze, A. (comp.), "Progress Report on Research Projects Sponsored by the Federal Ministry of Scientific Research and Applicable to the Reactor Safety Aspect", (Technischer Euberwachungs-Verein e. V., Cologne (West Germany). Institut fuer Reaktorsicherbeit). Translated for Oak Ridge National Lab., Tenn., from report IRS-F-2. 51p, 1969.

1968

Anderson, T.T., Grate, T.A., "Acoustic Boiling Detection in Reactor Vessels", Reactor Engineering Division, Argonne National Laboratory 15th Nuclear Science Symposium, Montreal, Canada, October 1968.

Argarwall, A.B.L., "An Investigation of the Behavior of the Acoustic Emission from Metals and a Proposed Mechanism for its Generation", Ph.D. Thesis, The University of Michigan, Ann Arbor, Michigan, 1968.

Baker, G.S., "Acoustic Emission and Prefracture Processes in High-Strength Steels", AFML-TR-67-266, Aerojet-General Corporation, Wright-Patterson AFB, March 1968.

Chuch, Y.P., Hardy, H.R., Jr., and Stefanko, R., "An Investigation of the Frequency Spectra of Microseismic Activity in Rock under Tension", Proceedings of the Tenth Rock Mechanics Symposium, Austin, Texas, May 1968.

Day, C.K., "An Investigation of Acoustic Emission from Defect Formation in Stainless Steel Weld Coupons", BNWL-902, Battelle-Northwest, Richland, Washington, November 1968.

Dunegan, H.L., Harris, D.O. and Tatro, C.A., "Fracture Analysis by Use of Acoustic Emission", Engineering Fracture Mechanics, 1, 105-122, June 1968.

Dunegan, H.L., Brown, A.E., and Knauss, P.L., "Piezoelectric Transducers for Acoustic Emission Measurements", UCRL-50553, Lawrence Radiation Laboratory, December 1968.

Dunegan, H, Harris, D., "Acoustic Emission - A New Nondestructive Testing Tool", (Univ. of California, Livermore). pp 203-38 of Proceedings - 1968 Symposium on the NDT of Welds and Materials Joining. Evanston, Ill., The American Society for Nondestructive Testing, Inc., 1968, and the 3rd Annual Symposium on Non-destructive Testing of Welds and Materials Joining, Los Angeles, Calif.

Engle, R.B. and Dunegan, H.L., "Acoustic Emission: Stress Wave Detection as a Tool for Nondestructive Testing and Material Evaluation", UCRL-71267, Lawrence Radiation Laboratory, Deptember 1968. Proceedings of the Eighth Symposium on Physics and Nondestructive Testing, Schiller Park, Ill., 1968.

Hartbower, C.E., Gerberich, W.W., and Crimmins, P.P., "Spontaneous Strain Aging as a Mechanism of Slow Crack Growth," presented at the American Welding Society Annual Conference, Chicago, Illinois, April 1968. The WELDING JOURNAL, Vol. 47(10), Oct. 1968.

Hartbower, C.E., Gerberich, W.W., Reuter, W.G. and Crimmins, P.P., "Stress-Wave Characteristics of Fracture Instability in Constructional Alloys", Final Report on Contract N00014-66-C-0340, July 1968. AD-674-881.

Hartbower, C.E. and Crimmins, P.P., "Fracture of Structural Metals as Related to Pressure-Vessel Integrity and In-Service Monitoring", presented at the ICRPG/AIAA 3rd Solid Propulsion Conference (AIAA Paper 68-501), Atlantic City, June 1968.

Hutton, P. H., "Acoustic Emission in Metals as a NDT Tool", Materials Evaluation, 26, 125-128, July 1968.

Hutton, P.H., "Nuclear Reactor System Noise Analysis, Dresden I Reactor, Commonwealth Edison Company", BNWL-867, Battelle-Northwest, Richland, Washington, October 1968.

Jolly, W.D., "An In-Situ Weld Defect Detector Acoustic Emission", BNWL-817, Battelle-Northwest, Richland, Washington, September 1968.

Liptai, R.G., Dunegan, H.L. and Tatro, C.A., "Acoustic Emissions Generated During Phase Transformations in Metals and Alloys", UCRL-50525, Lawrence Radiation Laboratory, September 1968.

Michaels, T.E., "Acoustic Emission of Zircaloy-2 During Tensile and Fatigue Loading", BNWL-727, Battelle-Northwest, Richland, Washington, August 1968, 30p.

Pollock, A.A., "Stress-Wave Emission - A New Tool for Industry", Ultrasonics, 6, 88-92, April 1968.

Reuter, W.G., Green, A.T., Hartbower, C.E., and Crimmins, P.P., "Monitoring of Crack Growth in Ti-6A1-4V Alloy by the Stress Wave Analysis Technique", Final Report on Contract NAS 9-7759, Dec. 1968.

Sedgwick, R.T., "Acoustic Emission from Single Crystals of LiF and KCl",
Journal of Applied Physics, 39, 1728-1740, February 1968.

Waite, E.V. and Moore, K. V., "ACOUST--A Digital Program for Acoustic
Triangulation of Nuclear Vessels", IDO-17280, Phillips Petroleum Company,
Idaho Falls, Idaho, November 1968, 19p.

Worlton, D.C., "Review of Selected Nondestructive Testing Activities at
Battelle Northwest Laboratory", (Battelle-Northwest, Richland, Wash.),
pp 353-60 of Materials Technology: An Interamerican Approach. New York;
American Society of Mechanical Engineers (1968). From Inter-American
Conference on Materials Technology, San Antonio, Tex.

1967

Baker, G.S. and Green, A.T., "Stress-Wave and Fracture of High-Strength Metal",
USAF AFML Symposium on Correlation of Material Characteristics with Systems
Performance, Orlando, Florida, May 1967.

Baker, G.S., "Acoustic Emission and Pre-Fracture Processes in High-Strength
Steels", Final Report on Contract USAF AF 33(615)-5027, July 1967.

Beal, J.B., "Ultrasonic Emission Detector Evaluation of Strength of Bonded
Materials", Nondestructive Testing Trends and Techniques, NASA SP-5082,
1967.

Dunegan, H.L., and Tatro, C.A., "Passive Pressure Transducer Utilizing Acoustic
Emission", UCRL-14981, Lawrence Radiation Laboratory, Livermore, California,
1967, and Review of Scientific Instruments, Vol. 38, No. 8, August 1967.

Dunegan, H.L., Harris, D.O., Tatro, C.A., "Fracture Analysis by Use of Acoustic
Emission", National Symposium on Fracture Mechanics, Lehigh University, June 1967.
Published in Engineering Fracture Mechanics, Vol. 1, p. 105, June 1968.

Fisher, R.M. and Lally, J.S., "Microplasticity Detected by an Acoustic Technique",
Canadian Journal of Physics, Vol. 45, No. 2, Part 3, Feb. 1967, pp. 1147-1159.

Gerberich, W.W., Baker, G.S., "On the Toughness of Two-Phase 6A1-4V Titanium
Microstructures,"ASTM Titanium Symposium, Los Angeles, Calif., April 1967.

Gerberich, W.W., Baker, G.S., Reuter, W.G., Crimmins, P.P., Hartbower, C.E.,
"Materials Investigation--Titanium", Naval Ship Research and Development Center,
N600(61533)-65927, Aug. 1967.

Gerberich, W.W., Hartbower, C.E., "Monitoring Crack Growth of Hydrogen Embrittle-
ment and Stress Corrosion Cracking by Acoustic Emission", Conference on Funda-
mental Aspects of Stress Corrosion Cracking, Ohio State University, Sept. 1967.

Gerberich, W.W., Hartbower, C.E., "Stress-Wave Emission as a Criterion for Discontinuous Crack Extension", ASM Metal Science Forum on Criteria for Brittle Crack Extension, Cleveland, Ohio, Oct. 1967.

Gerberich, W.W., Hartbower, C.E., "Some Observations on Stress-Wave Emission as a Measure of Crack Growth", International Journal of Fracture Mechanics, Vol. 3, No. 3, Sept. 1967.

Green, A.T., "Testing of 10-in. Glass Hemispheres Using Stress-Wave Analysis Technique", Naval Ship Research and Development Center, N00014-67-C-0333, Sept. 1967.

Green, A.T. and Hartbower, C.E., "Stress-Wave Analysis Technique for Detection of Incipient Failure", Aerojet-General Corp., Presented at ORNL Conference on Incipient Failure Diagnosis for Assuring Safety and Availability of Nuclear Power Plants, Gatlinburg, Tennessee, October 1967. Published in the PROCEEDINGS of the AEC Conference.

Hartbower, C.E., Gerberich, W.W. and Crimmins, P.P., "Mechanisms of Slow Crack Growth in High-Strength Steels", AFML-TR-67-26, Vol. 1, Aerojet-General Corp., February 1967.

Hartbower, C.E., Gerberich, W.W., Liebowitz., H., "Investigating of Crack-Growth Stress-Wave Relationships," National Symposium on Fracture Mechanics, Lehigh, 1967, Journal of Applied Fracture Mechanics, Vol. 1, No. 2, p. 291, Aug 1968.

Hartbower, C.E., Gerberich, W.W., Reuter, W.G., Crimmins, P.P., "Stress-Wave Characteristics of Fracture Instability in Constructional Alloys", ONR Contract N00014-66-C0340, July 1967.

Hartbower, C.E., Gerberich, W.W., Crimmins, P.P., "Monitoring Subcritical Crack Growth by Detection of Elastic Stress-Waves, American Welding Society, Houston, Texas, Oct. 1967, published in The Welding Journal, Vol. 47, No. 1, Jan. 1968. (received the SPRARAGEN AWARD as the best research paper published in The WELDING JOURNAL in the year 1968.).

Hoppman, W.H., "Statics and Dynamics of Deformation of Physical Models of Crystalline Materials Which Exhibit Couple Stress Effects", AD-822-861, Rensselaer Polytechnic Institute, Troy, New York, September 1967.

Hutton, P.H., "Crack Detection in Pressure Piping by Acoustic Emission", Nuclear Safety Quarterly Progress Report January-March 1967, NVWL-433, Battelle-Northwest, Richland, Washington, June 1967.

Hutton, P.H., "Crack Detection in Pressure Piping by Acoustic Emission", Nuclear Safety Quarterly Progress Report April-June 1967, BNWL-537, Battelle-Northwest, Richland, Washington, September 1967.

Hutton, P.H., "Acoustic Emission in Metals as a NDT Tool", Battelle, Northwest, BNWL-SA-1262. 27th National Conference of the Society for Nondestructive Testing, Cleveland, Ohio, Oct. 1967.

Kubiak, E.J., "New NDT Techniques for Aerospace Materials and Structures", General American Transportation, Niles, Illinois, from the Symposium on Correlation of Material Characteristics with Systems Performance, Orlando AFB, Florida, May 1967.

Michaels, T.E. and Fraser, M.C., "Acoustic Emission Behavior of Zircaloy-2 Pressure Tubing Under Applied Stress", BNWL-545, Battelle-Northwest, Richland, Washington, September 1967.

Parry, D.L., "Nondestructive Flaw Detection in Nuclear Power Installations", USAEC report, Conference Proceedings, Incipient Failure Diagnosis for Assuring Safety and Availability of Nuclear Power Plants, Gatlinburg, Tenn., Nov. 1967. Also TRANS. American Nuclear Society, Vol. 10, No. 1, 1967.

Parry, D.L., "Nondestructive Flaw Detection by Use of Acoustic Emission", IDO-17230, Phillips Petroleum Company, Idaho Falls, Idaho, May 1967.

Pollock, A.A., "Stress Wave Emission During Stress Corrosion Cracking of Titanium Alloys", D 1-82-0658, Boeing Airplane Company, October 1967.

Schofield, B.H., "Kaiser Effect: Noise from Plastically Deformed Metals; Tin Cry", Encyclopaedic Dictionary of Physics, Supplementary Volume 1, Pergamon Press 1967.

Wildermuth, D., "Pressure Testing of AFRM-017 Service Propulsion System Fuel Tank Utilizing Aerojet-General Corporation's Stress-Wave Analysis Technique", NAS 9-6766, 1967.

Worlton, D.C., et al., "Nuclear Safety Quarterly Report Jan, Feb, Mar, 1967 for Nuclear Safety Branch of USAFC Division of Reactor Development and Technology," Battelle-Northwest BNWL-433, July 1967.

Worlton, D.C., et al., "Nuclear Safety Quarterly Report April, May, June, 1967 for Nuclear Safety Branch of USAEC Division of Reactor Development and Technology", Battelle-Northwest BNWL-537.

1966

Antsferov, M.S., Ed., "Seismo-Acoustic Methods in Mining", S.E. Hall, Trans. Consultant's Bureau, New York, 1966.

Bolles, Milton Moris, "Investigation and Design of a Fluid Coupled Acoustic Transducer System for the Detection of Acoustic Emission, Tulane University, Ph.D. Dissertation, 1966.

Downing, T.J., "The Acoustic Analysis of Materials in Dynamic Applications", Memorandum Report N67-6-1, Frankford Arsenal, Philadelphia, Pennsylvania, September 1966.

Egle, D.M. and Tatro, C.A., "Analysis of Acoustic Emission Strain Waves, Journal of the Acoustical Society of America, Vol. 41, No. 2, p. 321, June 1966.

Engle, R.B., "Acoustic Emission and Related Displacements in Lithium Fluoride Single Crystals", Ph.D. Thesis, Michigan State University, East Lansing, Michigan, 1966.

Fisher, R.M. and Lally, J.S., "Microplasticity Detected by an Acoustic Technique", Proceedings of the Conference on Deformation of Crystalline Solids, Ottawa, Canada, 1966.

Gerberich, W.W., Hartbower, C.E., "Feasibility Study for Measuring Fatigue Crack Growth Rate in Welded HY-80 Steel Using Stress-Wave Emission", USN-N600 (167)-64934(X)(FBM), July 1966.

Green, A.T., "Stress-Wave Detection, Saturn S-II," NASA CR-61161, Dec 1966.

Green, A.T., Lockman, C.S., Brown, S.J., Steele, R.K., "Feasibility Study of Acoustic Depressurization System," NASA CR-55472, March 1966.

Hartbower, C.E., Gerberich, W.W., Crimmins, P.P., "Monitoring Subcritical Crack Growth by an Acoustic Technique", Weld Imperfections Symposium, Lockheed Research, Palo Alto, Calif., Sept. 1966. Published in WELD IMPERFECTIONS, Addison-Wesley, Menlo Park, Calif.

Hartbower, C.E., Gerberich, W.W., Crimmins, P.P., "Characterization of Fatigue-Crack Growth by Stress-Wave Emission", NAS 1-4902, Report CR-66303, June 1966.

Hartbower, C.E., Gerberich, W.W., "Mechanisms of Slow Crack Growth in High Strength Steel", A progress report on Contract AF 33(615)-2788, February 1966.

Hutton, P.H., "Pressure Piping Crack Monitoring Detection of Metal Overstress by Acoustic Emission", BNWL-CC-673, Battelle-Northwest, Richland, Washington, August 1966.

Hutton, P.H., "Pressure Piping Crack Monitoring Detection of Metal Overstress by Acoustic Emission", Nuclear Safety Quarterly Progress Report July-September 1966, BNWL-CC-900, Battelle-Northwest, Richland, Washington, December 1966.

Lockman, C.S., Green, A.T., Steele, R.K., "Acoustic Monitoring During Proof Testing, Weld Imperfections Symposium, Lockheed Research, Palo Alto, Calif., Sept. 1966. Published in WELD IMPERFECTIONS, Addison-Wesley, Menlo Park, Calif.

Notvest, K., "Effect of Thermal Cycles in Welding D6aC Steel", The WELDING JOURNAL, Vol. 45(4), p. 173-s, April 1966.

Schmitz, G.L. and Frank, L.M., "Nondestructive Testing of Adhesive Bonds", General American Transportation Corp., Presented at the Third Annual Aerospace Conference on NDT, Georgia Institute of Technology, May 1966.

Schofield, B.H., "A Study of the Applicability of Acoustic Emission to Pressure Vessel Testing", Summary Report ML-TR-66-92, Lessels and Associates, November 1966.

Srawley, J.E., "Investigation of Hydrotest Failure of Thiokol Chemical Corp., 260-in.-Dia. Motor Case", NASA TM-X-1194, Jan. 1966.

Watson, R.W., Becker, K.R., and Gibson, F.C., "Stress Waves in Bounded Media", Pittsburgh Explosives Research Center Quarterly Report December 1965-February 1966, AD-480-403, Bureau of Mines, April 1966.

Weiss, V., Nash, G., Krause, G., Marchetto, G., and Sessler, J., "Crack Initiation and Crack Propagation in Structural Metal Alloys", Final Report on Navy Contract NOw-65-0355-d, Syracuse University Research Institute Report SURI Met-E-1289-0666-F, June 1966.

1965

Baker, G.S. and Bainbridge, D.W., "Influence of Strain Rate on Acoustic Emission from Hardened D6aC During Increment Crack Growth", Internal Memorandum, Aerojet-General Corp., November 1965.

Baker, G.S. and Bainbridge, D.W., "Sources of Pre-Fracture Acoustic Emission", Internal Memorandum, Aerojet-General Corp., October 1965.

Brown, W.F., and Srawley, J.E., "Fracture Toughness Testing and Its Applications", Fracture Toughness Testing Methods, ASTM Special Technical Publication No. 381, Philadelphia, Pennsylvania, American Society for Testing and Materials, pp. 133-244, 1965.

Butenko, A.N. and Gumenyuk, V.S., "Acoustic Device for Ultrasonic Wire Inspection", Industrial Laboratory, 31, 1757-1758, November 1965.

Egle, D.M., "A Comprehensive Analysis of an Acoustic Emission Detection System", Ph.D. Thesis, Tulane University, New Orleans, Louisiana, 1965.

Goodman, R.E. and Blake, W., "Rock Noise in Landslides and Slope Failures", University of California Press, Berkeley, Calif.,1965.

Green, A.T., Hartbower, C.E., and Lockman, C.S., "Feasibility Study of Acoustic Depressurization System:, Report NAS 7-310, Aerojet-General Corporation, February 1965.

Kerawalla, J.N., "An Investigation of the Acoustic Emission from Commercial Ferrous Materials Subjected to Cyclic Tensile Loading", Ph.D. Thesis, University of Michigan, Ann Arbor, Michigan, 1965. University microfilm 66-6632.

Kuttruff, H. and Wolfrum, J., "Acoustical Detection of Electromagnetically Produced Shock Waves", Nachr Akad Wiss Cöttingen, Math-Phys. Kl. N.3. (in German), 1965.

McCauky, M.L., "Engineering Geology", Association of Engineering Geologists, AEGBA, Vol. 2, 1965, p. 1.

Mitchell, L.D., "An Investigation of the Correlation of the Acoustic Emission Phenomenon with the Scatter in Fatigue Data", Ph.D. Thesis, University of Michigan, Ann Arbor, Michigan (Univ. Microfilms 66-6657), 1965.

Moss, G.L., "Fracture of Fe With Stress Waves", Report BRL-1289, Ballistic Research Labs, Aberdeen Proving Ground, Maryland, July 1965.

Schofield, B.H., "Investigation of Applicability of Acoustic Emission", Technical Report, ML TR-65-106, Lessels and Associates, May 1965.

Srawley, J.E. and Brown, W.F., "Fracture Toughness Testing Methods", ASTM STP-381, American Society for Testing and Materials, 133-244, 1965.

Steele, R.K., Green, A.T. and Lockman, C.S., "Structural-Seismology Techniques for Prevention of Failure of Rocket Chambers", ICPRG, Aerojet-General Corp., 1965.

Susuki, K., Sasaki, Z., Siohara, Z., and Kirota, T., in Proceedings of the International Conference on Strata Control and Rock Mechanics, Columbia University, New York, 1965, p. 1.

Swann, P.R. and Embury, J.D., "Microstructural Aspects of Stress Corrosion Failure", High Strength Materials, John Wiley and Sons, New York, 1965.

Weiss, V., Krause, G., Chave, C., Jr., and Marchetto, G., "Crack Initiation in Metallic Materials", Progress Report on Contract NOw-65-0355-d, 1965.

1964

Braddock, P.H., "New Method for NDT Uses Ultrasonic Waves from Loads", Metalworking News, Fairchild News Service, October 1964.

Brown, W.F., Jr., and Jones, M.H., "Acoustic Detection of Crack Initiation in Sharply Notched Specimens", Materials Research and Standards, Vol. 4, No. 3, March 1964.

Dunegan, H.L., Harris, D.O., and Tatro, C.A., "Acoustic Emission Research Status Report, December 1963-August 1964", UCID-4868 Rev. 1, Lawrence Radiation Laboratory, November 1964.

Steele, R.K., Green, A.T., Lockman, C.S., "Acoustic Verification of Structural Integrity of Polaris Chambers", Society of Plastic Engineers, Atlantic City, N.Y., Jan. 1964. Published in Modern Plastics, Vol. 41, pp. 137-139, July 1964.

Kroll, R.J., "Stress-Wave Propagation in Axially Symmetric Test Specimens", Experimental Mechanics, Vol. 4, No. 5, 129-134, May 1964.

Schofield, B.H., "Acoustic Emission Under Applied Stress", ASD-TDR-63-509, Part II, May 1964.

Schofield, B.H., "Acoustic Emission under Cyclic Stress", Final Report TR 796/P81, Lessels and Associates, July 1964.

1963

Borchers, H. and Tensi, H.M., "Piezoelektische Impulsmessungen bei der Phasenanderung von unlegierten Proben der binaren Legierungen Blei-Sinn, Blei-Antimon und Kadmium-Zink," Z. Metallkunde, 17. 784, 1963.

Green, A.T., Lockman, C.S., and Haines, H.K., "Acoustic Analysis of Filament-Wound Polaris Chambers", Report 0672-01F, Aerojet-General Corp., Sacramento, California, September 1963.

Jones, M.H. and Brown, W.F., Jr., "An Acoustic Method for Determining the Onset of Crack Propagation in Sharply Notched Specimens", paper presented at the ASTM Annual Meeting, June 1963.

Liptai, R.G., "An Investigation of the Acoustic Emission Phenomenon", Ph.D. Thesis, Michigan State University, East Lansing, Michigan, 1963.

Liptai, R.G. and Tatro, C.A., Proceedings of the Fourth Annual Symposium on Nondestructive Testing of Aircraft and Missile Components, Southwest Research Institute, San Antonio, Texas, 1963, pp 287-341.

Schofield, B.H., "Acoustic Emission from Metals, Its Detection, Character-istics, and Source", Proceedings of the Symposium on Physics and Nondestructive Testing, Southwest Research Institute, San Antonio, Texas, October 1963.

Schofield, B.H., "Acoustic Emission Under Applied Stress", ASD-TDR-63-509, Part I, 1963.

1962

Borchers, H. and Teusi, H.M., "Piezoelektrische Impulsmessungen Wahrend der Mechanischem Beansprunchung von Al, MgO, und A199", Z. Metallkunde, 1962.

R.J. Kroll, "Stress Waves in Test Specimens due to Simulated Acoustic Emission", Ph.D. Tehsis, Michigan State University, East Lansing, Michigan, 1962.

Tatro, C.A. and Liptai, R.G., "Acoustic Emission from Crystalline Substances", Proceedings of the Symposium on Physics and Nondestructive Testing, Southwest Research Institute, San Antonio, Texas, 145-158, October 1962.

1961

Borchers, H. and Tensi, H.M., "Eine verbesserte piezoelektrische Methode zur Untersuchung von Vorgangen in Metallen bei mechanischer Beanspruchung und bei Phasenanderung", Z. Metallkunde, 51, 212, 1961.

Christensen, R.H., "Cracking and Fracture in Metals and Structures", Proceedings of the Crack Propagation Symposium, Granfield, England, Vol. II, 1961.

Schofield, B.H., "Acoustic Emission Under Applied Stress", Report ARL-150, Lessels and Associates, December 1961.

1960

Borchers, H. and Tensi, H.M., "Eine Verbesserte Piezoelektrische Methode", Z. Metallkunde, Vol. 51, No. 4, 212-218, 1960.

1959

Tatro, C.A., "Sonic Techniques in the Detection of Crystal Slip in Metals", Progress Report, Division of Engineering Research, Michigan State University, East Lansing, Michigan, January 1959.

1958

Borchers, H. and Kaiser, J., "Akustische Effekte bei Phasenuberganen im System Blei-Zinn", Z. Metallkunde, 49, 95-100, 1958.

Lean, J.B., Plateau, J., Bachet, C. and Crussuard, C., "Sur la deformation d'ondes Sonores, au Cours d'essais de traction, dans des Eprouvettas Metalliques", Comptes Rendus des Seances de l'Academie des Sciences, 246, 19, May 1958.

Schofield, B.H., Bareis, R.A., Kyrala, A.A., "Acoustic Emission Under Applied Stress", WADC Technical Report 58-194, ASTIA Doc. No. AD155674, April 1958.

1957

Borchers, H. and Tensi, H.M., "Eine Verbesserte Piezoelektrische Methode", Z. Metallkunde, 23, 1957.

Kaiser, J., "Uber das Auftreten von Gerauschen beium Schmelzen und Erstarren von Metallen", Forschg. Ing. Wes., Vol. 23, No. 1-2, p. 38, 1957.

1950

Kaiser, J., "Untersuchungen uber das Auftreten Gerauschen Beim Sugversuch", Ph.D. Thesis, Techn. Hochsch., Munchen, 1950, and <u>Arkiv Fur das Eisen-huttenwesen</u>, Vol. 24, No. 1-2, Jan./Feb. 1953, pp. 43-45.

1948

Mason, W.P., McSkimin, H.J. and Shockley, W., "Ultrasonic Observation of Twinning in Tin", <u>Physical Review</u>, Vol. 73, No. 10, pp. 1213-1214, May 1948.

1942

Obert, L. and Duvall, W., "Use of Subaudible Noises for the Prediction of Rock Bursts, Part II", RI-3654, US Bureau of Mines, 1942.

1928

Joffe', A., <u>The Physics of Crystals</u>, McGraw-Hill, New York, 1928.